

004
KAK

T 287

<p>CENTRAL LIBRARY TEZPUR UNIVERSITY</p> <p>Accession No. <u>T-287</u></p> <p>Date <u>21/7/14</u></p>

THESES & DISSERTATION
SECTION
CENTRAL LIBRARY, T.U.

A Biomimetic Hand with EMG based Grasp Emulation

A thesis submitted in partial fulfillment of the requirements for the degree of
Doctor of Philosophy

Nayan Moni Kakoty
Registration No. 012/2013



Department of Computer Science and Engineering
School of Engineering
Tezpur University
Napaam - 784028, Assam, India
April 2014

To my Mother and the memory of my Father

Abstract

Despite serious research efforts, electromyogram (EMG) based prosthetic hands (both commercial variants and research prototypes) are nowhere near the original counterparts they intended to replace. EMG based prosthetic hands are non-intuitive in the sense that user is required to learn to associate muscle remnants action to unrelated postures of the prosthesis or being limited to few hand postures based on higher number of EMG channels. Moreover, present prosthesis are non-anthropomorphic in terms of the functional geometry. These are some of the main reasons for non-acceptance of prostheses by the amputees. Development of a biomimetic hand capable of reproducing grasping operations involved during daily living activities (dla) based on low channel EMG signals holds promise. This would involve recognition of grasp types based on EMG signals and a biomimetic hand development inspired by human hand anatomy.

Therefore, the prime concerns to be addressed in this research involve: a. Recognition of six grasp types involved during 70% of dla based on two channel EMG signals and b. Development of a biomimetic hand; a five fingered extreme upper limb inspired by human hand anatomy capable of emulating the grasps based on EMG signals.

Acknowledgements

I am indebted to my advisor Professor Shyamanta Moni Hazarika for letting me get involved in this research in the first place; and very thankful for his guidance and support through the years. I appreciate his considerate and understanding personality as a mentor, who set realistic goals that always kept me motivated for research. He always gave positive feedback and has a good sense of humor while dealing with disappointments or unforeseen circumstances. It has been a genuine pleasure working with him.

I am also grateful to the members of the doctoral committee, Professor Dilip Kumar Saikia and Dr. Bhogeswar Borah. As individuals, they offered continuous encouragement and constructive criticism for this dissertation to take its current shape.

I would like to thank my laboratory mates in the Biomimetic and Cognitive Robotics Lab, Tezpur University for their friendship and for sharing days and nights with me. My special thanks to Pritom, Achyanta and Dushyanta for their inspiring words.

I would like to express my sincere thanks to the Department of Electronics and Information Technology, Government of India for the financial assistance for this research under the project entitled Design and Development of Bio-signals Controlled Prosthetic Hand: 1(9)/2008 - ME & TMD. Thanks are also due to the fund of BARC/BRNS Programme for Autonomous Robotics at Indian Institute of Technology, Delhi to support a short stay of mine during the work for this dissertation.

I am grateful to my family members for their support throughout my education life. My deepest gratitude goes to my parents. This thesis is indeed a realization of their dream. Thank you "Maa" for all the trouble you have taken to ensure I get the best out of life.



Department of Computer Science and Engineering
Tezpur University

Dr. Shyamanta Moni Hazarika
B. E., M. Tech.(IIT Kanpur, INDIA)
Ph. D. (University of Leeds, England)
Professor

Phone: 03712 - 275354
Fax: 03712 - 267005
e-mail: smh@tezu.ernet.in

Certificate

This is to certify that the thesis entitled A Biomimetic Hand with EMG based Grasp Emulation submitted to the School of Engineering, Tezpur University in part fulfillment for award of the degree of Doctor of Philosophy in Computer Science and Engineering is a record of research work carried out by Nayan Moni Kakoty under my supervision and guidance. All help received by him from various sources have been duly acknowledged. No part of this thesis has been reproduced elsewhere for award of any other degree.

(Shyamanta Moni Hazarika)

Professor

Department of Computer Science and Engineering


School of Engineering

Tezpur University

Declaration

I, Nayan Moni Kakoty, declare that the thesis entitled A Biomimetic Hand with EMG based Grasp Emulation and the work presented in it are my own. I confirm that:

- This work was done entirely while in candidature for a research degree at Tezpur University.
- Where any part of this thesis has previously been submitted for a degree or any other qualification at this University or any other institution, this has been clearly stated.
- Where I have consulted the published work of others, this is always clearly attributed.
- Where I have quoted from the work of others, the source is always given. With the exception of such quotations, this thesis is entirely my own work.
- I have acknowledged all main sources of help.

..... 

(Nayan Moni Kakoty)

Date: 30.04.2014.

Place: Tezpur, INDIA

Contents

List of Figures	xix
List of Tables	xxii
List of Abbreviations	xxiv
1 Introduction	1
1.1 EMG Controlled Prosthesis	2
1.1.1 Problems with EMG Controlled Prosthetic Hands	3
1.2 Objectives	4
1.3 Thesis Outline	5
2 Background and Literature Review	7
2.1 Introduction	7
2.2 Electrical Signals from Muscle - Electromyogram	8
2.2.1 Origin of EMG Signals	8
2.2.2 Characteristics of EMG Signal	9
2.2.2.1 Noises in EMG Signals	9
2.2.3 EMG signal Acquisition	10
2.2.3.1 Requirements of EMG Acquisition	10
2.2.3.2 Types of EMG Electrodes	11
2.3 EMG Features and Classifiers	12
2.3.1 EMG Features	12
2.3.1.1 Time Domain Features	13
2.3.1.2 Frequency Domain Features	14
2.3.1.3 Time/ Frcquency Domain Features	15

CONTENTS

2.3.2	EMG Classifiers	16
2.3.2.1	Linear Discriminant Analysis (LDA)	17
2.3.2.2	Support Vector Machine (SVM)	18
2.3.2.3	Artificial Neural Networks (ANN)	20
2.3.2.4	Fuzzy Logic (FL)	20
2.3.2.5	k Nearest Neighbour Classifier (kNN)	21
2.4	EMG based Grasp Classification	23
2.4.1	State of Art	23
2.4.2	Limitations	24
2.4.3	Focus of our Work	24
2.5	Review of Prosthetic Hands	25
2.5.1	Human Hand	25
2.5.1.1	Human Hand Grasping	27
2.5.2	Prosthetic Hands: State of Art	28
2.5.2.1	Brief History of Prosthetic Hands	29
2.5.2.2	Commercially Available Prosthetic Hands	30
2.5.2.3	Research Prototypes of Prosthetic Hands	31
2.5.2.4	Limitations	36
2.5.2.5	Focus of our Work	37
2.6	Summary	37
3	EMG based Grasps Recognition: Initial Results	39
3.1	Materials and Methods	40
3.1.1	Subjects and Experiment	40
3.1.1.1	Experimental Protocol	40
3.2	EMG Acquisition and Preprocessing	41
3.2.1	EMG Acquisition	41
3.2.2	EMG Preprocessing	43
3.3	Grasp Recognition Architecture-I	44
3.3.1	Feature Set	45
3.3.2	Classifier	45
3.3.3	Results of Grasp Recognition Architecture-I	47
3.4	Grasp Recognition Architecture-II	49

3.4.1	Normalization	49
3.4.2	Feature Set	50
3.4.3	Classifier	51
3.4.4	Results of Grasp Recognition Architecture-II	52
3.5	Grasp Recognition Architecture-III	55
3.5.1	Feature Set	56
3.5.2	Classifier	56
3.5.3	Results of Grasp Recognition Architecture-III	59
3.6	Summary	60
4	EMG based Grasps Recognition: Results with Statistical Analysis	61
4.1	Grasps Recognition Architecture-IV	61
4.1.1	Classification with Time Domain Feature	62
4.1.1.1	Feature Set	62
4.1.1.2	Classifier	64
	Classifier Parameter Setting	64
4.1.1.3	Results with Time Domain Features	65
	Cross Validation	65
4.1.1.4	Linear Relationship	67
4.1.2	Classification with Frequency Domain Feature	69
4.1.2.1	Feature Set	69
4.1.2.2	Classifier	70
	Classifier Parameter Setting	71
4.1.2.3	Results with Frequency Domain Features	71
	Cross Validation	71
4.1.2.4	Linear Relationship	73
4.1.3	Classification with Time/ Frequency Domain Feature	74
4.1.3.1	Feature Set	74
4.1.3.2	Classifier	77
	Classifier Parameter Setting	77
4.1.3.3	Results with Time/ Frequency Domain Features	77
	Cross Validation	77
4.1.3.4	Linear Relationship	79

4.1.4	Classification with PCA of Time/ Frequency Domain Feature . .	81
4.1.4.1	Feature Sct	81
4.1.4.2	Classifier Parameter Setting	82
4.1.4.3	Results with PCA of Time/ Frequency Domain Features	82
	Cross Validation	82
4.1.4.4	Linear Relationship	84
4.2	Statistical Analysis	85
4.2.1	ANOVA analysis	85
4.2.2	Shecfc's Post hoc Test	87
4.3	Summary	89
5	A Biomimetic Hand: Prototype 1.0	91
5.1	Biomimetic Approach	92
5.1.1	Material selection	93
5.1.2	Bio-mechanical Structure	94
5.1.2.1	Tendon System	96
5.1.3	Development of Control Architecture	98
5.1.3.1	Superior Hand Control	99
5.1.3.2	Local Hand Control	99
5.2	Kinematics, Statics and Dynamics	100
5.2.1	Kinematic Analysis of a Finger	100
5.2.1.1	Tendon Actuation	101
5.2.2	Static Analysis of a Finger	103
5.2.2.1	Joint Torques and Fingertip Forces	103
5.2.2.2	Tendon Forces and Joint Torques	106
5.2.3	Dynamic Analysis of a Finger	108
5.2.3.1	Equations of motion	108
5.2.3.2	Torques for Natural Curling	112
5.2.4	PID Control	117
5.2.4.1	System Linearity	117
5.2.4.2	System Transfer Function	118
5.2.4.3	PID Controller Design	119
5.2.4.4	Simulation Results	119

CONTENTS

5.3	Graspability of Prototype 1.0	122
5.4	Summary	123
6	Characteristics of Prototype 1.0 and A Similarity Index	124
6.1	Characteristics of Prototype 1.0	125
6.1.1	Physical Characteristics	125
6.1.1.1	Size	125
6.1.1.2	Weight	126
6.1.1.3	Degrees of Freedom	127
6.1.2	Kinematic Characteristics	128
6.1.2.1	Dynamic Constraints	128
6.1.2.2	Range of Motion	128
6.1.2.3	Number of Actuators and Hand Complexity	129
6.1.3	Dynamic Characteristics	129
6.1.3.1	Achievable Grasps	129
6.1.3.2	Finger Tip Force	130
6.2	Biomimetic Similarity Index	130
6.2.1	Metric for Similarity	131
6.2.2	Function-Vector Characteristics	134
6.2.3	Derivation of A Biomimetic Similarity Index	136
6.3	Summary	139
7	Conclusions and Future Work	140
7.1	Conclusions	140
7.1.1	EMG based Grasp Recognition	141
7.1.2	A Biomimetic Hand with EMG based Grasp Emulation	142
7.1.3	A Biomimetic Similarity Index	142
7.2	Future Work	143
7.2.1	Further evaluation of the EMG based Grasp Recognition	143
7.2.1.1	Use of Different Classifier	143
7.2.1.2	Use of Different Data Sets	143
7.2.2	Implementation into a Microcontroller	144
	Bibliography	145

CONTENTS

Appendix-I: IEMG and nIEMG Signals	164
Appendix-II: EMG Signals in Time/ Frequency Domain	169
Appendix-III: Simulation Results of Prototype 1.0	200
List of Publications	207

List of Figures

1.1	Schematic of EMG controlled Prosthetic Hand	2
1.2	Grasp types involved in 70% of daily living activities	4
2.1	Superposition of MUAP to form EMG signals	8
2.2	EMG Electrodes	11
2.3	SVM Classifier with hyperplane H and margin of width 2γ	18
2.4	Bones and Joints of Human Hand	26
2.5	Muscles on Extreme Upper Limb	27
2.6	The i-Limb Hand (From (1)).	30
2.7	The Manus Hand (From (2)).	32
2.8	The Southampton Hand (From (3)).	33
2.9	The DLR-II Hand (From (3)).	34
2.10	The RTR-II Hand (From (4)).	36
3.1	Electrode placement on the Forearm Muscles	42
3.2	Experimental Set-up during Acquisition of EMG Signals	43
3.3	Schematic of the Grasp Recognition Architecture-I	45
3.4	Confusion matrix for classification based on Architecture-I	48
3.5	Schematic of the Grasp Recognition Architecture-II	49
3.6	Grasp Recognition Architecture-III	56
3.7	Confusion matrix for classification based on Architecture-III	59
4.1	Proposed EMG based Grasp Recognition Architecture	62
4.2	Classification with TD Features	64
4.3	Results of Grid search for TD features	65
4.4	Recognition Rate with TD Features	66

LIST OF FIGURES

4.5	Confusion Matrix for classification based on TD features	66
4.6	Classification with FD Features	71
4.7	Results of Grid search for FD features	71
4.8	Recognition Rate with FD Features	72
4.9	Confusion Matrix for classification based on FD Features	73
4.10	Classification with TFD Features	78
4.11	Results of Grid search for TFD features	79
4.12	Recognition Rate with TFD Features	79
4.13	Confusion Matrix for classification based on TFD features	80
4.14	Results of Grid search for PCA of TFD features	82
4.15	Recognition Rate with PCA of TFD features	83
4.16	Confusion Matrix for classification based on PCA of TFD features	84
4.17	Grasp Recognition Error Average across all Subjects	90
5.1	Biomimetic Approach followed for development of Prototype 1.0	92
5.2	Schematic of the Index Finger	95
5.3	Ventral View of Prototype 1.0	96
5.4	Schematic of Control Architecture	98
5.5	Schematic of point contact between the object and finger tip	106
5.6	Human Finger Joint Trajectories	113
5.7	Digitized and Curve Fitted Finger Joint Trajectories	114
5.8	Linearity range of the System	118
5.9	Response of the PID controller with different values of the Gains	120
5.10	Schematic of the Simulation Model	120
5.11	Simulated DIP, PIP and MCP Joint Trajectories of Fingers	121
5.12	Prototype 1.0 performing grasp types	122
6.1	Weights versus number of Joints of Prosthetic Hands	126
6.2	Weights versus number of Actuators of Prosthetic Hands	127
6.3	DoF versus Number of Joints for Prosthetic Hands	127
6.4	Number of Actuator versus DoF	129
6.5	Precision Grasp Force versus weights of Prosthetic hands	130
6.6	Precision Grasp Force versus number of actuators of Prosthetic hands	131
6.7	Graphical interpretation of prosthesis function-vector similarity projection	133

LIST OF FIGURES

6.8 Concept Lattice for the context of anthropomorphism 135

List of Tables

2.1	Typical EMG Recognition for Prosthesis Control	16
2.2	Finger joint range of motion of human hand	25
3.1	Placement of EMG Electrode	42
3.2	Bio-amplifier specification settings during EMG Acquisition	44
3.3	Results of SVM Classifier	46
3.4	Results of FFT Classifier	47
3.5	Recognition Rates of Architecture-I	47
3.6	Average recognition rates over six grasp types through CWT coefficients at different scale index	52
3.7	Entropy Measure of Wavelet coefficients	53
3.8	Entropy Measure of nIEMG Signals for Grasp Types Under Study	53
3.9	Recognition rate of six grasp types through DWT at third, fourth and fifth level of decomposition	54
3.10	Recognition Rates of Architecture-III	59
4.1	Recognition rates based with TD features	65
4.2	ANOVA with TD Features	68
4.3	Recognition rates based with FD features	72
4.4	ANOVA with FD Features	73
4.5	Recognition rates based with TFD features	78
4.6	ANOVA with TFD Features	80
4.7	Recognition rates based with PCA of TFD features	83
4.8	ANOVA with PCA of TFD Features	84
4.9	ANOVA Results for TD (G_1) and FD (G_2) features	86

LIST OF TABLES

4.10	ANOVA Results for TD (G_1) and TFD (G_2) features	86
4.11	ANOVA Results for TD (G_1) and PCA of TFD (G_2) features	87
4.12	ANOVA Results for FD (G_1) and TFD (G_2) features	87
4.13	ANOVA Results for FD (G_1) and PCA of TFD (G_2) features	87
4.14	ANOVA Results for TFD (G_1) and PCA of TFD (G_2) features	88
4.15	Results of Sheffes post hoc test	88
4.16	Comparison of Grasp Types Recognition Rates	90
5.1	Comparison of primitive characteristics	93
5.2	Building blocks of Human hand versus the Prototype 1.0	93
5.3	Finger joint range of motion of the prototype	94
5.4	Specification of the Actuating Motors	96
5.5	Characteristics of Human hand and Prototype 1.0	97
5.6	Denavit-Hartenberg Parameters of the Finger	101
5.7	Curve Fitted Finger Joint Trajectories for Natural Curling	115
5.8	Average Finger Joint Torques for Natural Curling Operations	116
5.9	Average Fingertip Forces corresponding to the Joint Torques	117
5.10	Process followed for Controller Gain Selection	119
6.1	Size of Human hand and Prototype 1.0	125
6.2	Length of Prosthetic Hands and Prototype 1.0	126
6.3	Finger joint RoM and Dynamic Constraints	128
6.4	Formal Context of Anthropomorphism.	135
6.5	Concepts of Anthropomorphism	136

List of Abbreviations

EEG	Electroencephalogram	1
EMG	Electromyogram	1
dla	Daily living activities	4
SHC	Superior Hand Control	6
LHC	Local Hand Control	6
BSI	Biomimetic Similarity Index	6
sEMG	Surface Electromyogram	8
MUAP	Motor Unit Action Potential	9
SNR	Signal to Noise Ratio	10
CMRR	Common Mode Rejection Ratio	11
TD	Time Domain	12
FD	Frequency Domain	12
TFD	Time/ Frequency Domain	12
MAV	Mean Absolute Value	13
VAR	Variance	13
IAV	Integrated Absolute Value	13
MAVS	Mean Absolute Value Slope	13
WAMP	Willison Amplitude	13
ZC	Zero Crossing	13
SSC	Slope Sign Changes	13
WL	Wavelength	13
DoF	Degrees of Freedom	13
PS	Power Spectrum	14
FMD	Frequency Median	14
FMN	Frequency Mean	14

LIST OF ABBREVIATIONS

FR	Frequency Ratio	14
NN	Neural Network	14
FFT	Fast Fourier Transform	14
STFT	Short Time Fourier Transform	15
WT	Wavelet Transform	15
WPT	Wavelet Packet Transform	15
CWT	Continuous Wavelet Transform	15
DWT	Discrete Wavelet Transform	15
PCA	Principal Component Analysis	17
FL	Fuzzy Logic	17
LDA	Linear Discriminant Analysis	17
SVM	Support Vector Machine	18
ANN	Artificial Neural Network	20
MLP	Multilayer perceptron neural network	20
kNN	k Nearest Neighbour	21
RoM	Range of Motion	25
DC	Direct Current	30
RBF	Radial Basis Function	40
IEMG	Integrated Electromyogram	44
BZC	Baseline Zero Crossing	45
TP	Turning Points	45
DFT	Discrete Fourier Transform	46
MVC	Maximum Voluntary Contraction	49
nIEMG	Normalized Integrated Electromyogram	49
RMS	Root Mean Square	49
SWC	Sum of Wavelet Decomposition Coefficients	56
ANOVA	Analysis of Variance	61
PSD	Power Spectral Density	70
EWC	Energy of Approximate Wavelet Coefficients	75
MWC	Mean Absolute value of Wavelet Decomposition Coefficients	76
VWC	Variance of Wavelet Decomposition Coefficients	76
ZWC	Zero Crossings of Wavelet Decomposition Coefficients	76
TWC	Turning points of Wavelet Decomposition Coefficients	76

LIST OF ABBREVIATIONS

RMSWC	RMS Value of Wavelet Decomposition Coefficients	77
RPM	Revolution per Minute	96
PID	Proportional Integral Derivative	100
PWM	Pulse Width Modulation	117
ARAT	Action Research Arm Test	124
SHAP	Southampton Hand Assessment Procedure	124
FCA	Formal Concept Analysis	132
EU	European Union	142

1

Introduction

The development of interfaces that link the human musculoskeletal system with robotic devices has been a major area of research within *rehabilitation robotics*. Most of the research is focused on restoration of motor and sensory functions to those with degenerative diseases, injury or amputees. The basic goal is to enhance capability for independent living and vocational productivity by restoring the physical functionality through use of prosthesis. One of the key focus has been upper limb prostheses for people with manipulative disabilities. Bio-signals driven prosthetic hands have been found to be suitable; wherein control is through conveying human's intention to the prosthesis. There are two possible bio-signal based schemes covering the approaches for conveying human's intention to the prosthesis.

- Electroencephalogram (EEG) based approaches
- Electromyogram (EMG) based approaches

EEG based approaches are implemented through an interface between the brain and the prosthetic hand to be controlled. The activity of the brain is recognized based on the EEG signals (5). On successful recognition of brain's activity; the prosthesis emulate the amputee's intention through the interface. Due to localization of brain activities and multidimensional aspect of the EEG signals, analysis and classification of EEG signals are challenging. Moreover, the appropriate number of channels as well as their specific location on the scalp requires identification. Failing to do so results in degradation of system performance. In many cases, there is no clear agreement about the number and location of necessary channels to collect EEG signals. Using a small

number of channels may cause loss of important information. Conversely, including more channels for data collection provides redundant information, which could degrade the system performance.

In EMG based approaches, an indirect interface between the brain and the prosthetic hand to be controlled is established based on the muscles' activity through EMG signals (6). EMG is the electrical manifestation of the neuromuscular activities and is known to reflect the voluntary intention of the central nervous system (7). Interpreting the content of the EMG implies the interpretation of the brain's activity to contract a muscle or a group of muscles. EMG based approaches for prosthetic hand control is a targeted reinnervation as it collects information from specific muscles; responsible for specific functions

1.1 EMG Controlled Prosthesis

The concept of EMG control has emerged essentially as a control paradigm for prosthetic hands in which the EMG signals are acquired from the muscles remnant in the amputee's stump. This still have normal innervations (8) and thus subjected to voluntary control. It allows amputees intuitively to use the same mental process to effectively control their prosthesis. A schematic of EMG controlled prosthetic hand is shown in Figure 1.1.

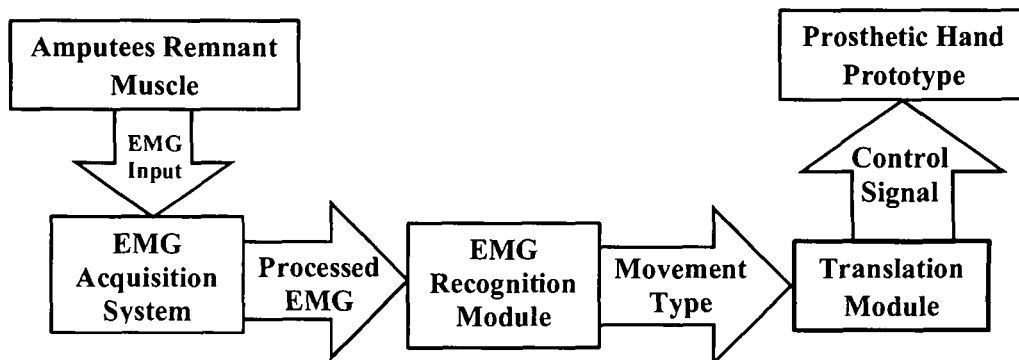


Figure 1.1: Schematic of EMG controlled Prosthetic Hand

EMG signals generated from the remnant muscles of the amputee are collected through an EMG Acquisition System. Based on the EMG signals, the type of movement attempted by the user is identified in the EMG Recognition Module using signal processing and machine learning techniques. The information about the identified movement is passed to the Translation Module wherein a control is developed to command the prosthetic hand to emulate the identified movement.

1.1.1 Problems with EMG Controlled Prosthetic Hands

Although the concept of EMG controlled prosthesis has been known for several decades, there remain several issues to be addressed for its successful implementation. Despite serious research efforts, EMG based prosthetic hands (both commercial variants and research prototypes) are nowhere near to the original counterparts they intended to replace.

The lack of acceptance stems from an inadequate controllability. EMG based prostheses are non-intuitive in the sense that user is required to learn to associate muscle remnants action to unrelated postures of the prosthesis or being limited to few hand postures based on higher number of EMG channels. Most of the work on EMG based prosthesis control concentrates in EMG based classification of hand movements instead of correlated grasping for the control purpose.

Grasp is the interface between the subject's hand and the object to be handled. A single grasp can perform different specific tasks. Such as a hook grasp can be used for pick and place operation of a mug as well as for pouring water from the mug; i.e. grasps are generic and task are specific in nature. For an effective extreme upper limb prosthesis, EMG based grasp classification holds promise (9). This thesis focus on the six grasp types as shown in Figure 1.2.

Even though classification of EMG signals has been the subject of considerable research; *recognition has been either poor while using low channel EMG or only for a limited set of grasps based on higher number of EMG channels*. EMG based grasp classification performance depends on type of features (10). Therefore, derivation of a feature vector resulting in higher recognition rate of grasp types based on lower number of EMG channels is one of the important issues.

Another important reason for non-acceptance of prosthetic hands by the amputees is their non-anthropomorphism. Present prosthesis are far from human hand in terms

of the functional geometry i.e the anatomical geometry that effects the functionality of the hand (11). Functional geometry can be expressed in terms of static and dynamic constraints. Static constraints involve dimensions, weight and joint range motions. The dynamic constraints involve linear inter-joint angular relationships in human finger (12).

1.2 Objectives

The work presented in this thesis stems from the desire to develop a biomimetic hand with EMG based grasp emulation. Although the use of advanced machine learning and signal processing techniques have proved useful in EMG based prostheses; higher recognition rate of grasp types based on low number of EMG channels is still a challenge. Eventhough multifingered hand prostheses using surface EMG (1), (13) have appeared in the market and advanced research prototypes (2), (14), (15), (16) have been developed; they are far from the human hand in terms of the functional geometry as well as controllability. A recognition architecture for grasp types used during daily living activities (dla) based on low number of EMG channels along with the development of a biomimetic hand emulating the recognized grasps holds promise. The prime objectives in this research include:

- Recognition of six grasp types (shown in Figure 1.2) involved during 70% of dla based on two channel EMG signals - derivation of a low dimensional yet informative and distinguishing feature vector through exploration of time domain, frequency domain and time/ frequency domain feature sets.

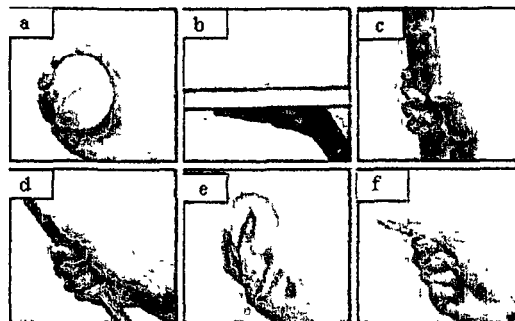


Figure 1.2: Grasp types: a. Power b. Palm-up c. Hook d. Oblique e. Precision and f. Pinch. These six grasp types are significant for they are involved in 70% of dla (17)

- Development of a biomimetic hand - a five fingered extreme upper limb inspired by human hand anatomy capable of emulating the above grasps based on EMG signals through a biomimetic approach satisfying the static and dynamic constraints of the human hand

This thesis, however, does not address the issues for embedment of the control architecture for the biomimetic hand. The embedment of the EMG acquisition unit, control architecture as well as customization of the power supply are not within the purview of this thesis. Research is limited to the development of an extreme upper limb prototype emulating the grasp types based on EMG signals. To evaluate or compare prosthesis based on their conceptual closeness to the human hand, I have also worked on the following:

- Development of an anthropomorphic similarity index for evaluation of anthropomorphism of the biomimetic hand prototype - evolve a framework for quantification of anthropomorphism for prosthetic hands.

1.3 Thesis Outline

The remainder of this thesis is divided into six chapters and the content of each is summarised below in order to simplify the reading.

Chapter 2: Background and Literature Review

Prior to presenting the development of a biomimetic hand with EMG based grasp emulation and its evaluation, it is useful to have a historical perspective. This chapter provides the basic concepts of EMG signals and the literature review on the major components of this thesis: (a) EMG signals and its features for classification of hand gestures and grasp types, (b) human hand including its characteristics during grasping operations (c) commercially available prosthetic hands and research prototypes and (d) EMG based control for prosthetic hand operations.

Chapter 3: EMG based Grasps Recognition: Initial Results

This chapter begins by discussing the materials and methods followed for acquisition of EMG signals. The initial results on grasp classification are presented. Three grasps classification architecture developed for recognition of six grasp types are described. Entropy as a measure to find the closeness of a mother wavelet function coefficients with the grasp types is reported. Also sum of wavelet decomposition coefficients has

been established as a primal feature for grasp recognition.

Chapter 4: EMG based Grasps Recognition: Results with Statistical Analysis

Following the initial work on EMG based grasp recognition for six grasp types reported in chapter 3, this chapter proposes grasp recognition architecture-IV. The focus is on the derivation of a low dimensional yet informative and distinguishing feature set to significantly increase the performance of grasp types recognition based on lower number of EMG channels. A recognition rate of 97.5% is reported using principal components of discrete wavelet transform based EMG features. The recognition rate obtained is comparable to that reported in literature and better in terms of number of grasp types vis-a-vis number of EMG channels. The experimental results are statistically evaluated through analysis of variance and Sheffe's post hoc test.

Chapter 5: A Biomimetic Hand: Prototype 1.0

Development of a biomimetic hand: Prototype 1.0 inspired by human hand anatomy is described in this chapter. A comparison of Prototype 1.0 vis-a-vis the human hand is presented. The kinematic, static and dynamic analysis of Prototype 1.0 satisfying the dynamic constraints of human hand is presented. This chapter also presents a two layered control architecture comprising of superior hand control (SHC) and local hand control (LHC) for the developed prototype. The SHC is to perceive the type of grasps attempted by the user based on the results reported in Chapter 4. The LHC is for emulating the identified grasp type into Prototype 1.0.

Chapter 6: Characteristics of Prototype 1.0 and A BSI

In this chapter, the performance requirements of the prostheses and Prototype 1.0 based on the research in prosthetic hands and their clinical use are set forth. A framework for quantification of anthropomorphism leading to a biomimetic similarity index (BSI) for prosthetic hands is proposed. Prototype 1.0 has been compared with five fairly established prosthetic hands with reference to human hand through the BSI.

Chapter 7: Conclusions and Future Work

It summarize the work presented in Chapter 2 through Chapter 6 with the concluding remarks. The issues to be encountered for further development of Prototype 1.0 are mentioned leading to future orientation of this research.

2

Background and Literature Review

2.1 Introduction

A long standing goal in *Rehabilitation Robotics* is the development of anthropomorphic artificial appendages that can be used as biological counterparts. Although tremendous technological progress has been made since the days of the wooden peg leg; contemporary orthoses and prostheses can not be used during daily living activities (dla) (4). However, last four decades have shown continuous advancement in anthropomorphic artificial limbs leading to improvements in the quality of life for the physically challenged.

The driving issue for realization of multifingered hand prostheses is to mimic human hand capabilities. Although commercial versions of prosthetic hands including bio-signals controlled ones have appeared in the market, there still exists a gap between the current state of art and prostheses that can *emulate* human hand grasping. This chapter covers a basic introduction to electromyogram (EMG) signals, which provides an useful non-invasive measure of ongoing muscle activity and have been used for controlling robotic prosthesis (18, 19). The chapter also review the classification of hand gestures and grasp types based on EMG signals. Commercially available prosthetic hands and research prototypes are reviewed. Human hand including its characteristics

2.2 Electrical Signals from Muscle - Electromyogram

during grasping operations is discussed for completeness. Finally EMG based control for prosthetic hand operations are discussed. In addition, the chapter highlight the shortcomings of the currently available prosthetic hands that this research aims to overcome.

2.2 Electrical Signals from Muscle - Electromyogram

EMG signal is the graphical representation of the electrical activity of muscles. It is the electrical manifestation of neuromuscular signals associated with muscle contraction. Surface EMG (sEMG) is the non-invasive electrical recording of muscle activity from the surface. EMG signal, an accurate and computationally efficient means of classifying muscle activity have increasingly gained attention for research in prosthesis control (18, 20, 21, 22, 23). The use of advanced machine learning and signal processing techniques have proved useful in EMG application to control prostheses; which otherwise presented a challenge due to the complexity of the EMG signal.

2.2.1 Origin of EMG Signals

EMG represents the current generated by the ionic flow across the membrane of the muscle fibers that propagates through the intervening tissues to reach the detection surface. Muscles fibers are innervated in groups called motor units, which activate on

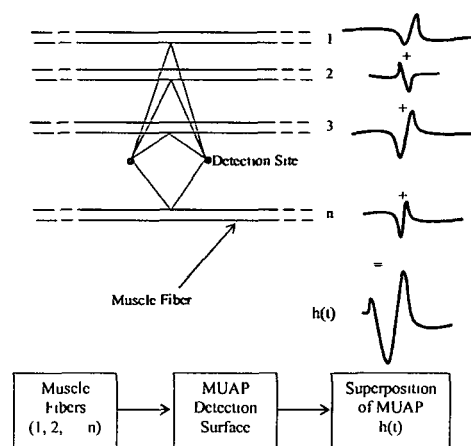


Figure 2.1: Superposition of MUAP to form EMG signals

2.2 Electrical Signals from Muscle - Electromyogram

achieving neural signals from nervous system and generate a motor unit action potential (MUAP). The activation of MUAP from the central nervous system is repeated continuously for as long as the muscle is required to generate force or action. These MUAP from the concurrently active motor units superimpose to form the EMG signal. A schematic representation of the genesis of a MUAP is presented in Figure 2.1.

2.2.2 Characteristics of EMG Signal

EMG signal is stochastic in nature. The amplitude of the EMG signal ranges from 0 to 10 mV and dominant energy is limited to the 0 to 500 Hz frequency range (24). EMG signals are often affected by external and internal sources of noises. The EMG signal acquired from the surface needs to be preprocessed for accurate recording, display and analysis.

2.2.2.1 Noises in EMG Signals

Three main sources from where noise may emanate are:

Inherent noise. The electronic components used in the detection and recording of EMG signals generate electrical noise. This noise has frequency components that range from 0 Hz to several thousand Hz which cannot be eliminated. It can only be reduced by using high quality electronic components, intelligent circuit design and construction techniques.

Ambient noise: This noise originates from sources of electromagnetic radiation, such as radio and television transmission, electrical-power wires, fluorescent lamps etc. The surfaces of our bodies are constantly exposed to electromagnetic radiation and it is impossible to avoid this exposure. The dominant concern for the ambient noise arises from the 50 Hz (or 60 Hz) radiation from power sources.

Motion artifacts: There are two main sources of motion artifact: one from the interfacing layers between the detection surface of the electrode and the skin; the other from movement of the cable connecting the electrode to the amplifier. The electrical signals of both noise sources have most of their energy in the frequency range from 0 to 20 Hz.

2.2 Electrical Signals from Muscle - Electromyogram

2.2.3 EMG signal Acquisition

It is important to use an EMG acquisition unit that provides minimal distortion and highest signal to noise ratio (SNR) (25). A good acquisition of the EMG signal is a prerequisite for good signal processing. EMG signal is easily affected by undesired signal that come from different sources. In addition, for surface electrode instrumentation, complicating issues may arise due to its coupling with skin. Concerns such as impedance of the skin, its superficial oil content and the density of its dead cell layers are to name a few.

2.2.3.1 Requirements of EMG Acquisition

The following characteristics are important for achieving the requirements during EMG acquisition.

Electrode stability: When an electrode is placed on the site of EMG acquisition, the detection surfaces come in contact with the electrolytes in the electrode. A chemical reaction takes place which requires some time to stabilize. This reaction should remain stable during EMG acquisition and should not change if the electrical characteristics of the skin change for sweating or humidity.

Input impedance: The source impedance at the interface of the skin and EMG electrode ranges from several thousand ohms to several megohms for dry skin. To prevent attenuation and distortion of the acquired signal due to the effects of source impedance, the input impedance of the differential amplifier should be as large as possible.

Differential Amplification: In order to eliminate the noise signal, a differential amplification is required. The signal is detected at two sites; electronic circuitry subtracts the two signals and then amplifies the difference. Any signal that is common to both detection sites will be removed and signals that are different at the two sites will be amplified. Signals that originate far away from the detection sites will appear as a common signal, whereas signals in the immediate vicinity of the detection surfaces will be different and consequently will be amplified. Thus, relatively distant noise signals will be removed and relatively local EMG signals will be amplified. The accuracy with

of the functional geometry i.e the anatomical geometry that effects the functionality of the hand (11). Functional geometry can be expressed in terms of static and dynamic constraints. Static constraints involve dimensions, weight and joint range motions. The dynamic constraints involve linear inter-joint angular relationships in human finger (12).

1.2 Objectives

The work presented in this thesis stems from the desire to develop a biomimetic hand with EMG based grasp emulation. Although the use of advanced machine learning and signal processing techniques have proved useful in EMG based prostheses; higher recognition rate of grasp types based on low number of EMG channels is still a challenge. Eventhough multifingered hand prostheses using surface EMG (1), (13) have appeared in the market and advanced research prototypes (2), (14), (15), (16) have been developed; they are far from the human hand in terms of the functional geometry as well as controllability. A recognition architecture for grasp types used during daily living activities (dla) based on low number of EMG channels along with the development of a biomimetic hand emulating the recognized grasps holds promise. The prime objectives in this research include:

- Recognition of six grasp types (shown in Figure 1.2) involved during 70% of dla based on two channel EMG signals - derivation of a low dimensional yet informative and distinguishing feature vector through exploration of time domain, frequency domain and time/ frequency domain feature sets.

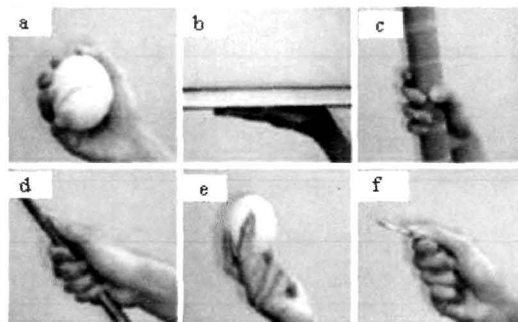


Figure 1.2: Grasp types: a. Power b. Palm-up c. Hook d. Oblique e. Precision and f. Pinch. These six grasp types are significant for they are involved in 70% of dla (17)

conductive medium, they have a higher inherent noise level. Also, these electrodes do not have long term reliability because their dielectric properties are susceptible to change with the presence of perspiration. For these reasons, they have not yet found a significant place in electromyography. Figure 2.2 (b) shows an active surface electrode.

Needle Electrodes: The most common invasive electrode is the needle electrode. The concentric needle electrode is the most common. This monopolar configuration contains one insulated wire in the cannula. The tip of the wire is bare and acts as a detection surface. The bipolar configuration contains a second wire in the cannula and provides a second detection surface. The two main advantages of the needle electrode are:

- It has relatively small pickup area enabling the electrode to detect individual MUAPs during relatively low force contractions.
- The electrodes may be conveniently repositioned within the muscle so that the signal quality may be improved. Figure 2.2 (c) shows a needle electrode.

2.3 EMG Features and Classifiers

2.3.1 EMG Features

Features are the characteristic pattern representation of a signal with reduced dimensionality. The goal of feature extraction is to find a small number of features that are particularly most distinguishing and informative. EMG features are studied in time domain (TD), frequency domain (FD) and time/frequency domain (TFD). TD representation is the representation of the signal characteristics versus time. TD features identifies the attributes of the signal that characterize its temporal structure. The representation of the signal characteristics versus frequency is the FD representation. Frequency spectrum of any signal indicates what frequencies exist in that signal. TFD features provides the information about both temporal and spectral characteristics of the signal. For classification of EMG signals, a variety of features has been considered; each feature individually as well as a number of features (in groups) in TD, FD and TFD (25, 26).

2.3 EMG Features and Classifiers

2.3.1.1 Time Domain Features

TD features based on EMG signal amplitude are the first features considered (27). Their direct extraction without the need for mathematical transformation makes these features the best choice from a computational perspective. Typical TD features are: mean absolute value (MAV) (27, 28), integrated absolute value (IAV) (29), variance (VAR) (28, 30), mean absolute value slope (MAVS) (27), Willison amplitude (WAMP) (30), zero crossing (ZC) (27), slope sign changes (SSC) (31), waveform length (WL) (31) and EMG histogram (32).

Square integral methods were among the first to be introduced for features extraction of the EMG signals in TD. This represents the energy of the signal as temporal characteristics. However the energy in EMG signal is usually not evenly distributed. The variation of energy upon time actually contains the most important attribution for muscles movements. A higher degree of muscle activity usually recruits more motors units and consequently release more MUAP to be detected as EMG.

For instance, a burst of energy in EMG signal produces an intense muscle contraction and fast motion causing the EMG signal to cross a threshold value. This makes the TD features more suitable than FD features for real time control of prosthetic hands for opening and closing operations (33). Moreover the FD features are much more expensive than TD approaches in terms of computational time (34). The RMS of the EMG signal was also used to represent features for EMG classification. Ajiboye and Weir (35) calculated the RMS of each EMG channel using a 64 sample window to determine the signal envelop. Four subjects: two healthy and two amputees was used for real time analysis. EMG pattern belonging to three different classes were successfully discriminated and the overall classification accuracy ranged from 94-99%.

On the other hand, the work done by Shenoy et al. (36) demonstrated the effectiveness of the RMS of the steady state EMG signals in classifying between many classes of the arm movements. Two experiments were done by Shenoy's group. In the first experiment, the group explored the current classification based paradigms for myoelectric control to obtain high accuracy (92-98%) on an eight class off-line classification problem. In the second experiment, an on-line control system for a four degrees of freedom (DoF) robot was implemented giving a classification accuracy of more than 90%. This shows that TD features have capability for real time control of prosthetic

hands with lower DoF. Although pattern recognition using TD features were successful to some extent, however it is argued in literature that pattern recognition results using TD features may not provide high success rate (37).

2.3.1.2 Frequency Domain Features

Frequency domain (FD) features include power spectrum (PS) , mean and median of signal frequencies (FMN , FMD) (38), frequency ratio (FR) (25) etc. A fundamental concept in the study of signals is the notion of the frequency content of a signal, i.e. the contribution of each specific frequency in the signal. The need for the study of the frequency contents of signals emerged due to the fact that the information that can not be readily seen in the TD can be seen in the FD. FD features are more reliable and accurate than TD features (39).

One of the well known techniques for discovering the frequency content of signals is Fourier series for periodic signals and Fourier transform for aperiodic signals. The basic idea behind Fourier analysis in general is to generate the frequency content by decomposition of the original signal into weighted orthogonal components given by sinusoids of specific magnitude and phases. The relative weights of the frequency component composing the signal are considered as a major factor in determining the shape of the signal. The magnitudes of the different frequency components are considered as features when Fourier transform is employed in the feature extraction process (40).

Many experiments exist within the literature in which the authors utilized Fourier transform for feature extraction from the EMG signals. Nishikawa et al. (41) developed a discrimination system using a Neural Network (NN) for EMG control prosthesis. The NN was used in the system to learn the relation between the power spectrum of EMG signal analyzed by fast Fourier transform (FFT) and the movement desired by the amputee. It was shown that the discrimination system with the NN was able to discriminate seven hand movements from the EMG signals with the probability of 61%. In another attempt, Matsumura et al. (42) proposed a system to classify EMG signals into seven categories of movements by employing the FFT for feature extraction with the analysis window length of 256 msec and an increment of 128 msec. The classifier used was a back propagation NN with an average accuracy rate of 71.67%.

Although this approach is still being used in EMG control, but it is noticed that in general the classification results when employing the FFT based features are low. An

example include the work presented by Matsumura et al. (42) in which the authors claimed that they presented an effective approach for EMG classification by using FFT and back propagation NN, while achieving a maximum accuracy of 87.5-89.5% which is still far from optimal. This can be justified by the fact that it is well established in literature that the FFT is a powerful tool to discover the frequency spectrum of a certain class of signals i.e. stationary signals. On the other hand, the FFT is not the optimum tool to be used with non stationary signals such as the EMG as it is unable to localize the observed frequency components in time.

2.3.1.3 Time/ Frequency Domain Features

TD feature of a signal indicates only the temporal characteristics. FD feature indicates the spectral characteristics of the signal. TFD features are localized in both time and frequency domain. Some of the methods used in TFD are short time Fourier transform (STFT) , wavelet transform (WT) and wavelet packet transform (WPT) . In STFT, the EMG signal is mapped into frequency components that present within an interval of time. A suitable window size must be determined as small window will give good time resolution but poor frequency resolution and vice versa. The partitioning ratio of the STFT is fixed once specified, each cell has an identical aspect ratio. Further, STFT analysis does not lead to high recognition rate of hand gestures based on EMG (43). WT gives good frequency resolution and poor time resolution for low frequencies; whereas, poor frequency resolution and good time resolution for high frequencies (44). In EMG signals, high frequency component exist for short duration of time whereas low frequency component exist for longer time (45). Therefore, WT features are better suited for EMG signal analysis. Wavelets forming a continuous wavelet transform (CWT) are subject to the uncertainty principle of Fourier analysis (46). In contrast, discrete wavelet transform (DWT) provides sufficient information for analysis and synthesis of the original signal, with a significant reduction in the computation time (47). WPT is the generalization of the WT method that allows the best adapted analysis of the signal and cause long processing time as compared to WT (48, 49). Table 2.1 summarizes some of the methods used for feature extraction and EMG based on pattern recognition for upper-limb prosthesis control.

2.3 EMG Features and Classifiers

Table 2.1: Typical EMG Recognition for Prosthesis Control

Classifier	Features	EMG Pattern Recognition Rate
Bayes (18)	Zero Variance	91%
Non Linear Discriminant Function (50)	Coefficient of AR Model	99%
Fuzzy System (51)	FFT Results	80-90%
Neural Network (52)	MAV, Zero Crossing	70-90%
Mchalanobis Function (53)	Envelope Amplitude	90%
Fuzzy System (8)	Zero Crossing Absolute Value slope	90%
Linear Discriminant Analysis (49)	Auto/Cross Correlation Short Time Fourier Transform Wavelet Decomposition Wavelet packet Transform	96% 96.5% 97-98% 98%
Neural Network (54)	Harmonic Wavelet Packet Transform	95%

However, the percentage obtained by each study is subjective. It depends upon the number of control channels used and the number of movements to be recognized. Englehart et al. (48, 49) investigated four channel sEMG signal in classifying four types of upper limb motion by using the TFD method. In comparison with Hudgins et al. (27) that used two sEMG channel in discriminating four types of upper limb motion, a lower classification rate was obtained. Even though Ajiboye and Weir (35) also used four surface EMG channels in their study but they have a lower classification accuracy compared to the work of Englehart et al. (48, 49). This is possibly due to the feature used to extract the information from the EMG signal that might be not accurate enough in giving the best information.

2.3.2 EMG Classifiers

For controlling a prosthetic hand with EMG signals, the user must produce different muscle activities that will be identified by a system and then translated into commands. In most of the cases, this identification is accomplished through a classification algo-

rithm i. e. a classifier that estimates the class of data as represented by a feature vector representing the original signal in reduced dimensionality. Several classification algorithms were employed for recognition of EMG signals (8, 20, 25, 55, 56). This section review the most popular classification algorithms for EMG recognition and their important properties are highlighted.

Several pattern recognition algorithms have been used over the past decades to correctly classify desired limb motions (8, 20, 25, 55, 56). Lee and Saridis (57) had constructed a proof of concept on EMG signal pattern recognition system for real-time control of a prosthetic arm. Early approaches in this area involved simple single channel signal identification and included work by Graupe (58) for EMG classification using an autoregressive model with reasonable success. Park and Lee (28) presented a fuzzy based decision making system to classify six distinct motions: elbow flexion and extension, wrist pronation and supination and in and out humeral rotation for six subjects. Englerhart et al. (48) compared FD and TD methods to preprocess EMG signals and introduced WPT with satisfactory results. Englerhart et al. (49) applied combination of wavelet packet and principal component analysis (PCA) to extract suitable features from myoelectric signals to classify six classes of hand motions. Identification of limb motion based on EMG signals have been attempted through various methods including multilayer NN (49), self-organized maps (59) and fuzzy logic (FL) (20).

2.3.2.1 Linear Discriminant Analysis (LDA)

The aim of LDA (also known as Fisher's LDA) is to find the hyper-planes that separate the data representing different classes (60, 61). LDA assumes normal distribution of the data with equal covariance matrices. The separating hyper-plane is obtained by seeking the projection that maximizes the distance between the means of the classes and minimizes the inter-class variance. LDA classification rule is to assign an object to the group with highest conditional probability (i. e. Bayes's rule) (18). LDA classifier is derived as the minimum error classifier for normally distributed classes with equal covariance matrices. Assuming each group belonging to a certain class has multivariate normal distribution and all groups have the same covariance matrix, one get what is

called a linear discriminant analysis formula that is given by:

$$g_i(x) = \log[P(w_i)] - \frac{1}{2} \mu_i \sum^{-1} \mu_i + \mu_i^T \sum^{-1} x = w_{i0} + w_i^T x$$

where g_i represent a set of linear functions, $g_i, i = 1, 2, \dots, c$ for a c class problem, $P(w_i)$ is the probability of class, w_i, μ_i is the mean of class i and \sum represent its covariance matrix. Assuming all class covariance matrices are the same i. e. $\sum = \sum_i$. $w_{i0} \dots$ and $w_i \dots$ are the coefficient of the linear discriminant function g_i .

LDA is one of the simplest linear classifier. However, it is optimum only for data normal distribution with equal covariance matrices. In some application, the assumption of equal covariance is reasonable because the properties of the noise do not change very much from one signal to another. However in complex non-linear pattern recognition, the assumption of equal covariance is not true. Although these are not optimum, the simplicity and robustness of the linear classifier compensate for the loss in performance in many cases (62).

2.3.2.2 Support Vector Machine (SVM)

The SVM is a relatively new classification technique developed by Vapnik (63). SVM belong to the family of kernel based classifiers. It has shown better performance in a number of real world problems (64). SVM implicitly map the data into the feature space where a decision boundary separates the classes that may exist (65). If data is

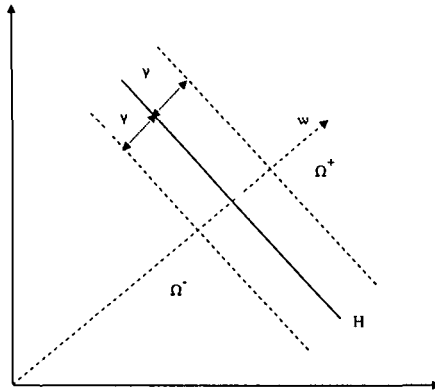


Figure 2.3: SVM Classifier with hyperplane H and margin of width 2γ

linear, a linear kernel separating hyper plane may be used to classify the data and is

known as linear SVM. Figure 2.3 illustrates this. The chosen hyperplane H separates the two regions Ω_+ and Ω_- , representing the two classes of points respectively. The dotted lines indicate the margin. Now let w be the normal to the hyperplane H . The classifier labels a data point x as $+1$ or -1 , based on whether $(w \cdot x + b)$ is greater than 1 or less than -1 . b is the bias term chosen to maximize the margin of the decision boundary γ while still classifying the data points correctly.

For the classification of non-linear and high transitional data, the formulation of linear hyper plane is extended to build non-linear SVM kernel. Non-linear kernel transforms the input data into feature space of higher dimensions. In this high dimensional space, data can be linearly separable by applying linear SVM formulation (66). It implicitly maps the data to another space, generally of much higher dimensionality, using a kernel function. It tries to find the optimal decision boundary by maximizing the margin between the boundaries of different classes controlled through a regularization constant c .

Grid search

During classification through SVM, there are two parameters: c and γ . The goal is to identify good c and γ so that the classifier can accurately classify the testing data. The standard method of exploring the value of c and γ on the two dimensional space is via grid-search; wherein the grid points are generally chosen on a logarithmic scale and classifier accuracy is estimated for each point on the grid. There is a range of parameter values that yield optimal classifier performance; furthermore, these equivalent points in parameter space fall along a ridge in parameter space.

The grid-search is straightforward but seems naive. In fact, there are several advanced methods which can save computational cost, for example, approximating the cross-validation rate. However, there are two motivations why I prefer the simple grid-search approach. One is that, psychologically, it may not be safe to use methods which avoid doing an exhaustive parameter search by approximations or heuristics. The other reason is that the computational time required to find good parameters by grid search is not much more than that by advanced methods since there are only two parameters. Furthermore, the grid-search can be easily parallelized because each c and γ is independent. Many of advanced methods are iterative processes, e.g. walking along a path, which can be hard to parallelize.

2.3.2.3 Artificial Neural Networks (ANN)

An ANN is an information processing paradigm inspired by the way of biological nervous systems. It is comprised of parallel arrays of non-linear interconnected processing elements called neurons. An ANN is configured for a specific application like pattern recognition through a learning process. An ANN learns as people learns by examples. Learning in biological systems involves adjustments to the synaptic connection that exist between the biological neurons. This is true for ANN as well (67). Multilayer perceptron neural network (MLP) trained with back propagation algorithm is the most well known paradigm of ANN employed in the classification of EMG signals (68). It is suitable structures for non-linearly separable input data. In an MLP model, the neurons are organized in the form of layers. Neurons in a layer get input from the previous layer and feed their output to the next layer. In this type of networks, connections to the neurons in the same or previous layers are not permitted. The back propagation training algorithm is an interactive gradient algorithm design to minimize the mean square error between the actual output of a MLP and the desired output (69) done by modifying the connection weights between the layers.

The MLP is one of the first classifiers that proved effective for EMG based control (70). The MLP structure is usually determined by trial and error, as the most appropriate number of hidden layers and the number of neurons per layer vary from problem to problem. Englehart et al. (48) proved that despite the fact that the MLP enjoys an advantage over LDA of being capable of prescribing non-linear class boundaries, but the LDA performance was shown to out performs that of MLP when dealing with EMG features (38).

2.3.2.4 Fuzzy Logic (FL)

In recent years, FL proved to bring new possibilities in the biomedical signal analysis problems. Several studies were found in the literature on the application of FL based algorithm for EMG based control (71), most of which reported to achieved much better results than those achieved by conventional methods (50, 72). Fuzzy clustering methods like the fuzzy c-means algorithm (8) and the ISO-FUZ (51) methods were utilized in different ways in EMG recognition problems as classifiers and in both cases they achieved good accuracies, depending on the complexity of the problem. The work

done by Chen et al (71) came with better result than that achieved by Hudgins et al. (27) while using fuzzy clustering techniques on the same data set. The Fuzzy c-means clustering was also utilized with features extracted by the WT and projected with independent component analysis reporting a promising performance (73). But application of FL for EMG based control has some limitations like: the output in FL is not binary, it classifies data points from the continuous variable domain; it is quite arbitrary to determine a number of fuzzy sets, relationship among different rules that should be done a-priori is unclear as well as the design and computing algorithm can be hard to follow (74).

2.3.2.5 k Nearest Neighbour Classifier (kNN)

The kNN classifier is a quite trivial, where it simply memorizes the training data. All the work is done by the classifier at run-time. Given a new instance, x to be classified, the classifier finds the k-training examples that are most similar to x , and looks at their labels. Whichever labels occurs most frequently among the k nearest neighbours; is chosen as the predicted label for x . Loote et al (75) reported that kNN algorithms are not very popular in the EMG classification problem probably because they are known to be very sensitive to the curse of dimensionality, which made them fail in several EMG classification experiments (76).

Another two important aspects related to the classification of EMG signals along with the feature sets and classification algorithms are dimensionality reduction of features and cross validation of the classification results

Dimensionality Reduction of Features

The dimensionality reduction of feature sets as well as deriving a feature vector with uncorrelated feature components is often necessary for increasing classification performance. This process should preserve as much of the relevant information as possible while reducing the number of dimensions. The two main strategies of dimensionality reduction are feature selection and feature projection.

Feature Projection. This method, instead of searching the best subset of features (v), tries to determine the best combination of the original features (V) to form a new

feature set (Z), generally smaller than the original one. Moreover, if the map $f: V \rightarrow Z$ is linear, finding the coefficients of this projection could be quite a fast and simple process. PCA or Singular Value Decomposition provides a linear map from the original set of variables into a reduced-dimensional set of uncorrelated variables (the principal components); minimizing the mean-square error between the original feature set and the projected one. The transformed variables are ranked according to their variance, thereby reflecting a decreasing effectiveness in representing the original set of variables.

Feature Selection: In this case, the best subset $z \in Z \subseteq \mathbb{R}^L$ of the original feature set $v \in V \subseteq \mathbb{R}^M$ is chosen according to some criteria for judging whether one subset is better than another. The ideal criterion for classification should be the minimization of the probability of misclassification, but generally simpler criteria based on the ability to distinguish classes are chosen. In general, feature selection methods use class membership to determine discriminant power. As the original identity of the features is maintained, the utility of each individual feature is known.

Cross-validation

Cross-validation is a statistical method of evaluating and comparing learning algorithms by dividing data into two segments: one used to learn or train a model and the other used to test the model. In typical cross-validation, the training and testing sets must cross-over in successive rounds such that each data point has a chance of being tested. The basic form of cross-validation is k-fold cross-validation. In k-fold cross-validation, the data is first partitioned into k equally or nearly equally sized folds. Subsequently k iterations of training and testing are performed such that within each iteration a different fold of the data is held-out for testing while the remaining k-1 folds are used for learning. Kohavi (77) compared several approaches to estimate accuracy: cross-validation (including regular cross-validation, leave-one-out cross-validation, stratified cross-validation) and bootstrap (sample with replacement), and recommended 10-fold cross-validation as the best model selection method, as it tends to provide less biased estimation of the accuracy. In 10-fold cross validation, data are divided into ten subsets. Nine out of ten subsets are used for training and the remaining one subset is used for testing. This procedure is then repeated for ten times, using a different subsets for testing in each case. The ten test performances obtained

are averaged and the average test performance is declared as the estimate of the true generalized performance of the classifier.

2.4 EMG based Grasp Classification

2.4.1 State of Art

Even though a number of classification and pattern recognition techniques of EMG signals for hand gestures (55, 56) and robotic control (8) has been reported, discriminating grasping operations is still an open problem. Elliott (78) appear to be the first to work on classification of grasp types based on EMG signals. This work proposed four feature extraction techniques: Envelope Maxima, Legendre Polynomials, Haar wavelets, EMG histogram for classification of six grasp types: small cylinder, large cylinder, small sphere, large sphere, small disk and key grasps. Among these, EMG histogram based feature extraction produced maximum classification rate of 81%. The reported results were based on four channel EMG signals and are subject dependent. Ferguson and Dunlop (43) are among the pioneer to report the classification of grasp types based on EMG signals. They have developed a system for identification of grasp types based on muscle movements. Four electrodes were placed on extensor muscles of the forearm. Four grasp types: cylindrical, spherical, pinch and key were under study. The feature set and the classifiers vary from subject to subject. Features used include FFT, Autoregressive modelling, wavelet decomposition, deconvolution analyses followed by the classifier based on neural network and Mahalanobis classifier. Mean value of the success rates was around 75-80%. Martelloni et al. (79) have performed the classification of three grasp types: cylindrical, spherical and key grasps based EMG signals. The classification was using MAV of EMG signals through SVM. The reported result was for a limited group of subjects; only three with a recognition rate of 84-93% based on eight EMG channels.

More recently, Castellini et al. (22) have reported classification of only *three* distinct types of grasps. index precision grasp, other fingers precision grasp and power grasp based on *ten* surface electrodes with a recognition rate of 90%. Castellini et al. (80) has shown the classification of two grasp types. precision and power based on seven channel EMG signals. The classification was using TD features through SVM. The results reports classification of the grasp types with cross-subject analysis. The experimental

results showed a classification of 97% in the baseline condition i.e. while the subject would keep her/his arm still and relaxed on a table and was asked to grasp and 95% in the dfa condition. More recently, Liarokapis et al. (81) have reported the classification of three grasp types used during dfa based on 16-number of EMG channels. Six classifier performances are evaluated and Liarokapis et al. (81) reported highest recognition rate of 99% for Random Forest classifier.

2.4.2 Limitations

From the review on recognition of grasp types based on EMG signals, it can be seen that the results reported by the Elliott (78) et al. is limited to a recognition rate of 81% only. Further, both Ferguson's and Martelloni's results are subject dependent as well as the recognition rates are low. Both of their experiments involve higher number of EMG channels for lower number of grasp types recognition. Although recent results by Castellini et al. (22) and Liarokapis et al. (81) have shown higher recognition rates, their results are limited to a fewer number of grasp types. Castellini et al. results are based on ten number of EMG channels and that of Liarokapis et al. on 16-number of EMG channels; which are significantly higher.

2.4.3 Focus of our Work

It has been seen that a serious effort for classification of grasp types based on EMG signals have been done by the researchers for last two decades. Grasp recognition is an important step for anthropomorphic movement control of extreme upper limb prosthesis. Furthermore, the goal should be towards higher recognition rate based on lower EMG channel for more number of grasp types used during dfa. Therefore, an EMG based grasps classification architecture based on lower number of EMG channels with higher recognition rates holds promise. In this line, this research concentrated on the derivation of a low dimensional yet informative and distinguishing feature set for classification of six grasp types used during 70% of dfa based on two channels EMG signals.

2.5 Review of Prosthetic Hands

This section reviews the current status of the prosthetic hand development covering their function, mechanical structure and control mechanisms. A brief history and commercially available prosthetic hands are also included in this chapter. An introductory explanation of the human hand and physiology is also included.

2.5.1 Human Hand

The human hand is a complex anatomical structure consisting of bones, muscles, tendons, skin and the complex relationships between them. It consists of five digits: four fingers and one thumb. Each finger constitutes of three interlinking segments: proximal, intermediate and distal phalanges. Thumb is made up of only the proximal and distal phalanges. The first phalanx is connected to the metacarpal bone. The metacarpal bones constitute the palm and are connected to the carpal bones. Movements of carpal bones allow the hand to rotate with respect to the arm. The joints on the finger are named: distal interphalangeal (DIP), proximal interphalangeal (PIP), metacarpophalangeal (MCP) joints. Figure 2.4 shows the bones and joints of the hand.

Each joint is characterized by the geometry of the contacting surfaces and by a joint range of movement (RoM) as illustrated in Table 2.2.

Table 2.2: Finger joint range of motion of human hand (in degrees) (83)

	Thumb	Index	Middle	Ring	Little
MCP (Abduction / Adduction)	0 to 90	-30 to 30	-20 to 20	-30 to 30	-30 to 30
MCP Flexion	0 to 100	-30 to 90	-30 to 90	-30 to 90	-30 to 90
PIP Flexion		0 to 110	0 to 110	0 to 110	0 to 110
DIP Flexion	0 to 90	0 to 70	0 to 70	0 to 70	0 to 70

Each finger can move in the frontal plane to go closer to the medial axis (adduction); can move far from the medial axis (abduction); can flex and extend in sagittal plane (plane at right angles to the frontal plane) at each of the joints. Each digit (except the thumb) has three flexion/extension and one abduction/adduction DoF. Thumb is able to move in opposition with other fingers along with abduction and adduction. Thumb

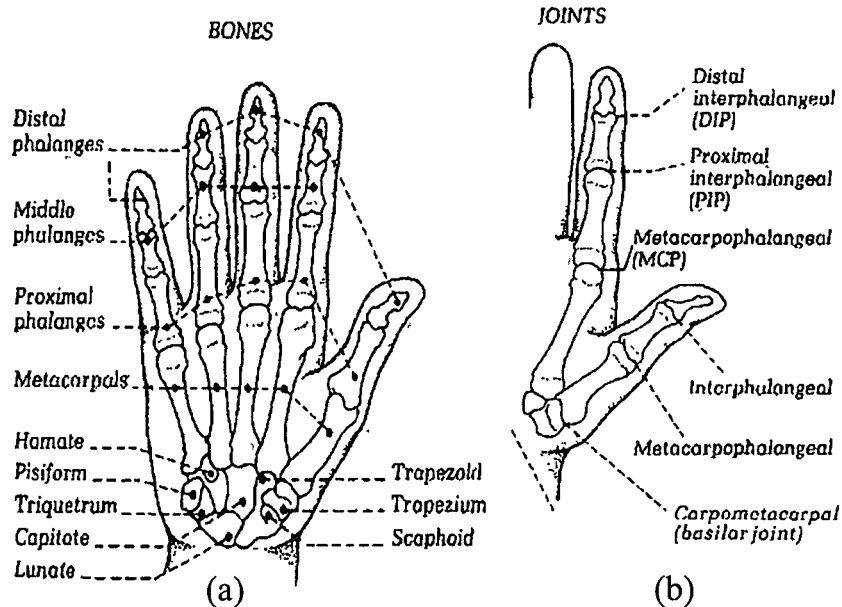


Figure 2.4: (a) Bones and (b) Joints of Human Hand (Figure is adapted from (82))

is missing one joint therefore have two flexion/extension DoF. This makes a total of $(4 \times 4 + 3) = 19$ DoF excluding the wrist. The wrist has three rotational DoF, hence the human hand have 22 DoF in total. These fingers and DoFs are selectively used during different grasping operations. The forearm muscles are connected to the bones via the tendons which act as transmission media for actuation of the fingers (84). Figure 2.5 shows the muscles on extrem upper limb of the human hand.

According to the grasp to be formed, the neuromuscular signals generates the EMG signals for actuation of the muscles. These EMG signals carries the information about the grasp type to be performed by the amputees and can be used to identify it. Using the EMG signals to direct the prototype for emulating the attempted grasp gives a natural feeling of control.

The constraints of the human hand are categorized as static and dynamic constraints. Static constraints includes dimensions of the hand, finger phalanges and palm, finger joint RoM and DoF. The linear inter-joint angular relationships in human finger are expressed as dynamic constraints and results in a natural curling motion of the fingers (12). These are defined as follows:

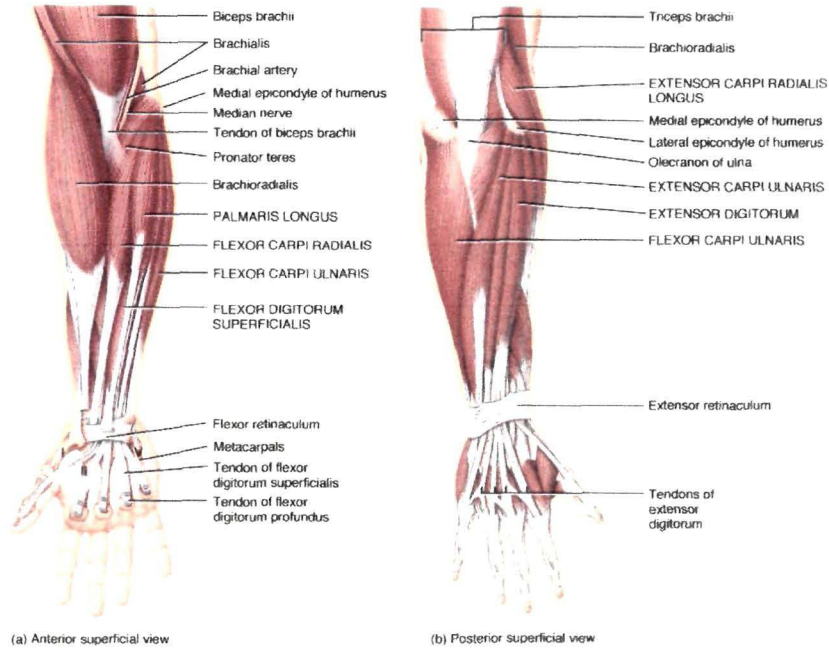


Figure 2.5: Muscles on Extreme Upper Limb (Figure is adapted from (82))

$$PIP = 2 \times MCP \quad (2.1)$$

$$PIP = 1.5 \times DIP \quad (2.2)$$

2.5.1.1 Human Hand Grasping

Type of grasp is the interface between a person's hand and the object being handled. For activities such as lifting, lowering, carrying, pushing and pulling etc., different type of grasp is required. Different studies have reported a number of basic grasp types. Studies on the number of possible grasps have resulted in different categorizations based on different parameters such as:

- Grasp appearance (85)
- Contact area involved (86)
- Functions (87)

Taylor and Schwartz (85) have defined six grasp types: Cylindrical, fingertip, hook, palm up, spherical and lateral based on the shape of the grasps. According to Napier (86), grasps are classified as power and precision. When people use objects in everyday tasks, the choice of grasp is dictated less by the size and shape of the objects than by the task they want to accomplish. Even during the course of a single task with a single object, the hand adopts different grasp types. An extensive list of grasp types based on the functions to be performed during dfa is available in (87). This allows one to understand the relationship between the task requirements and the grasping solutions adopted to meet those requirements. Heumer et al. (88) identified six different grasp types, whereas Fiex et al. (89) has a classification that identifies seventeen grasp types.

In this thesis, six grasp types: power, palm-up, hook, oblique, precision and pinch as shown in Figure 1.2 were considered. Power grasp involves having larger contact area between the palm and the fingers of the hand with the grasped objects. Power grasp is mostly used in situations where an object needs to be grasped with stability. Holding an object like a book or a plate on the palm without curling the fingers forms a palm-up grasp. This grasp is mostly used during lifting or pushing an object. Hook grasp involves holding the objects within the hollow formed by the thumb, palm and the other fingers. The oblique grasp differs from the hook in the sense that the thumb supports the object in lateral to the other fingers instead of in opposition in the case of hook grasp. Holding an object with the thumb, index and middle finger having contact of the object with the distal and middle phalanges forms the precision grasps. Grasp like holding a pen or pencil with the fingertip of the index, middle and thumb leads to the formation of the pinch grasp. The power, palm-up, oblique and hook are concentrated more towards the stability during the grasping while the pinch and precision focus more on the sensitivity and dexterity. These six grasp types are significant for they are involved in 70% of dfa (17). These grasp types has been explored for classification using surface EMG and the Prototype 1.0 is developed to execute the above grasps.

2.5.2 Prosthetic Hands: State of Art

Prosthetic hands are designed to provide a replacement for upper limb amputees and are mainly categorized as passive and functional types. A passive prosthesis is a cosmetic type where it just provides visual replacement of the amputation, while the functional

prostheses are used to mimic the function of a natural hand. The functional type can be divided into two categories: body powered and externally powered.

2.5.2.1 Brief History of Prosthetic Hands

Prosthetic hands have been found centuries ago with the main aim to provide the amputees with a replacement of their natural arm. It had been found as early as 330 BC on an Egyptian mummy; which was a cosmetic hand prosthesis (90). In the 15th century, passive hand prostheses were developed and used for several decades. Passive prosthetic hands involve a moveable thumb only or by using knob activation to lock the thumb and fingers configuration to select the chosen position (90).

The beginning of 19th century showed the start of actively operated prostheses. These prostheses are called body powered; where a harness is tied to the shoulder and connected to device via a cable. When the user moves the shoulder, the cable is tightened and cause the device to open and close. Count of Beaufort from France had designed a body powered prosthesis back in 1860 where the hand was made of wood and the moveable thumb was controlled by a cable connected to a shoulder girdle (90).

World War I had caused a large number of amputees. The development and use of the body powered prostheses were boosted during this time. Plastic materials were introduced into prosthetics after the World War II and further development on the body powered prostheses continued with gradual growth.

External powered prostheses were introduced at the end of 19th century and can be divided two types: pneumatically and electrically powered. Pneumatically powered used carbon dioxide to power up the prostheses while electrically powered used rechargeable batteries. However, the pneumatically powered device was not practical as it was noisy and more difficult to operate. Later, EMG based prostheses had been introduced where an electrical signals is generated with the muscle contraction to control the prosthetic device. When a skeletal muscles contracts, small voltages can be detected on the skin surface which are amplified and conditioned to operate an electrically powered prosthesis. It has been reported that the EMG controlled prosthetic hand was first proposed and built by Reiter in 1948. By end 70's, the EMG controlled prosthetic hands became popular in the area of rehabilitation robotics (90).

2.5.2.2 Commercially Available Prosthetic Hands

i-Limb: The prosthetic hand i-Limb by Touch Bionics is a five fingered hand. All fingers are identical and consists of two phalanxes: the proximal and intermediate one; the distal phalanx is actually fused in a fixed position with the intermediate phalanx. *The thumb is identical to the other fingers and is fixed on a passive joint that allows to move it in opposition to other fingers.* Each finger is actuated by an independent direct current (DC) motor placed in the palm. Motion is transmitted to the finger by means of a rigid transmission based on a toothed belt. The hand is meant to be used by mono lateral amputees in order to perform a grasp. The subject should use healthy hand to rotate the thumb and send an EMG closing command. At this point all fingers start to move towards the palm and independently stop until a force level is reached. The hand can perform pinch, power and lateral grasps (1). Figure 2.6 shows the i-Limb.

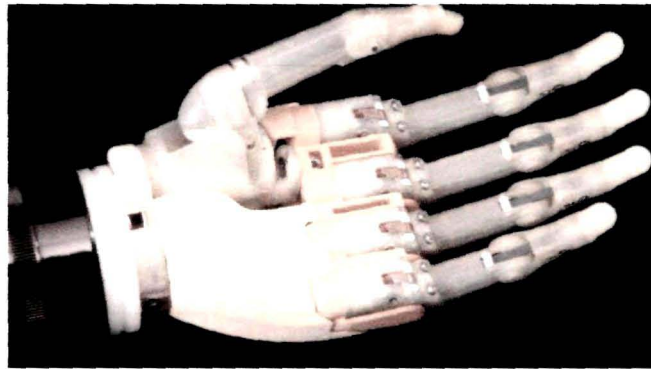


Figure 2.6: The i-Limb Hand (From (1)).

This hand is the first to market prosthetic device with five individually powered digits. The finger kinematics is fixed; the dynamic relationship between MCP and PIP joint angle, while the finger is moving is fixed. The independent actuation, results in a short of compliant grasp since each finger effectively flex when the object has been gripped and high number of contact points between hand and object is present. The hand is covered by a soft cosmetic glove, that mimics the natural skin and improved compliance.

There is no scientific literature or available information regarding the sensory system of the hand, from the analysis of the mechanical design (where no structurally integrated

sensors are placed in the fingers), and from viewing the available material from the company website, it is reasonable to think that only sensors available, are related to the DC motors and could be both encoders and current sensors. The desired finger speed is controlled through instantaneous EMG signal amplitude of the muscle employed for closing. In this manner, all fingers close until there is muscle activity but those fingers that get in contact with the object before the others, inevitably start gripping until their motor current becomes higher than the limit value. In the second case, the desired torque proportional to the DC motor current is proportional to the EMG signal amplitude, the fingers move with fixed velocity and stop when the torque value is reached.

Even though EMG controlled prosthetic devices have gained increasingly importance, the search for something better has continued to achieve human like functionality and controllability.

2.5.2.3 Research Prototypes of Prosthetic Hands

MANUS Hand: Among the research prototypes, MANUS hand was developed with enhanced mobility so that the basic grasping modes i.e. hook, precision, cylindrical, power, tip and lateral grasp of human hand could be reached. MANUS hand possesses three DoF. The other joints are coupled to the driven ones by underactuated mechanisms. It possess five fingers and the resulting prototype is approximately 20% larger than an average human hand. It weights around 1200 gram; which is more than twice than that of a human hand. It could achieved a maximum grasping force of 60 Newton (N) was obtained at the fingertip (2).

MANUS Hand proposes a prosthesis having 10 joints of which three are independently driven and others are coupled to the driven ones through different types of mechanisms. Three independent mechanisms can be found in the MANUS Hand prototype:

- The index/ middle mechanism coupling six DoFs
- The thumb mechanism coupling three DoFs
- The wrist mechanism

In addition to the active joints, bendable joints have been included in the fourth and fifth fingers, using a martensitic structure so they can be placed manually in a position

and assist the index and middle fingers. The index and middle fingers are actuated by means of one single brush-less DC motor and the MCP joints of the two fingers are linked. Figure 2.7 shows the Manus hand. The force and position sensors are distributed

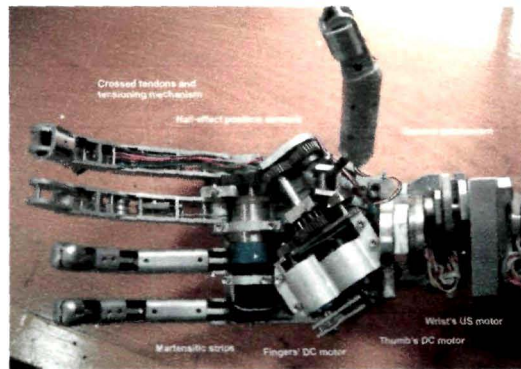


Figure 2.7: The Manus Hand (From (2)).

in the hand. Both kinds of sensors were specifically designed from Hall effect pick-ups. Position sensors were developed by placing a permanent magnet opposite to the Hall effect sensor. In between, a cam made of ferromagnetic steel modifies the reluctance of the magnetic circuit resulting in a linear relation between cam rotation and output voltage. The force sensors are embedded in the finger tips and are also based on Hall effect pick-ups. In this case, the permanent magnet is spring mounted and the resulting magnetic field at the Hall effect sensor location results in a linear relationship between force exerted and output voltage.

The control architecture of MANUS Hand comprises a host microcontroller (master) and three local microcontrollers (slaves). Each local controller is in charge of the active compliance control of each active joint. The host controller is also in charge of the EMG command decoding. The digit specific control scheme is through an impedance control that allow the fingers to behave as virtual springs. For every grasping mode, the finger performance is determined by a set of desired positions and finger stiffness.

Southampton Hand: It is a five fingered hand, actuated through six electrical motors. Two of them are used to actuate the flexion/ extension and rotation of the thumb while the remaining four motors are assigned to individual finger flexion/ extension.

Each finger is made from six bar linkages, which when flexed or extended, curl in an anthropomorphic trajectory. It possesses six DoF with with 14 joints in it. The hand weights around 520 gram including the actuation system which is close to that of a human hand. The grasping force at the end of each fingertip is 9 N. Figure 2.8 shows the Southampton hand.

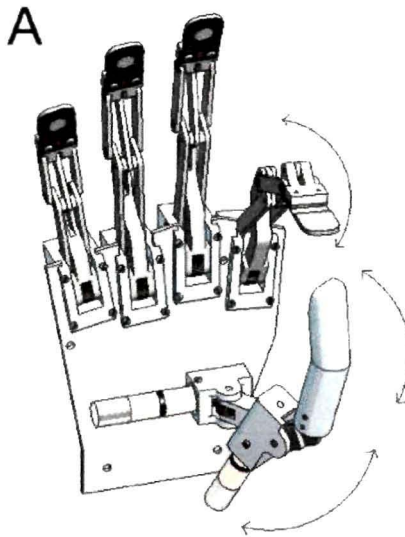


Figure 2.8: The Southampton Hand (From (3)).

Each finger is equipped with an array of film sensors which can be used to monitor the force exerted by the finger as well as to detect the onset of object slip and measure temperature. These are located on a cantilever type structure placed on the distal phalanx of each finger. The array consist of three different types of sensor included upon the fingertip cantilever: static force sensors, dynamic force sensors and temperature sensors.

Southampton hand is controlled through sEMG signals in the conventional two site manner while a microprocessor and sensor system provide feedback for the prosthesis to self regulate prehensile movement and grip force. It is the hierarchical control philosophy, the Southampton Adaptive Manipulation Scheme (SAMS) that co-ordinates the different DoF to achieve a stable grip. It attempts to minimize the contact force between the hand and object by maximizing the contact between them. The controller

achieves this by selecting between the different possible grips by detecting the object with sensors on the surface of the fingers and then adopting the most appropriate posture and applying the lightest possible touch. If the object slips, this is detected and the hand automatically increases the grip force until the sliding stops. Consequently the operator only needs to make the strategic decisions and the rest of the control is devolved to the microprocessor (3).

DLR Hand - II: In 1997, DLR developed one of the first articulated hands with completely integrated actuators and electronics (91). Due to the maintenance problems with *Hand-I* and in order to reduce weight and production cost, the fingers and base joints of *Hand-II* were realized as an open skeleton structure. The open structure is covered by four semi-shells and fingertip housing realized in stereolithography and vacuum mold. This enables to test the influence of different shapes of the outer surfaces on the grasping tasks without redesigning finger parts. Figure 2.9 shows the DLR-II hand.

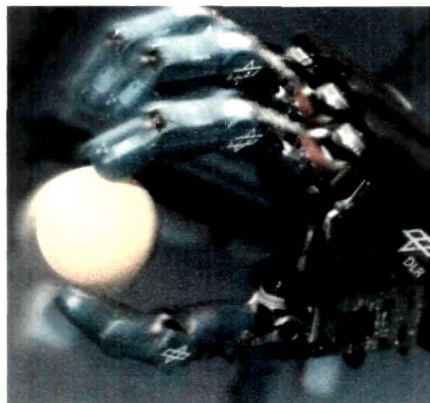


Figure 2.9: The DLR-II Hand (From (3)).

The three independent joints of each finger are equipped with appropriate actuators. The actuation systems essentially consist of brushless DC motors, tooth belts, harmonic drive gears and bevel gears in the base zone. The configuration differs between the different joints. The base joint with its 2 DoF is of differential bevel gear type, the harmonic drive gears for geometric reasons being directly coupled to the motors. The

differential type of joint allows to use the full power of the two actuators for flexion or extension. Since this is the motion where most of the available torque has to be applied, it allows to use the torque of both actuators jointly for most of the time. The actuation system in the medial joint is designed to meet the conditions in the base joints when the finger is in stretched position and can apply a force of upto 10 Newton on the fingertip.

Each joint in the hand is equipped with strain gauge base joint torque sensors and specially designed potentiometers based on conductive plastics. Besides the torque sensors in each joint, each fingertip is equipped with six dimensional force torque sensors. Salisbury (92) implemented cartesian stiffness control by using fingertip force sensors. The stiffness control scheme has the disadvantage of not being able to actively control the complete system dynamics, specifically the system damping parameter. When the hand performs any fine manipulation, there is always need that the fingertip should be soft in the direction normal to the contact surface and hard tangential to the contact surface. Therefore the impedance should be adaptable to the orientation of the fingertip. Therefore a cartesian impedance controller has been build. In steady state, all measured and desired velocity and acceleration values are zero. This induces that the value of the steady state torque is stiffness multiplied by the steady state deformation and the fingertip behaves like a programmable spring.

RTR-II Hand: In 2002, the Scuola Superiore Sant' Anna, Italy has been working in this field for almost two decades firstly providing the MARCUS hand (93) and then proposed a novel three articulated fingered, under-actuated prosthetic hand named RTR-II (4). The hand has been developed with the aim of replicating the natural fingers movement, and allowing different prehensile patterns: precision, power and lateral grasp. The hand has three fingers: middle, index and the thumb. Since the under-actuated mechanisms based on Soft gripper proposed by S. Hirose (94), have been applied to both fingers and thumb, these are able to automatically wrap around the objects. Figure 2.10 shows the RTR-II hand.

Two DC motors, located in the carbon fibre palm structure, actuate the 9 DoFs hand: one motor is applied for the thumb opposition movement, the other for the contemporary flexion of all fingers. The index and middle fingers are connected to the motors by means of an adaptive grasp mechanism based on a linear slider and



Figure 2.10: The RTR-II Hand (From (4)).

two compression springs, the slider is connected to the motor through a lead/ screw transmission. In order to reduce the number of actuators and to perform an adaptive grasp between the fingers, a differential grasp system based on compression springs and a linear slider has been designed.

The RTR II is provided with position sensors for the thumb opposition and the flexion/ extension slider. A cable tension sensor on the cable that drives the index finger and a force sensor on the tip of the thumb were used. Both the slider position sensor and the thumb position sensor are based on Hall effect sensor. The Hand is provided with a hierarchical control architecture composed of a top level control module (TCM), a low level control module (LCM) and a sensory processing module (SPM). Core of the system is the LCM that deals both with sensory triggers detected by the SPM and with high level commands generated by the TCM based on user intentions.

2.5.2.4 Limitations

Although the prosthetic hands discussed above are closer to the natural counterpart in terms of geometry, they deviate from the human hand in terms of dynamic constraints, joint range of motion, number of joints, number of fingers, weight etc. A detailed comparison of all the static and dynamic constraints are presented in Chapter 6. Further, the control through EMG signals is non-intuitive.

The MANUS Hand is controlled via EMG signals from of the residual muscle of

the user. In this technique, signal muscle EMG signal is used to generate the grasping commands. In order to do this, a command language comprising of three bits has been developed based on the EMG signal amplitude. Each bit has defined three bit levels. Accordingly, an input comprise of three muscle contraction to generate three EMG levels and 27 commands. However no information relevant to the pattern recognition has been published authors (95). The opening and closing of the Southampton Hand is being controlled through two site switch mechanism activated by EMG signals. No EMG based control was available originally for the DLR Hand-II. The control of the hand and the fingers was done through an external computer. Later, Castellini et al. (80) proposed seven channel EMG based control for the Hand. Following the proposed method, DLR Hand-II can perform precision and power grasps. The RTR-II Hand can perform grasping task limited to only opening and closing by means of EMG signals generated by two antagonist muscles of forearm.

Therefore, the development of a biomimetic hand replicating the human hand in form and function is of importance so that the user can feel it as if it were a natural part of the body. Furthermore, it requires a more intuitive control method through proper pattern recognition.

2.5.2.5 Focus of our Work

The work presented in this thesis focus on the development of a prosthetic hand prototype following a biomimetic approach. The aim is to harmonize both physical and functional aspects to mimic the human hand satisfying the static and dynamic constraints. The prototype is to be controlled more intuitively for performing six grasp types used during 70% of dla. The control is through recognition of six grasp types based on two channel EMG signals. The emphasis is on following the human finger joint trajectories by the prototype finger joints during the emulation of six grasp types.

2.6 Summary

In this chapter, a background on the basic concepts related to EMG and its acquisition is discussed. The chapter reviews the TD, FD and TFD features for recognition of EMG patterns. The limitations exhibited by the features in different domains were also mentioned. The pattern recognition algorithms contributing towards EMG pattern

2.6 Summary

recognition and their shortcomings were also reviewed. This review emphasizes that the recognition of grasp types to be emulated by a prosthetic hand holds promise. Towards the end of the chapter, current prosthetic hands; both commercial variants and research prototypes were discussed. The focus of the thesis in order to minimize the gaps between the state of art and a prosthesis to be used during dla is mentioned.

3

EMG based Grasps Recognition: Initial Results

Upper limb prosthesis and their control interfaces have changed in the past four decades. Most of the prosthesis developed earlier would be inappropriate due to their non-anthropomorphic actuation. EMG implies the interpretation of the brain's activity to contract a muscle or a group of muscles; and extreme upper limb amputees can generate EMG from residual forearm muscles similar to the healthy subject (8). Grasp recognition based on EMG signals holds promise.

This chapter presents three grasp recognition architectures based on EMG signals. It starts with the materials and methods for acquisition of EMG signals generated during grasping operations. Six grasp types used during 70% of dfa (as detailed in Chapter 1) have been investigated. Higher grasp recognition rate based on lower number of EMG channels for higher number of grasp types is a challenge; further, major difficulties (are detailed in section 2.2.3) are attenuation and distortion due to the effects of input impedance, inherent EMG noises, electrode stability etc. The grasp recognition architectures in this Chapter investigate the recognition of six grasp types as detailed in Chapter 1 based on two channel EMG.

With a set of computationally less complex features: baseline zero crossing, turning points (96, Chapter 8) and Fast Fourier Transform (FFT) phase angle (97), grasp recognition architecture-I is a two tier classifier comprising of linear kernel Support Vector Machine (SVM) followed by a FFT classifier. Classification with linear kernel SVM and FFT classifier is computationally less time consuming and less complex (65,

97). Architecture-I yields an average recognition rate of 77% (98), which is low vis-a-vis the results reported in literature (22). Following the advantages of TFD features over TD and FD features as stated in Chapter 2, grasp recognition architecture-II has reported a recognition rate of 80% using continuous wavelet transform (CWT) coefficients and 84% using Discrete Wavelet Transform (DWT) as the feature set (99); and Radial Basis Function (RBF) kernel SVM as the classifier. In grasp recognition architecture-III, sum of DWT coefficients has been established as a primal feature for classification of grasp types with an average recognition rate of 86% (100).

3.1 Materials and Methods

3.1.1 Subjects and Experiment

Eighty subjects (sixty male and twenty female) in the age group of 20 to 45 years, without any known history of neuromuscular disorder took part in the experiment. The study used healthy subjects and relied on the fact that amputees who have lost their hand are able to generate EMG signals from the forearm muscles that are very similar to that generated by healthy subjects (8). The acquisition of EMG signals from the subjects was after the administrative permission from the Tezpur University Ethics Committee.

3.1.1.1 Experimental Protocol

EMG signals were acquired continuously from the state of pre-shape initiation by the user for the six grasp types. We categorized six types of macro stages as enumerated below (M0 to M5) during the process of grasping. These stages are along the lines of (101).

M0: Rest position: The starting point of the grasp preparation. Fingers stay at rest in half closed arrangement. They are motionless.

M1. Grasp preparation: Fingers are opening or closing taking the posture depending on the type of grasp to be performed.

M2. Grasp Closing: Precedes the grasp. The fingers move taking the posture depending on the size of the object to be grasped.

M3. Grasping: The fingers squeeze the object with a force dependant on the knowledge and observed behavior of the object.

3.2 EMG Acquisition and Preprocessing

M4. Maintaining the Grasp: With force adjustment, fingers decrease or increase the squeeze depending on the object deformation and slip.

M5. Releasing the Grasp and returning to Rest: Fingers slowly reduce squeeze and return to half close position of rest.

A period of around 40 seconds was allowed between two consecutive grasps during signal collection. This is in order to meet the features of robotic rehabilitation interventions (102).

3.2 EMG Acquisition and Preprocessing

3.2.1 EMG Acquisition

At the start of the experiment, subjects were given a demonstration towards maintaining fingers at rest position and how to perform the six grasping operations. Prior to the recording, the participants were encouraged to familiarize themselves with the experimental protocol and with the EMG acquisition equipment. Each subject was asked to rest the right arm on the arm rest of the chair with the fingers in a half closed state in horizontal direction. The skin where electrodes are to be placed was moistened using an electrode gel. Ag/AgCl electrodes are used over 80% of surface EMG applications (103, chapter 8: p 299) and are superior than other surface electrodes because they are non-polarized in nature (104). Table 3.1 shows the placement of the Ag/AgCl electrodes over the forearm muscles and their respective functions. This follows the electrode placement discussed in (8), without following any optimization algorithm for it. Figure 3.1 shows the muscles for placement of electrodes on a subject's forearm.

The electrodes were placed such that the longitudinal axes of the electrodes were parallel to the longitudinal axis of the muscle (101). A total of (80 subjects \times 6 grasp types) = 480 two channel EMG signals were acquired. In most previous works, more than two number of EMG channel have been used for patterns recognition (8, 79). However, users suffer from the inconvenience of carrying many cabled electrodes (105). This fact is most obvious while using prosthesis. Further, more number of channels includes increased processing as well as cost of the system. Based on these facts, two channel EMG signals have been used in this experiment. Figure 3.2 shows the experimental set-up during EMG acquisition

3.2 EMG Acquisition and Preprocessing

Table 3.1: Placement of EMG Electrode

Electrode Number	Electrode Leads	Specific Muscle	Functions (82)
Electrode1	Lead11	Extensor Digitorum	Extension of proximal, middle and distal phalanges of fingers
	Lead12	Flexor Digitorum	Flexion of proximal, middle distal phalanges of fingers and wrist
Electrode2	Lead21	Flexor Carpi Ulnaris	Flexion-Extension and abduction-adduction of the wrist
	Lead22	Extensor Carpi Radialis Longus	Abduction of the wrist and flexion-extension of the palm

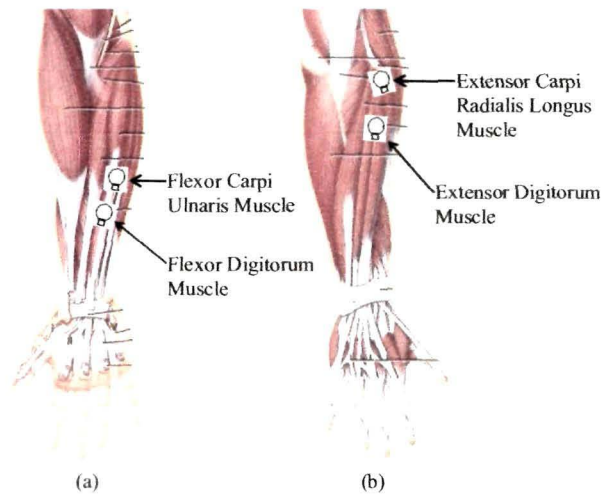


Figure 3.1: Electrode placement on the Forearm Muscles with (a) anterior view and (b) posterior view. Longitudinal axes of the electrodes are placed in line with the longitudinal axes of the corresponding muscles.

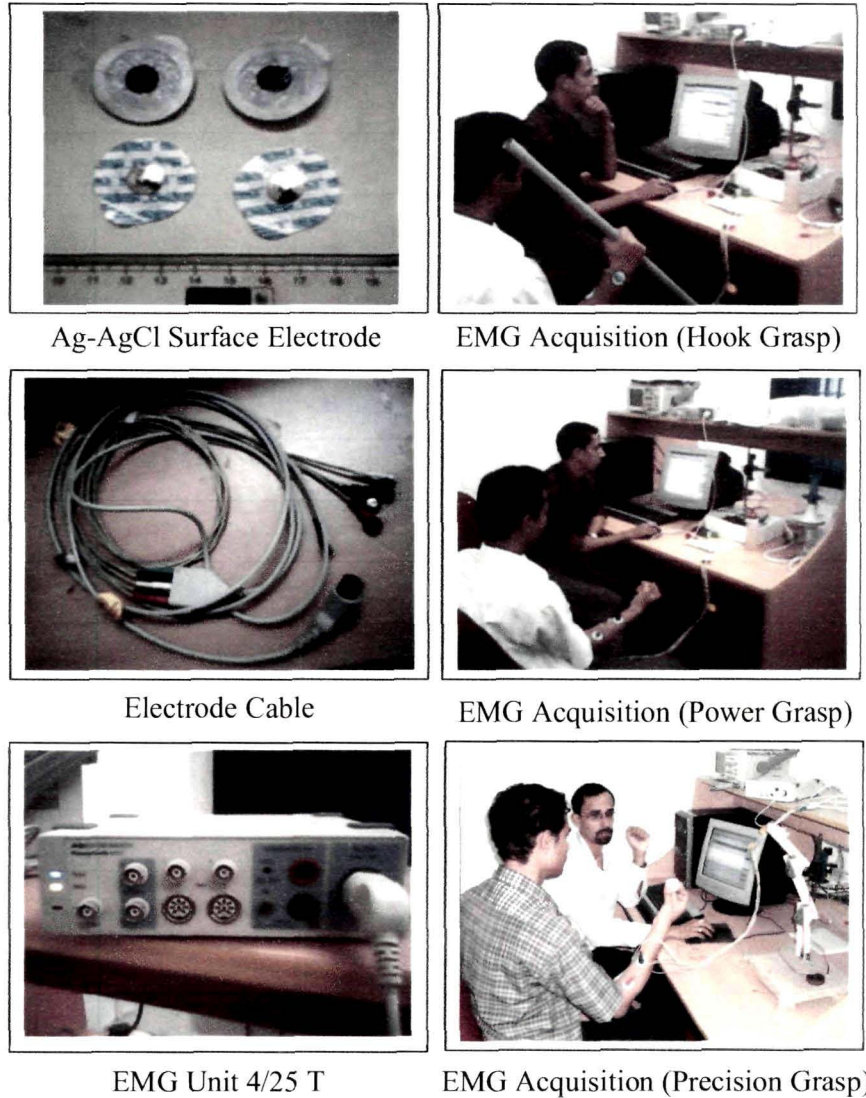


Figure 3.2: Experimental Set-up during Acquisition of EMG Signals

3.2.2 EMG Preprocessing

The raw EMG signals obtained for six grasp types needs to be preprocessed for accurate record, display and analysis. After the signal acquisition, EMG signals were filtered using a band pass filter; consisting of a high pass filter to reduce motion artefacts

3.3 Grasp Recognition Architecture-I

and a low pass filter to reduce base line drift. The signal is next amplified with an instrumentation amplifier of high common mode rejection ratio (CMRR) of 110 dB. Also a notch filter is incorporated to eliminate power line noise. This is performed using the bio-amplifier ML4818 in AD Instrument's Power Lab 4/25T EMG unit with the specification settings as detailed in Table 3.2. The EMG signal obtained after filtration and amplification is called integrated electromyogram (IEMG) signal. Even though the term integrated EMG refers to amplified and filtered signal including rectification; it is used in this research to refer to the preprocessed EMG signal only; without rectification. The preprocessed IEMG signal was digitized at a sampling rate of 10 kHz. Two channel EMG signals were recorded for a period of 250 msec. This is to meet the real time constraint that the response time of myoelectric control system should be less than 300 msec (106). The collected IEMG signals from one subject for the six grasp types are shown in Figure I:1 through Figure I:6 in Appendix-I.

Table 3.2: Bio-amplifier specification settings during EMG Acquisition

Parameter	Value
CMRR	110 dB
Low pass cutoff	2 kHz
High pass cutoff	10 Hz
Notch filter cutoff	50 Hz
Amplification range	+/-5 V

3.3 Grasp Recognition Architecture-I

Figure 3.3 shows the schematic diagram of the grasp recognition architecture-I. The fundamental blocks are the EMG Unit, Feature Extraction Unit and the Classifier Unit. The preprocessing in the EMG Unit is as per steps detailed in section 3.2.2. The characteristic pattern representation of a signal with reduced dimensionality called features are extracted in the Feature Extraction Unit. Feature extraction is the step to extract the useful informations of the signals for successful classification. Based on these features, the classifier perform the classification operation.

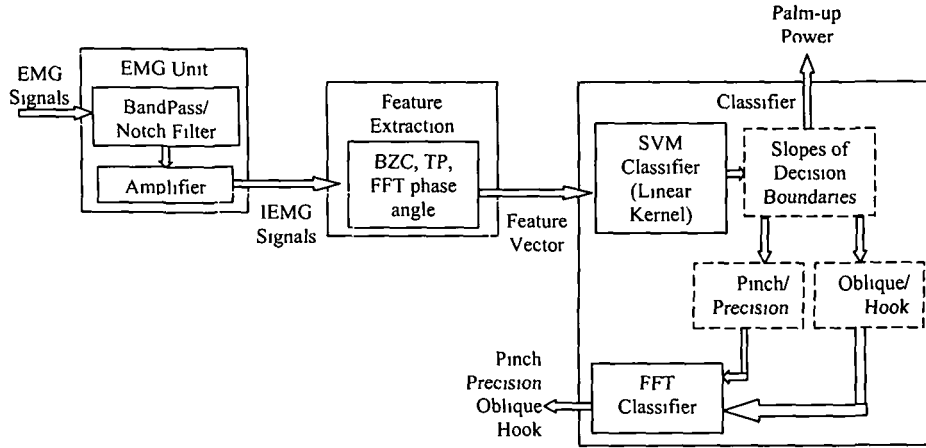


Figure 3.3: Schematic of the Grasp Recognition Architecture-I

3.3.1 Feature Set

Following set of features are used for grasps classification in architecture-I:

- Baseline Zero Crossings (BZC): Number of times a signal crosses the zero amplitude line.
- Turning Points (TP) : Sum of number of peaks and valleys in a given signal.
- FFT phase angle: Phase angle of a Fourier transformed signal.

Features are extracted from the IEMG signals in 50 msec frame. Rectangular window function was applied in each frame. BZC and TP extracted from EMG signals represents muscle strength and fatigue (107). I used these features for classification as the strength involved during different grasping are different (108). FFT phase angle possess many important informations of the signal and is alone sufficient to completely reconstruct the signal (109).

3.3.2 Classifier

The classification is in two stages. Number of BZC and TP of five individual windows were considered as the input features in stage I. The feature for classification in stage II is FFT phase angle.

Stage I: SVM Classifier

Classification of the extracted feature set in the SVM classifier was accomplished in two phases: training and testing. In the training phase, 40 numbers of user wearing the electrodes performs the grasp type decided a priori. The feature set is extracted from IEMG signals. This constitutes the training data set; which is passed through a linear kernel SVM classifier. SVM performs the classification of the feature set following the mathematical formulation stated in section 2.3.2.2 in Chapter 2. The slope of the separating hyperplane was considered for classification of the grasp types. For testing, another 40 subjects were allowed to perform the six grasp types randomly twice. The feature vector for each IEMG signal was extracted and fed to the classifier. Power and palm-up were classified correctly. Hook/ oblique were included in a single cluster; pinch/ precision into another cluster. These results are tabulated in Table 3.3.

Table 3.3: Results of SVM Classifier

Grasp Types	Decision Boundary Slopes	Clusters
Power	0.4 to 0.52	Cluster 1
Palm-up	-0.22 to -0.32	Cluster 2
Hook / Oblique	-0.55 to -1.88	Cluster 3
Pinch / Precision	3.9 to 6.6	Cluster 4

Stage II: FFT Classifier

For sampled vector data, Fourier analysis is performed using the discrete Fourier transform (DFT) . The FFT is an efficient algorithm for computing the DFT of a sequence. FFT has been used to detect muscle fatigue, force production and muscle fiber signal conduction velocity (54). Important information about a transform sequence includes its magnitude and phase. I have used the FFT phase angle (109). However, the performance of the FFT classifier was not considered against any other classifier. The slope of the FFT phase angle at discrete frequencies was the observation parameter for

3.3 Grasp Recognition Architecture-I

categorizing cluster 3 into hook and oblique; cluster 4 into pinch and precision. The results of the FFT classifier are tabulated in Table 3.4.

Table 3.4: Results of FFT Classifier

Grasp Types	Slope of FFT Phase angle	
	400 Hz	600 Hz
Oblique	-0.42 to -0.25	0.46 to 0.58
Hook	0.26 to 0.34	0.78 to 0.88
Pinch	0.51 to 0.62	-0.26 to -0.11
Precision	0.93 to 1.3	0.12 to 0.34

3.3.3 Results of Grasp Recognition Architecture-I

The architecture-I for recognition of grasp types using low channel forearm EMG signals has identified six grasps in two stages. Following Subasi et al. (110), the average recognition rate for each grasp types was calculated as:

$$\text{Recognition rate} = \frac{N}{G} \times 100\%$$

where

N = Number of correctly classified grasp during testing

G = Total number of grasps used in testing

Table 3.5 shows the grasp recognition results of architecture-I. An average recognition rate of around 77% is achieved (98). The confusion matrix in Figure 3.4 shows

Table 3.5: Recognition Rates of Architecture-I

Grasp Type Identified	Recognition Rate
Power	75%
Palm-up	75%
Oblique	75%
Hook	62.6%
Pinch	87.5%
Precision	87.5%

3.3 Grasp Recognition Architecture-I

the classification and misclassification of grasp types obtained through architecture-I. 80 number of input signals pertaining to each grasp type was passed to classifier. 75% of power grasp are classified correctly; 25% are misclassified as oblique. 75% of palm-up are classified correctly; 25% are misclassified as power and oblique. 75% of oblique are classified correctly; 25% are misclassified as hook and power. 62.5% of hook are classified correctly; 37.5% are misclassified as power and oblique. 87.5% of pinch are classified correctly; 12.5% are misclassified as precision and 87.5% of precision are classified correctly; 12.5% are misclassified as pinch. The main limitation of the grasp

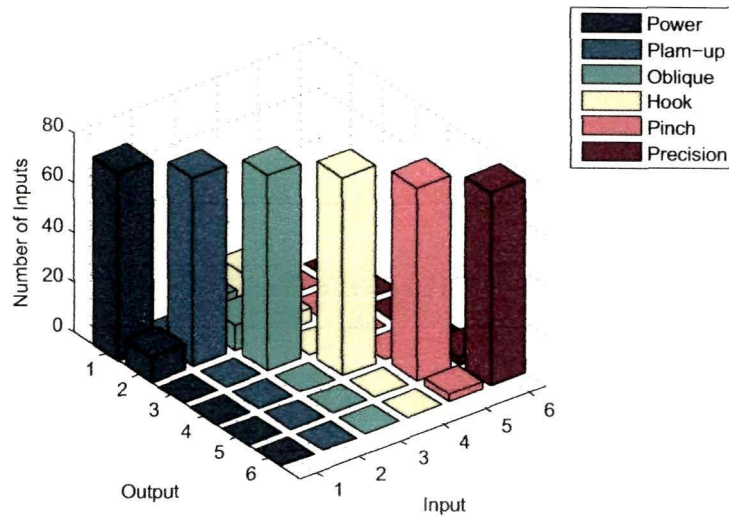


Figure 3.4: Confusion matrix for classification based on Architecture-I

recognition architecture-I was its lower recognition rate. It produced an average error rate of 23%. One of the main reason for low recognition rate was that architecture-I does not take into account subjectivity of the EMG signals. The EMG signals of different subjects for the same grasp type are never absolute because of the variation in impedance between the muscle of interest and electrodes (111). Furthermore it is dependent upon electrode application and placement (112), muscle fatigue (113), contraction velocity and muscle length, cross talk from nearby muscles and slight variation in task execution (114) etc. It would be almost impossible to control all these factors during EMG acquisition. Therefore, some kind of technique is required wherein all the EMG signals are converted into a scale that is common to all measurement occurrences.

Normalization controls for the aforementioned variables and facilitates the comparison of EMG signals between subjects as well between days for the same subject (115).

3.4 Grasp Recognition Architecture-II

The schematic diagram of grasp recognition architecture-II is shown in Figure 3.5. The preprocessing of the EMG signals were as detailed in section 3.3. In order to overcome the limitation of subjectivity as in architecture-I, a Normalization Unit as detailed in section 3.4.1 is introduced in the grasp recognition architecture-II.

As detailed in section 2.3.1.3 in Chapter 2, WT is better suited for EMG classification therefore, grasp recognition architecture-II and III are based on WT features.

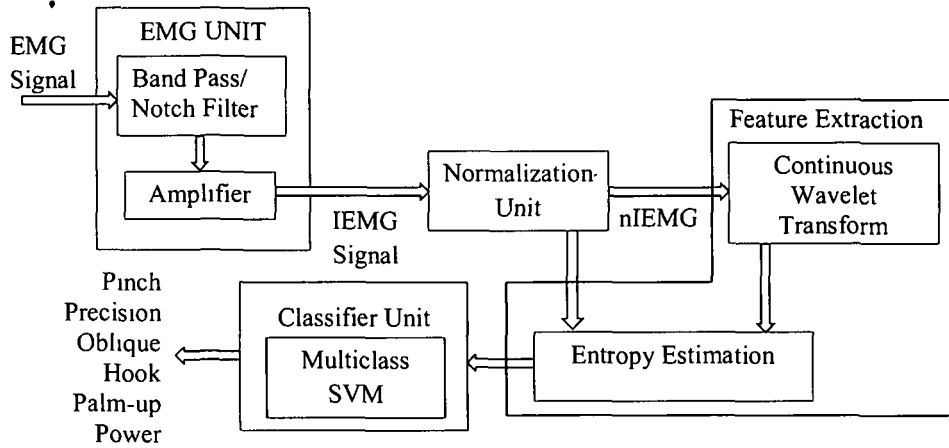


Figure 3.5: Schematic of the Grasp Recognition Architecture-II

3.4.1 Normalization

To reduce the influence of EMG signal subjectivity as discussed towards the end of the section 3.3.3, signals were normalized for making the method to work for all subjects. Normalization is through maximum volunteer contraction (MVC) as reference point (116). However, working of the method for all subjects can be evaluated only after clinical trials; which is not within the purview of this thesis. The IEMG signal on normalization is called normalized IEMG (nIEMG) signals. The normalized Root Mean Square (RMS) of IEMG signals is obtained as follows:

Normalized RMS of IEMG =

$$\frac{RMS(IEMG_i) - MinimumRMS(IEMG)}{MaximumRMS(IEMG) - MinimumRMS(IEMG)}$$

where

$IEMG_i = i^{th}$ sample value of IEMG signal

$RMS(IEMG_i) =$ RMS value of i^{th} sample of IEMG

$MaximumRMS(IEMG) =$ maximum RMS value of IEMG

$MinimumRMS(IEMG) =$ minimum RMS value of IEMG

The nIEMG signals for the six grasp types under study are shown in Figure I:7 through Figure I:12 in Appendix-I.

3.4.2 Feature Set

The feature vector for grasp classification in architecture-II was derived using CWT. The proper wavelet basis function was selected through computation of entropy of the preprocessed EMG signals and WT coefficients of six different wavelet families: Gaussian, Daubechies, Morlet, Meyer, Mexicanhat and Symlet. The CWT coefficients were derived at 11, 21, 35 and 101 scale index. The purpose of CWT is to decompose a signal into localized contributions characterized by scale parameter. The CWT of a signal $f(x)$ is defined as an inner product of the signal and the wavelet bases as follows:

$$W(s, b) = \langle f(x), \psi_{s,b}(x) \rangle \quad (3.1)$$

Where $\psi_{s,b}(x)$ is referred to as wavelet bases and $W(s, b)$ is referred to as WT coefficient of signal $f(x)$. The $\psi_{s,b}(x)$ can be formed from a basic wavelet $\psi(x)$ by a series of scaling and shifting operations. The wavelet base is defined as:

$$\psi_{s,b}(x) = 1/s \cdot \psi((x - b)/s) \quad (3.2)$$

Where $s > 0$ and b are any real numbers. The variable s indicates the scale of the particular basis function and the variable b specifies its shift operation. Using the wavelet bases in equation 3.2, the wavelet transform defined in equation 3.1 can be computed as:

$$W(s, b) = 1/\sqrt{s} \cdot \int_{x=-\infty}^{\infty} f(x) \cdot \psi((x - b)/s) \quad (3.3)$$

The CWT given by equation 3.3 is the convolution of signal with the wavelet function shifted over the entire signal defined by the wavelet scale (117). The transform coefficients produce by this process are the correlation of the basis function with the signal. CWT based feature extraction for efficient classification of grasp types is dependent on the appropriate choice of the mother wavelet function. This work proposed entropy measure to select an optimum wavelet function.

The entropy is a measure of uncertainty of information in a statistical description of a system. The features extraction through CWT is followed by the entropy estimation. The entropy of wavelet transform coefficients of the wavelet families under study are estimated. The entropy H for random variable X is defined as (118):

$$H(X) = \sum_i P(X = a_i) \log_2 P(X = a_i) \quad (3.4)$$

Where i is the possible values of X . To select the optimum wavelet function in representing the EMG signals of grasp types, the entropy of nIEMG signal of six grasp types with entropy of the decomposition coefficients of wavelet functions under study were compared. The selection of the CWT mother wavelet function based on entropy measurement is detailed in section 3.4.4.

3.4.3 Classifier

In this study, One-vs-All method is carried out for classification of grasp types. The classification steps of One-vs-All SVM for six grasp types are:

- Label all the training samples of the one of the grasp types as positive samples.
- Label all the training samples of other grasp types as negative samples.
- Use all positive and negative samples as input to train a SVM and corresponding classification planes are obtained.
- Label the trained SVM as SVM_1 ; representing that SVM_1 is used for differentiating the grasp type used for training from other five grasp types.
- Repeat the previous step for other five grasp types, finally six of the SVMs are obtained as $SVM_1, SVM_2, SVM_3, SVM_4, SVM_5, SVM_6$.

3.4 Grasp Recognition Architecture-II

3.4.4 Results of Grasp Recognition Architecture-II

Following the formulation for recognition rate as stated in section 3.3.3, the average recognition rates for six grasp types obtained using CWT coefficients at scale index 11, 21, 35 and 101 are shown in Table 3.6. Results with Gaussian CWT has been found highest with an average recognition rate of 80% over six grasp types. To investigate the relation of recognition rate with scale index, a range of scale index have been considered to access the changes of accuracies with wavelet functions. Table 3.6 shows variation of scale index has little effect on the average recognition rates of six grasp types.

Table 3.6: Average recognition rates over six grasp types through CWT coefficients at different scale index

Wavelet Functions	Recognition Rate			
	scale index 11	scale index 21	scale index 35	scale index 101
Gaussian	79%	80%	80%	81%
Morlet	77%	77%	76%	76%
Meyer	75%	74%	74%	74%
Symlet 4	74%	74%	73%	74%
Db	72%	73%	73%	74%
Mexicanhat	70%	71%	71%	72%
Haar	62%	62%	62%	62%

The arrangement of wavelet functions into an increasing order of grasp recognition rates result in the following sequence 3.5.

$$Haar < Mexicanhat < Daubechies8 < Symlet4 < Meyer < Morlet < Gaussian \quad (3.5)$$

Table 3.7 shows the entropy values of CWT coefficients of nIEMG signal. The average entropy of the nIEMG signals for the six grasp types are estimated as shown in Table 3.8. From Table 3.8, average entropy of the nIEMG signal is measured as 1.09×10^3 .

Table 3.7: Entropy Measure of Wavelet coefficients

Wavelet Function	Average Entropy Values
Gaussian	3.07×10^3
Morlet	3.46×10^3
Meyer	4.22×10^3
Symlet 4	4.25×10^3
Daubechies 8	4.33×10^3
Mexicanhat	5.12×10^3
Haar	8.60×10^3

Table 3.8: Entropy Measure of nIEMG Signals for Grasp Types Under Study

Grasp Types	Average Entropy Values
Hook	1.01×10^3
Oblique	1.04×10^3
Palm-up	1.04×10^3
Pinch	1.26×10^3
Power	1.04×10^3
Precision	1.19×10^3

The increasing order of entropy values of wavelet transform coefficients and nIEMG signals results into the sequence 3.6.

$$Haar > Mexicanhat > Daubechies\ 8 > Symlet\ 4 > Meyer > Morlet \\ > Gaussian > nIEMG \quad (3.6)$$

From sequence 3.5 and 3.6, it is clear that (a) wavelet function coefficients having entropy values close to that of the nIEMG signal produces higher recognition rate (b) wavelet function coefficients having entropy values far from that of nIEMG results into lesser recognition rate. Based on this result, it has been hypothesized that wavelet function coefficients having entropy values close to the entropy values of nIEMG possesses maximum informations about the grasp types. Gaussian wavelet function was reported to be possessing maximum information about the grasp types producing an average recognition rate of 80% (119).

In continuation to the grasp recognition results with CWT, eight DWT coefficients: Bior 1.3, Bior 2.3, Coif 3, Coif 4, Symlet 4 (Sym 4), Symlet 8 (Sym 8), Haar and

3.4 Grasp Recognition Architecture-II

Daubichies 8 (dB8) at third, fourth and fifth level of decomposition have been considered for classification of grasp types under study through grasp recognition architecture-II. The approximate coefficients contain the most important information of the signal (120) and have been used to constitute the feature set. Table 3.9 shows the results of the grasp recognition architecture-II with DWT coefficients as feature set.

Table 3.9: Recognition rate of six grasp types through DWT at third, fourth and fifth level of decomposition

Wavelet Function		Grasp Types					
		Power	Palm-up	Hook	Oblique	Precision	Pinch
Bior 1.3	third level	82%	82%	71%	90%	80%	95%
	fourth level	72%	80%	64%	84%	72%	72%
	fifth level	70%	82%	72%	85%	82%	92%
Bior 2.2	third level	80%	83%	64%	87%	76%	90%
	fourth level	80%	82%	72%	85%	76%	82%
	fifth level	88%	82%	78%	86%	80%	92%
Coif 3	third level	82%	82%	83%	88%	70%	81%
	fourth level	74%	82%	68%	84%	74%	74%
	fifth level	84%	82%	72%	78%	84%	88%
Coif 4	third level	80%	82%	64%	88%	82%	90%
	fourth level	84%	82%	72%	84%	74%	84%
	fifth level	80%	82%	80%	78%	74%	88%
Sym 4	third level	82%	83%	80%	88%	82%	84%
	fourth level	84%	82%	72%	84%	74%	84%
	fifth level	86%	84%	86%	78%	76%	88%
Sym 8	third level	80%	83%	78%	88%	84%	94%
	fourth level	84%	80%	66%	84%	72%	84%
	fifth level	84%	82%	82%	78%	78%	90%
Haar	third level	82%	82%	65%	87%	80%	88%
	fourth level	82%	82%	64%	84%	82%	82%
	fifth level	86%	83%	70%	80%	78%	94%
dB8	third level	82%	82%	65%	88%	82%	95%
	fourth level	86%	82%	64%	84%	76%	90%
	fifth level	86%	83%	70%	86%	82%	90%

At the third level of decomposition, even though the recognition rate of oblique, palm-up, pinch and power grasps based on Haar wavelet is better than that of Symlet 8; the average recognition rate over all six grasp types is poor compared to Symlet 8. At the fourth level of decomposition, all of the wavelets have similar recognition rates for oblique and palm-up grasp types. For pinch and power, recognition based on Symlet 8 wavelet is better than the other wavelets. At the fifth level of decomposition, except for pinch grasp, where classification with Symlet 8 wavelet have higher recognition rate, other wavelets exhibit similar recognition rates for all other grasp types. Irrespective of the wavelet function, the average recognition rate is higher at third level of decomposition.

An average recognition rate of 80% using CWT and 84% using DWT were achieved. Moreover, the CWT computation may consume significant amount of time and resources depending on the resolution required. The DWT, which is based on sub band coding is found to yield a fast computation of WT. DWT is easy to implement and reduces the computation time and resources required. Based on the results, DWT is recommended as more efficient and suitable for EMG based grasps recognition (121).

The classification results obtained from grasp recognition architecture-II is not high enough as compared to those reported in the literature (122). Moreover, When the energy of the signal is finite, not all values of a decomposition are needed to exactly reconstruct the original signal. In such cases, DWT is sufficient and CWT is redundant (123). Energy of EMG signals are finite (124). Furthermore, the wavelet coefficients of Haar WT function was found to possess the frequency informations of the original signal (125, 126, 127, 128) as well results based on Haar WT was found better for more number of grasp types. Therefore DWT Haar wavelet coefficients were used in the grasp recognition architecture-III.

3.5 Grasp Recognition Architecture-III

Figure 3.6 shows the schematic diagram of the grasp recognition architecture-III. The fundamental blocks: EMG Unit, Normalization Unit, Feature Extraction Unit and the Classifier Unit are as detailed in section 3.3 and 3.4.

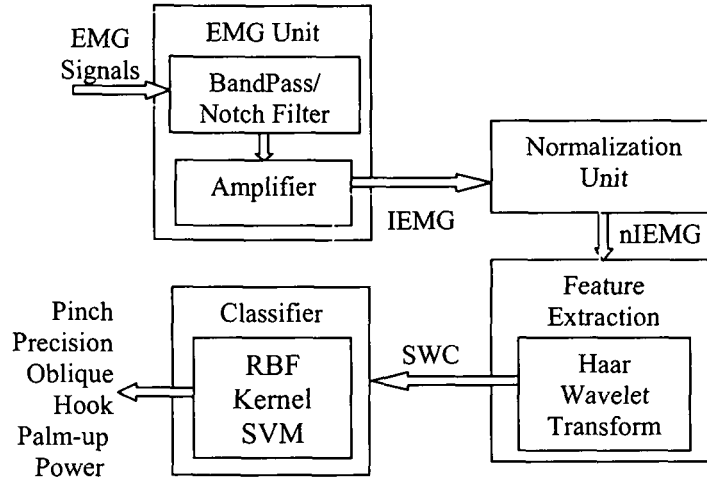


Figure 3.6: Grasp Recognition Architecture-III

3.5.1 Feature Set

Grasp recognition architecture-III explores sum of discrete wavelet decomposition coefficients (SWC). SWC can be interpreted as the difference between two approximations at subsequent scales (125) and corresponds to the frequency components of the original signal (126, 127). During grasping, the number of motor units firing varies according to the involvement of the forearm extensor and flexor muscles (129). Further, the firing rate of motor units associated with control and co-ordination of finger movements during grasping operations, varies according to the grasps (128). Consequently EMG for each of the grasp types is the composite of different frequency components. Therefore, it has been hypothesized that SWC is a primal feature for classification of grasp types based on EMG signals (98).

3.5.2 Classifier

For the classification of non-linear and high transitional data, the formulation of linear SVM hyperplane as discussed in section 3.4.3 is extended to build non linear SVM kernel. Non linear kernel transforms the input data into feature space of higher dimensions. In this high dimensional space, data can be linearly separable by applying linear SVM formulation (24).

In continuation to the mathematical formulation of SVM in section 2.3.2.2 in Chapter 2, the optimal hyper plane is characterized by:

- Maximum margin of separation between any training point and hyper plane i.e.

$$\begin{aligned} \max_{(w,b)} \min \|x - x_i\| : x \in H, \langle w, x \rangle + b = 0; \\ i = 1, 2, \dots, m \end{aligned}$$

- The normal vector that leads to the largest margin is calculated as

$$\min_{(w \in H, b \in R)} \tau(w) = \frac{1}{2} \|w\|^2 \quad (3.7)$$

subjected to

$$y_i (\langle w, x \rangle + b) \geq 1; i = 1, 2, \dots, m \quad (3.8)$$

where y_i is label corresponding to the i^{th} training sample and

$$\begin{aligned} y_i &= +1 \text{ if } \langle w, x_i \rangle + b > 1 \text{ or} \\ y_i &= -1 \text{ if } \langle w, x_i \rangle + b < -1 \end{aligned}$$

The function τ in equation 3.7 is called the objective function and equation 3.8 is inequality constraint. Together they form a constrained optimization problem. By introducing Lagrange multipliers $\alpha_i \geq 0$ and Lagrangian

$$L(w, b, \alpha) = \frac{1}{2} \|w\|^2 - \sum_{i=1}^m \alpha_i (y_i (\langle w, x \rangle + b) - 1) \quad (3.9)$$

The Lagrangian L has to be minimized with respect to the primal variables w and b and maximized with respect to the dual variable α_i i.e.

$$\frac{\partial}{\partial b} L(w, b, \alpha) = 0 \text{ and } \frac{\partial}{\partial w} L(w, b, \alpha) = 0$$

which leads to

$$\sum_{i=1}^m \alpha_i y_i = 0 \text{ and } w = \sum_{i=1}^m \alpha_i y_i x_i \quad (3.10)$$

By substituting the above in equation 3.9, the primal variables w and b are eliminated and arrived at the dual optimization problem:

$$\max_{\alpha} w(\alpha) = \sum_{i=1}^m \alpha_i - \frac{1}{2} \sum_{i,j=1}^m \alpha_i \alpha_j y_i y_j \langle x_i, x_j \rangle$$

subjected to $\alpha_i \geq 0, i=1,2,..,m$ and

$$\sum_{i=1}^m \alpha_i y_i = 0$$

Using equation 3.10, the hyper plane decision function can be written as

$$f(x) = \text{sgn}\left(\sum_{i=1}^m y_i \alpha_i \langle x, x_i \rangle + b\right)$$

By applying kernel trick (k), the normal vector becomes an expansion in feature space and no longer correspond to a single vector from input space. Thus the decision function is of the form

$$f(x) = \text{sgn}\left(\sum_{i=1}^m y_i \alpha_i k(x, x_i) + b\right)$$

and the following quadratic problem

$$\max_{\alpha} w(\alpha) = \sum_{i=1}^m \alpha_i - \frac{1}{2} \sum_{i,j=1}^m \alpha_i \alpha_j y_i y_j k(x_i, x_j)$$

subjected to

$$\alpha_i \geq 0 \text{ and } \sum_{i=1}^m \alpha_i y_i = 0; 0 \leq \alpha_i \leq c$$

where c is the regularization constant.

In terms of selecting a kernel function to use with the SVM, there is no method that can determine what kernel function should be used for a particular application. According to (130), the RBF kernel should be the first choice. Another reason to use the RBF kernel is that there are less difficulties with mathematical computations. A RBF kernel is used as the kernel function k in our method,

$$k(x_i, x) = \exp(-\gamma(\|x_i - x\|)^2)$$

where γ is the kernel parameter. The $\gamma = 2^{-3}$ and $c = 2^3$ are selected through a random iterative process for the experiment.

3.5.3 Results of Grasp Recognition Architecture-III

Recognition rates of classifying the EMG signals into six grasp types using the grasps recognition architecture-III are tabulated in Table 3.10. Given these rates, the average rate of recognition of a grasp types was 86% (100).

Table 3.10: Recognition Rates of Architecture-III

Identified Grasp Types	Recognition Rate
Hook	94%
Oblique	94%
palm-up	88%
Pinch	88%
Power	88%
Precision	66%

The confusion matrix in Figure 3.7 shows the classification and misclassification of grasp types obtained through Architecture-III. 80 number of input signals pertaining to

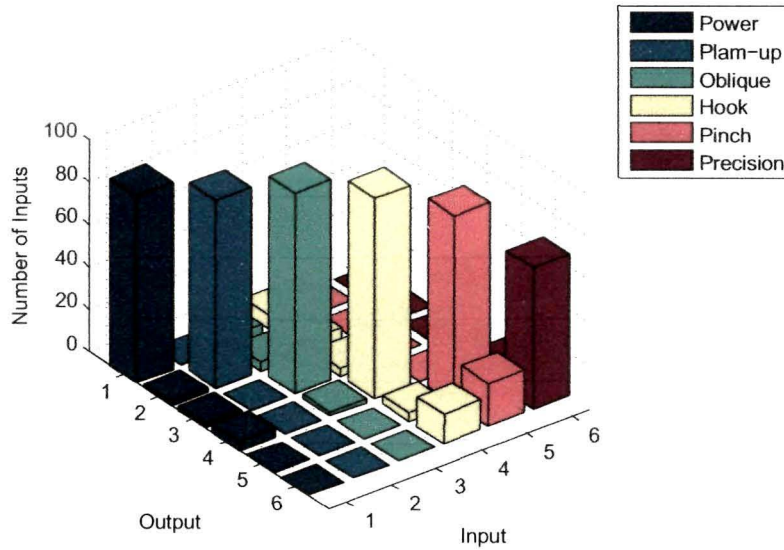


Figure 3.7: Confusion matrix for classification based on Architecture-III

each grasp type was passed to classifier. 88% of power grasp are classified correctly; 12% are misclassified as oblique. 88% of palm-up are classified correctly; 12% are misclassified

as power and oblique. 94% of oblique are classified correctly; 6% are misclassified as hook. 94% of hook are classified correctly; 6% are misclassified as oblique. 88% of pinch are classified correctly; 12% are misclassified as precision and 66% of precision are classified correctly; 34% are misclassified as precision. A much lesser misclassification rate than that of 14% is desirable for a reliable emulation of grasp types by a prosthetic hand.

3.6 Summary

A strategy for classification of grasp types based on two channel EMG signals is presented. Three grasp recognition architectures have been proposed. Architecture-I is a two stage classifier with an average recognition rate of 77%. From experiments in Architecture-II, it has been hypothesized that CWT function coefficients of the EMG signals having entropy values close to the entropy values of preprocessed EMG signals possess maximum informations about the grasp types. In Architecture-III, SWC is established as a primal feature for classification of grasp types with an average recognition rate of 86%. Derivation of a wholesome feature set for increasing the recognition rate is the focus of work for Chapter 4.

4

EMG based Grasps Recognition: Results with Statistical Analysis

Following the initial work on EMG based grasp recognition for six grasp types reported in Chapter 3, this chapter focus on the derivation of a low dimensional yet informative and distinguishing feature set to significantly increase the performance of a low channel EMG based grasps recognition architecture. In quest of an efficient feature set for higher recognition rate, grasps classification experiments have been carried out with four groups of features: Time Domain (TD), Frequency Domain (FD), Time/Frequency Domain (TFD) and Principal Component Analysis (PCA) of TFD features. The transition from one feature set to another is based on the linear relationship of each feature set with the grasp types based on R^2 -value of analysis of variance (ANOVA). Classification is through grasp recognition architecture-IV using RBF kernel SVM; cross validated through 10-fold cross validation. Following the experiments on grasps recognition, the classification results are evaluated through statistical analysis finding the relative performance of the feature sets through Sheffe's post hoc test.

4.1 Grasps Recognition Architecture-IV

Figure 4.1 shows the schematic diagram of the proposed EMG based grasp recognition architecture-IV. The architecture comprises of four fundamental units: EMG Unit, MVC normalization Unit, Feature Extraction Unit followed by the Classifier Unit. The EMG unit comprises of the amplifier, band pass and notch filter. The pre-processing

and normalization of the raw EMG signals are in line with the experimental details reported in section 3.4.1 of Chapter 3. The TD, FD, TFD and PCA of TFD features extracted from the nIEMG in the Feature Extraction Unit are fed to the classifier in separate groups. The classifier is a RBF kernel SVM with a 10-fold cross validation unit. Identifying the RBF kernel parameters c and γ through grid search and 10-fold cross validation of the classifier results are as stated in section 2.3.2.2 and 2.3.2.5 of Chapter 2.

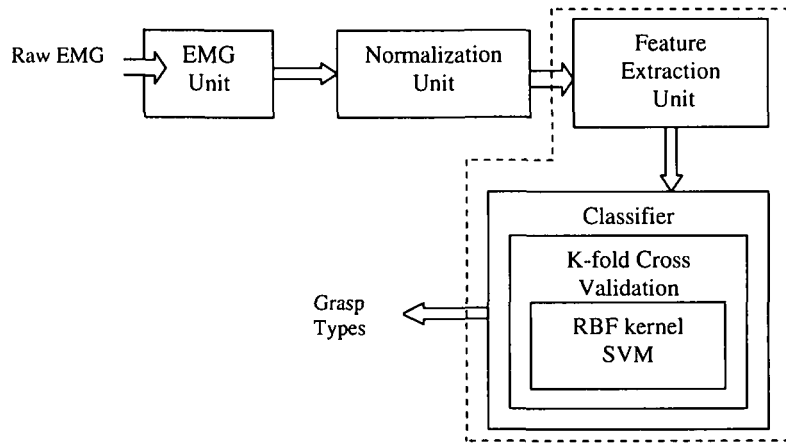


Figure 4.1: Proposed EMG based Grasp Recognition Architecture

4.1.1 Classification with Time Domain Feature

4.1.1.1 Feature Set

In continuation to the discussion on TD features in Chapter 2, following TD features have been used for recognition of grasp types through the grasp recognition architecture-IV.

- Mean Absolute Value (MAV)

This is the mean absolute value of a signal and is measured as (34):

$$MAV = 1/N \sum_{k=1}^N |x_k|$$

where

N = Total number of samples in the signal

$x_k = k^{th}$ sample value of the signal.

- Root Mean Square (RMS) Value

RMS is modeled as amplitude modulated Gaussian random process and is related to the constant force and non-fatiguing contraction (106) and can be expressed as

$$RMS = 1/N \sqrt{\sum_{n=1}^N x_k^2}$$

- Variance (VAR)

This feature is the measure of the of EMG signal's power (34) and is measured as

$$VAR = 1/(N - 1) \sum_{k=1}^N x_k^2$$

- Characteristic point counts

TP and ZC were viewed as the characteristic points describing a waveform. The turn count registered a local extreme value as a turning point and the zero-crossing count was determined as the number of times the signal completely traversed both sides of the baseline (106).

The TP count increased by one if

$$\begin{aligned} &x_k - x_{k+1} < 0 \text{ and } x_k - x_{k+1} < 0 \\ \text{or } &x_k - x_{k-1} > 0 \text{ and } x_k - x_{k+1} > 0 \end{aligned}$$

and the ZC count increased by one if

$$\begin{aligned} &x_k > 0 \text{ and } x_{k+1} < 0 \\ \text{or } &x_k < 0 \text{ and } x_{k+1} > 0 \end{aligned}$$

4.1.1.2 Classifier

During experiment with TD features, the Feature Extraction and Classification Unit shown in Figure 4.1 is as shown in Figure 4.2. The TD features ZC, MAV, RMS value, VAR, TP are extracted from the nIEMG signals following the mathematical definitions as detailed in section 4.1.1.1.

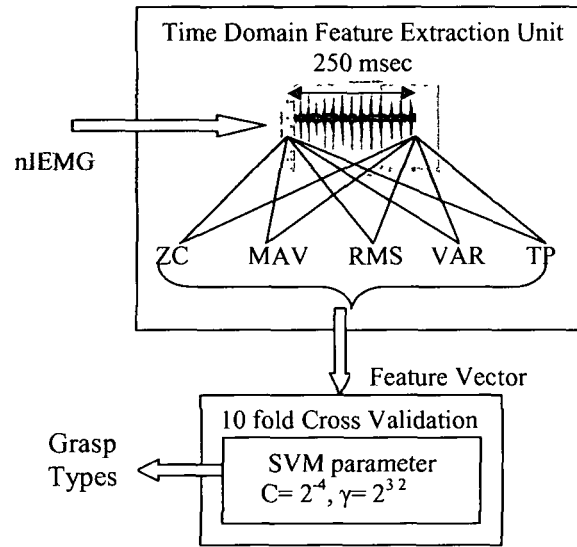


Figure 4.2: Classification with TD Features

Classifier Parameter Setting In the classifier, various values of c and γ are tried and one of the best set obtained through grid search is picked up for grasp classification. The grid search is used with 10 search intervals for γ and 11 search intervals for c and hence the classifier evaluates a total of $10 \times 11 = 110$ grid points. A range of value of $\log_2 c = \{-5, -4, -3, \dots, 5\}$ and $\log_2 \gamma = \{2, 2.2, 2.4, \dots, 3.8\}$ are considered for grid search. Figure 4.3 shows the grid search result for TD features. A value of $c = 2^{-4}$ and $\gamma = 2^{3.2}$ is chosen for classification. The lowest value of γ and corresponding c value is chosen from the set in order to avoid overfitting of the classifier (131).

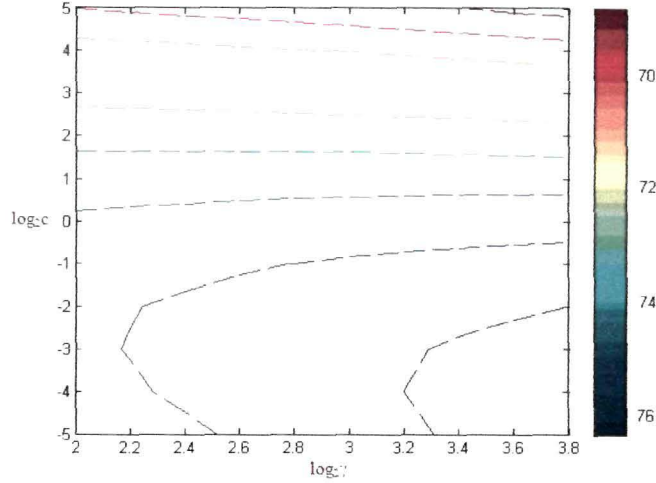


Figure 4.3: Results of Grid search for finding the values of C and γ with TD features

4.1.1.3 Results with Time Domain Features

Cross Validation Table 4.1 shows the recognition rates obtained during each test for 10-fold cross validation for the six grasp types under study. The average of the 10-fold test results produce average recognition rate of grasp types.

Table 4.1: Recognition rates in % with the testing folds along the columns and grasp types along the rows obtained through 10-fold cross validation. Classification is based on TD features

	1st	2nd	3rd	4th	5th	6th	7th	8th	9th	10th
Hook	62.5	75	75	87.5	62.5	75	75	87.5	75	75
Oblique	75	75	62.5	75	87.5	87.5	75	75	62.5	75
Palm-up	75	75	87.5	75	62.5	75	87.5	87.5	87.5	62.5
Power	87.5	87.5	87.5	75	87.5	87.5	87.5	75	87.5	87.5
Pinch	62.5	62.5	87.5	62.5	62.5	75	62.5	75	75	62.5
Precision	62.5	62.5	87.5	62.5	62.5	62.5	87.5	87.5	87.5	62.5

Following the formulation for recognition rate as stated in section 3.3.3, the average recognition rate for each grasp types with TD features is shown in Figure 4.4.

The confusion matrix in Figure 4.5 shows the classification and misclassification of

4.1 Grasps Recognition Architecture-IV

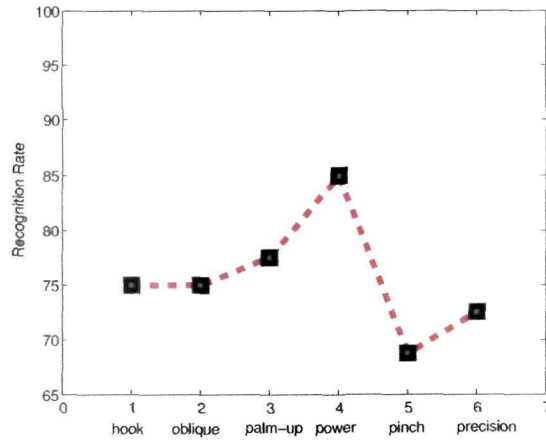


Figure 4.4: Recognition Rate with TD Features

grasp types based on TD features. 80 number of input signals (pertaining to each grasp

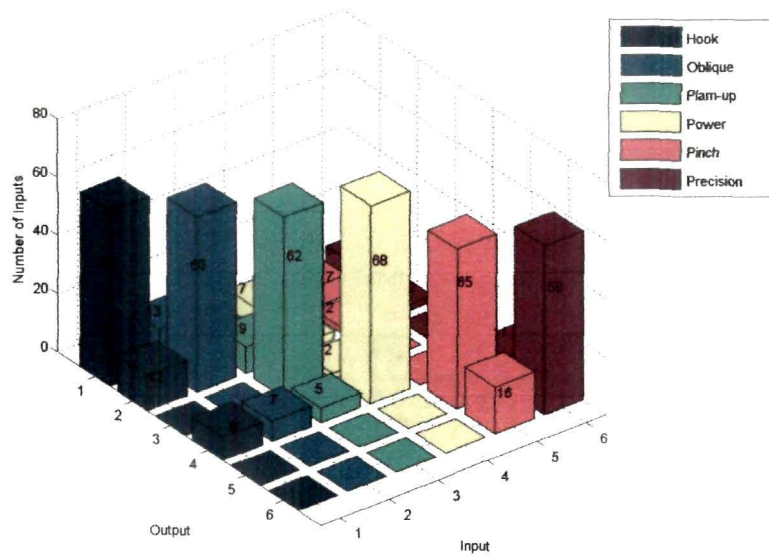


Figure 4.5: Confusion Matrix for classification based on TD features

type) was passed to classifier; Figure shows classification as well as misclassification for each of these signals. Numeric value (on bars) represent the number of signals classified for the particular type corresponding to color legend shown. For example corresponding to input 1: 80 signals of hook type are passed; 60 are classified as hook (aka input 1),

12 are misclassified as oblique (aka output 2) and 8 are misclassified as power (aka output 4).

Following (132), the misclassification rate (R) is calculated as:

$$R = \frac{\text{Number of off-diagonal data in confusion matrix}}{\text{Total number of Testing data}}$$

From Figure 4.5, it is found that the TD features gives an average misclassification rate of 24%; 25% hook is misclassified as oblique and power, 25% oblique is misclassified as hook and power, 22.5% palm-up is misclassified as hook, oblique and palm-up, 15% power is misclassified as hook, oblique and palm-up, 31.25% pinch is misclassified as hook, oblique and precision, 27.5% precision is misclassified as hook, oblique and pinch. The average recognition rate for six grasp types with TD features is 76%.

4.1.1.4 Linear Relationship

The purpose of ANOVA is to test for significant differences between means of several groups of data and provide statistical significance. Basically ANOVA is performed using two techniques: One-way ANOVA and two-way ANOVA. In a one-way ANOVA, one test simultaneously whether there exist differences between two or more group's means. This differs from a two-way ANOVA approach in that in a one-way ANOVA test, one evaluate whether all groups' means are equal or not, but do not care which ones differ and which ones are equal. In this test, assumption is that one have independent samples from each groups. Two-way ANOVA is an extension of one-way ANOVA and differ in that the groups in a two-way ANOVA have two categories of defining characteristics instead of one. ANOVA can express the statistical significance of the groups in terms of p-value and R^2 -value.

P value: The p-value tests the null hypothesis that data from all groups are with identical means. Therefore, the p-value answers:

- If all the groups have the same mean, what is the chance that random sampling would result in means as far apart?
- If the overall p-value is large, the data do not give you any reason to conclude that the means differ. Even if the group means were equal, it would not be surprised to find sample means this far apart just by chance.

4.1 Grasps Recognition Architecture-IV

- If the overall p-value is small, then it is unlikely that the differences you observed are due to random sampling. One can reject the idea that all the groups have identical means. This doesn't mean that every mean differs from every other mean, only that at least one differs from the rest.

R^2 - Value: R^2 -Value is the fraction of the overall variance of all the data in all the groups attributable to differences among the group means. It compares the variability among group means with the variability within the groups. A large value means that a large fraction of the variation is due to the treatment that defines the groups. The R^2 -value is calculated from the results of ANOVA and equals the between group sum-of-squares divided by the total sum-of-squares. It is a descriptive statistic that quantifies the strength of the relationship between group membership and the variable measured. A higher linear relationship of a feature set with the grasp types depicted by higher R^2 -value, which reflects that the feature set possess more information about the grasp types.

Force involved during grasping varies with grasp types (133). The average EMG provides direct measurement of force involved during grasping (134). Average EMG is a function of features. From these facts, it has been hypothesized that the linear relationship of the force with the average EMG depicts the relationship of the features with the grasps. Based on the above facts, the next step is followed to search the linear relationship of the feature set with the grasp types. The R^2 -value for the TD features with the grasp types was derived through one-way ANOVA. The results of ANOVA analysis is tabulated in Table 4.2.

Table 4.2: ANOVA with TD Features

<i>Source</i>	<i>ss</i>	<i>df</i>	<i>MS</i>	F	Prob.
Columns	1.172721e+011	1	1.17234e+011	5.43	0.0481
Errors	1.72721e+011	8	2.15901e+010		
Total	2.89955e+011	8			

where

ss = sum of squares

df = degrees of freedom

MS = mean square

F = F-ratio

Prob. = Probability or significance of F

The R^2 -value is calculated as follows:

$$\begin{aligned} R^2 - value &= 1 - SS(Error)/SS(Total) \\ &= 1 - 0.59 \\ &= 0.41 \end{aligned}$$

Having noted a poor linear relationship of the TD features with the grasp types as well as a low recognition rates as comparable to those reported in the literature (122); the next experiment is on the recognition of grasp types based on FD features.

4.1.2 Classification with Frequency Domain Feature

4.1.2.1 Feature Set

In continuation to the discussion on FD features in Chapter 2, following FD features have been used for recognition of grasp types through grasp recognition architecture-IV.

- **FFT Phase Angle:** Fast Fourier Transform has been used to detect muscle fatigue, force production and fibre signal conduction velocity (54). Important information about a transform sequence includes its magnitude and phase. The FFT phase angle $\phi(F(f(x)))$ of a signal $f(x)$ is calculated as follows:

$$\begin{aligned} FFT(f(x)) &= F(x) \\ &= \int_{-\infty}^{\infty} f(x)e^{-i2\pi ux} dx \\ &= \int_{-\infty}^{\infty} f(x)(\cos(2\pi ux) - i\sin(2\pi ux))dx \end{aligned}$$

where $i = \sqrt{-1}$ and $u (=1,2,3,\dots,u)$ is called the frequency variable.

The FFT phase angle is defined as

$$\phi(F(x)) = \tan^{-1}(b/a)$$

4.1 Grasps Recognition Architecture-IV

where $a=\cos(2\pi ux)$ and $b=\sin(2\pi ux)$

- Power Spectral Density (PSD) : The PSD of the EMG provides information on muscle properties such as fatigue and force production (135). The PSD defines how the power of a signal is distributed with frequency and is defined as

$$PSD = |F(x)|^2$$

- Frequency Median (FMD): FMD is the frequency at which the spectrum is divided into two regions with equal power (106). It can be expressed as:

$$FMD = 1/2 \sum_{j=1}^M P_j$$

where P_j is the EMG power spectrum at frequency bin j .

- Frequency Mean (FMN)
FMN is the average frequency. FMN is calculated as the sum of the product of the power spectrum and the frequency divided by the total sum of spectrogram intensity (106). FMN is calculated as

$$FMN = \frac{\sum_{j=1}^M f_j P_j}{\sum_{j=1}^M P_j}$$

where f_j is the frequency of spectrum at frequency bin j .

- Frequency Ratio (FR): FR indicates the extent of contraction and relaxation of muscle. A high FR means that the degree of contraction of the muscle is high, a low FR means the opposite (25). By applying the FFT to the EMG in TD, the FR is calculated as:

$$FR = |F(x)|_{lowfrequency} / |F(\tau)|_{highfrequency}$$

4.1.2.2 Classifier

During experiment with FD features, the Feature Extraction and Classification Unit are as shown in Figure 4.6. The FD features: FFT phase angle, PSD, FMD, FMN and FR are extracted from the nIEMG signals following the mathematical definitions as detailed in section 4.1.2.1.

4.1 Grasps Recognition Architecture-IV

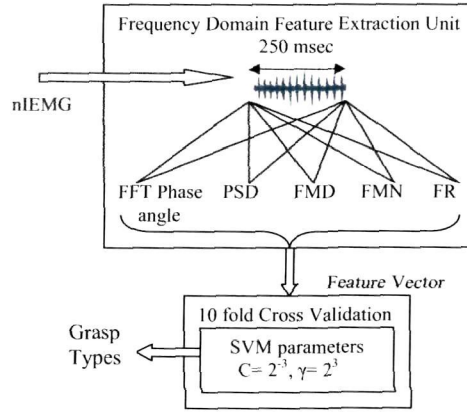


Figure 4.6: Classification with FD Features

Classifier Parameter Setting A range of value of $\log_2 c = \{-5, -4, -3, \dots, 5\}$ and $\log_2 \gamma = \{2, 2.2, 2.4, \dots, 3.8\}$ is considered for grid search. Figure 4.7 shows the grid

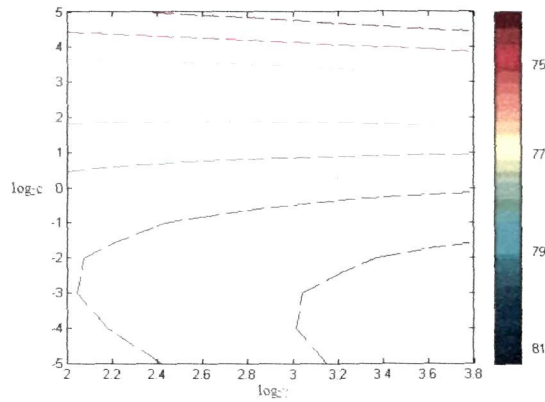


Figure 4.7: Results of Grid search for finding the values of C and γ with FD features

search result for FD features. A value of $c = 2^{-3}$ and $\gamma = 2^3$ was chosen for classification.

4.1.2.3 Results with Frequency Domain Features

Cross Validation The results of each testing fold for 10 fold cross validation based on FD features are shown in Table 4.3. The average recognition rate for each grasp type with FD features during each test for 10-fold cross validation is shown in Figure 4.8.

4.1 Grasps Recognition Architecture-IV

Table 4.3: Recognition rates in % with the testing folds along the columns and grasp types along the rows obtained through 10-fold cross validation based on FD Features.

	1st	2nd	3rd	4th	5th	6th	7th	8th	9th	10th
Hook	62.5	75	75	75	75	75	100	100	100	75
Oblique	87.5	87.5	75	75	75	75	87.5	87.5	75	75
Palm-up	75	75	100	100	87.5	87.5	87.5	87.5	87.5	87.5
Power	75	87.5	87.5	75	87.5	87.5	87.5	87.5	87.5	87.5
Pinch	75	75	75	75	75	62.5	87.5	87.5	62.5	75
Precision	62.5	62.5	87.5	87.5	62.5	62.5	87.5	87.5	62.5	62.5

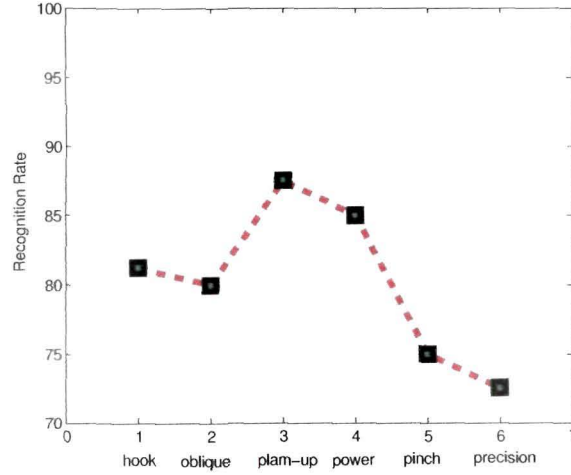


Figure 4.8: Recognition Rate with FD Features

The confusion matrix in Figure 4.9 shows the classification and misclassification of the grasp types based on FD features. Following the formulation for recognition rate as detailed in section 4.1.1.3 and results from Figure 4.8 and Figure 4.9, it is found that the FD features gives an average misclassification rate of 19%; 18.75% hook is misclassified as oblique and power, 20% oblique is misclassified as hook and power, 12.5% palm-up is misclassified as hook and oblique, 15% power is misclassified as hook and oblique, 25% pinch is misclassified as precision and hook, 27.5% precision is misclassified as hook and pinch. The average recognition rate for six grasp types with FD features is 81%.

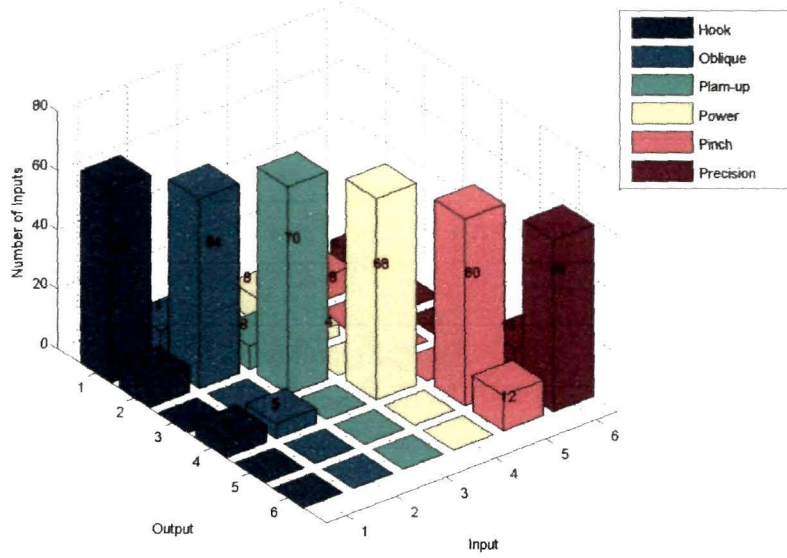


Figure 4.9: Confusion Matrix for classification based on FD Features

Table 4.4: ANOVA with FD Features

Source	ss	df	MS	F	Prob.
Columns	1.01156e+008	1	1.01156e+008	12.34	0.0079
Errors	6.56027e+007	8	8.20033e+006		
Total	1.66759e+008	9			

4.1.2.4 Linear Relationship

Finding the recognition rates of the grasp types based on FD features; the linear relationship of the FD features has been evaluated following the formulation in section 4.1.1.4. The R^2 -value derived through one-way ANOVA. The results of ANOVA analysis is tabulated in Table 4.4.

The R^2 -value is calculated as follows:

$$\begin{aligned}
 R^2 - \text{value} &= 1 - SS(\text{Error})/SS(\text{Total}) \\
 &= 1 - 0.39 \\
 &= 0.61
 \end{aligned}$$

It has been found that the average recognition rate with FD features is higher as com-

pared to TD features. The R^2 - value for FD features also reflect that FD features are having more information about the grasp types than TD features. In search of a feature set with a higher grasp recognition rate as well as with a higher linear relationship with the grasp types; rest experiments have been conducted with TFD features.

4.1.3 Classification with Time/ Frequency Domain Feature

4.1.3.1 Feature Set

WT provides a time/ frequency representation of a signal. The WT is a signal decomposition method on a set of basis functions, obtained by dilations, contractions and shifts of a unique function, the wavelet prototype. They are much better suited for representing short bursts of high-frequency signals or long-duration, slow varying signals. EMG signals do have such behavior and hence wavelet transform should be an ideal tool for their analysis (45).

WT can be classified as CWT and DWT. The wavelets forming a CWT are subjected to the uncertainty principle of Fourier analysis (44). Further in CWT, calculating wavelet coefficients at every possible scale is a fair amount of work and it generates an awful lot of data (136). In contrast, DWT may be considered in the context of uncertainty principle (44) as well as for dealing with smaller size coefficients. In the case of DWT, a time-scale representation of the signal is obtained using digital filtering techniques and the scale is determined by up sampling and down sampling operations (45). The signal to be analyzed is passed through filters with different cut-off frequencies at different levels. At each decomposition level, the half band filters produce signals spanning only half the frequency band. This doubles the frequency resolution as the uncertainty in frequency is reduced by half. With this approach, the time resolution becomes arbitrarily good at high frequencies, while the frequency resolution becomes arbitrarily good at low frequencies (44). DWT decomposes a signal into an approximation signal and detail signal. The detail coefficients D_j and the approximation coefficients A_j at level j can be obtained by filtering the signal with an L -sample high pass filter g , and an L -sample low pass filter h . Both approximation and detail signals

are down sampled by a factor of two (137). This can be expressed as follows:

$$A_j[n] = H\langle A_{j-1}[n] \rangle = \sum_{k=0}^{L-1} h[k]A_{j-1}[2n - k]$$

$$D_j[n] = G\langle D_{j-1}[n] \rangle = \sum_{k=0}^{L-1} g[k]A_{j-1}[2n - k]$$

where H and G represent the convolution/ down sampling operators. Sequences g[n] and h[n] are associated with wavelet function $\psi(t)$ and the scaling function $\phi(t)$ through inner products:

$$g[n] = \langle \psi(t), \sqrt{2}.\psi(2t - n) \rangle$$

$$h[n] = \langle \phi(t), \sqrt{2}.\phi(2t - n) \rangle$$

In theory, there exist an infinite set of wavelet functions. Following Phinyomark (138), we consider five basic wavelet functions: Symlet 4, Coiflet 2, Daubechies (db2), Biorthogonal (bior 1.3) and Harr. The dominant energy of EMG signals is concentrated in the range of 10-150 Hz (138). In order to extract the most important features, we used third level of DWT decomposition approximate coefficients for feature extraction (139). The approximate coefficients contain the most important information of the signal (120) and is therefore used for deriving the feature set. The approximate coefficients obtained through Symlet 4, Coiflet 2, db2, bior 1.3 and Haar DWT for the six grasp types are shown in Figure 7.0 through 7.0 in Appendix-II. The energy, zero crossings, turning points, mean absolute value, RMS value, variance, sum of DWT approximate coefficients constitute the feature set. The DWT based EMG features were derived as follows:

- Energy of Approximate Wavelet Decomposition Coefficients (EWC)

$$EWC = \int_{-\infty}^{\infty} A_j[n]^2 dt$$

where

$A_j[n]$ is the wavelet decomposition approximate coefficients at level j.

- Sum of Wavelet Decomposition Coefficients (SWC¹)

$$SWC = \sum_{n=1}^N A_j[n]$$

- Mean Absolute Value of Wavelet Decomposition Coefficients (MWC)

$$MWC = 1/N \sum_{n=1}^N |A_j[n]|$$

where

N is the total number of wavelet coefficients.

- Variance of Wavelet Decomposition Coefficients (VWC)

$$VWC = 1/N - 1 \sum_{n=1}^N A_j[n]^2$$

- Zero Crossings of Wavelet Decomposition Coefficients (ZWC)

$$ZWC = \sum_{n=1}^N F(A_j[n].A_j[n-1])$$

where

$$\begin{aligned} F &= 1 \text{ if } A_j[n].A_j[n-1] < 0. \\ &= 0 \text{ elsewhere} \end{aligned}$$

- Turning points of Wavelet Decomposition Coefficients (TWC)

$$TWC = \sum F(((a-1) - a) < 0)$$

where

$$\begin{aligned} a &= 1 \text{ if } A_j[n] > A_j[n-1] \\ a &= -1 \text{ if } A_j[n] < A_j[n-1] \\ F &= 1 \text{ if } ((a-1) - a) < 0. \end{aligned}$$

¹SWC corresponds to the frequency components of the original signal (100)

- RMS Value of Wavelet Decomposition Coefficients (RMSWC)

$$RMSWC = 1/N \sqrt{\sum_{n=1}^N A_j[n]^2}$$

With the wavelet mother function as rows and above features as columns, the feature matrix is constructed. The feature set of seven features obtained for two channel EMG signals; over 5 discrete wavelet functions constitute the feature matrix of size (5 × 14).

4.1.3.2 Classifier

During experiment with TFD features, the Feature Extraction and Classification Unit of the proposed architecture shown in Figure 5.4 is as shown in Figure 4.10. The nIEMG signal is transformed into TFD through Symlet 4, Coiflet 2, db2, bior 1.3 and Harr wavelet functions. The approximate coefficients at third level of decomposition of each wavelet function is used for feature extraction. The energy, zero crossings, turning points, mean absolute value, RMS value, variance, sum of DWT approximate coefficients has been derived following the mathematical definitions described in section 4.1.3.1.

Classifier Parameter Setting A range of value of $\log_2 c = \{-5, -4, -3, \dots, 5\}$ and $\log_2 \gamma = \{2, 2.2, 2.4, \dots, 3.8\}$ is considered for grid search. Figure 4.11 shows the grid search result for TFD features. A value of $c = 2^{-2}$ and $\gamma = 2^{2.6}$ is chosen for classification.

4.1.3.3 Results with Time/ Frequency Domain Features

Cross Validation The results obtained with 10-fold cross validation based on TFD features are shown in Table 4.5. The average of the 10-fold cross validation results gives the average recognition rate for each grasp types.

Figure 4.12 shows the recognition rate for each grasp types with TFD features. The classification and misclassification of the grasp types based on the TFD features are shown in the confusion matrix in Figure 4.13. From Figure 4.13, it is found that the TFD features gives an average misclassification rate of 11.03%; 8.75% hook is misclassified as oblique and power, 10% oblique is misclassified as hook and power, 12.5% palm-up is misclassified as hook, oblique and power, 10% power is misclassified

4.1 Grasps Recognition Architecture-IV

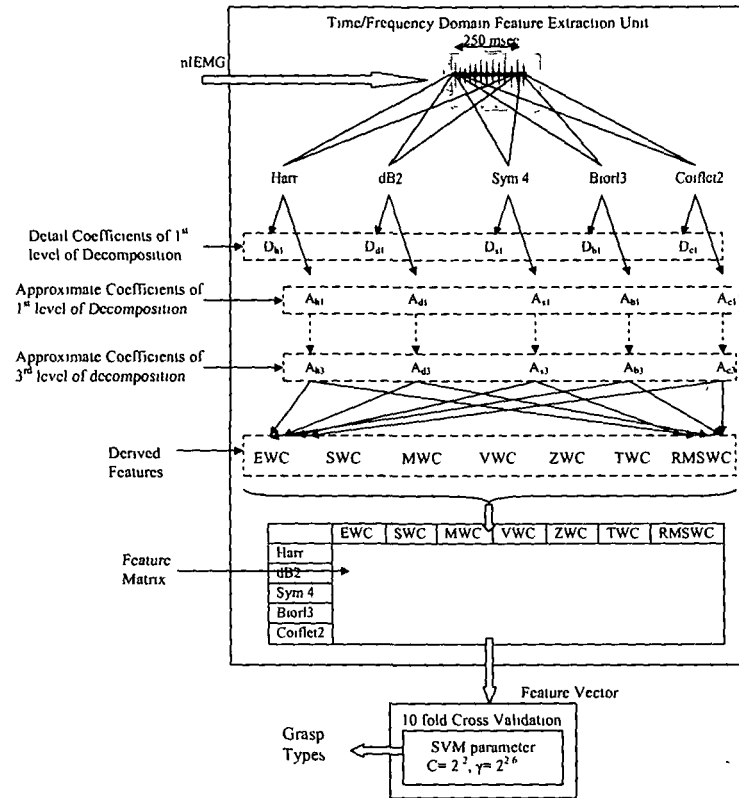


Figure 4.10: Classification with TFD Features

Table 4.5: Recognition rates in % with the testing folds along the columns and grasp types along the rows obtained through 10-fold cross validation based on TFD Features.

	1st	2nd	3rd	4th	5th	6th	7th	8th	9th	10th
Hook	75	87.5	87.5	87.5	100	87.5	100	100	100	87.5
Oblique	87.5	87.5	100	87.5	75	87.5	100	75	100	100
Palm-up	87.5	87.5	87.5	100	100	87.5	75	87.5	87.5	75
Power	87.5	87.5	100	87.5	87.5	100	75	100	75	100
Pinch	87.5	100	100	87.5	87.5	87.5	100	75	75	100
Precision	87.5	87.5	87.5	87.5	100	75	100	75	100	100

as hook and oblique, 10% pinch is misclassified as hook and precision, 10% precision is misclassified as hook and pinch. Provided these classification accuracy, the average

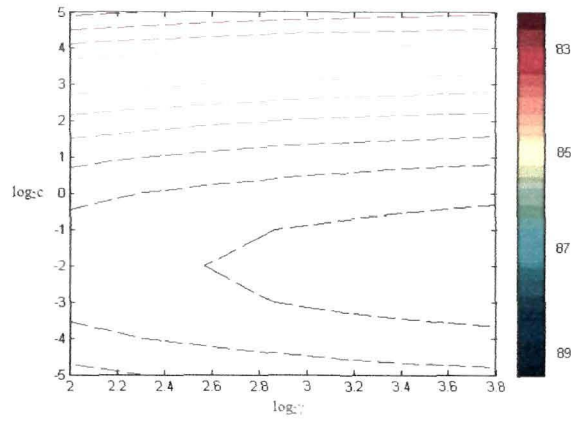


Figure 4.11: Results of Grid search for finding the values of C and γ with TFD features

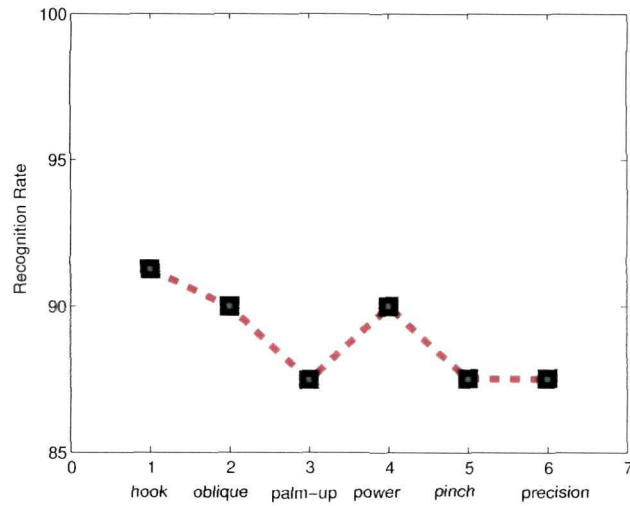


Figure 4.12: Recognition Rate with TFD Features

recognition rate for six grasp types with TFD features is 88.97%.

4.1.3.4 Linear Relationship

Finding the recognition rates of the grasp types based on TFD features; the linear relationship of the TFD features has been evaluated following the formulation in section 4.1.1.4. The R^2 -value derived through one-way ANOVA. The results of ANOVA analysis is tabulated in Table 4.6. The R^2 -value is calculated as follows:

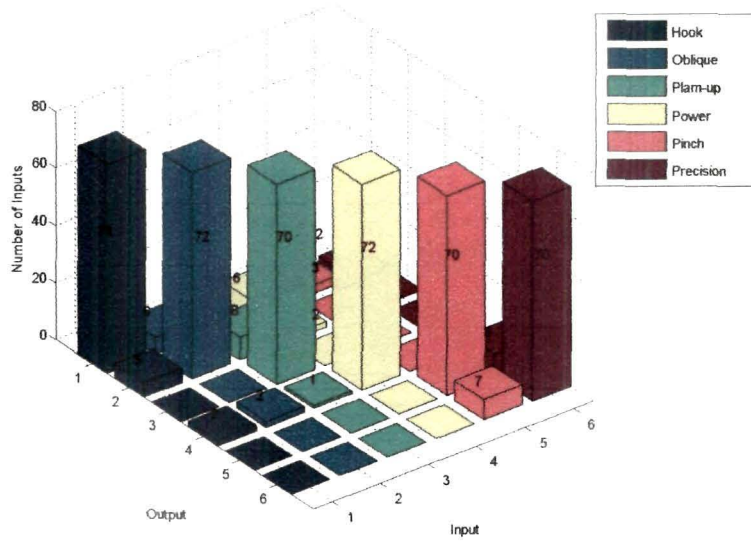


Figure 4.13: Confusion Matrix for classification based on TFD features

Table 4.6: ANOVA with TFD Features

Source	ss	df	MS	F	Prob.
Columns	1.94525	1	1.94525	18.48	0.0026
Errors	0.84226	8	0.10528		
Total	2.78751	9			

$$\begin{aligned}
 R^2 - \text{value} &= 1 - SS(\text{Error})/SS(\text{Total}) \\
 &= 1 - 0.30 \\
 &= 0.70
 \end{aligned}$$

It has been found that the recognition rate with TFD features is higher than that of TD and FD features. Also the linear relationship as reflected by R^2 -value is higher for TFD features than TD and FD features.

4.1.4 Classification with PCA of Time/ Frequency Domain Feature

4.1.4.1 Feature Set

The reduction in dimensionality of the feature set as well as deriving a feature vector with uncorrelated feature components is often necessary for increasing classification performance. This process preserve as much of the relevant information as possible while reducing the number of dimensions. Feature projection methods such as PCA identifies the best subset of features combining the original features into a smaller feature set (123).

In order to obtain the most informative and distinguishing low dimensional feature vector, PCA is applied on the feature matrix of DWT based EMG features derived in section 4.1.3.1. By dimensionality reduction, classes can be computed more efficiently and easily by the classification algorithm (42). The steps for PCA implementation is presented in equations from 4.1 to 4.4.

1. Subtract the mean from the data to accomplish zero mean data

$$\bar{x}[n] = x[n] - E[x] \quad (4.1)$$

where $x[n]$ and $E[x]$ are the data and mean respectively.

2. Obtain the covariance matrix of the data

$$C_x = \frac{1}{N}(E[x]E[x]) \quad (4.2)$$

3. Determine the eigenvectors and corresponding eigen values of the covariance matrix.

$$[\vec{v}, \nu] = eig(C_x) \quad (4.3)$$

where \vec{v} represents the eigen vectors and ν is the eigen values.

4. After sorting the eigenvalues in descending order, first three corresponding eigen values are chosen for further experiment. The projected data which contains the feature vector is given by equation 4.4.

$$y = x[n].\vec{v}(1 : k) \quad (4.4)$$

where $n > k$ and k is the desired reduced dimension. This algorithm tunes the signal for classification and generally improves classification accuracy (140).

The covariance matrix is of size (5×5) whose eigen vectors are principal components (PCs) and respective eigen values are PC weights (i.e. the amount of explained variance). The PCs are then ordered in descending order according to their weights and first three PCs are chosen for further experiment. Now multiplying the PCs matrix by original feature matrix, a new (3×14) dataset is obtained whose values are uncorrelated. This new dataset is the derived feature vector. The classifier used for classification with PCA of TFD features is the one detailed in section 4.1.3.2 followed by the steps discussed in section 4.1.4.1.

4.1.4.2 Classifier Parameter Setting

A range of value of $\log_2 c = \{-5, -4, -3, \dots, 5\}$ and $\log_2 \gamma = \{2, 2.2, 2.4, \dots, 3.8\}$ is considered for grid search. Figure 4.14 shows the grid search for result for PCA of TFD features. A value of $c = 2^{-1}$ and $\gamma = 2^{2.2}$ is chosen for classification.

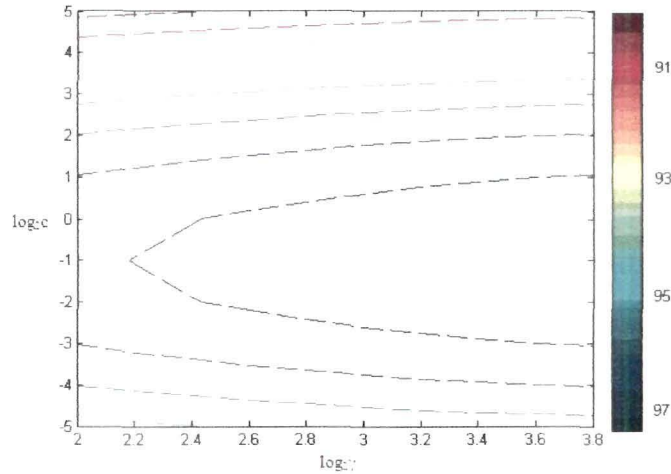


Figure 4.14: Results of Grid search for finding the values of C and γ with PCA of TF domain features

4.1.4.3 Results with PCA of Time/ Frequency Domain Features

Cross Validation The results obtained during 10-fold cross validation based on the PCA of TFD features are shown in Table 4.7.

Table 4.7: Recognition rates in % with the testing folds along the columns and grasp types along the rows obtained through 10-fold cross validation based on PCA of TFD features.

	1st	2nd	3rd	4th	5th	6th	7th	8th	9th	10th
Hook	100	100	100	100	100	100	100	100	87.5	100
Oblique	100	87.5	100	100	100	87.5	100	100	100	100
Palm-up	100	100	100	100	87.5	100	100	100	100	87.5
Power	87.5	100	100	100	100	100	100	100	100	100
Pinch	100	100	87.5	100	100	100	100	75	100	100
Precision	100	100	100	100	75	100	100	100	100	87.5

Figure 4.15 shows the recognition rate for each grasp types with PCA of TFD features. The classification and misclassification of the grasp types based on the PCA

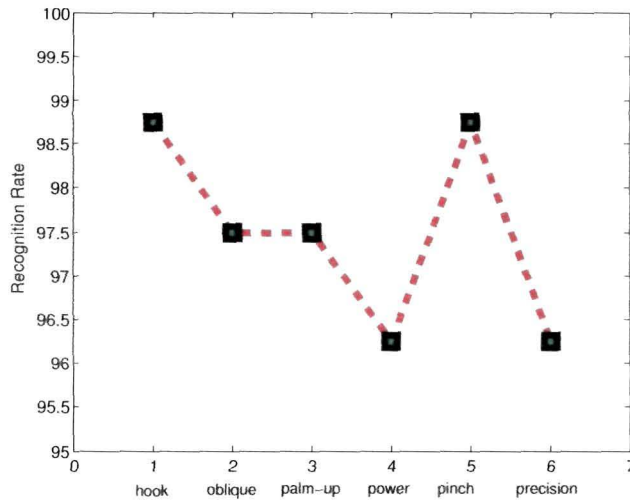


Figure 4.15: Recognition Rate with PCA of TFD features

of TFD features are shown in the confusion matrix in Figure 4.16. From Figure 4.16, it is found that the PCA of TFD features gives an average misclassification rate of 2.5%; 1.25% hook is misclassified as oblique, 2.5% oblique is misclassified as hook, 2.5% palm-up is misclassified as oblique, 3.5% power is misclassified as hook, 1.25% pinch is misclassified as precision, 3.75% precision is misclassified as pinch. The average recognition rate for six grasp types with PCA of TFD features is 97.5% (141).

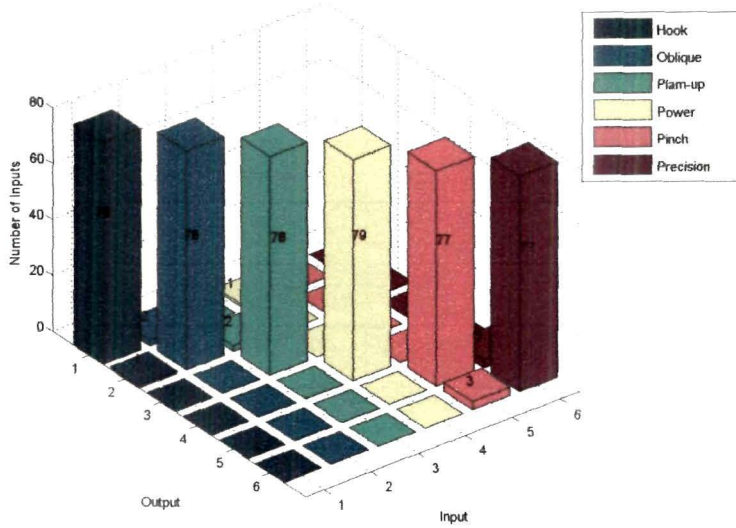


Figure 4.16: Confusion Matrix for classification based on PCA of TFD features

Table 4.8: ANOVA with PCA of TFD Features

Source	ss	df	MS	F	Prob.
Columns	1.24737e+008	1	1.24737e+008	25.63	0.001
Errors	3.89392e+007	8	0 4.86741e+006		
Total	1.63676e+008	9			

4.1.4.4 Linear Relationship

Finding the recognition rates of the grasp types based on PCA of TFD features; the linear relationship of the PCA of TFD features has been evaluated following the formulation in section 4.1.1.4.

The R^2 -value is derived through one-way ANOVA. The results of ANOVA analysis is tabulated in Table 4.8.

The R^2 -value is calculated as follows:

$$\begin{aligned}
 R^2 - value &= 1 - SS(Error)/SS(Total) \\
 &= 1 - 0.23 \\
 &= 0.77
 \end{aligned}$$

It is seen that the PCA of TFD features have highest linear relationship with the grasp types as well as the grasp recognition rate obtained using PCA of TFD features is comparable to that reported in the literature (122). Following these, the next step of the experiment has been done for evaluating the relative performance of the feature sets.

4.2 Statistical Analysis

The purpose of statistical analysis in pattern recognition is to assess the classification results (142). Although the uncertainty associated with engineering experiments is generally far less and can often be quantified through carefully controlled experiments; the interest for statistical evaluation for the experiments on EMG classification have changed over the past decade due to its complex patterns and random behaviour. Moreover, the pattern recognition algorithms are probabilistic in nature (143). Furthermore, many of the experimental results are subjected to database samplings and sizes. To know the truth of the experimental results, one needs to evaluate it through statistical means. Statistical analysis is used to evaluate the relative significance of the feature sets considered for classification of grasp types vis-a-vis the results of grasp recognition architecture-IV. Please note that statistical analysis as discussed here has no role in distilling the decided feature vector and is not required to be performed in real-time environment. Statistical analysis has been accomplished in two main steps:

- First the feature groups under study were subjected to one-way ANOVA with feature set as a factor and rejects the null hypothesis of equal means. In order to find the differences between two groups of feature sets, ANOVA was performed between TD and FD, TD and TFD, TD and PCA of TFD, FD and TFD, FD and PCA of TFD, TFD and PCA of TFD.
- The relative performance of the feature sets have been evaluated through Scheffe's post hoc test using the results of ANOVA.

4.2.1 ANOVA analysis

Following the discussion on ANOVA analysis in section 4.1.1.4, one way ANOVA was performed to find the significance of variance of the four feature sets under study using

the Statistical Toolbox in Matlab 2009. The results of ANOVA analysis for each two feature sets under study are tabulated in Table 4.9 through Table 4.14 wherein MS = Mean square error, df = Degrees of freedom, p-value = probability value. The number of groups represents the number of feature sets under study and the size of groups represents the number of features in the feature sets. These results provides the significance of variance for the features sets under study. It is common to declare that a ANOVA result is significant if the p-value is less than 0.05 (144). From the Table 4.9, it is seen that the variance of TD and FD features are not of significance.

Table 4.9: ANOVA Results for TD (G_1) and FD (G_2) features

Parameters	Values
MS	0.003
df	9
Number of Groups (G_N)	2
Size of Group 1 (G_1)	5
Size of Group 2 (G_2)	5
p-value	0.11

From the Table 4.10 through Table 4.14, it is clear that the variance of TD features with TFD as well as with PCA of TFD features; FD features with TFD as well as with PCA of TFD features are of significant. These values are evaluated to find the relative significance of the features sets under study through Scheffe's post hoc test.

Table 4.10: ANOVA Results for TD (G_1) and TFD (G_2) features

Parameters	Values
MS	0.0003
df	9
Number of Groups (G_N)	2
Size of Group 1 (G_1)	5
Size of Group 2 (G_2)	35
p-value	0.02

Table 4.11: ANOVA Results for TD (G_1) and PCA of TFD (G_2) features

Parameters	Values
MS	0.0001
df	9
Number of Groups (G_N)	2
Size of Group 1 (G_1)	5
Size of Group 2 (G_2)	25
p-value	0.005

Table 4.12: ANOVA Results for FD (G_1) and TFD (G_2) features

Parameters	Values
MS	0.0001
df	9
Number of Groups (G_N)	2
Size of Group 1 (G_1)	5
Size of Group 2 (G_2)	25
p-value	0.0153

Table 4.13: ANOVA Results for FD (G_1) and PCA of TFD (G_2) features

Parameters	Values
MS	0.00008
df	9
Number of Groups (G_N)	2
Size of Group 1 (G_1)	5
Size of Group 2 (G_2)	25
p-value	0.014

4.2.2 Sheefe's Post hoc Test

The relative significance of the feature groups were evaluated through Sheefe's post hoc test. Whenever an ANOVA is used to examine the differences among more than two groups, a post hoc procedure is used to compare differences between all pairs of

Table 4.14: ANOVA Results for TFD (G_1) and PCA of TFD (G_2) features

Parameters	Values
MS	0.00008
df	9
Number of Groups (G_N)	2
Size of Group 1 (G_1)	35
Size of Group 2 (G_2)	25
p-value	0.0075

means. Post hoc comparisons are more appropriate for multiple tests. Sheffe's post hoc test is a statistical test that is used to make comparisons among group means in ANOVA experiment. Sheffe's post hoc test are used when [i] sample sizes are unequal and [ii] most conservative test is desired. Following the ANOVA analysis results in section 4.2.1, Sheffe's post hoc test are performed using the on-line tool available at www.statstodo.com (145). Table 4.15 shows the significance levels among the pairs of features. The bold entries represent a mean difference among the feature sets that are

Table 4.15: Results of Sheffes post hoc test upon the recognition obtained using four sets of features

Feature Set I	Feature Set II	Significance, P
Time Domain	Frequency Domain	0.110
	Time/ Frequency Domain	0.020
	PCA of Time/ Frequency Domain	0.005
Frequency Domain	Time Domain	0.110
	Time/ Frequency Domain	0.025
	PCA of Time/ Frequency Domain	0.014
Time/ Frequency Domain	Time Domain	0.020
	Frequency Domain	0.025
	PCA of Time/ Frequency Domain	0.027
PCA of Time/ Frequency Domain	Time Domain	0.005
	Frequency Domain	0.014
	Time/ Frequency Domain	0.027

significant. From the experiment between TD features with other three feature sets, it has been found that the difference of TD features with respect to TFD and PCA of TFD features are significant but not the case with FD features. From the experiment between FD features and other feature sets, it has been found that the difference of the FD features with respect to the TFD and PCA of TFD features are significant but not the case with TD features. This satisfies the significant level between TD and FD features as found in the experiment with TD features. From the experiment between TFD features with other features, it has been found that the difference of the TFD features with respect to the TD, FD as well as PCA of TFD features are significant. From experiment between PCA of TFD with other feature sets, it has been found that the difference of the PCA of TFD features is significant with respect to the TD, FD and TFD features. This is in line to the results of the experiments with the other three feature sets. Moreover, the significant levels resulted in Sheffe's post hoc test are in line with the recognition rates obtained using TD, FD, TFD and PCA of TFD features through the grasp recognition architecture-IV. e.g. Recognition rates with TD and FD features are not of much difference as compared to that with the TFD and PCA of TFD features. Likewise, the case is true for FD, TFD and PCA of TFD features.

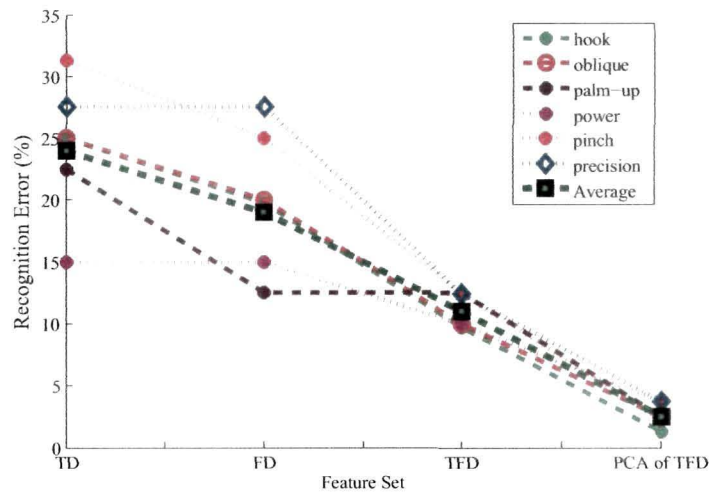
4.3 Summary

Four sets of EMG features: TD, FD and TFD were evaluated for classification of six grasp types used during 70% of DLA. Features obtained through PCA of DWT based EMG features produced highest recognition rate of 97.5%. As tabulated in Table 4.16, grasp classification based on PCA of TFD feature vector is better as compared to those reported in literature in terms of [i]. recognition rate [ii]. number of EMG channels used and [iii]. number of grasp types recognized. Figure 4.17 shows grasp recognition error averaged across the subjects for the four feature sets. The recognition rate increases as the feature set progresses from TD to PCA of TFD. Further, PCA of TFD have lowest recognition error across all grasp types. The results of this chapter highlight the following:

- PCA of TFD have the highest linear relationship with grasp types.
- PCA of TFD is the most superior feature set among the feature sets examined.

Table 4.16: Comparison of Grasp Types Recognition Rates

Author	Number of Grasp Types	Number of EMG Channels	Recognition Rates
Ferguson and Dunlop(43)	Four	Four	75-80%
Martelloni et al. (79)	Three	Eight	84-93%
Castellini et el. (22)	Three	Ten	90%
Castellini et al. (80)	Two	Seven	97%
PCA based Classification (141)	Six	Two	97.5%

**Figure 4.17:** Grasp Recognition Error Average across all Subjects; Also shown is the grasp recognition error for each grasp type

- There is a distinct trend towards improvement of recognition rates in TD features → frequency domain features → TFD features → PCA of TFD features.

The superior result using PCA of TFD features can be substantiated by the fact that statistical independence of the features is achieved through dimensionality reduction using PCA. In the original feature set, information is liberally dispersed amongst the original feature set, PCA consolidate this information much more effectively by discarding less useful information. TD and FD features possess only temporal and spectral features respectively; whereas TFD features represents the original signal over both time and frequency.

5

A Biomimetic Hand: Prototype 1.0

This chapter details the development of a five fingered extreme upper limb prosthetic hand prototype: Prototype 1.0. The focus is on emulating the six grasping operations involved during 70% of dfa using EMG based grasps classification.

The approach for development of an anthropomorphic hand should be to take reference of human hand (146). Biomimetic approach for development of a prosthetic hand has appeared as a significant opportune towards mimicking the natural counterparts (147) as well in tackling the challenges of present artificial hands (148). Biomimesis is the understanding of nature, its models, systems, processes and elements to emulate or take inspiration from these designs and processes; and imitate them into artificial system (149, 150). Although some of the laboratory prototypes (2, 14, 15) have been developed following biomimetic approaches, they are far from the human hand in terms of the static and dynamic constraints (12).

The biomimetic approach is followed to harmonize both physical and functional aspects of the human hand. The emulation of grasp types is through a two layered architecture: SHC and LHC. SHC is for recognition of user's intended grasp based on EMG signals and LHC is for actuating the fingers in the prototype to emulate the identified grasp. Prototype 1.0 can perform the six grasp types under static and dynamic constraints, which are responsible for natural movement (151).

5.1 Biomimetic Approach

An ideal upper limb prototype should be perceived as a part of the natural body by the amputees. Towards this goal, Prototype 1.0 is developed following a biomimetic approach as shown in Figure 5.1. The approach comprises of five steps. It involves: [i] Study of the human hand physiology [ii] Material selection based on the expected properties in the prototype [iii] development of bio-mechanical structure ¹ [iv] development of control architecture [v] development of biomimetic hand prototype. Study of

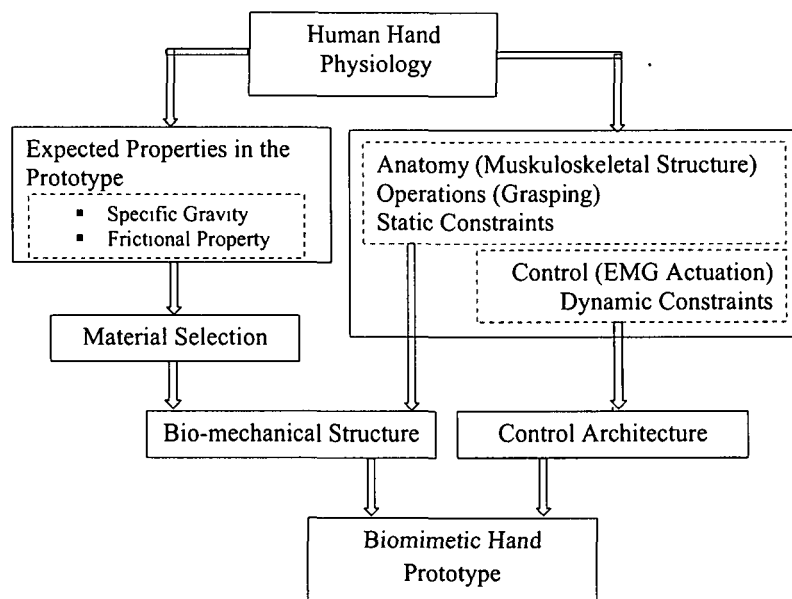


Figure 5.1: Biomimetic Approach followed for development of Prototype 1.0

the human hand physiology in terms of the anatomy, grasping operations, static and dynamic constraints, EMG based actuation; the first stage of the biomimetic approach is detailed in Chapter 2.

¹With reference to (152), bio-mechanical structure means the the physical representation of human hand anatomy quantitatively for this research

5.1.1 Material selection

The approach for building the prototype is to duplicate any of the features and properties which affect the characteristics of human hand. So the work seek to use materials that can mimic the human hand properties. The goal has always been for size and weight similar to human hands vis-a-vis grasp functionality. Following (153), two properties, specific gravity and coefficient of friction have been considered for material selection. Heavy weight is one of the main reasons for non-acceptance of artificial hands by the amputees (154). Moreover, an object grasped by the hand should not slip. These leads to specific gravity and coefficient of friction as the important properties for selection of the material to be used for development of the prototype. Following (153) and (155), four materials: nylon, teflon, steel and aluminum are under study. From Table 5.1, nylon and teflon are found to bear properties close to that of human hand. Nylon is stable, undeformable and has low friction and low specific gravity. Further, cost of nylon is more than five times lesser than that of teflon. Therefore, nylon is selected for the skeletal structure of the hand. The building blocks of the human hand and that of Prototype 1.0 are tabulated in Table 5.2.

Table 5.1: Comparison of primitive characteristics (required to replicate human hand properties) for four materials under study

	Nylon	Teflon	Steel	Aluminum	Human Hand
Specific Gravity	1.13	2.15	7.85	2.64	0.96 - 1.2
Co-efficient of friction	0.15 - 0.25	0.04	0.8	1.35	0.72 - 0.7

Table 5.2: Building blocks of Human hand versus the Prototype 1.0

Human Hand	Prototype 1.0
The skeletal of the hand	Nylon as links, joints and palm
Set of muscles, which are embedded in between the skin surface and skeleton	A set of DC geared motors embedded in the palm
Mass-spring system, inter-linking the skin, skeleton and muscle	Tendon system interlinking the skeletal and actuators
Joint hierarchy which matches the structure of the skeleton	A joint hierarchy which matches the structure of natural hand

5.1.2 Bio-mechanical Structure

The development of the mechanical prototype is based on the knowledge gathered from the study of the human hand physiology. The skeletal structure of the prototype is developed using the material selected with reference to the study carried out in section 5.1.1.

Human anatomical terminologies has been used to describe Prototype 1.0. The prototype comprises of five fingers. Each finger consists of three links replicating the distal, middle and proximal phalanges of human finger; thumb consist of two links. The links are connected through revolute joints corresponding to DIP, PIP and MCP joints. The palm is two piece and can move inward and outward to form grasp modes. The palm accommodates the actuators. The wrist is of two concentric cylindrical structures made of nylon.

In the prototype, the joints have been obtained with an extended knuckle structure at each link to prevent the backward movement of the succeeding link. The curvature of the phalanges are with reference to the human anatomical structure and therefore can flex and extend in the joint range corresponding to the human finger as recorded in Table 5.3.

Table 5.3: Finger joint range of motion of the prototype (in degrees) measured using Jamar Plastic Goniometer

	Thumb	Index	Middle	Ring	Little
MCP Flexion	0 to 100	0 to 90	0 to 90	0 to 90	0 to 90
PIP Flexion		0 to 110	0 to 110	0 to 110	0 to 110
DIP Flexion	0 to 90	0 to 70	0 to 70	0 to 70	0 to 70

Figure 5.2(a) shows the dimensional representation of the index finger. Figure 5.2(b) is a planner schematic structure of the index finger and 5.2(c) represents the routing of the tendons through the joints of the finger. Figure 5.2(b) and (c) are for kinematic and dynamic analysis of the prototype as detailed in section 5.1.3.

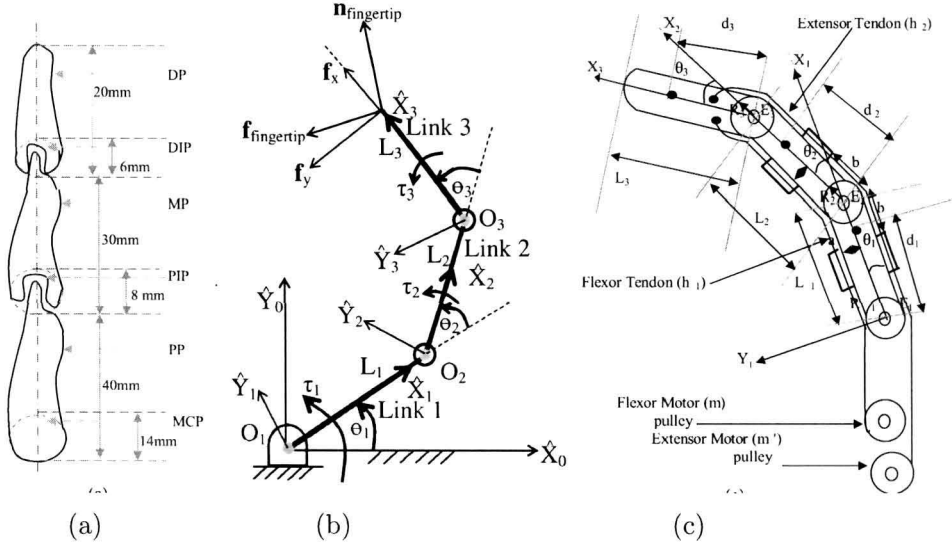


Figure 5.2: (a) Dimensional representation of the index finger. The lengths of the proximal, middle and distal phalanges are 40 mm, 30 mm and 20 mm respectively. The radius of rotation (R_1, R_2, R_3) of the three joints (MCP, PIP and DIP) are 14 mm, 8 mm and 6 mm respectively. (b) A planner schematic structure of a finger (other than the thumb). Each link L_i ($i = 1, 2, 3$) corresponds to the proximal, middle and distal phalanges. MCP, PIP and DIP joint angles are θ_1, θ_2 and θ_3 respectively. (c) Tendon routing the finger joints. d_1, d_2 and d_3 are the distance of the center of mass of the phalanges from the respective joints MCP, PIP and DIP (E_1, E_2 and E_3) respectively. I_1, I_2 and I_3 are the moment of inertias of the three phalanges about an axis passing through their center of masses. m_1, m_2 and m_3 are the masses of the proximal, middle and distal phalanges respectively. a and b are half the finger width and distance of the tendon guides from the finger joints.

Each finger is actuated with two motors; one for flexion and another for extension. The little and ring finger are actuated through the common motors. Abduction and adduction is not implemented in Prototype 1.0. The prehension of the palm is obtained through one single motor. The wrist of the prototype is actuated through three DC motors placed in mutually perpendicular axes. The developed prototype possess a total of $(3 \times 3 \text{ of fingers} + 2 \text{ of thumb} + 1 \text{ of the palm} + 3 \text{ of wrist}) = 15 \text{ DoF}$. Arrangement of the actuators and tendons as well as the digits of the prototype in its ventral view is shown in Figure 5.3. Each finger tip is equipped with film like force sensors to measure the fingertip force. The specification of the used actuator units (geared DC motors) are in Table 5.4.

Table 5.4: Specification of the Actuating Motors

Parameter	Finger Motor	Wrist Motor
Gear Ratio	0.03	0.06
No load Speed	250 Revolutions Per Minute (RPM)	300 RPM
No Load Torque	0.076 Nm	0.090 Nm
Diameter	160 mm	160 mm
Length	300 mm	350 mm
Diameter of motor pulley	10 mm	10 mm

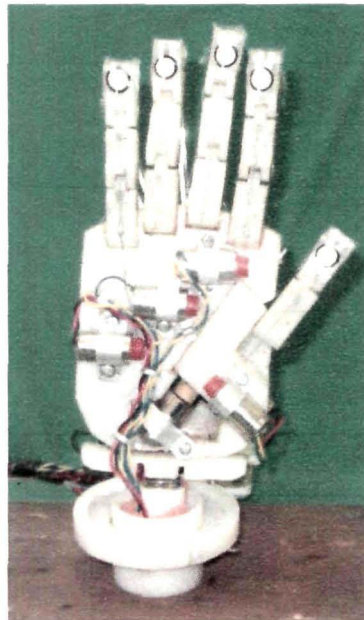


Figure 5.3: Ventral View of Prototype 1.0

5.1.2.1 Tendon System

$N + 1$ tendon configuration is used as media to transmit forces from actuators to the finger's joints. $N+1$ tendon configuration is one in which a single tendon pulls on all the joints in one direction and one or more additional tendons which generate torques in opposite direction (156). Such a system is important from a biomimetic point of view

5.1 Biomimetic Approach

as most of the muscles and tendons involve in flexion-extension of the human body parts form agonist-antagonist pair. In the prototype, the agonist and antagonist tendons mimic the flexor digitorum superficialis and flexor digitorum profundus; extensor digitorum communis and extensor indicis tendons of human finger (82). Thin tendons made of polymeric fibers have been used. Extensor and flexor tendons are placed on the dorsal and ventral side of each finger and connected to individual actuation unit in the palm. The tendons connected to the pulley of the motor, passing through a series of hollow guides are fixed at the finger tips. This replicates the agonist-antagonistic tendon system of human hand (157). Table 5.5 shows the characteristics of a human hand vis-a-vis Prototype 1.0.

Table 5.5: Characteristics of Human hand and Prototype 1.0

Characteristics	Human Hand	Prototype 1.0
Number of DoF	22	15
Wrist Mobility	03	03
Total Volume	50 cc	47cc
Each finger length	92 mm	90 mm
Each finger diameter	14 mm	14 mm
Wrist width	65 mm	65 mm
Palm width and thickness	90 mm and 45 mm	90 mm and 45 mm
Total weight	400 gram	520 gram

In this comparison, one of the distinguishing feature of the biomimetic hand from the human hand is the number of DoF. The thumb of Prototype 1.0 possess significantly lower DoF - two DoF as compared to the five DoF of the human hand thumb. Prototype 1.0 thumb possess two flexion-extension axis of rotation at DIP and MCP joint. However in human thumb, the DIP joint have one flexion-extension DoF, MCP and CMC joints have one flexion-extension and one abduction-adduction DoF in each. Further, the abduction-adduction of the remaining four fingers are not implemented in Prototype 1.0. This results in Prototype 1.0 with seven DoF lesser than that of the human hand.

5.1.3 Development of Control Architecture

The proposed control architecture is two layered: superior hand control (SHC) and local hand control (LHC). Figure 5.4 shows the schematic representation of the developed control architecture. SHC is to perceive the type of grasps attempted by the user and the LHC is to compute the grasp primitives i.e. finger joint torques and angles to emulate the identified grasp type.

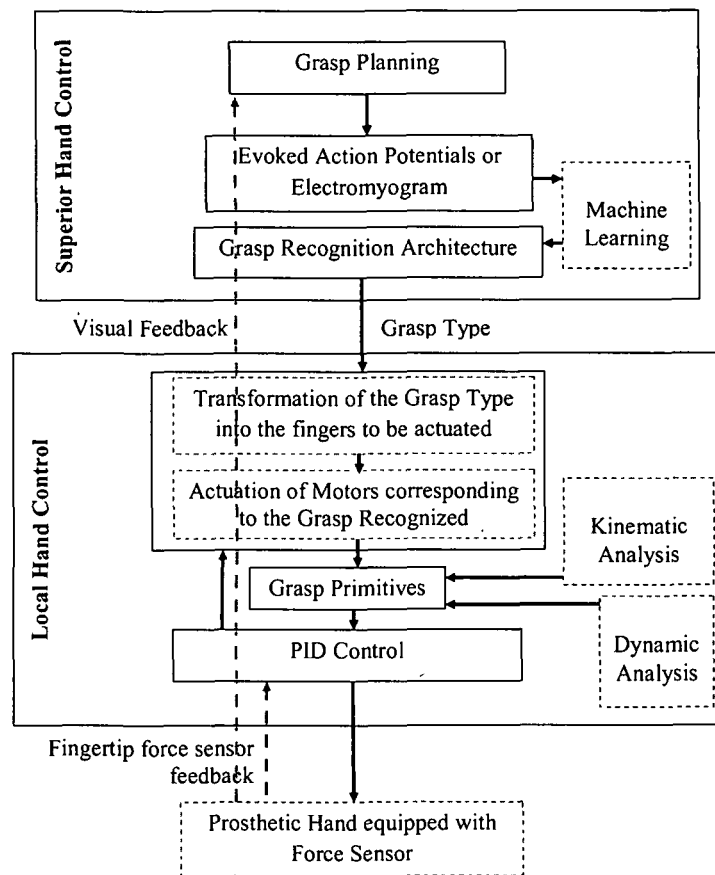


Figure 5.4: Schematic of Control Architecture indicating two main states: Superior Hand Control and Local Hand Control

5.1.3.1 Superior Hand Control

The SHC provides the information about the grasp types to be performed by Prototype 1.0 based on EMG signals acquired from forearm muscles. In accordance to the visual information about the object to be grasped, the human brain plans the type of grasp to be formed for holding the object. Accordingly, the motor commands generated in the brain are sent down through the spinal cord to the forearm muscles. The motor commands initiate the forearm surface EMG. The grasp recognition architecture recognizes the grasp type attempted by the user based on the forearm EMG.

The grasp recognition module comprises of four fundamental units: EMG Unit, MVC normalization Unit, Feature Extraction Unit followed by the Classifier Unit. The EMG unit comprises of the amplifier, band pass and notch filter. The EMG signals were acquired following the experimental protocol as detailed in section 3.1.1.1 in Chapter 3. The raw EMG signals extracted from the subjects required processing for accurate recording, display and analysis. The EMG signal obtained after filtration and amplification is called IEMG signal. The MVC normalization unit applies normalization algorithm to avoid the test case subjectivity and generates nIEMG signals. The characteristic patterns of a signal in a reduced dimension called *features* are extracted from nIEMG signals in the feature extraction unit and a feature vector is generated. The feature vector: PCA of TFD EMG feature is fed to the classifier. The classifier is a RBF kernel SVM. The details of the grasp recognition architecture is elaborate in Chapter 4 and here mentioned in brief for completeness. The information about the identified grasp type is passed to the LHC.

5.1.3.2 Local Hand Control

The LHC is the interface between the SHC and Prototype 1.0. Human hands are capable of grasping objects with dexterous motion. As such, fingers typically grasp by curling around the objects following stereotypical trajectories (158). Manual grasping is more stable and secure than the current prosthesis grasping. Therefore, it is of interest to reproduce the natural movement of fingers in order to perform stable grasping operations by the prosthetic hands.

LHC identifies the fingers to be actuated for performing the grasp type identified via SHC. The derivation of the grasp primitives are through kinematic, static and

dynamic analysis. Based on the kinematic and static analysis of the finger model as shown in Figure 5.2, the LHC determines the relation between the finger joint torques and the actuating motor torque. This is achieved satisfying the human finger dynamic constraints; responsible for stable grasping (151). Based on the joint angles for natural curling of the human finger (159), the finger joint torques are determined through dynamic analysis such that the joint angle trajectories are similar to that of the human finger. The corresponding finger-tip force is determined through kinematic and static analysis. A proportional integral derivative (PID) controller is implemented to maintain the fingertip force.

5.2 Kinematics, Statics and Dynamics

For kinematic, static and dynamic analysis, the index finger of Prototype 1.0 is schematically represented as shown in Figure 5.2(b). L_{c1}, L_{c2} and L_{3c} are the distance of the center of mass of the phalanges from the respective joints PIP, MCP and DIP shown as d_1, d_2 and d_3 respectively in Figure 5.2(b). R_1, R_2 and R_3 are the radius of the joints E_1, E_2 and E_3 . I_1, I_2 and I_3 be the moment of inertias of the three phalanges about an axis passing through their center of masses. m_1, m_2 and m_3 are the masses of the proximal, middle and distal phalanges respectively. The distance from the end of tendon guide to the finger joint is b and radius of the finger is a .

5.2.1 Kinematic Analysis of a Finger

The Denavit-Hartenberg parameters describing finger kinematics are illustrated in Table 5.6; where θ_i is the joint angle from X_{i-1} axis to X_i axis about Z_{i-1} axis, d_i is the distance from the origin of $(i-1)^{th}$ coordinate frame to the intersection of Z_{i-1} axis with X_{i-1} axis along Z_{i-1} axis, a_i is the offset distance from intersection of Z_{i-1} axis with X_i axis and α_i is the offset angle from Z_{i-1} axis to Z_i axis about the X_i axis with $i = 1, 2, 3$.

Direct kinematic equations are used to obtain the fingertip position and orientation according to the joint angles. With three revolute joints, the finger has three rotational DoF ($\bar{\theta} = \{\theta_1, \theta_2, \theta_3\}^T$) leading to the finger end effector having pose ($\bar{x} = \{x, y, \alpha\}^T$). To analyze the three joint link shown in Figure 5.2(b), the first step is to establish the mapping from joint angles (the vector of three generalized rotational coordinates

Table 5.6: Denavit-Hartenberg Parameters of the Finger

Link	α_{i-1}	a_{i-1}	d_i	θ_i
1	0	0	0	θ_1
2	0	$L_1 = 40 \text{ mm}$	0	θ_2
3	0	$L_2 = 30 \text{ mm}$	0	θ_3

$\bar{\theta} = \{\theta_1, \theta_2, \theta_3\}^T$) to link end point position and orientation of the finger for a given set of link lengths $\bar{L} = \{L_1, L_2, L_3\}$. From the Denavit-Hartenberg parameters of the finger as stated in Table 5.6, the fingertip pose \bar{x} with respect to the base frame can be computed as:

$$\bar{x} = G(\bar{\theta}) = \begin{bmatrix} G_x(\bar{\theta}) \\ G_y(\bar{\theta}) \\ G_\alpha(\bar{\theta}) \end{bmatrix}$$

$$\begin{bmatrix} x \\ y \\ \alpha \end{bmatrix} = \begin{bmatrix} L_1 C_1 + L_2 C_{12} + L_3 C_{123} \\ L_1 S_1 + L_2 S_{12} + L_3 S_{123} \\ \theta_1 + \theta_2 + \theta_3 \end{bmatrix} \quad (5.1)$$

where $G(\bar{\theta})$ is the geometric model defined by the trigonometric equations for the end point position $\{x, y\}^T$ and orientation $\{\alpha\}$ of the last link as a function of $\bar{\theta}$ and link lengths of the finger \bar{L} . C_1, C_{12} and C_{123} denotes $\cos\theta_1, \cos(\theta_1 + \theta_2)$ and $\cos(\theta_1 + \theta_2 + \theta_3)$ and S_1, S_{12} and S_{123} denotes $\sin(\theta_1), \sin(\theta_1 + \theta_2)$ and $\sin(\theta_1 + \theta_2 + \theta_3)$ respectively.

5.2.1.1 Tendon Actuation

Flexion and extension of the fingers is performed by pulling and releasing the flexor and extensor tendons. The finger joint angles depends on the tendon length pulled l_m and released $l_{m'}$ by the flexor motors. Tendon length while the finger is maximally extended is $l_o = L_1 + L_2 + L_3$. When the finger is flexed, the flexor tendon is pulled by the motor. Let l_x be the resulting flexor tendon length and $\theta_1, \theta_2, \theta_3$ be the joint angles respectively. Change in flexor tendon length l_m is the difference of l_o and l_x .

$$\begin{aligned}
 l_m &= l_o - l_x \\
 &= (L_1 + L_2 + L_3) - \\
 &\quad (L_1 C_1 + L_2 C_{12} + L_3 C_{123})
 \end{aligned} \tag{5.2}$$

Both anatomical and empirical studies show a linear inter-joint angular relationships in human finger expressed as dynamic constraints (12) and results in a natural curling motion of the fingers. The dynamic constraints of human hand finger is represented using the following

$$DC1 = \frac{\theta_1}{\theta_2} = 0.5 \tag{5.3}$$

$$DC2 = \frac{\theta_2}{\theta_3} = 1.5 \tag{5.4}$$

In order to replicate the natural motion of human finger into the prototype, the dynamic constraints of human fingers have been considered for computation of the tendon length. Substituting the constraints in equations (5.3) and (5.4) into equation (5.2), following relation between θ_1 and l_m is obtained.

$$\begin{aligned}
 l_m &= (L_1 + L_2 + L_3) - \\
 &\quad (L_1 \cos(\theta_1) + L_2 \cos(2.\theta_1) + L_3 \cos(4.\theta_1/3))
 \end{aligned} \tag{5.5}$$

In a similar way, the length of the extensor tendon released by the extensor motor is given as:

$$\begin{aligned}
 l_{m'} &= (L_1 + L_2 + L_3) + \\
 &\quad (L_1 \cos(\theta_1) + L_2 \cos(2.\theta_1) + L_3 \cos(4.\theta_1/3))
 \end{aligned} \tag{5.6}$$

Since, l_m is the length of the tendon pulled by the motor; l_m can be computed using equation 5.6 given diameter of the pulley connected to the motor, D ; time of rotation of the motor, δt and revolution per minute of the motor, N .

$$l_m = \pi DN \delta t \quad (5.7)$$

The values of D and N are known a priori as in Table 5.4. δt is computed from force sensory feedback. The start time is achieved from initiation of the actuating signal to the motor and the time of contact is on receiving a feedback signal from fingertip sensor.

5.2.2 Static Analysis of a Finger

5.2.2.1 Joint Torques and Fingertip Forces

The joint torques exactly balances finger tip forces in static equilibrium situations. The rotational kinetic input to the end effector is net of three torques ($\tau = \{\tau_1, \tau_2, \tau_3\}^T$) at MCP, PIP and DIP joints respectively to produce the output wrench vector

$$\bar{W} = \begin{pmatrix} {}^0\mathbf{f}_{fingertip} \\ {}^0\mathbf{n}_{fingertip} \end{pmatrix} \quad (5.8)$$

The Jacobian transpose maps finger tip forces into equivalent joint torques (156). The joint torques τ which balances the wrench vector \bar{W} is given as:

$$\tau = J(\theta)^T \bar{W} \quad (5.9)$$

Where $J(\theta)$ is the Jacobian matrix relating the joint space to the fingertip space.

The three link finger as shown in Figure 5.2(b) is applying force and moment through the fingertip on the environment. These are given by the following equations:

$${}^0\mathbf{f}_{fingertip} = (f_x, f_y, 0)^T \quad (5.10)$$

$${}^0\mathbf{n}_{fingertip} = (0, 0, n_z)^T \quad (5.11)$$

Let the forces ${}^{fingertip}\mathbf{f}_{fingertip}$ and moment ${}^{fingertip}\mathbf{n}_{fingertip}$ be denoted as $(f'_x, f'_y, 0)^T$ and $(0, 0, n'_z)^T$.

$$\begin{pmatrix} f'_x \\ f'_y \\ 0 \end{pmatrix} = \begin{bmatrix} C_{123} & S_{123} & 0 \\ -S_{123} & C_{123} & 0 \\ 0 & 0 & 1 \end{bmatrix} \cdot \begin{pmatrix} f_x \\ f_y \\ 0 \end{pmatrix} \quad (5.12)$$

and

$$(0, 0, n'_z)^T = (0, 0, n_z)^T \quad (5.13)$$

5.2 Kinematics, Statics and Dynamics

Equation 5.13 results from the fact that rotation matrix 0_1R in equation 5.12 has $(0 \ 0 \ 1)$ in the last column and row. In order to obtain static forces and moments acting on links of a serial manipulator, when the fingertip (or end effector) is subjected to external forces and moments; the joints of the manipulator are assumed to be locked. The manipulator can be viewed as a structure. Using equations of static equilibrium, the following pair of equations (5.14 and 5.15) are obtained [Please refer to (160, pp. 167) for complete derivation].

$${}^i\mathbf{f}_i = {}^i_{i+1}[R]^{i+1}\mathbf{f}_{i+1} \quad (5.14)$$

$${}^i\mathbf{n}_i = {}^i_{i+1}[R]^{i+1}\mathbf{n}_{i+1} + {}^i\mathbf{O}_{i+1} \times {}^i\mathbf{f}_i \quad (5.15)$$

Here \mathbf{f}_i = force exerted on the link $\{i\}$ by link $\{i - 1\}$, \mathbf{n}_i = moment exerted on link $\{i\}$ by link $\{i - 1\}$. ${}^i\mathbf{O}_{i+1}$ is the vector from O_i to O_{i+1} . ${}^i_{i+1}\mathbf{R}$ = Rotation matrix of $\{i + 1\}^{th}$ frame with respect to $\{i\}^{th}$ frame. The leading superscript i signifies that the vectors are described in $\{i\}^{th}$ frame.

Above equations can be used to compute forces and moments when the forces and moments at the fingertip are known. Applying the above iterative formula at the fingertip going towards the base for the finger shown in Figure 5.2(b).

for $i = 3$

$${}^3\mathbf{f}_3 = (f'_x, f'_y, 0)^T \quad (5.16)$$

$${}^3\mathbf{n}_3 = (0, 0, n'_z + l_3 \cdot f'_y)^T \quad (5.17)$$

for $i = 2$

$${}^2\mathbf{f}_2 = (C_3 \cdot f'_x - S_3 \cdot f'_y, S_3 \cdot f'_x + C_3 \cdot f'_y, 0)^T \quad (5.18)$$

$${}^2\mathbf{n}_2 = (0, 0, n'_z + l_2(S_3 \cdot f'_x + C_3 \cdot f'_y) + l_3 \cdot f'_y)^T \quad (5.19)$$

for $i = 1$

$${}^1\mathbf{f}_1 = (C_{23} \cdot f'_x - S_{23} \cdot f'_y, S_{23} \cdot f'_x + C_{23} \cdot f'_y, 0)^T \quad (5.20)$$

$${}^1\mathbf{n}_1 = (0, 0, n'_z + l_1(S_{23} \cdot f'_x + C_{23} \cdot f'_y) + l_2(S_3 \cdot f'_x + C_3 \cdot f'_y) + l_3 \cdot f'_y)^T \quad (5.21)$$

The joints can only apply torques about \hat{Z} axis in order to have static equilibrium. Therefore for a serial link manipulator with rotary joints, the torque required at joint i can be computed by equation 5.22 (160, pp. 168).

$$\tau_i = {}^i\mathbf{n}_i \cdot {}^i\hat{\mathbf{Z}}_i \quad (5.22)$$

Where ${}^i\widehat{\mathbf{Z}}_i$ is a vector along \widehat{Z} axis at joint i .

Torques required at the joints to keep the finger in equilibrium are as follows:

$$\begin{aligned}\tau_1 &= {}^1\mathbf{n}_1 \cdot {}^1\widehat{\mathbf{Z}}_1 \\ &= n'_z + f'_x(l_1S_{23} + l_2S_3) + f'_y(l_1C_{23} + l_2C_3 + l_3)\end{aligned}\quad (5.23)$$

$$\begin{aligned}\tau_2 &= {}^2\mathbf{n}_2 \cdot {}^2\widehat{\mathbf{Z}}_2 \\ &= n'_z + f'_xl_2S_3 + f'_y(l_2C_3 + l_3)\end{aligned}\quad (5.24)$$

$$\begin{aligned}\tau_3 &= {}^3\mathbf{n}_3 \cdot {}^3\widehat{\mathbf{Z}}_3 \\ &= n'_z + f'_yl_3\end{aligned}\quad (5.25)$$

Rearranging equations 5.23 through 5.25, the joint torques can be expressed as:

$$\begin{pmatrix} \tau_1 \\ \tau_2 \\ \tau_3 \end{pmatrix} = \begin{bmatrix} L_1S_{23} + L_2S_3 & L_1C_{23} + L_2C_3 + L_3 & 0 & 0 & 0 & 1 \\ L_2S_3 & L_2C_3 + L_3 & 0 & 0 & 0 & 1 \\ 0 & L_3 & 0 & 0 & 0 & 1 \end{bmatrix} \begin{pmatrix} f'_x \\ f'_y \\ 0 \\ 0 \\ 0 \\ n'_z \end{pmatrix}\quad (5.26)$$

Substituting from equations 5.12 and 5.13 into equation 5.26:

$$\begin{pmatrix} \tau_1 \\ \tau_2 \\ \tau_3 \end{pmatrix} = \begin{bmatrix} -L_1S_1 - L_2S_{12} - L_3S_{123} & L_1C_1 + L_2C_{12} + L_3C_{123} & 0 & 0 & 0 & 1 \\ -L_2S_{12} - L_3S_{123} & L_2C_{12} + L_3C_{123} & 0 & 0 & 0 & 1 \\ -L_3S_{123} & L_3C_{123} & 0 & 0 & 0 & 1 \end{bmatrix} \begin{pmatrix} f_x \\ f_y \\ 0 \\ 0 \\ 0 \\ n_z \end{pmatrix}\quad (5.27)$$

The term in the square bracket is the transpose of the Jacobian $J(\theta)$.

The contact between the object to be grasped and fingertip (of the three link finger) is assumed to be point contact with friction as shown in Figure 5.5. The contact can not resist any moment applied around its normal. Thus $n_z = 0$ (161).

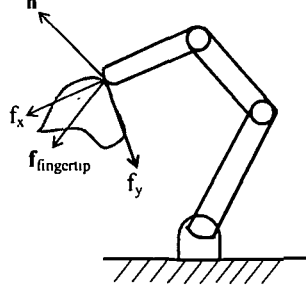


Figure 5.5: Schematic of point contact between the object and fingertip

With this assumption, equation 5.27 can be reduced to

$$\begin{pmatrix} \tau_1 \\ \tau_2 \\ \tau_3 \end{pmatrix} = \begin{bmatrix} -L_1 S_1 - L_2 S_{12} - L_3 S_{123} & L_1 C_1 + L_2 C_{12} + L_3 C_{123} & 0 \\ -L_2 S_{12} - L_3 S_{123} & L_2 C_{12} + L_3 C_{123} & 0 \\ -L_3 S_{123} & L_3 C_{123} & 0 \end{bmatrix} \begin{pmatrix} f_x \\ f_y \\ 0 \end{pmatrix} \quad (5.28)$$

From 5.28, the fingertip force (f_x, f_y) in terms of the joint torques can be computed as:

$$f_x = \frac{(L_2 C_{12})\tau_1 - (L_1 C_1 + L_2 C_{12})\tau_2 + L_1 C_1(\tau_3)}{L_1 L_2 (C_1 S_{12} - S_1 C_{12})} \quad (5.29)$$

$$f_y = \frac{(L_2 S_{12})\tau_1 - (L_1 S_1 + L_2 S_{12})\tau_2 + L_1 S_1(\tau_3)}{L_1 L_2 (C_1 S_{12} - S_1 C_{12})} \quad (5.30)$$

5.2.2.2 Tendon Forces and Joint Torques

Next step is to describe how forces applied at the end of the tendons are related to the torque applied at the joints. Figure 5.2(c) illustrates the flexor (h_1) and extensor (h_2) tendons routing the finger joints. Following (156, pp. 293), the extension function for the flexor and extensor tendons are given as:

$$h_1(\theta) = l_m + 2\sqrt{a^2 + b^2} \cos(\tan^{-1}(a/b) + \theta_1/2) - 2b - R_2\theta_2 - R_3\theta_3 \quad (5.31)$$

$$h_2(\theta) = l_{m'} + R_1\theta_1 + R_2\theta_2 + R_3\theta_3 \quad (5.32)$$

5.2 Kinematics, Statics and Dynamics

Where (R_1, R_2, R_3) are radius of rotation of the three joints (MCP, PIP and DIP) respectively. a and b are half the finger width and distance of the tendon guides from the finger joints as shown in Figure 5.2(c).

The coupling matrix relating the force at the ends of the tendons and the joint torques is as given below.

$$H_c = \begin{bmatrix} \partial h_1 / \partial \theta_1 & \partial h_2 / \partial \theta_1 \\ \partial h_1 / \partial \theta_2 & \partial h_2 / \partial \theta_2 \\ \partial h_1 / \partial \theta_3 & \partial h_2 / \partial \theta_3 \end{bmatrix} \quad (5.33)$$

The joint torque in terms of tendon force is computed as:

$$\tau = H_c \cdot F \quad (5.34)$$

$$= \begin{bmatrix} -2\sqrt{a^2 + b^2} \sin(\tan^{-1}(a/b) + \theta_1/2) & R_1 \\ -R_2 & R_2 \\ -R_3 & R_3 \end{bmatrix} \cdot \begin{bmatrix} F_1 \\ F_2 \end{bmatrix} \quad (5.35)$$

Where $F = [F_1 \quad F_2]^T$; F_1 and F_2 are the forces on the flexor and extensor tendons respectively.

Considering the motor torque $T = [T_1 \quad T_2]^T$; T_1 for flexion and T_2 for extension of the finger:

$$\begin{bmatrix} F_1 \\ F_2 \end{bmatrix} = \begin{bmatrix} \frac{1}{r_1} & 0 \\ 0 & \frac{1}{r_2} \end{bmatrix} \begin{bmatrix} T_1 \\ T_2 \end{bmatrix} \quad (5.36)$$

Where r_1 and r_2 ; are the radius of the pulleys connected to the flexor and extensor motors.

Using equation 5.35 and 5.36, the joint torques can be expressed as a function of motor torques as follows:

$$\tau_1 = -2\sqrt{a^2 + b^2} \sin(\tan^{-1}(a/b) + \theta_1/2) \frac{T_1}{r_1} + R_1 \frac{T_2}{r_2} \quad (5.37)$$

$$\tau_2 = -R_2 \frac{T_1}{r_1} + R_2 \frac{T_2}{r_2} \quad (5.38)$$

$$\tau_3 = -R_3 \frac{T_1}{r_1} + R_3 \frac{T_2}{r_2} \quad (5.39)$$

For a tendon network; the tendon forces chosen to exert a given vector of joint torques have the form

$$F = H_c^+ \tau + F_N \quad (5.40)$$

Where $H_c^+ = (H_c)^T((H_c)(H_c)^T)^{-1}$ is the pseudo-inverse of the coupling matrix. F_N is tendon internal force to ensure that tendons remain taut and chosen as small as possible.

Using equation 5.36 in equation 5.40, the relation between the motor torque and joint torque is obtained as:

$$T = \begin{bmatrix} r_1 & 0 \\ 0 & r_2 \end{bmatrix} [H_c^+ \tau + F_N] \quad (5.41)$$

Using the values of τ_1 , τ_2 and τ_3 from equation 5.37 through 5.39 into equation 5.29 and 5.30; the fingertip force (f_x, f_y) can be computed in terms of the tendon actuation motor torque as:

$$\begin{aligned} f_x = & \{ (L_2 C_{12}) (-2\sqrt{a^2 + b^2} \sin(\tan^{-1}(a/b) + \theta_1/2) \frac{T_1}{r_1} \\ & - (L_1 C_1 + L_2 C_{12}) (-R_2 \frac{T_1}{r_1} + R_2 \frac{T_2}{r_2}) + L_1 C_1 (-R_3 \frac{T_1}{r_1} + R_3 \frac{T_2}{r_2}) \} \\ & \{ L_1 L_2 (C_1 S_{12} - S_1 C_{12}) \}^{-1} \end{aligned} \quad (5.42)$$

$$\begin{aligned} f_y = & \{ (L_2 S_{12}) (-2\sqrt{a^2 + b^2} \sin(\tan^{-1}(a/b) + \theta_1/2) \frac{T_1}{r_1} + R_1 \frac{T_2}{r_2} \\ & - (L_1 S_1 + L_2 S_{12}) (-R_2 \frac{T_1}{r_1} + R_2 \frac{T_2}{r_2}) + L_1 S_1 (-R_3 \frac{T_1}{r_1} + R_3 \frac{T_2}{r_2}) \} \\ & \{ (L_1 L_2 (C_1 S_{12} - S_1 C_{12})) \}^{-1} \end{aligned} \quad (5.43)$$

5.2.3 Dynamic Analysis of a Finger

The goal of dynamic analysis is to determine the motor torque required to be applied such that the finger joints follow the human finger joint trajectories. Finger joint torques for Prototype 1.0 for emulating the natural curling is to be estimated. In order to do this, joint torques as a function of velocity and acceleration are determined for a finger of Prototype 1.0 using equations of motion for a serial link manipulator as detailed in (160, pp. 159).

5.2.3.1 Equations of motion

The equations of motion for a serial link manipulator is given as:

$$[M(\theta)]\ddot{\theta} + [C(\theta, \dot{\theta})]\dot{\theta} + G(\theta) = \tau \quad (5.44)$$

5.2 Kinematics, Statics and Dynamics

Where $[M(\theta)]$ is the $n \times n$ mass matrix. $C(\theta, \dot{\theta})$ is the $n \times n$ matrix with $[C(\theta, \dot{\theta})]\dot{\theta}$ representing an $n \times 1$ vector of centripetal and Coriolis terms. $G(\theta)$ is an $n \times 1$ vector containing the gravity terms and τ is the $n \times 1$ vector of joint torques.

L_{c1}, L_{c2} and L_{c3} are the distances of the center of mass of the three phalanges (of the finger) from their respective joint origins, viz. O_1, O_2 and O_3 . Let the masses of the three links be m_1, m_2 and m_3 and their link inertia about the axis through center of masses are I_1, I_2 and I_3

The end effector velocity can be computed as a function of the joint velocities $\dot{\theta} = \dot{\theta}_1, \dot{\theta}_2, \dot{\theta}_3, \dots, \dot{\theta}_i$ through the Jacobian matrix J . The same methodology can be used to compute the velocity of a generic point of the manipulator, and in particular the velocity $V_{c_i} = \dot{c}_i$ of the center of mass p_{c_i} that results function of the joint velocities $\dot{\theta}_1, \dot{\theta}_2, \dot{\theta}_3$ only: [Please refer to (162)]

$$\dot{c}_i = J_{c1}^i \dot{\theta}_1 + J_{c2}^i \dot{\theta}_2 + \dots + J_{c_i}^i \dot{\theta}_i \quad (5.45)$$

$$= J_c^i \dot{\theta}_i \quad (5.46)$$

$$\omega_i = J_{\omega 1}^i \dot{\theta}_1 + J_{\omega 2}^i \dot{\theta}_2 + \dots + J_{\omega_i}^i \dot{\theta}_i \quad (5.47)$$

$$= J_{\omega}^i \dot{\theta}_i \quad (5.48)$$

$$(5.49)$$

Where

$$J_{c,i} = [J_{c1}^i, J_{c2}^i, \dots, J_{c_i}^i, 0 \quad 0] \quad (5.50)$$

$$J_{\omega,i} = [J_{\omega 1}^i, J_{\omega 2}^i, \dots, J_{\omega_i}^i, 0 \quad 0] \quad (5.51)$$

$$(5.52)$$

With

$$\begin{bmatrix} J_{c_j}^i \\ J_{\omega_j}^i \end{bmatrix} = \begin{bmatrix} Z_{j-1} \times (p_{c_i} - p_{j-1}) \\ Z_{j-1} \end{bmatrix} \quad (5.53)$$

Jacobians $J_{\omega,i}^i$ and $J_{c,i}^i$ for computing the mass matrix with reference to the base frame $\{X_o, Y_o\}$ for the three link finger under study are yielded as follows

for $i = 1$

$$J_{\omega,1} = \begin{bmatrix} 0 & 0 & 0 \\ 0 & 0 & 0 \\ 1 & 0 & 0 \end{bmatrix} \quad (5.54)$$

$$J_{c,1} = \begin{bmatrix} -L_{c1}S_1 & 0 & 0 \\ L_{c1}C_1 & 0 & 0 \\ 0 & 0 & 0 \end{bmatrix} \quad (5.55)$$

for $i = 2$

$$J_{w,2} = \begin{bmatrix} 0 & 0 & 0 \\ 0 & 0 & 0 \\ 1 & 1 & 0 \end{bmatrix} \quad (5.56)$$

$$J_{c,2} = \begin{bmatrix} -L_1S_1 - L_{c2}S_{12} & -L_{c2}S_{12} & 0 \\ L_1C_1 + L_{c2}C_{12} & L_{c2}C_{12} & 0 \\ 0 & 0 & 0 \end{bmatrix} \quad (5.57)$$

for $i = 3$

$$J_{w,3} = \begin{bmatrix} 0 & 0 & 0 \\ 0 & 0 & 0 \\ 1 & 1 & 1 \end{bmatrix} \quad (5.58)$$

$$J_{c,3} = \begin{bmatrix} -L_1S_1 - L_1S_{12} - L_{c3}S_{123} & -L_2S_{12} - L_{c3}S_{123} & -L_{c3}S_{123} \\ L_1C_1 + L_2C_{12} + L_{c3}C_{123} & L_2C_{12} + L_{c3}C_{123} & L_{c3}C_{123} \\ 0 & 0 & 0 \end{bmatrix} \quad (5.59)$$

The equation for mass matrix; which is positive definite and symmetric is given as follows [Please refer to (163, pp. 175)];

$$M = \sum_{i=1}^n \bar{M}_i \quad (5.60)$$

$$= \sum_{i=1}^n m_i J_{c,i}^T J_{c,i} + J_{w,i}^T M_i J_{w,i} \quad (5.61)$$

For the three link finger under study, the elements of the mass matrix are as follows:

$$M_{11} = I_1 + I_2 + I_3 + m_1(L_{c1})^2 + m_2(L_1^2 + L_{c2}^2 + 2L_1L_{c2}C_2) + m_3(L_1^2 + L_2^2 + L_{c3}^2 + 2L_1L_2C_2 + 2L_2L_{c3}C_3 + 2L_1L_{c3}C_{23}) \quad (5.62)$$

$$M_{12} = M_{21} = I_2 + I_3 + m_2(L_{c2}^2 + L_1L_{c2}C_2) + m_3(L_2^2 + L_{c3}^2 + L_1L_2C_2 + L_1L_{c3}C_{23} + 2L_2L_{c3}C_3) \quad (5.63)$$

$$(5.64)$$

$$\begin{aligned} M_{13} &= M_{31} \\ &= I_3 + m_3(L_{c3}^2 + L_1L_{c3}C_2S_3 + L_2L_{c3}C_3) \end{aligned} \quad (5.65)$$

$$M_{22} = I_2 + I_3 + m_2L_{c2}^2 + m_3(L_2)^2 + L_{c3}^2 + 2L_2L_{c3}C_3 \quad (5.66)$$

$$\begin{aligned} M_{23} &= M_{32} \\ &= I_3 + m_3(L_{c3}^2 + L_2L_{c3}C_3) \end{aligned} \quad (5.67)$$

$$M_{33} = I_3 + m_3L_{c3}^2 \quad (5.68)$$

The $[C(\theta, \dot{\theta})]\dot{\theta}$ is a $n \times 1$ vector \mathbf{V} whose elements are quadratic functions of joint velocities $\dot{\theta}$. The k^{th} element of this vector is given as [Please refer to (162)]

$$V_k = \sum_{j=1}^n C_{kj} \dot{\theta}_j \quad (5.69)$$

Where the elements C_{kj} are computed as

$$C_{kj} = \sum_{i=1}^n C_{ij} \dot{\theta}_i \quad (5.70)$$

With

$$C_{ijk} = \frac{1}{2} \left(\frac{\partial M_{kj}}{\partial \theta_i} + \frac{\partial M_{ki}}{\partial \theta_j} - \frac{\partial M_{ij}}{\partial \theta_k} \right), \text{ which is known as Christoffel symbols} \quad (5.71)$$

Following the above formulation, the elements of $[C(\theta, \dot{\theta})]$ for the three link finger shown in Figure 5.2 are

$$\begin{aligned} C_{11} &= -(m_2L_1L_{c3}S_2 + m_3L_1L_2S_2 + m_3L_1L_{c3}S_{23})\dot{\theta}_2 \\ &\quad -(m_3L_2L_{c3}S_3 + m_3L_1L_{c3}S_{23})\dot{\theta}_3 \end{aligned} \quad (5.72)$$

$$\begin{aligned} C_{12} &= -(m_2L_1L_{c2}S_2 + m_3L_1L_2S_2 + m_3L_1L_{c3}S_{23})\dot{\theta}_1 - (m_2L_1L_{c2}S_2) \\ &\quad + m_3L_1L_2S_2 + m_3L_1L_{c3}S_{23})\dot{\theta}_2 - (m_3L_1L_{c3}S_{23} + m_3L_2L_{c3}S_3)\dot{\theta}_3 \end{aligned} \quad (5.73)$$

$$\begin{aligned} C_{13} &= -(m_3L_2L_{c3}S_3 + m_3L_1L_{c3}S_{23})\dot{\theta}_1 - (m_3L_1L_{c3}S_{23} + m_3L_2L_{c3}S_3)\dot{\theta}_2 \\ &\quad -(m_3L_1L_{c3}S_{23} + m_3L_2L_{c3}S_3)\dot{\theta}_3 \end{aligned} \quad (5.74)$$

5.2 Kinematics, Statics and Dynamics

$$C_{21} = -(m_2 L_1 L_{c2} S_2 + m_3 L_1 L_2 S_2 + m_3 L_1 L_{c3} S_{23}) \dot{\theta}_1 - (m_3 L_2 L_{c3} S_3) \dot{\theta}_3 \quad (5.75)$$

$$C_{22} = -(m_2 L_2 L_{c3} S_3) \dot{\theta}_3 \quad (5.76)$$

$$C_{23} = -(m_3 L_2 L_{c3} S_3) \dot{\theta}_1 - (m_3 L_2 L_{c3} S_3) \dot{\theta}_2 - (m_3 L_2 L_{c3} S_3) \dot{\theta}_3 \quad (5.77)$$

$$C_{31} = (m_3 L_2 L_{c3} S_3 + m_2 L_1 L_{c3} S_{23}) \dot{\theta}_1 + (m_3 L_2 L_{c3} S_3) \dot{\theta}_2 \quad (5.78)$$

$$C_{32} = (m_3 L_2 L_{c3} S_3) \dot{\theta}_1 + (m_3 L_2 L_{c3} S_3) \dot{\theta}_2 \quad (5.79)$$

$$C_{33} = 0 \quad (5.80)$$

Finally the gravity terms G_i of the gravity vector $G(\theta)$ are computed from the expression [Please refer to (163, pp. 177)]:

$$G_i = - \sum_{j=1}^n m_j \mathbf{g}^T J_{c,j}^i \quad (5.81)$$

Where

$$\mathbf{g} = [0 \quad -g \quad 0]^T; \mathbf{g} \text{ being the acceleration due to gravity}$$

Which results into the gravity terms as follows:

$$G_1 = m_1 g L_{c1} C_1 + m_2 g (L_{c1} + L_{c2} C_{12}) + m_3 g (L_1 C_1 + L_2 C_2 + L_{c3} C_{123}) \quad (5.82)$$

$$G_2 = m_2 g L_{c2} C_{12} + m_3 g (L_2 C_{12} + L_{c3} C_{123}) \quad (5.83)$$

$$G_3 = m_3 g L_{c3} C_{123} \quad (5.84)$$

Using the mass matrix from equation 5.60, centripetal and coriolis matrix from equation 5.70 and gravity terms from 5.81, the joint torques are computed as follows:

$$\begin{bmatrix} \tau_1 \\ \tau_2 \\ \tau_3 \end{bmatrix} = \begin{bmatrix} M_{11} & M_{12} & M_{13} \\ M_{21} & M_{22} & M_{23} \\ M_{31} & M_{32} & M_{33} \end{bmatrix} \begin{Bmatrix} \ddot{\theta}_1 \\ \ddot{\theta}_2 \\ \ddot{\theta}_3 \end{Bmatrix} + \begin{bmatrix} C_{11} & C_{12} & C_{13} \\ C_{21} & C_{22} & C_{23} \\ C_{31} & C_{32} & C_{33} \end{bmatrix} \begin{Bmatrix} \dot{\theta}_1 \\ \dot{\theta}_2 \\ \dot{\theta}_3 \end{Bmatrix} + \begin{bmatrix} G_1 \\ G_2 \\ G_3 \end{bmatrix} \quad (5.85)$$

5.2.3.2. Torques for Natural Curling

In order to find the motor torques to be applied to the flexor and extensor motors for natural curling of the finger, the velocity and acceleration corresponding to the human finger joints during natural curling are obtained. These velocities and accelerations are used for finding the joint torques through the equations of motion which in turn is used for determining the flexor and extensor motor torques. The steps followed for determination of the finger joint torques are enlisted below:

5.2 Kinematics, Statics and Dynamics

- The human finger joint trajectories have been adopted from the Figure 3 reported in (159) and are shown in Figure 5.6.

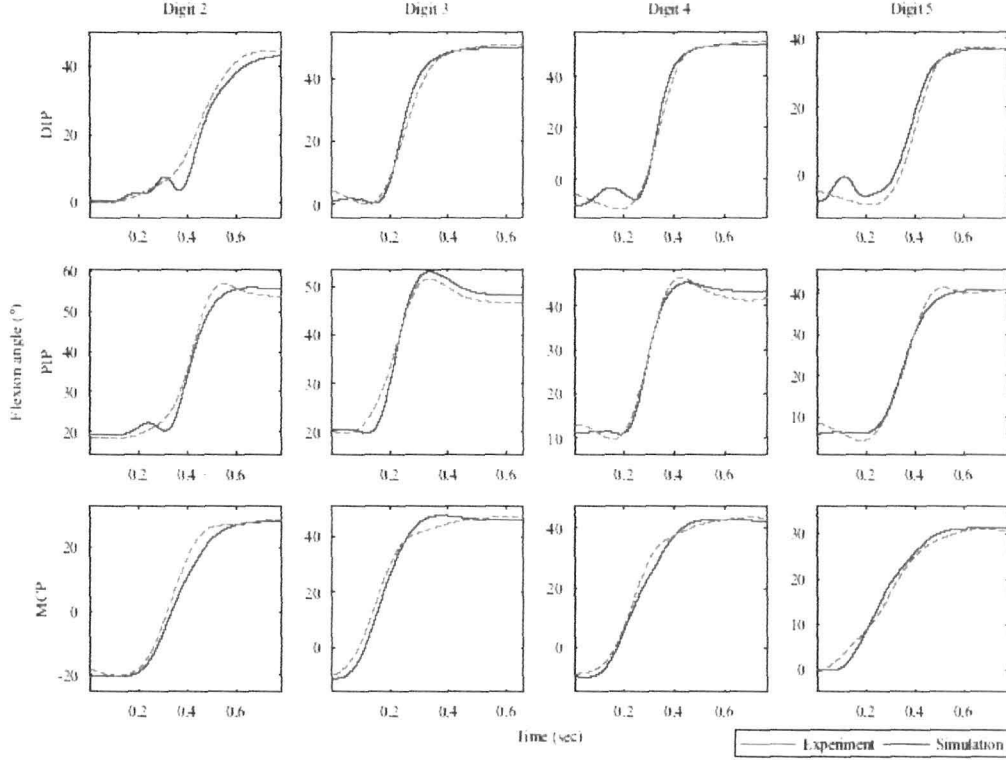


Figure 5.6: Human Finger Joint Trajectories. The trajectories in red are for human fingers and in blue are for the dynamic model of human hand proposed in (159). Digit 2, 3, 4, 5 in the figure represents the index, middle, ring and little finger. The x-axis is the flexion angle in degree and y-axis is the time in sec.

- The trajectories in Figure 5.6 are digitized using Engauge Digitizer 5.1 (164) that converts an image file showing a graph into numbers.
 - The equation representing the digitized finger joint trajectories are obtained through polynomial curve fitting. Figure 5.7 and Table 5.7 shows the digitized finger joint trajectories and representative equations respectively. The choice of a particular polynomial order was based on absolute value error between the digitized and curve fitted trajectories.

5.2 Kinematics, Statics and Dynamics

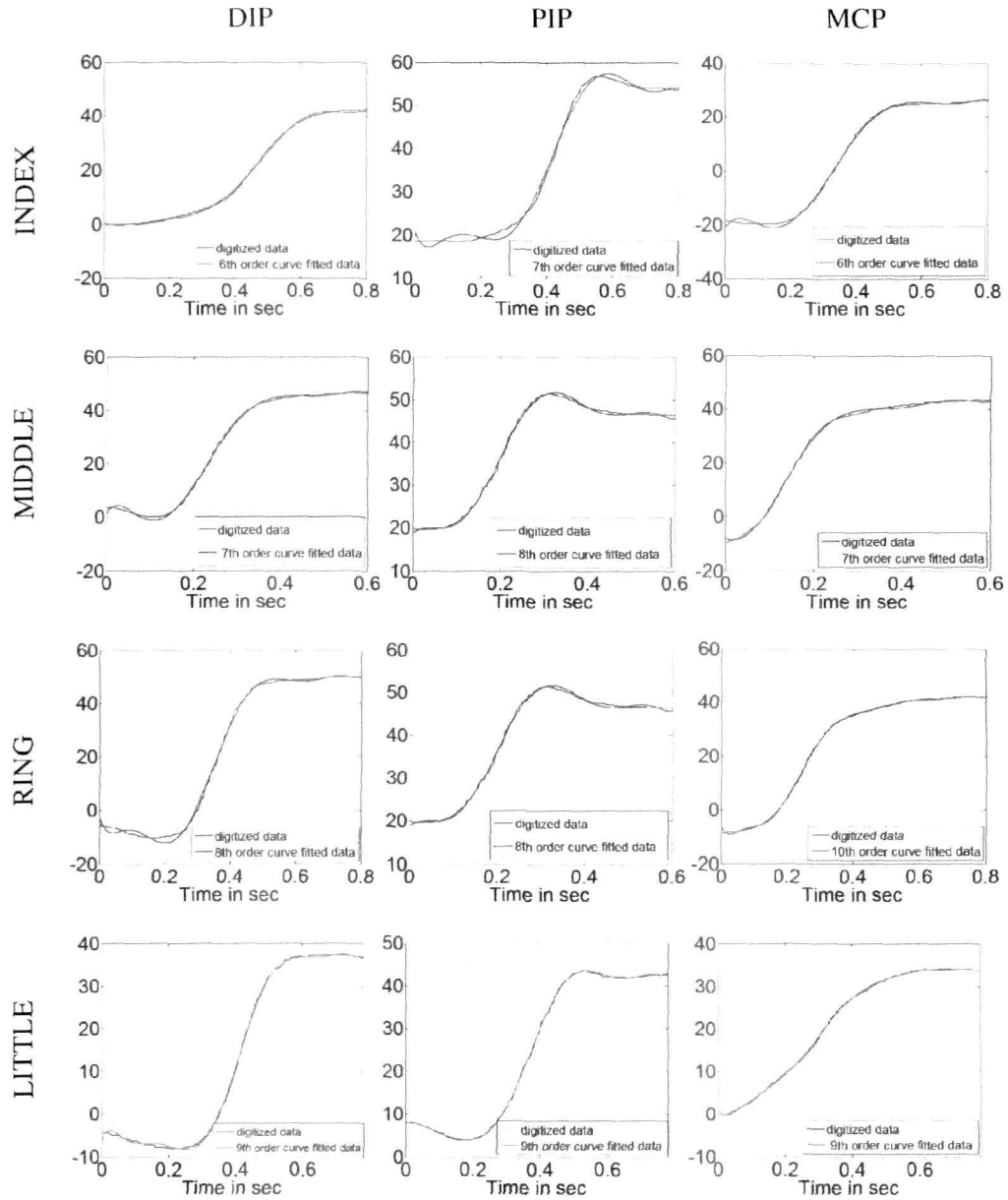


Figure 5.7: Digitized and Curve Fitted Finger Joint Trajectories. The x-axis is the flexion angle in degree and y-axis is the time in sec.

Table 5.7: Curve Fitted Finger Joint Trajectories for Natural Curling

Fingcr	Joints	Curve Fitted Trajectories
Index	MCP	$1.1e + 004x^6 - 2.5e + 004x^5 + 1.9e + 004x^4 - 6.7e + 003x^3 + 1.1e + 003x^2 - 64x + 0.85$
	PIP	$-7.3e + 004x^7 + 2.1e + 005x^6 - 2.4e + 005x^5 + 1.3e + 005x^4 - 3.7e + 004x^3 + 4.7e + 003x^2 - 2.3e + 002x + 21$
	DIP	$-1.5e + 004x^6 + 3.9e + 004x^5 - 3.9e + 004x^4 + 1.7e + 004x^3 - 3e + 003x^2 + 1.8e + 002x - 21$
Middle	MCP	$1.2e + 005x^7 - 3.6e + 005x^6 + 4.1e + 005x^5 - 2.3e + 005x^4 + 6.3e + 004x^3 - 7.2e + 003x^2 + 2.6e + 002x + 1.4$
	PIP	$9.6e + 005x^8 - 2.1e + 006x^7 + 1.8e + 006x^6 - 6.7e + 005x^5 + 9.3e + 004x^4 + 3.9e + 003x^3 - 1.3e + 003x^2 + 67x + 19$
	DIP	$2.1e + 005x^7 - 4.2e + 005x^6 + 3.2e + 005x^5 - 1e + 005x^4 + 8.7e + 003x^3 + 1.7e + 003x^2 - 66x - 8.1$
Ring	MCP	$3.9e + 005x^8 - 1.3e + 006x^7 + 1.8e + 006x^6 - 1.3e + 006x^5 + 5.1e + 005x^4 - 1e + 005x^3 + 1e + 004x^2 - 4.3e + 002x - 2.3$
	PIP	$5e + 006x^{10} + 2e + 007x^9 - 3.4e + 07x^8 + 3.1e + 07x^7 - 1.7e + 07x^6 + 5.9e + 06x^5 - 1.3e + 06x^4 + 1.7e + 05x^3 - 1.3e + 04x^2 + 5.1e + 02x + 6.7$
	DIP	$2.9e + 006x^{10} - 1.2e + 007x^9 + 2.3e + 007x^8 - 2.3e + 007x^7 + 1.4e + 007x^6 - 5.5e + 06x^5 + 1.3e + 06x^4 - 1.6e + 05x^3 + 1.1e + 04x^2 - 3.2e + 02x - 6.1$
Little	MCP	$1.2e + 006x^9 - 4.6e + 006x^8 + 7e + 006x^7 - 5.7e + 006x^6 + 2.6e + 006x^5 - 7.2e + 005x^4 + 1.1e + 005x^3 - 8.6e + 003x^2 + 2.6e + 002x - 6.5$
	PIP	$5.8e + 005x^9 - 2e + 006x^8 + 2.9e + 006x^7 - 2.1e + 006x^6 + 8.8e + 005x^5 - 2.1e + 005x^4 + 2.9e + 004x^3 - 2.3e + 003x^2 + 52x + 7.7$
	DIP	$-1.9e + 005x^9 + 7.8e + 005x^8 - 1.3e + 006x^7 + 1.2e + 006x^6 - 6.8e + 005x^5 + 2.2e + 005x^4 - 4e + 004x^3 + 3.9e + 003x^2 - 1.3e + 002x + 1.2$

- The finger joint velocity and acceleration corresponding to the equation representing the finger joint trajectories are determined.
- Velocity and acceleration values corresponding to the natural curling operations of the human finger along with the finger specification of Prototype 1.0 were fed into equation 5.85 to find the corresponding joint torques.
- The corresponding average joint torques required for replicating the finger joint angles are presented in Table 5.8. The simulation results for finger joint trajectories, velocity and acceleration are presented in Figure III.1 through Figure III.12 in Appendix-III.
- Using Equation 5.41, motor torques required corresponding to the finger joint torques are determined.

Table 5.8: Average Finger Joint Torques for Natural Curling Operations

Finger	Joints	Torque (Nm)
Index	MCP	0.090
	PIP	0.051
	DIP	0.020
Middle	MCP	0.110
	PIP	0.071
	DIP	0.021
Ring	MCP	0.081
	PIP	0.061
	DIP	0.022
Little	MCP	0.071
	PIP	0.041
	DIP	0.011
Thumb	MCP	0.070
	DIP	0.031

- The fingertip forces corresponding to the motor torques are determined through Equation 5.42 and 5.43. Table 5.9 shows the average fingertip forces corresponding to the joint torques.

Table 5.9: Average Fingertip Forces corresponding to the Joint Torques

Finger	Average Fingertip Force
Index	1.12 N
Middle	1.30 N
Ring	1.00 N
Little	0.91 N
Thumb	1.32 N

In the preceding sections, the methods for computing the joint torques required by Prototype 1.0 to replicate the natural curling operations were presented. Given these joint torques, equation to determine the motor torques for a tendon driven system is presented. Finally fingertip forces corresponding to the motor torques for natural curling are determined. In the next section we discuss a feedback control based on the fingertip forces.

5.2.4 PID Control

This section reports the simulation of a PID controller for emulating the grasp types by Prototype 1.0. The goal of the PID controller is to inhibit the fingertip force from exceeding the desired force. The selection of the PID controller is based on the fact that it has better static and dynamic performance (165). The input to the actuator required for generating the fingertip force as in Table 5.9 is applied through a PID controller. The difference of the required force and the actual actual force is fed as error into the PID controller. The steps for design and simulation of the PID controller is detailed in the following sections.

5.2.4.1 System Linearity

The system linearity is checked by applying a pulse width modulated (PWM) voltage to the driver circuit of the motor and finding the corresponding output of the fingertip force. Figure 5.8 represents the relationship of the input voltage versus the fingertip force sensor outputdirect determining the linearity range of the system. It has been found that the system is linear within a range of input voltage 1.75 volt (V) to 10.00 V with an output fingertip force in the range of 0.6 N to 45 N.

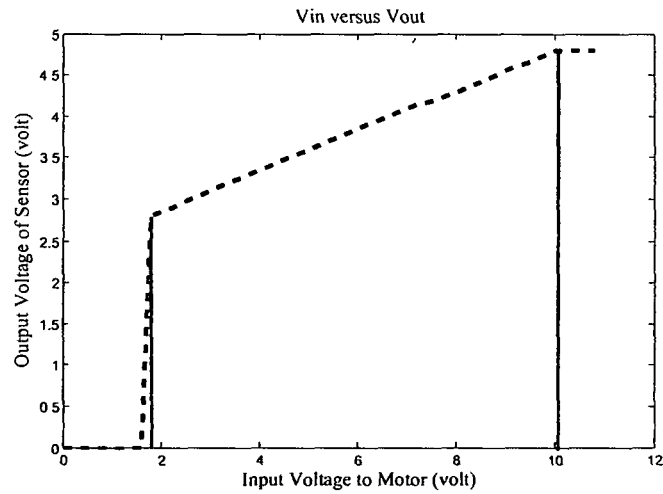


Figure 5.8: Linearity range of the System

5.2.4.2 System Transfer Function

Once the linear operating range of the system is obtained, the next step is to find the transfer function for the system. The transfer function relating the input voltage v_a and output angular velocity ω of the motor in Laplace domain is as follows (163):

$$\frac{\omega(s)}{v_a(s)} = \frac{K_t}{(Ls + R)(Js + b) + K_t K_e} \quad (5.86)$$

Where

Moment of inertia of the rotor (J) = 0.01

Motor viscous friction constant (b) = 0.1 Nmsec

Electromotive force constant (K_e) = 0.01 V/radian/sec

Motor torque constant (K_t) = 3.3 Nm/ Amp

Electric resistance (R) = 1 ohm

Electric inductance (L) = 0.5 Henry

The transfer function of the used DC geared motor used determined using the above specifications (166) as follows:

$$G(s) = \frac{3.3}{0.005s^2 + 0.06s + 0.1001} \quad (5.87)$$

5.2.4.3 PID Controller Design

Following design criteria are set for design of the PID controller.

- Overshoot < 5%
- Settling Time < 0.5 sec
- Steady state error < 2%

The transfer function of a PID controller (165) is given as follows:

$$T(s) = K_p + K_I/s + K_Ds \tag{5.88}$$

where

K_P = Proportional Gain

K_D = Differential Gain

K_I = Integral Gain

The values of the controller gains have been selected through manual tuning using proportional gain K_P to decrease the rise time, differential gain K_D to reduce the overshoot and settling time and integral gain K_I to eliminate the steady-state error. The process is followed in line with (167) and is tabulated in Table 5.10. The response

Table 5.10: Process followed for Controller Gain Selection

Parameters	Rise Time	Overshoot	Small Change	Steady State Error
K_p	Decrease	Increase	Small Change	Decrease
K_I	Decrease	Increase	Increase	Eliminate
K_D	Small Change	Decrease	Decrease	No Change

of the PID controller with different values of the gains is shown in Figure 5.9. A set of values of $K_p = 1.7$, $K_D = 5.35$ and $K_I = 0.0085$ are selected for almost zero steady state error, zero overshoot and 0.2 sec setting time.

5.2.4.4 Simulation Results

The simulation of the designed PID controller was carried out in MATLAB. The schematic of the simulation model is shown in Figure 5.10.

The fingertip force corresponding to the joint torques for the desired finger joint trajectories obtained from the dynamic and static analysis is fed to the PID controller. The gains of the PID controller were set as obtained in section 5.2.4.3. The PID control

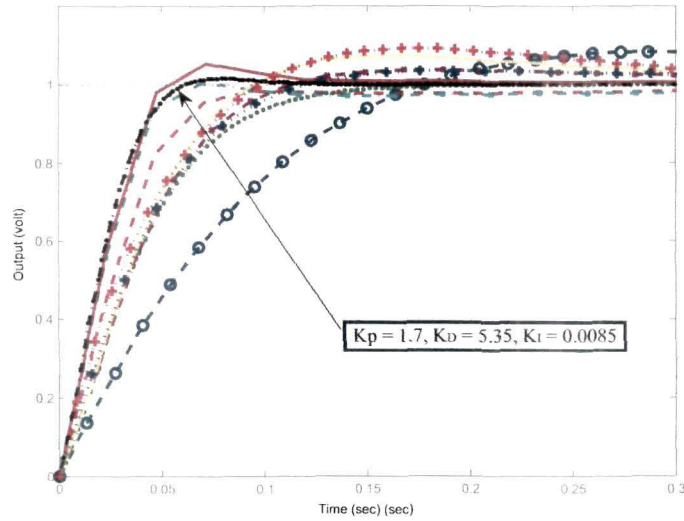


Figure 5.9: Response of the PID controller with different values of the Gains. The arrow shows the response selected for the Experiment

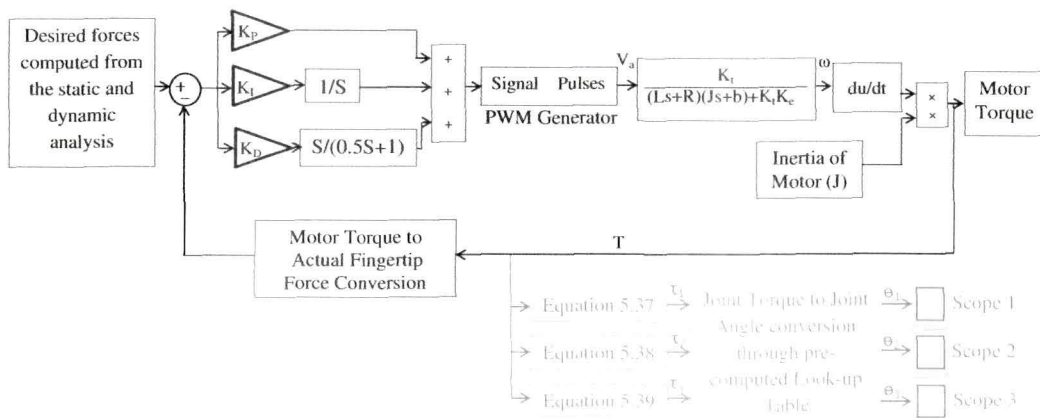


Figure 5.10: Schematic of the Simulation Model

signal is converted into a PWM signal through a PWM generator. The PWM signal drive the motor actuating the fingers on Prototype 1.0. The torques measured at the output of the motor was fed back through the feedback path. The force corresponding to the resulting torque i.e. actual fingertip force obtained through the feedback transfer

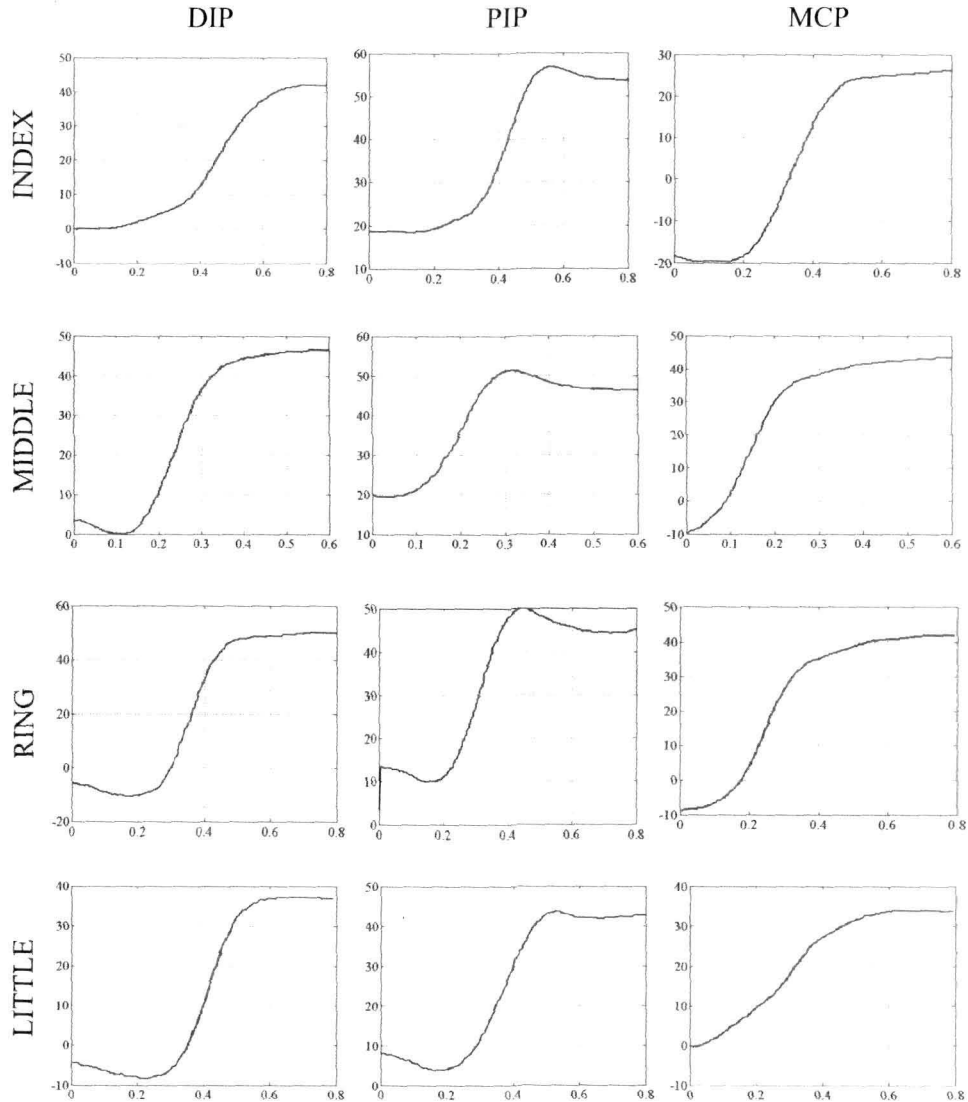


Figure 5.11: Simulated DIP, PIP and MCP Joint Trajectories of Index, Middle, Ring and Little Finger. The x-axis is Time in Sec and Y-axis is flexion angle in degree

function is fed back to the PID controller. The controller minimizes the difference of the actual fingertip force and desired fingertip force. In the simulation, the corresponding joint torques are computed as a function of the motor torque using Equation 5.41. Resulting finger joint trajectories are shown in Figure 5.11.

5.3 Graspability of Prototype 1.0

Figure 5.12 shows Prototype 1.0 performing the six grasp types under study. The

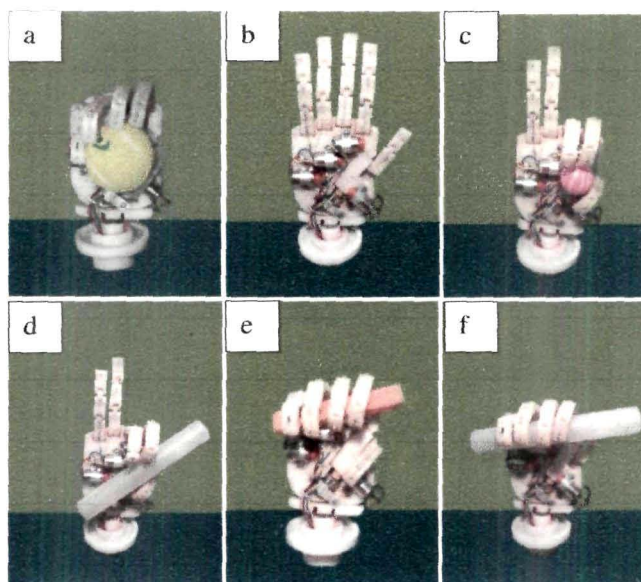


Figure 5.12: Prototype 1.0 performing grasp types: a. Power b. Palm-up c. Precision d. Hook e. Pinch and f. Oblique

posture and/ or number of fingers involved in each grasps are different as detailed in section 2.5.1.1 in Chapter 2. Prototype 1.0 can grasp a the objects like cricket tennis ball, square bar, circular bar and table tennis ball stably. The video of Prototype 1.0 performing six grasp types through off-line EMG controlled is available in <http://www.tezu.ernet.in/bcr/video.html>.

While grasping, Prototype 1.0 is subjected to the limitation of grasping an object with the thumb mimicking the thumb of human hand. This is mainly because of its lesser DoF as discussed towards the end of the section 5.1. The thumb being only of two DoF, can not grasp an object with its tip. Further, for the absence of abduction-adduction of four fingers, Prototype 1.0 can not grasp objects of larger size. However, it can emulate all the six grasp under study.

5.4 Summary

This chapter presented the development of a biomimetic hand prototype: Prototype 1.0. The prototype has been developed following a biomimetic approach inspired by human hand anatomy. It mimics the human hand both in geometry and function. The prototype exhibits all the functionality except abduction/ adduction movement of the digits. During grasping operations by human hand, objects are held firmly because of the palm prehension; which is achieved in the prototype by making the palm a two piece structure in order to have proper grasp modes. The human wrist is a complex structure with eight carpal bones of semicircular surface giving three DoF. This is achieved in the prototype by arranging three motors in mutually perpendicular axes. The thumb mechanism in the prototype is a simplified version of the human thumb. Further, the dynamic constraints have been considered for tendon actuation in the hand as stated in section 5.2.1.1. This is subsequently used in the control of the hand.

Following a two layered control architecture, the prototype reproduce the grasping operations involved during 70% of dla with 97.5% accuracy. Control is two layered: a SHC recognizes grasp type attempted by the user based on EMG signals; a LHC was implemented to control the finger joint torques and angles in the prosthesis for the grasp attempted. SHC recognized six grasp types used during 70% of dla. Grasp recognition was through RBF kernel SVM using PCA of TFD features. The control in the LHC was based on kinematic, static and dynamic analysis. Prototype 1.0 emulates the grasping operations following the joint angle trajectories of the human finger during natural curling operations.

6

Characteristics of Prototype 1.0 and A Similarity Index

Extreme upper limb prosthesis is a well researched topic. There are number of research prototypes and a few commercially launched variants. For a wider acceptance among amputees, prosthetic hands need to be anthropomorphic i.e. replicate the human hand in form and function. However it is difficult to compare and rank prosthetic hands on the extent of their being anthropomorphic. Therefore this chapter focus to evolve a framework for quantification of anthropomorphism for prosthetic hands.

Prototype 1.0 is evaluated in terms of the performance requirements of prosthetic hands. The requirements listed here are based on the research in prosthetic hands and their clinical use (16, 168, 169, 170). The characteristics indicating the anthropomorphism are categorized as physical, kinematic and dynamic characteristics. The selection of the characteristics are based on the functional requirements of human hand to have a clinical score such as Action Research Arm Test (ARAT) (168) and Southampton Hand Assessment Procedure (SHAP) (16) equivalent to that of normal upper limb (16, 168). These characteristics includes joint range of motion (RoM), DoF, dynamic constraints and fingertip force; requirements of a robotic hand to be used as prosthesis (169) such as number of joints, number of fingers and number of actuators; geometrical and general characteristics to mimic the human hand in form and function (84, 170) such as weight and length. The characteristics of Prototype 1.0 vis-a-vis five established prosthetic hands viz. DLR Hand, Manus Hand, i-Limb, Southampton Hand and Utah/MIT Hand are evaluated.

6.1 Characteristics of Prototype 1.0

In continuation to the characteristics evaluation, the chapter propose a framework for quantification of anthropomorphism of prosthetic hands. A Biomimetic Similarity Index (BSI) for comparison of prosthetic hands is reported following the quantification of anthropomorphism. The BSI of Prototype 1.0 is compared with five fairly established prosthetic hands vis-a-vis human hand.

6.1 Characteristics of Prototype 1.0

6.1.1 Physical Characteristics

6.1.1.1 Size

Prosthetic hands are expected to possess the shape and size of a human hand. A prosthetic hand with unnatural shape and size is far from human hand in terms of the functional geometry; which makes it unappealing to the user (20). The size of Prototype 1.0 has been computed in terms of the finger length, finger diameter, hand length, palm width, palm thickness and total volume. Table 6.1 illustrates the size of Prototype 1.0 with respect to the human hand.

Table 6.1: Size of Human hand and Prototype 1.0

Performance	Human Hand	Prototype 1.0
Each finger diameter	14 mm	14 mm
Each finger length	92 mm	96 mm
Hand Length	210 mm	190 mm
Total Volume	50 cc	47cc
Wrist width	65 mm	65 mm
Palm width and thickness	90 mm	90 mm
Palm thickness	45 mm	45 mm

The size of prosthetic hands are commonly expressed in terms of the extreme upper limb length (171). The prosthetic hand structure should have a length between 180-198 mm and a width of 75-90 mm to match normal human hand size (1). Table 6.2 shows the length of prosthetic hands including Prototype 1.0. Lengths are in the ranges of 180 mm to 210 mm.

Table 6.2: Length of Prosthetic Hands and Prototype 1.0

Hands	Length in mm
DLR Hand	190
Manus Hand	198
i-Limb	180
Southampton Hand	185
Utah/ MIT Hand	188
Prototype 1.0	210

6.1.1.2 Weight

Weight is one of the main reasons for non-acceptance of prosthetic hands by the amputees (154). Kay and Rakic (172) have set a requirement that the hand including cosmetic glove should remain under 370 grams while other group (173) advocate a 500 gram weight limit. According to (2), an adult-sized prosthetic hand should weigh less than 400 grams; the average weight of human hand (171). The weight of Prototype 1.0 is 520 grams. Figure 6.1 shows the weight of prosthetic hands versus number of joints. Figure 6.2 shows the weight of prosthetic hands versus number of actuators.

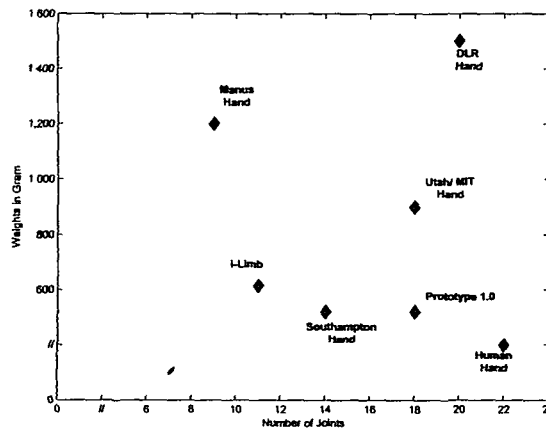


Figure 6.1: Weights of Prosthetic Hands and Research prototypes versus number of Joints (Adapted from (171, Table I and II))

6.1 Characteristics of Prototype 1.0

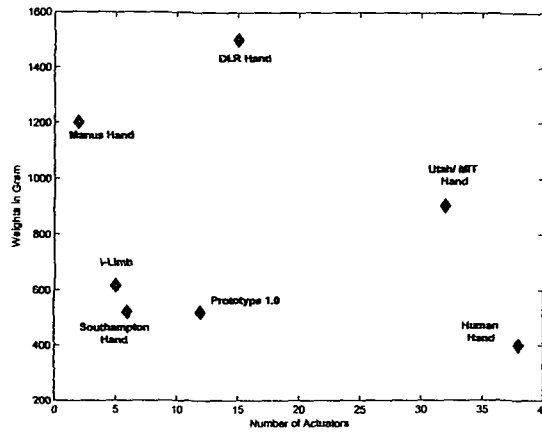


Figure 6.2: Weights of Prosthetic Hands and Research prototypes versus number of Actuators (Adapted from (171, Table I and II))

6.1.1.3 Degrees of Freedom

Low DoF characterize low grasping functionality, lesser flexibility and may lead to unstable grasps (4). Figure 6.3 shows the DoF of prosthetic hands (including Prototype 1.0) versus the number of joints. It is seen that the DoF increases with the increase in number of joints. The human hand possess 22 DoF.

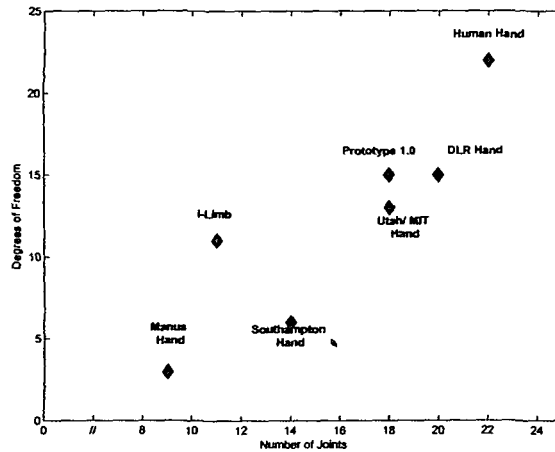


Figure 6.3: DoF versus Number of Joints for Prosthetic Hands (Adapted from (171, Table I and II))

6.1.2 Kinematic Characteristics

6.1.2.1 Dynamic Constraints

The finger joint motions must integrate among themselves to form stable grasps. Human finger joint angles follow inter-joint angular relationships. Dynamic constraints (12) ensure such an integration during motion (168) as detailed in Chapter 5. ARAT score revealed that dynamic constraints are highly disrupted in stroke subjects (168). Table 6.3 shows the dynamic constraints for Prototype 1.0 vis-a-vis prosthetic hands. Dynamic constraints for Prototype 1.0 are evaluated following the mathematical formulation in equation 2.1 and 2.2 in Chapter 2; and from simulation results in Chapter 5.

6.1.2.2 Range of Motion

Finger joint range of motion (RoM) is one of the characteristics that determines the work volume of the hand. For an anthropomorphic prosthetic hand, the finger joint RoM should be close to that of human finger. Each joint in human hand is characterized by the geometry of the contacting surfaces and by an angle of movement. Table 6.3 lists the RoM of Prototype 1.0 vis-a-vis other prosthetic hands. The RoM of Prototype 1.0 is measured using Jamar Plastic Goniometer.

Table 6.3: Finger joint RoM and Dynamic Constraints (Adapted from (171, Table III and IV))

	MCP Flexion	PIP Flexion	DIP Flexion	Dynamic Constraints	
				DC1	DC2
i-Limb	0 to 90	0 to 90	0 to 20	1	4.5
Manus Hand	0 to 70	0 to 40	0 to 40	1.57	1
Utah/ MIT Hand	0 to 90	0 to 90	0 to 90	1	1
DLR Hand	0 to 90	0 to 90	0 to 90	1	1
Southampton Hand	0 to 90	0 to 110	0 to 70	0.8	1.57
Prototype 1.0	0 to 90	0 to 110	0 to 70	0.8	1.57

6.1.2.3 Number of Actuators and Hand Complexity

Number of actuators is one of the important characteristics of a prosthetic hand as it decides the number of DoFs and the weight of the hand. Furthermore, several joints results in unnatural movements by the prosthetic hands (84). One of the aims of biomimetic robotics is to reduce the number of actuators keeping similar hand dexterity (174). With this, the little and ring finger in Prototype 1.0 are actuated through common actuators. Moreover, these two fingers moves together for grasping all spherical objects (175). Figure 6.4 shows the number of actuators versus DoF of the prosthetic hands. Human hand possess 38 number of actuators (25).

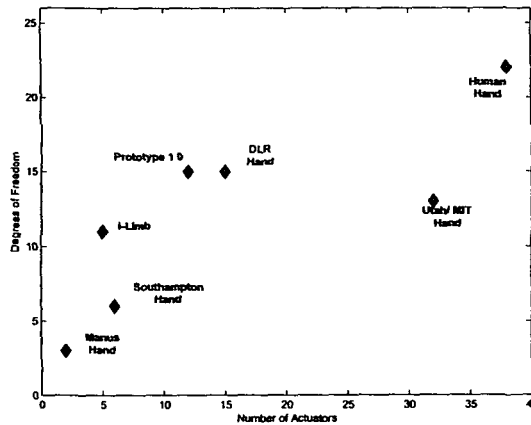


Figure 6.4: Number of Actuator versus DoF (Adapted from (171, Table I and II))

6.1.3 Dynamic Characteristics

6.1.3.1 Achievable Grasps

Increasing the number of achievable grasp types increases the functionality (176). Grasp-ability of the most of the prosthetic hands in literature are limited to two to four grasp types (177, 178). Prototype 1.0 can execute six grasp types: power, palm-up, oblique, hook, pinch and precision as shown in Figure 5.12.

6.1.3.2 Finger Tip Force

Figure 6.5 shows the precision grasp force of the prosthetic hands versus their weights. Figure 6.6 shows the precision grasp force versus number of actuators. A minimum of 3 N fingertip force is required in human hand to form a stable grasp (179). Human hand can generate a maximum of 20 N fingertip force. The fingertip force of the prosthetic hands under study ranges from 2 N to 60 N. Prototype 1.0 can generate a fingertip force in the range of 0.6 N to 45 N.

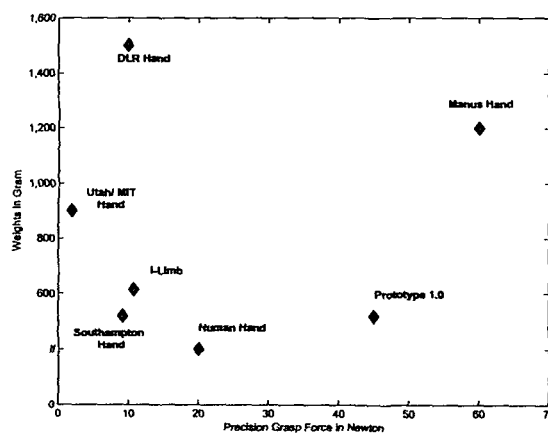


Figure 6.5: Precision Grasp Force of Prosthetic hands and research prototype versus weights (Adapted from (171, Fig.5))

In addition to the above characteristics, number of fingers is an important emphasis to mimic the human hand (180, chapter 23).

6.2 Biomimetic Similarity Index

For a wider acceptance among amputees, prosthetic hands intends to be anthropomorphic i.e. replicate the human hand in form and function. However, it is often difficult to compare and rank prosthetic hands on the extent of their being anthropomorphic. BSI reflects extent of anthropomorphism and allows a quantitative comparison of different prosthetic hands with reference to the human hand.

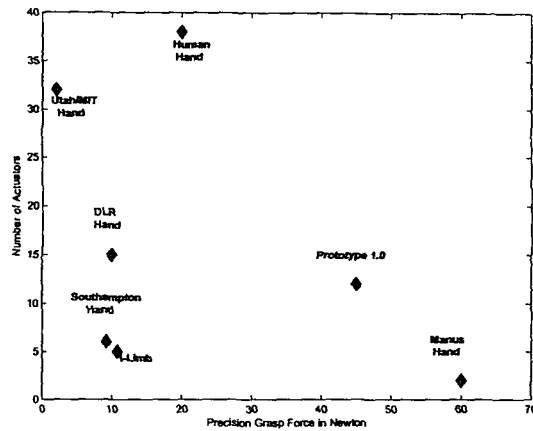


Figure 6.6: Precision Grasp Force of Prosthetic hands and research prototypes versus number of actuators (Adapted from (171, Fig.2))

6.2.1 Metric for Similarity

A similarity measure determines the relative closeness of the objects to a reference object. Ranking the objects based on the magnitudes of their similarity measure with respect to the reference object computes the degree of similarity of the objects vis-a-vis the reference object. This similarity measure can be mapped to the range 0 to 1; where 1 shows absolute similarity. A quantitative framework based on matrix algebra for computation of such a similarity measure for exploiting functionality of products in *design-by-analogy* have been put forward by McAdams and Wood (181). The similarity is influenced by customer needs which drive the product functions having a key impact on the resulting design. Along these lines, this section give a method for computing biomimetic similarity of prosthetic hands. BSI is intended to give the closeness of the prosthetic hands under investigation to the human hand. The philosophy of the similarity measure is that anthropomorphism of a prosthetic hand can be expressed in terms of functional, geometric and general characteristics. Given a similarity index for individual prosthesis, one could rank these prostheses; one with the highest similarity index being the closest to the human hand.

A function-vector would be required to represent the prosthesis' functional, geometrical and general characteristics influencing anthropomorphism. Although anthropomorphism is subjective, there exist characteristics that prompt one to project the

right characteristics (182). With this to bring objectivity to the process of defining biomimetic similarity based on anthropomorphism, the *context* of anthropomorphism is characterized within Formal Concept Analysis (FCA). This follows the work reported for creating a security pattern lattice in (183). This characterization is based on the surveys encompassing clinical practice in the literature (16, 168) as well as research in prosthetic hands (169, 170, 171, 178, 184). The central notion of FCA is Galois connection (185), a duality between objects and attributes in an application. The process of defining BSI makes explicit this relationship between requirements for anthropomorphism and expected functionalities of the prosthesis based on literature review.

Formal Context: A formal context is given as $\langle O, A, I \rangle$, where O is the set of objects (called the *extent*); A is the set of attributes (called the *intent*) and I is a mapping between O and A . Formal context can be seen as a table between objects and attributes.

Formal Concept: Formal concept analyzes data which describe relationship between a particular set of objects and a particular set of attributes. A formal concept for a context $\langle O, A, I \rangle$ is defined by a two tuple $\langle O_i, A_i \rangle$ such that

- i. $O_i \subseteq O$ and $A_i \subseteq A$
- ii. Every object in O_i has every attribute in A_i
- iii. For every object in O that is not in O_i , there is an attribute in A_i which that object does not have and
- iv. For every attribute in A that is not in A_i , there is an object in O_i that does not have that attribute.

Function-Vector: A function-vector is the description of the extreme upper limb in terms of its characteristics that are required to be achieved by the prosthesis in order to completely represent the natural counterpart. Concept covering the characteristics of anthropomorphism is taken as the function-vector. It is described in terms of functional, geometrical and general characteristics of prosthesis.

A formal context of anthropomorphism is constructed for [i.] clarity in understanding the object to attribute relation and [ii] deciding on the minimal set of attributes

covering all of the given objects. Table 6.4 shows the formal context of anthropomorphism.

Graphical interpretation of the prosthesis function-vector and similarity projection of such a vector on to the human hand is shown in Figure 6.7.

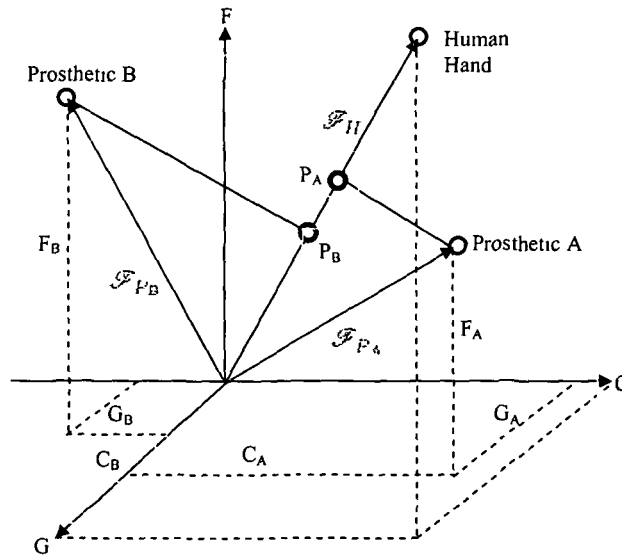


Figure 6.7: Graphical interpretation of prosthesis function-vector similarity projection on human hand

Each prosthesis is represented as P_i in terms of its function-vector \mathcal{F}_{P_i} . \mathcal{F}_H is the human hand function-vector. Prosthetic A (resp. Prosthetic B) is represented as a function of its functional, geometric and general characteristics $\langle F_A, G_A, C_A \rangle$ (resp. $\langle F_B, G_B, C_B \rangle$). The solid lines in Figure 6.7 represents the function-vectors for the prostheses and the human hand. The component characteristics of each prosthesis is represented as dotted lines. The projection of Prosthetic A (resp. Prosthetic B) to the human hand as shown in Figure 6.7 begets the BSI P_A (resp. P_B).

Prosthetic-Functional Matrix: In order to carry out similarity projection based on a function-vector, a prosthetic-functional matrix, Φ is constructed. The prosthetic-functional matrix results out of collecting the prostheses' function-vectors as rows and

prostheses under investigation as columns.

6.2.2 Function-Vector Characteristics

An approach to derive the concept that best describes the anthropomorphism is presented in this section. It is through FCA supported by the research in clinical practice and prosthetic hands (16, 168, 169, 170). Functional, geometric and general characteristics are the objects indicating anthropomorphism. Formal context of anthropomorphism is expressed as

$$\langle O, A, I \rangle$$

where

$O = \{\text{Functional, Geometric, General}\}$ is the set of objects

$A = \{\text{DoF, RoM:MCP, RoM:DIP, RoM:PIP, } DC1, DC2, \text{Fingertip Force, Number of Fingers, Number of Joints, Hand Length, Weight, Number of Actuators}\}$ is the set of attributes

I is the relation between O and A ; expressed as per Table 6.4. The object to attribute mapping is based on

- a. functional requirements of human hand to have a clinical score equivalent to that of normal upper limb (16, 168)
- b. requirements of a robotic hand to be used as prosthesis (169) and
- c. geometrical and general characteristics to mimic the human hand in form and function (84, 170).

The entries for I , the matrix of relation between objects and attributes is shown in Table 6.4. Figure 6.8 shows the formal concept lattice for the context of anthropomorphism (186). Eight concepts as tabulated in Table 6.5 are observed; including the functional, geometric and general characteristics as individual concepts.

6.2 Biomimetic Similarity Index

Table 6.4: Formal Context of Anthropomorphism.

Attributes \ Objects	Functional	Geometric	General
DoF	×		
RoM:MCP	×		
RoM:PIP	×		
RoM:DIP	×		
DC1	×		
DC2	×		
Fingertip Force	×		×
Number of Fingers		×	
Number of Joints	×	×	
Palm Length		×	×
Weight			×
Number of Actuators	×		

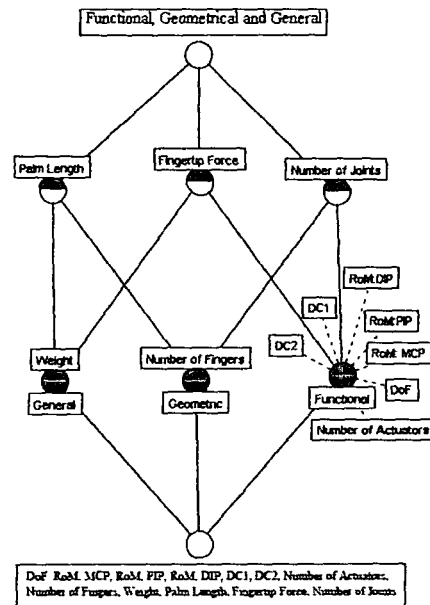


Figure 6.8: Concept Lattice for the context of anthropomorphism. Grey boxes are attributes and white boxes are objects

6.2 Biomimetic Similarity Index

Table 6.5: Concepts of Anthropomorphism

({General, Geometric},{Palm Length})
({General, Functional},{Fingertip Force})
({Geometric, Functional},{Number of Joints})
({General},{Weight})
({Geometric},{Number of Fingers})
({Functional},{DC1, DC2, RoM:MCP, RoM:DIP, RoM:PIP, DoF, Number of Actuators})
(},{DoF, RoM:MCP, RoM:DIP, RoM:PIP, DC1, DC2, Fingertip Force, Number of Fingers, Number of Joints, Palm Length, Weight, Number of Actuators})
({Functional, Geometric, General},{})

6.2.3 Derivation of A Biomimetic Similarity Index

McAdams and Woods (181) procedure is followed to arrive at a quantitative metric of similarity to a given reference for prosthetic hands. The human hand is considered as reference. To compensate the variations in function-vectors of the prosthetic hands, the elements of Φ are weighted using the weighing function:

$$V_{ij} = \Phi_{ij} \cdot \frac{\bar{\eta}}{\eta_j} \cdot \frac{\mu_j}{\bar{\mu}}$$

where

$$\begin{aligned} \Phi_{ij} &= \text{Element of the metric } \Phi \text{ at the } i^{\text{th}} \text{ row and } j^{\text{th}} \text{ column} \\ \bar{\eta} &= \frac{\text{sum of all the elements in } \Phi}{\text{number of columns}} \\ \eta_j &= \text{Columns sum of } \Phi \\ \mu_j &= \sum_{j=1}^m H(\Phi_{ij}) \text{ with } m = \text{total number of elements in } \Phi \\ \bar{\mu} &= \sum_{i=1}^m \sum_{j=1}^n H(\Phi_{ij}) \end{aligned}$$

H is the Heaviside function and is defined as

$$\begin{aligned} H(x) &= 1 \text{ when } x \neq 0 \\ &= 0 \text{ otherwise} \end{aligned}$$

6.2 Biomimetic Similarity Index

The weighted prosthetic-functional matrix is normalized to make its norm unity. The inner product of the normalized prosthetic-functional matrix and human hand function-vector \mathcal{F}_H gives projection of the prostheses on to the human hand. The index so obtained is a measure of biomimetic similarity and christened BSI. A BSI of unity represents the human hand.

The prosthetic-functional matrix Φ for i- Limb, Manus Hand, Utah/MIT Hand, DLR/HIT, Southampton and Prototype 1.0 are constructed as shown below.

	Prototype 1.0	i-Limb	Manus Hand	Utah/ MIT Hand	DLR Hand	Southampton	Human Hand
DoF	15	11	3	13	15	6	22
RoM: MCP Joint	90	90	70	90	90	90	90
:PIP Joint	110	90	40	90	90	70	110
:DIP Joint	70	20	40	90	90	70	70
Constraints: DC1	0.8	1	1.75	1	1	.8	.8
: DC2	1.57	4.5	1	1	1	1.57	1.57
Fingertip Force	45	10.8	60	2	10	9.2	20
Number of Fingers	5	5	5	4	5	5	5
Number of Joints	18	11	9	18	20	14	22
Palm Length	210	180	198	188	190	185	190
Weight	520	615	1200	900	1500	520	400
Number of Actuators	12	5	2	32	15	6	38

The human hand is considered as the reference. The human hand matrix S is given below.

	<i>HumanHand</i>
DoF	22
RoM: MCP Joint	90
:PIP Joint	110
:DIP Joint	70
Constraints: DC1	0.8
: DC2	1.57
Fingertip Force	20
Number of Fingers	5
Number of Joints	22
Palm Length	190
Weight	400
Number of Actuators	38

To make the importance of all the elements in the prosthetic-functional matrix equal, each elements of the prosthetic-functional matrix is weighted with the weighing

6.2 Biomimetic Similarity Index

function V_{ij} . The weighted matrix N is shown below.

	Prototype 1 0	r-Limb	Manus Hand	Utah/ MIT Hand	DLR Hand	Southampton	Human Hand
DoF	2 55	1 98	0 34	1 70	1 38	1 14	4 25
RoM MCP Joint	15 30	16 20	8 04	11 80	8 30	17 24	17 39
PIP Joint	18 70	16 20	4 59	11 80	8 30	13 41	21 26
DIP Joint	11 90	3 60	4 59	11 80	8 30	13 41	13 52
Constraints DC1	1 36	0 18	0 20	0 13	0 09	0 15	0 15
DC2	0 27	0 81	0 11	0 13	0 09	0 30	0 30
Fingertip Force	7 65	1 94	6 89	0 26	0 90	1 76	3 86
Number of Fingers	0 85	0 90	0 57	0 52	0 45	0 95	0 97
Number of Joints	3 06	1 98	1 03	2 34	1 84	2 68	4 25
Palm Length	35 70	32 40	22 76	24 44	17 56	35 40	36 72
Weight	88 40	110 70	137 95	117 00	138 64	99 66	77 30
Number of Actuators	2 04	0 90	0 23	4 16	1 38	1 14	7 34

To review the functional similarity of the prosthetic hands, the function-vectors in the weighted prosthetic-functional matrix is normalized so that their norm is unity. On normalization, N becomes \bar{N} and is given as:

	Prototype 1 0	r-Limb	Manus Hand	Utah/ MIT Hand	DLR Hand	Southampton	Human Hand
DoF	0 03	0 02	0 01	0 01	0 11	0 01	0 05
RoM MCP Joint	0 15	0 13	0 05	0 09	0 06	0 15	0 20
PIP Joint	0 18	0 13	0 03	0 09	0 06	0 12	0 23
DIP Joint	0 12	0 03	0 03	0 09	0 01	0 12	0 14
Constraints DC1	0 02	0 01	0 01	0 01	0 01	0 01	0 01
DC2	0 01	0 01	0 01	0 01	0 01	0 01	0 01
Fingertip Force	0 08	0 02	0 05	0 01	0 01	0 02	0 04
Number of Fingers	0 01	0 01	0 01	0 01	0 01	0 01	0 01
Number of Joints	0 03	0 02	0 01	0 02	0 02	0 02	0 05
Palm Length	0 35	0 27	0 16	0 20	0 33	0 33	0 40
Weight	0 89	0 94	0 98	0 96	0 91	0 91	0 85
Number of Actuators	0 02	0 01	0 01	0 03	0 01	0 01	0 08

The inner product of the reference matrix S and the \bar{N} gives the projection of the prosthetic hands onto the human hand in function-vector space. This is a measure of biomimetic similarity. The similarity index shows the extend of anthropomorphism of

the prosthetic hands under study including Prototype 1.0 with reference to the human hand.

$$\text{BSI} \begin{pmatrix} \text{Prototype 1.0} \\ \text{i-Limb} \\ \text{Manus Hand} \\ \text{Utah/ MIT Hand} \\ \text{DLR Hand} \\ \text{Southampton} \\ \text{Human Hand} \end{pmatrix} \begin{pmatrix} 0.96 & 0.94 & 0.89 & 0.92 & 0.89 & 0.95 & 1.00 \end{pmatrix}$$

6.3 Summary

A formalism have been presented to compute BSI for prosthetic hands. The BSI reflects extent of anthropomorphism and is a measure of closeness of a prosthetic hand to human hand. This allows a quantitative comparison of different prosthetic hands. This was computed over a set of functions that reflect functional and geometric biomimesis represented as a function-vector. The function-vector was characterized within a formal context of anthropomorphism; the context was constructed using FCA. This gives objectivity to what would one like to term as anthropomorphic and allows to decide which of the attributes contributes or best describes anthropomorphism of a prosthetic hand. The decision of the function-vector was arrived through a literature review of research in clinical practice and prosthetic hands. The objectivity of anthropomorphism is subjective to the set of attributes in the function-vector. A different set of attributes in the function-vector would result in different anthropomorphic measures. Defining the attributes in the function-vector remains as an open challenge.

Five prosthetic hands: DLR Hand, i-Limb, Manus Hand, Utah/ MIT Hand and Southampton Hand apart from the Prototype 1.0 have been considered for computing the BSI. It was interesting to note that BSI reflects quantitatively what one could qualitatively derive from (171). Southampton Hand and i-Limb could be categorized into one cluster and the remaining three (Manus, Utah/MIT and DLR) into another cluster as per tabulations reported in (171). Properties of Prototype 1.0 are closer to Southampton Hand and i-Limb. Prototype 1.0, Southampton and i-Limb have BSI of 0.96, 0.94 and 0.95 respectively; whereas the hands in the other cluster: Manus, Utah/MIT and DLR have BSI of 0.89, 0.92 and 0.89 respectively. BSI is a quantitative categorization of prosthetic hand's similarity.

Conclusions and Future Work

In this chapter, I shall summarize the main results of the thesis and point to the directions towards future work. First, I shall discuss the results on the EMG based recognition of six grasp types used during 70% of dla. Then, I shall summarize the results on the biomimetic hand with EMG based grasp emulation followed by the BSI for prosthetic hands. This summary leads to the issues to be encountered for future research and discussed in the final section.

7.1 Conclusions

In recent years, much research has been done in the area of rehabilitation robotics worldwide. I have presented a general understanding of the field and particular insight into the lines of research in Chapter 1, which originated and inspired the work undertaken in this thesis. The literature review starting from EMG based grasp recognition towards the control of a prosthetic hand grasping reveals that a biomimetic hand with EMG based grasp emulation holds promise.

This research highlighted some of the important issues involved in successful use of prosthetic hands as if it were a natural part of the body. Present prosthesis (both commercial and research prototypes) are far from the natural counterparts in terms of both EMG based control and functional geometry. Further, they are non-intuitive being controlled through dissociate muscle remnants action or higher number of EMG channels. The work reported in this thesis focused on the development of a biomimetic hand with EMG based grasp emulation. Development of such a hand involves the

recognition of grasp types used during dla as well as a biomimetic hand development inspired by human hand anatomy. I have concentrated on the recognition of six grasp types; power, palm-up, oblique, hook, pinch and precision based on EMG signals. These six grasps are of significance as they are used during 70% of dla. A biomimetic hand mimicking the functional geometry i.e. both static and dynamic constraints of the human hand was developed.

7.1.1 EMG based Grasp Recognition

The material and methods followed for acquisition of EMG signals were discussed in Chapter 3. An experimental protocol for acquisition of EMG signals from the resting state of the hand to grasping state followed by the releasing the grasp and returning to the rest has been presented. The chapter discusses three grasp recognition architectures and initial experimental results were presented. In architecture-I, six grasp types under study have been recognized with an average recognition rate of 77%. The classification was through a SVM classifier followed by a FFT classifier. In the grasp recognition architecture-II, classification was done in a single step through a linear kernel SVM and an average recognition rate of 80% and 84% were achieved using CWT and DWT features. SWC have been used as feature set for classification through a RBF kernel SVM in grasp recognition architecture-III. An average recognition rate of 86% was achieved for the six grasp types. Through these grasp recognition architectures, following facts have been established:

- CWT function coefficients of the EMG signals having entropy values close to the entropy values of preprocessed EMG signals possess maximum informations about the grasp types.
- SWC is established as a primal feature for classification of grasp types.

EMG based grasp recognition result comparable to that reported in the literature is presented in Chapter 4. This chapter focuses on the derivation of a low dimensional yet informative and distinguishing feature set to significantly increase the performance of low channel EMG based grasp types recognition. Grasps classification experiments have been carried out with four groups of features: TD, FD, TFD and PCA of TFD features in quest of an efficient feature set for higher recognition rate. The transition

from one feature set to another is based on the linear relationship of each feature set with the grasp types. It was based on the R^2 -value obtained through ANOVA. PCA of TFD features reported an average recognition rate 97.5% for the six grasp types under study based on two channel EMG. The reported result is better in terms of the number of EMG channels involved, number of grasp types and the recognition rate as presented in Table 4.16 in Chapter 4.

7.1.2 A Biomimetic Hand with EMG based Grasp Emulation

The development of a biomimetic hand inspired by human hand anatomy is reported in Chapter 5. The prototype has been developed following a biomimetic approach inspired by human hand anatomy. It mimics the human hand in its form satisfying the static and dynamic constraints. This results into a BSI of 0.96; which is the highest among the BSI of five fairly established prosthetic hands as elaborated in Chapter 6. Further, the dynamic constraints have been considered for tendon actuation in the hand as stated in section 5.2.1.1. This is subsequently used in the control of the hand. A two layered control architecture: SHC and LHC is presented in Figure 5.4. SHC is for the recognition of the grasp types attempted by the user based on the EMG signals. The LHC emulate the identified grasp type in Prototype 1.0. Prototype 1.0 follows the human-like finger joint trajectories and ensures stable grasping operations.

7.1.3 A Biomimetic Similarity Index

An index for comparative evaluation of the available prosthetic hands with reference to the human hand is of importance. Towards the end of this research, a BSI for evaluation of the prosthetic hands in terms of anthropomorphism is proposed in Chapter 6. Five fairly established prosthetic hands have been compared with Prototype 1.0. Prototype 1.0, developed through a biomimetic approach reports the highest BSI of 0.96. Biomimetic design leads to higher anthropomorphism of robotic hands; biomimetic design should result in a higher BSI. Prototype 1.0 is a case in point.

A similar metric for comparing the anthropomorphic motion capability of artificial hands have been reported parallel to my work by a group of researchers supported by European Union (EU) IST FP7 Integrated Project, EU European Research Council project and Swedish Foundation for Strategic Research. The metric is for comparing the anthropomorphic motion capability of robotic and prosthetic hands. The metric is

based on the evaluation of how many different postures or configurations a hand can perform by studying the reachable set of fingertip poses. It does not take into account the functional as well as geometric characteristics required to replicate a prosthetic hand as in the case of BSI reported in this thesis (187). Furthermore, although scores such as ARAT and SHAP can be used for evaluating prosthetic hands; it is often difficult to rank one with respect to other based on its extent of anthropomorphism. Therefore, formulation of a biomimetic index for comparison of prosthetic hands is novel and hitherto not reported in the literature. A high BSI i.e., anthropomorphism alone may not be the only criteria for wider acceptance of a prosthetic hands. Clinical studies can only evaluate BSI as a criteria.

7.2 Future Work

There remain many avenues for further research. Some of the issues to be explored for further improvement of Prototype 1.0 concern with the EMG based grasp recognition whilst others may lead to the application of Prototype 1.0 as a prosthetic hand for amputees.

7.2.1 Further evaluation of the EMG based Grasp Recognition

7.2.1.1 Use of Different Classifier

As presented in Chapter 3 and 4, the work concentrated on EMG based grasp classification through SVM. ANN, FL based classifiers are the most used method in classifying the EMG signals. Even though the developed grasp recognition system has shown its usefulness in classifying the EMG signals, a further evaluation using ANN, FL based classifiers is needed. In addition to this, a neuro-fuzzy classifier could also be investigated as it is a combination of ANN and fuzzy logic and may improve the system performance. All these methods would require training data from the individual user of the system which is a disadvantage.

7.2.1.2 Use of Different Data Sets

In the work presented in this thesis, the system was tested with EMG data from normal healthy subjects. It is expected that there will be not much difference in the system performance between healthy people and people with amputation based on the research

findings reported in (8). However, for final implementation of the prototype as a prosthesis, study on the grasp recognition system that uses amputees EMG from their remnant muscle is needed.

7.2.2 Implementation into a Microcontroller

A biomimetic hand prototype with EMG based grasp emulation: Prototype 1.0 has been developed. It is very important to implement the EMG based grasp emulation system in a microcontroller for a real time application to provide a practical and small system. The most critical part is to implement the EMG based grasp recognition architecture into a microcontroller. In addition, it should be accompanied with the miniaturization of the driver circuit so that the complete system can be fitted into an artificial slave. One of the challenges in this is to use a power supply (i.e. battery) of smaller size as well as longer back-up. Another task to be completed for real time application is to use a skin-covering to imitate the natural aesthetic. A dedicated clinical trials with the amputees is one of another important aspects so that the prototype can reach the end user with a good warranty.

Bibliography

- [1] W. Schwitzer, "Technical Below Elbow Amputee Issues - i-LIMB Pulse [new]," Touch EMAS Ltd., Tech. Rep., May 2010, Available at <http://www.swisswuff.ch/tech/?p=306>.
- [2] J. L. Pons, E. Rocon, R. Ceres, D. Reynaerts, B. Saro, S. Levin, and W. V. Moorlegheem, "The MANUS-HAND Dextrous Robotics Upper Limb Prosthesis: Mechanical and Manipulation Aspects," *Autonomous Robot*, vol. 16, no. 2, pp. 143–163, 2004.
- [3] P. J. Kyberd and P. H. Chappel, "The Southampton Hand: An Intelligent Myoelectric Prosthesis," *Journal of Rehabilitation Research and Development*, vol. 31, no. 4, pp. 326–334, 1994.
- [4] B. Massa, S. Roccella, M. C. Carrozza, and P. Dario, "Design and Development of an Underactuated Prosthetic Hand," in *IEEE International Conference on Robotics and Automation*, Washington, DC, 2002, pp. 3374–3379.
- [5] J. del R. Millan, F. Renkens, J. Mourino, and W. Gerstner, "Noninvasive Brain-Actuated Control of a Mobile Robot by Human EEG," *IEEE transactions on Biomedical Engineering*, vol. 51, no. 6, pp. 1026–1033, 2004.
- [6] P. K. Artemiadis and K. J. Kyriakopoulos, "An EMG-Based Robot Control Scheme Robust to Time-Varying EMG Signal Features," *IEEE transaction on Information Technology in Biomedicine*, vol. 14, no. 3, pp. 582–588, 2010.
- [7] M. Z. Jamal, *Signal Acquisition Using Surface EMG and Circuit Design Considerations for Robotic Prosthesis*. New York: Intech, 2012.

BIBLIOGRAPHY

- [8] B. Crawford, K. Miller, P. Shenoy, and R. Rao, "Real-Time Classification of Electromyographic Signals for Robotic Control," Department of Computer Science, University of Washington, Tech. Rep. 2005-03-05, 2005.
- [9] N. M. Kakoty and S. M. Hazarika, "A Two Layered Control Architecture for Prosthetic Grasping," *Paladyn. Journal of Behavioral Robotics*, vol. 4, no. 1, pp. 1–9, 2013.
- [10] N. Bu, J. Arita, and T. Tsuji, "A Novel Pattern Classification Method for Multivariate EMG Signals Using Neural Network," *Advances in Natural Computing*, vol. 3611, no. 1, pp. 165–174, 2005.
- [11] A. L. Hutchison and R. L. Hutchison, "Fibonacci, Littler and the Hand: A Brief Review," *Journal of Hand*, vol. 5, no. 4, pp. 364–368, 2010.
- [12] J. J. Kuch and T. S. Huang, "Vision Based Hand Modelling and Tracking for Virtual Teleconferencing and Telecollaboration," in *5th IEEE International Conference on Computer Vision*, Washington, 1995, pp. 666–671.
- [13] W. Schweitzer, "Technical Below Elbow Amputee Issues - Otto Bock Michelangelo Hand," Ottobock, Tech. Rep., March 2009, available at <http://www.swisswuff.ch/tech/?p=145>.
- [14] S. C. Jacobsen, E. K. Iversen, and D. F. Knutti, "Design of the UTAH/MIT Dextrous Hand," in *IEEE International Conference on Robotics and Automation*, San Francisco, 1986, pp. 1520–1532.
- [15] J. Butterfass, Grebenstein, H. Liu, and G. Hirzinger, "DLR Hand II: Next Generation of Dextrous Robot Hand," in *IEEE International Conference on Robotics and Automation*, Korea, 2001, pp. 109–114.
- [16] P. J. Kyberd, A. Murgia, M. Gasson, T. Tjerks, C. Metcalf, P. H. Chappell, K. Warwick, S. E. M. Lawson, and T. Barnhill, "Case Studies to Demonstrate the Range of Applications of the Southampton Hand Assessment Procedure," *British Journal of Occupational Therapy*, vol. 72, no. 5, pp. 212–218, 2009.

BIBLIOGRAPHY

- [17] F. Vecchi, S. Micera, M. C. Carrozza, A. M. Sabatini, and P. Dario, "A Sensorized Glove for Applications in Biomechanics and Motor Control," in *6th IFESS Conference*, San Francisco, CA, 2008, pp. 346–353.
- [18] S. Bitzer and P. van der Smagt, "Learning EMG Control of a Robotic Hand-Towards Active Prostheses," in *IEEE International Conference on Robotics and Automation*, Orlando, 2006, pp. 2819–2823.
- [19] M. Yoshikawa, M. Mikawa, and K. Tanaka, "A Myoelectric Interface for Robotic Hand Control Using Support Vector Machine," in *IEEE/RSJ International Conference on Intelligent Robots and Systems*, USA, 2007, pp. 2723–2728.
- [20] A. A. Aiboye and R. F. Weir, "A Heuristic Fuzzy Logic Approach to EMG Pattern Recognition for Multi-Functional Prosthetic Control," *IEEE Transactions on Neural Systems and Rehabilitation Engineering*, vol. 13, no. 3, pp. 280–291, 2005.
- [21] H. Arieta, R. Kato, H. Yokoi, and Y. Wenwei, "Development of a multi-DOF Electromyography Prosthetic System using the Adaptive Joint Mechanism," *Applied Bionics and Biomechanics*, vol. 3, no. 2, pp. 101–112, 2006.
- [22] C. Castellini, E. Fiorilla, and G. Sandini, "Multi-subject/ DLA Analysis of Surface EMG Control of Mechanical Hands," in *poster at GNB I, First Italian Bioengineering Congress, Italy, Pisa, Italy*, 2008.
- [23] O. Fukunda, T. Tsuji, M. Kancko, and A. Otsuka, "A Human-Assisting Manipulator Teleoperated by EMG Signals and Arm Motions," *IEEE transaction on Robotics and Automation*, vol. 19, no. 2, pp. 210–222, 2003.
- [24] G. D. Luca, "Fundamental Concepts in EMG Signal Acquisition," Delsys Inc., Tech. Rep., 2003.
- [25] M. Zecca, S. Micera, M. Carrozza, and P. Dario, "Control of Multifunctional Prosthetic Hands by Processing the Electromyographic Signal," *Journal of Biomedical Engineering*, vol. 30, no. 4-6, pp. 459–485, 2002.
- [26] M. Oskoei and H. Hu, "Myoelectric Control Systems A survey," *Journal of Biomedical Signal Processing and Control*, vol. 2, pp. 275–294, 2007.

BIBLIOGRAPHY

- [27] P. Hudgins, P. A. Parker, and R. Scott, "A New Strategy for Multifunction Myoelectric Control," *IEEE transaction of Bimedical Engineering*, vol. 40, no. 1, pp. 21–38, 1993.
- [28] S. H. Park and S. P. Lee, "EMG Pattern Recognition based on Artificial Intelligence Technique," *IEEE transactions on Rehabilitation Engineering*, vol. 6, no. 4, pp. 400–406, 1998.
- [29] S. Micera, A. M. Sabatini, and P. Dario, "On Automatic Identification of Upper Limb Movements using Small Sized Training Sets of EMG Signals," *Journal of Medical Engineering Physics*, vol. 22, no. 8, pp. 527–533, 2000.
- [30] F. V. G. Tanore, A. Ramos, A. Fahmy, S. Acharya, and R. Etninc-Cummings, "Decoding of Individual Finger Movements using Surface Electromyography," *IEEE transactions on Biomedical Engineering*, vol. 56, no. 5, pp. 1427–1434, 2009.
- [31] K. Farry, I. Walker, and R. Baraniuk, "Myoelectric Teleoperation of A Complex Robotic Hand," *IEEE transactions on Robot Automation*, vol. 12, no. 5, pp. 775–778, 1996.
- [32] M. Zardoshti-Kermani, B. Wheeler, K. Badie, and R. Hashemi, "EMG Feature Evaluation for movement control of upper extremity prosthesis," *IEEE transactions on Rehabilitation Engineering*, vol. 3, no. 4, pp. 459–485, 1995.
- [33] A. Phinyomark, A. Nuidod, P. Phukpattaranont, and C. Limsakul, "Feature Extraction and Reduction of Wavelet Transform Coefficients for EMG Pattern Classification," *Journal of Electronics and Electrical Engineering*, vol. 122, no. 6, pp. 27–32, 2012.
- [34] D. Tkach, H. Huang, and T. A. Kuiken, "Study of Stability of Time-Domain Features for Electromyographic Pattern Recognition," *Journal of NeuroEngineering and Rehabilitation*, vol. 7, pp. 1–13, 2010.
- [35] A. B. Ajiboye and R. F. Weir, "A Heuristic Fuzzy Logic Approach to EMG Pattern Recognition for Multifunctional Prosthesis Control," *IEEE Transaction on Neural System and Rehabilitation Engineering*, vol. 13, no. 3, pp. 280–291, 2005.

BIBLIOGRAPHY

- [36] P. Shenoy, K. J. Miller, B. Crawford, and R. N. Rao, "Online Electromyographic Control of a Robotic Prosthesis," *IEEE Transaction Biomedical Engineering*, vol. 55, pp. 1128–1135, 2008.
- [37] R. N. Khushaba, "Application of Biosignal-Driven Intelligent Systems for Multi-function Prosthesis Control," Ph.D. dissertation, University of Technology, Sydney, January 2010.
- [38] M. A. Oskoei, "Support Vector Machine-based Classification Scheme for Myoelectric Control Applied to Upper Limb," *IEEE Transaction on Biomedical Engineering*, vol. 55, no. 8, pp. 1956–1965, 2008.
- [39] K. Xing, Q. Xu, and Y. Lin, "Identification Scheme of Surface Electromyography of Upper Limb Movement," *Journal of Networks*, vol. 8, no. 4, pp. 895–902, 2013.
- [40] T. Oyama, Y. Matsumura, S. Karungaru, and Y. Mitsukura, "Recognition of Wrist Motion Pattern by EMG," in *International Joint Conference SICE-ICASE*, Busan, 2006, pp. 599–603.
- [41] D. Nishikawa, W. Yu, H. Yokoi, and Y. Kakazu, "EMG Prosthetic Hand Controller using Real-time Learning Method," in *IEEE International Conference on Systems Man and Cybernetics*, USA, 1999.
- [42] Y. Matsumura, M. Fukumi, and Y. Mitsukura, "Hybrid EMG Recognition System by MDA and PCA," in *IEEE International Joint Conference on Neural Networks*, Vancouver, BC, 2006, pp. 5294–5300.
- [43] S. Ferguson and G. R. Dunlop, "Grasp Recognition From Myoelectric Signals," in *Proceedings of Australian Conference on Robotics and Automation*, Auckland, 2002, pp. 82–84.
- [44] S. Mallat, *A Wavelet Tour of Signal Processing*. Paris: Academic Press, 1999.
- [45] V. J. Samar, A. Bopardikar, R. Rao, and K. Swartz, "Wavelet Analysis of Neuroelectric Waveforms: A Conceptual Tutorial," *Brain and Language*, vol. 66, no. 1, pp. 1–6, 1999.

- [46] W. C. Lang and K. Forinash, "Time frequency analysis with continuous wavelet transform," *American Journal Physics*, vol. 66, no. 9, pp. 794–796, 1998.
- [47] R. Polikar, "The Wavelet Tutorial: Part IV," Rowan University, Available at <http://users.rowan.edu/~polikar/WAVELETS/WTpart4.html>, Tech. Rcp., 2004.
- [48] K. Englehart, B. Hudgin, P. A. Parker, and M. Stevenson, "Classification of the Myoelectric Signal using Time-Frequency based Representations," *Journal of Medical Engineering and Physics*, vol. 21, no. 3, pp. 431–438, 1999.
- [49] K. Englehart and B. Hudgins, "A Robust, Real-Time Control Scheme for Multifunction Myoelectric Control," *IEEE transaction on Biomedical Engineering*, vol. 50, no. 7, pp. 848–854, 2003.
- [50] F. H. Y. Chan, Y.-S. Yang, F. K. Lam, Y.-T. Zhang, and P. A. Parker, "Fuzzy EMG Classification for Prosthesis Control," *IEEE transaction of Rehabilitation Engineering*, vol. 8, no. 3, pp. 305–11, 2000.
- [51] G. Wang, Z. Wang, W. Chen, and J. Zhuang, "Classification of Surface EMG Signals using Optimal Wavelet Packet Method Based on Davies-Bouldin Criterion," *International Federation for Medical and Biological Engineering*, vol. 44, 2006.
- [52] D. Graupe, J. Salahi, and K. H. Kohn, "Multifunction Prosthesis and Orthosis Control via Microcomputer Identification of Temporal Pattern Differences in Single-Myoelectric Signals," *Journal of Biomedical Engineering*, vol. 4, pp. 17–22, 1982.
- [53] H. Ido, "The Control Method for the Robot Hand Based on the Fuzzy Theory," *Journal of Robotics and Mechatronics*, vol. 4, pp. 262–267, 1992.
- [54] N. F. Guler and S. Kocer, "Classification of EMG Signals using PCA and FFT," *Journal of Medical Systems*, vol. 29, no. 3, pp. 241–250, 2005.
- [55] M. B. I. Reaz, M. S. Hussain, and F. Mohd-Yasin, "Techniques of EMG Signal Analysis: Detection, Processing, Classification and Applications," *Biological Proceedings Online*, vol. 8, no. 1, pp. 11–35, 2006.

BIBLIOGRAPHY

- [56] M. Yoshikawa, M. Mikawa, and K. Tanaka, "Hand Pose Estimation using EMG Signals," in *Proceedings of the 29th Annual International Conference of the IEEE*, Lyon, France, 2007, pp. 4830–4833.
- [57] S. Lee and G. N. Saridis, "The Control of a Prosthetic Arm by EMG Pattern Recognition," *IEEE transaction on Automatic Control*, vol. 29, no. 4, pp. 290–302, 1984.
- [58] D. Graupe, "EMG Pattern Analysis for Patient- Responsive Control of FES in Paralegics for Walker-Supported Walking," *IEEE trans. on Biomedical Engineering*, vol. 36, no. 7, 1989.
- [59] J. U. Chu, I. Moon, and M. S. Mun, "A Real-Time EMG Pattern Recognition System based on Linear-Nonlinear Feature Projection for a Multi-Function Myoelectric Hand," *IEEE transaction on Biomedical Engineering*, vol. 53, no. 11, pp. 2232–2239, 2006.
- [60] E.-C. Jeong, S.-J. Kim, Y.-R. Song, and S.-M. Lee, "Comparison of Wrist Motion Classification Methods using Surface Electromyogram," *Journal of Central South University, Springer*, vol. 20, no. 4, pp. 960–968, 2013.
- [61] D. Zhang, Y. Wang, X. Chen, and F. Xu, "EMG Classification for Application in Hierarchical FES System for Lower Limb Movement Control," *Intelligent Robotics and Applications, Springer*, vol. 7101, pp. 162–171, 2011.
- [62] H. Huang, F. Zhang, Y. L. Sun, and H. He, "Design of A Robust EMG Sensing Interface for Pattern Classification," *Journal of NeuroEngineering*, vol. 7, no. 5, pp. 1–19, 2010.
- [63] V. N. Vapnik, "The Nature of Statistical Learning Theory," in *Springer*, New York, 1995.
- [64] J. M. Moguerza and A. Munoz, "Support Vector Machines with Applications," *Journal of Statistical Science*, vol. 21, no. 3, pp. 322–336, 2006.
- [65] H. Cao, T. Naito, and Y. Ninomiya, "Approximate RBF Kernel SVM and Its Applications in Pedestrian Classification," in *International Workshop on Machine Learning for Vision-based Motion Analysis*, France, 2008, pp. 1–9.

BIBLIOGRAPHY

- [66] E. M. Tamil, N. S. Bashar, M. Y. I. Idris, and A. M. Tamil, "A Review on Feature Extraction and Classification Techniques for Biosignal Processing (Part III: Electromyogram)," in *Proceedings of IFBME, USA, 2008*, pp. 117–121.
- [67] K. Suzuki, *Artificial Neural Networks - Methodological Advances and Biomedical Applications*. Croatia: InTech, 2011.
- [68] M. Hamed, S. H. Salleh, M. Astaraki, and A. M. Noor, "Emg-based Facial Gesture Recognition through Versatile Elliptic basis Function Neural Network," *Journal of Biomedical Engineering*, vol. 12, no. 73, pp. 1–22, 2013.
- [69] H. Cardot, *Recurrent Neural Networks for Temporal Data Processing*. Croatia: InTech, February 2011.
- [70] F. Budak, N. Ycnigun, A. Ozbek, S. Orhan, and S. Komsuoglu, "Carpal Tunnel Syndrome in Carpet Weavers," *Electromyography and Clinical Neurophysiology*, vol. 41, no. 1, pp. 29–32, 2001.
- [71] S. A. Ahmad, A. J. Ishak, and S. H. Ali, "Speed Based Surface EMG Classification Using Fuzzy Logic for Prosthetic Hand Control," in *International Conference on Biomedical Engineering*, Lumpur, 2011, pp. 121–124.
- [72] S. George, K. S. Sivanandan, and K. P. Mohandas, "Fuzzy Logic and Probabilistic Neural Network for EMG Classification A Comparative Study," *International Journal of Engineering Research and Technology*, vol. 1, pp. 1–7, 2012.
- [73] S. Sindhumol, A. Kumar, and K. Balakrishnan, "Automated Brain Tissue Classification by Multisignal Wavelet Decomposition and Independent Component Analysis," *ISRN Biomedical Imaging*, vol. 2013, pp. 1–10, 2013.
- [74] A. Biswas, E. D. Lemaire, and J. Kofman, "Dynamic Gait Stability Index based on Plantar Pressures and Fuzzy Logic," *Australian Journal of Biomechanics*, vol. 41, pp. 1574–1581, 2008.
- [75] F. Bolner, "Decoding Movement Direction for Brain-Computer Interfaces using Depth and Surface EEG Recordings," Master's thesis, Aalborg University, Aalborg, June 2012.

BIBLIOGRAPHY

- [76] C. I. Christodoulou, P. A. Kaplanis, V. Murray, M. S. Pattichis, and C. S. Pattichis, "Comparison of AM-FM Features with Standard Features for the Classification of Surface Electromyographic Signals," in *Conference on Medical and Biological Engineering and Computing*, Greece, 2010, pp. 69–72.
- [77] R. Kohavi, "A Study of Cross-Validation and Bootstrap for Accuracy Estimation and Model Selection," in *14th International Joint Conference on Artificial Intelligence*, USA, 1995, pp. 1137–1143.
- [78] R. B. Elliott, "Feature Extraction Techniques for Grasp Classification," Master's thesis, University of Canterbury, New Zealand, August 1998.
- [79] C. Martellon, J. Carpaneto, and S. Micera, "Classification of upper arm emg signals during object-specific grasp," in *In 30th Annual International IEEE/EMBS Conference*, Canada, 2008, pp. 2061–5064.
- [80] C. Castellini, A. E. Fiorilla, and G. Sandini, "Multi-Subject/Daily-Life Activity EMG-based Control of Mechanical Hands," *ournal of NeuroEngineering and Rehabilitation*, vol. 4, no. 6, pp. 1–11, 2009.
- [81] M. V. Liarokapis, P. K. Artemiadis, P. T. Katsiaris, K. J. Kyriakopoulos, and E. S. Manolagos, "Learning Human Reach-to-Grasp Strategies: Towards EMG-based Control of Robotic Arm-Hand Systems," in *IEEE International Conference on Robotics and Automation*, Saint Paul, 2012, pp. 2287–2292.
- [82] H. Gray, *Anatomy of the Human Body*. Heidelberg: Philadelphia: Lea and Febiger, 1918.
- [83] L. J. Love, R. F. Lind, and J. F. Jansen, "Mesofluidic Actuation for Articulated Finger and Hand Prosthetics," in *IEEE International Conference on Intelligent Robots and Systems*, USA, 2009.
- [84] V. Bundhoo and E. J. Park, "Design of an Artificial Muscle Actuated Finger towards Biomimetic Prosthetic Hand," in *IEEE/ 12th Intl. Conference on Advance Robotics*, 2005, pp. 368–375.
- [85] C. L. Taylor and R. J. Schwartz, "The Anatomy and Mechanics of the Human Hand," *Artificial Limbs*, vol. 2, pp. 22–35, 1995.

BIBLIOGRAPHY

- [86] J. Napier, "The Prehensile Movements of the Human Hand," *Journal of Bone Joint Surgery*, vol. 2, pp. 902–913, 1956.
- [87] C. L. MacKenzie and T. Iberall, *The Grasping Hand*. North-Holland, Amsterdam: Elsevier, 1994.
- [88] G. Heumer, H. B. Amar, and B. Jung, "Grasp Recognition for un-calibrated Data Gloves: A machine learning Approach," *Journal of Medical Systems*, vol. 17, no. 2, pp. 121–142, 2008.
- [89] T. Fiex, R. Pawlik, H. B. Schmiedmayer, J. Romero, and D. Kragic, "A Comprehensive Grasp Taxonomy," in *Workshop on Understanding the Human Hand for Advancing Robotic Manipulation; Workshop at Robotics: Science and Systems Conference*, Austria, June, 2009.
- [90] D. H. Plottenburg, *Upper Extremity Prosthetics, Current Status and Evaluation*. Nederland: Delft Academic Press, 2006.
- [91] J. B. H. Liu and S. Knoch, "A New Control Strategy for DLR's Multisensory Articulated Hand," *IEEE Control Systems*, vol. 19, no. 2, pp. 47–54, 1999.
- [92] J. K. Salisbury and J. J. Craig, "Articulated Hands: Force Control and Kinematics Issues," *Journal of Robotics Research*, vol. 1, no. 1, pp. 4–17, 1982.
- [93] M. Bergamasco and S. S. Marchese, "The Mechanical Design of MARCUS Prosthetic Hand," in *IEEE International Conference on Robotics and Automation*, Tokyo, 1995, pp. 95–100.
- [94] S. Hirose and Y. Umetani, "The Development of Soft Gripper for the Versatile Robot Hand," *Mechanism and Machine Theory*, vol. 13, no. 3, pp. 351–359, 1978.
- [95] G. et al., *Recent Trends in EMG based Control Methods for Assistive Robots*. InTech, 2013.
- [96] G. Robertson, G. Caldwell, J. Hamill, G. Kamen, and S. Whittlesey, *Research Methods in Biomechanics*. USA: Library of Congress, 2004.
- [97] Y. Liao, "Phase and Frequency Estimation: High-Accuracy and Low-Complexity Techniques," Master's thesis, Worcester Polytechnic Institute, USA, 2011.

BIBLIOGRAPHY

- [98] N. M. Kakoty and S. M. Hazarika, "Recognition of Grasp Types Based on Electromyogram Signals," in *IEEE International Conference on Computing, Communication and Networking*, India, 2008.
- [99] —, "Towards Electromyogram based Grasps Classification," *International Journal of Biomechatronics and Biomedical Robotics, Inderscience*, vol. 4, no. 1, pp. 115–133, 2013.
- [100] —, "Classification of Grasp Types through Wavelet Decomposition of EMG Signals," in *IEEE Conf. on Biomedical Engineering and Informatics*, China, 2009.
- [101] N. A. Shrirao, N. P. Reddy, and D. R. Kosuri, "Neural Network Committees for Finger Joint Angle Estimation from Surface EMG Signals," *Journal of BioMedical Engineering OnLine*, vol. 38, no. 2, pp. 529–535, 2009.
- [102] S. Kousidou, N. G. Tsagarakis, C. Smith, and D. G. Caldwell, "Task-Orientated Biofeedback System for the Rehabilitation of the Upper Limb," in *IEEE 10th International Conference on Rehabilitation Robotics*, Netherlands, 2007, pp. 376–384.
- [103] G. R. Naik, *Computational Intelligence in Electromyography Analysis - A Perspective on Current Applications and Future Challenges*. Australia: InTech, 2012, pp. 136–149.
- [104] H. J. Hermens, B. Freriks, C. Disselhorst-Klug, and G. Rau, "Development of recommendations for SEMG sensors and sensor placement procedures," *Journal of Electromyography and Kinesiology*, vol. 10, pp. 361–374, 2000.
- [105] J. Kim, S. Mastnik, and E. Andre, "EMG-based Hand Gesture Recognition for Realtime Biosignal Interfacing," in *Proceedings of the 13th international Conference on Intelligent User Interfaces*, New York, 2008, pp. 30–39.
- [106] A. Phinyomark, C. Limsakul, and P. Phukpattaranont, "A Novel Feature Extraction for Robust EMG Pattern Recognition," *Journal of Computing*, vol. 1, pp. 71–80, 2009.

- [107] J. J. Im, D. H. Rho, Y. J. Jeon, N. B. Lee, and J. I. Chung, "Extraction of Parameters from EMG Signals for the Biofeedback Electrical Stimulation," in *In Proceeding of IEEE EMBS/BMES Conference*, Houston, 2002, pp. 133–134.
- [108] A. D. Astin, "Finger Force Capability: Measurement and Prediction using Anthropometric and Myoelectric Measures," Ph.D. dissertation, Virginia Polytechnic Institute and State University, Virginia, 1999.
- [109] A. V. Oppenheim and J. S. Lim, "The Importance of Phase in Signals," *IEEE Proceedings*, vol. 69, no. 5, pp. 529 – 541, 1981.
- [110] A. Subasi, M. Yilmaz, and H. R. Ozcalik, "Classification of EMG Signals using Wavelet Neural Network," *Journal of Neuroscience Methods*, vol. 156, no. 3, pp. 360–367, 2006.
- [111] B. Gerdle, S. Karlsson, S. Day, and M. Djupsjobacka, *Acquisition, Processing and Analysis of the Surface Electromyogram: Modern Techniques in Neuroscience Research*. Heidelberg: Springer-Verlag, 1999, pp. 705–755.
- [112] C. Jensen, O. Vasseljen, and R. Westgaard, "The Influence of Electrode Position on Bipolar Surface Electromyogram Recordings of the Upper Trapezius Muscle," *Journal of Applied Physiology and Occupational Physiology*, vol. 67, no. 3, pp. 266–273, 1993.
- [113] G. A. Hansson, U. Stromberg, B. Larsson, K. Ohlsson, I. Balogh, and U. Moritz, "Electromyographic Fatigue in Neck/Shoulder Muscles and Endurance in Women with Repetitive Work," *Journal of Ergonomics*, vol. 35, no. 11, pp. 1341–1352, 1991.
- [114] S. M. McGill, "Electromyographic Activity of the Abdominal and Low Back Musculature during the Generation of Isometric and Dynamic Axial Trunk Torque: Implications for Lumbar Mechanics," *Journal of Orthopaedic Research*, vol. 9, no. 1, pp. 91–103, 1991.
- [115] G. Lehman and S. McGill, "The Importance of Normalization in the Interpretation of Surface Electromyography: A Proof of Principle," *Journal of Manipulative and Physiological Therapeutics*, vol. 22, no. 7, pp. 369–370, 1999.

BIBLIOGRAPHY

- [116] M. B. I. Reaz and M. S. Hussain, "A Non-MVC EMG Normalization Technique for the Trunk Musculature: Part-I Method Development," *Journal of Electromyography and Kinesiology*, vol. 11, no. 1, pp. 1-9, 2001.
- [117] F. T. Santiago, J. L. Koncman, and A. Kok, "A Comparison of Different Methods for Estimating Single Trial p300 Latencies, Electroencephalogram," *Clin. neurophysics*, vol. 92, pp. 107-114, 1994.
- [118] H. A. Al-Nashash and N. V. Paul, J. S. and Thakor, "Wavelet Entropy Method for EEG Analysis: Application to Global Brain Injury," in *Proceedings of the 1st International IEEE EMBS Conference on Neural Engineering*, Italy, 2003, pp. 348-351.
- [119] A. Saikia, N. M. Kakoty, and S. M. Hazarika, "Wavelet Selection for EMG based Grasp Recognition through CWT," in *Conf. on Comp. and Comm.*, 2011, pp. 1116-24.
- [120] S. Li, J. Liao, and J. T. Kwok, "Wavelet-based Feature Extraction for Microarray Data Classification," in *IEEE International Conference on Neural Network*, Canada, 2006, pp. 5028-5033.
- [121] N. M. Kakoty, A. Saikia, and S. M. Hazarika, "Exploring a Family of Wavelet Transforms for EMG-based Grasp Recognition," *Journal of Signal, Image and Video Processing*, vol. Online First: 21st April 2013, pp. 1-7, 2013.
- [122] C. Castellini and S. Patrick, "Surface EMG in Advanced Hand Prosthetics," *Biological cybernetics*, vol. 100, no. 1, pp. 35-47, 2009.
- [123] K. Englehart, B. Hudgin, and P. A. Parker, "A Wavelet-based Continuous Classification Scheme for Multi-Function Myoelectric Control," *IEEE transaction on Biomedical Engineering*, vol. 48, no. 3, pp. 302-311, 2001.
- [124] H. Xiao, W. Zhi-zhong, and R. Xiao-mei, "Classification of Surface EMG Signal with Fractal Dimension," *Journal of Zhejiang University SCIENCE*, vol. 6B, no. 8, pp. 844-848, 2005.

- [125] S. Karasawa and H. Sakuraba, "Use of haar wavelet transform based multiple teplate matching for analyses of speech voice," in *Proc. of Euro-American Conf. on Telematics and Information System*, Portugal, 2007.
- [126] S. Karasawa, "Discrete Wavelet Transform based Multiple Template-Matching for Speech Recognition," in *Pattent Application No: 2006-357183*, Japan, 2006.
- [127] M. Santello, M. Flander, and J. F. Soechting, "Postural Hand Synergies for Tool Use," *Journal of Neuroscience*, vol. 18, no. 23, pp. 10 105–10 115, 1998.
- [128] B. E. Boser, I. M. Guyon, and V. N. Vapnik, "A Training Algorithm for Optimal Margin Classifiers," in *5th Annual ACM Workshop on COLT*, Pittsburgh, 1992.
- [129] S. L. Kilbrcath, R. B. Gorman, J. Raymond, and S. C. Gandevia, "Distribution of the forces produced by motor unit activity in the human flexon digitorium profundus," *J. of Physiology*, vol. 543, no. 1, pp. 289–296, 2002.
- [130] C. W. Hsu, C. C. Chang, and C. J. Lin, "A Practical Guide to Support Vector Classification," National Taiwan University, Taiwan, Tech. Rep., April 2010, available at <http://www.csie.ntu.edu.tw/~cjlin/libsvm>.
- [131] A. Ben-Hur and J. Weston, "A Users Guide to Support Vector Machines," *Methods in Molecular Biology*, vol. 609, pp. 223–239, 2010.
- [132] M. Taft, R. Krishnan, M. Hornick, D. Muhkin, G. Tang, S. Thomas, and P. Sten-gard, *Oracle Data Mining Concepts*. Oracle, Redwood City, CA, 2005.
- [133] M. Roa, M. Argus, D. Leidner, C. Borst, and G. Hirzinger, "Power Grasp Planning for Anthropomorphic Robot Hands," in *International Conference on Robotics and Automation*, 2012, pp. 563–569.
- [134] T. J. Roberts and A. M. Gabaldon, "Interpreting Muscle Function from EMG: Lessons Learned from Direct Measurements of Muscle Force," *Integrative and Comparative Biology*, vol. 48, no. 2, pp. 312–320, 2008.
- [135] M. Solomonow and R. Baratta, "Methods for Accurate EMG Power Spectrum Assesment for Biomechanical Applications," <http://www.asbweb.org/>.

BIBLIOGRAPHY

- [136] H. Khorrami and M. Moavenian, "A comparative study of dwt, cwt and dct transformations in ecg arrythmias classification," *Expert Systems with Applications*, vol. 37, no. 8, pp. 5751-5757, 2010.
- [137] I. R. Carrco and M. Vuskovic, "Wavclot Transform Momonts for Feature Extraction from Temporal Signals," *Informatics in Control, Automation and Robotics*, vol. 2, no. 3, pp. 235-242, 2007.
- [138] A. Phinyomark, C. Limsakul, and P. Phukpattaranont, "Evaluation of Wavelet Function Bascd on Robust EMG Featurec Extraction," in *The Seventh PSU Engineering Conference*, 2009, pp. 277-281.
- [139] S. Li, C. Liao, and J. T. Kwok, "Wavclot Bascd Feature Extraction for Microaray Data Classification," in *IEEE International Conference on Neural Network*, Canada, 2006, pp. 5028-5033.
- [140] M. A. Hearst, "Trends and Controversises: Support Vector Machines," *IEEE Intelligent Systems*, vol. 13, no. 4, pp. 18-28, 1998.
- [141] N. M. Kakoty and S. M. Hazarika, "Recognition of Grasp Types through PCs of DWT bascd EMG Features," in *International Conference on Rehabilitation Robotics*, Zurich, Switzerland, 2011, pp. 478-482.
- [142] G. Bohm and G. Zech, *Introduction to Statistics and Data Analysis for Physicists*. Hamrg: Verlag Deutsches Elektronen-Synchrotron, 2010.
- [143] A. R. Webb, *Statistical Pattern Recognition*. England: John Wiley and Sons, Ltd, 2002.
- [144] R. V. Hogg and J. Ledolter, *Engineering Statistics*. MacMillan Publishing Company, 1987.
- [145] K. D. Hopkins, B. R. Hopkins, and G. V. Glass, "Basic Statistics for the Behavioral Scienccs," Necdham Hcights, MA, Tech. Rcp., 1996.
- [146] Y. Bar-Cohen, "Biomimetics: mimicking and inspired-by biology," in *Proceedings of the SPIE Smart Structures Conference*, San Diego, CA, 2005, pp. 1-8.

BIBLIOGRAPHY

- [147] —, “Biomimetics using nature to inspire human innovation,” *Bioinspiration and Biomimetics*, vol. 1, pp. 1–12, 2006.
- [148] H. Herr, G. P. Whiteley, and D. Childress, *Cyborg Technology - Biomimetic Orthotic and Prosthetic Technology*. Bellingham, Washington: SPIE Press, 2003, pp. 103–143.
- [149] N. M. Kakoty and S. M. Hazarika, “Biomimetic Design and Development of a Prosthetic Hand: Prototype 1.0,” in *15th National Conference on Machines and Mechanisms*, India, 2011, pp. 499–06.
- [150] —, “Development of an Electromyographic Controlled Biomimetic Prosthetic Hand,” *International Journal Computational Vision and Robotics, In Press*, 2013.
- [151] M. Ferre, S. Cobos, J. Ortego, and M. A. Sanchez-Uran, “First Prototype of Hand Model, Sufficient for Mimicking Realistic Hand Motions, but not Full Hand Manipulation of Objects Yet,” Tech. Rep., May 2007, available at <http://www.immersence.info>. Retrieved on June, 2008.
- [152] O. Warlow, “Kinematic and Anatomical Measurement for Biomechanical Finger Models,” Ph.D. dissertation, Newcastle University, UK, April 2012.
- [153] M. Folgheraiter and G. Gim, “Blackfingers an Artificial Hand that Copies Human Hand in Structure, Size, and Function,” in *Proceedings of IEEE Humanoids*, MIT, Cambridge, 2000, pp. 1–10.
- [154] R. Gailey, L. V. McFarland, R. A. Cooper, J. Czerniccki, J. M. Gambel, S. Hubbard, C. Maynard, D. G. Smith, M. Raya, and G. E. Reiber, “Unilateral Lower-Limb Loss. Prosthetic Device Use and Functional Outcomes in Servicemembers from Vietnam War and OIF/OEF Conflicts,” *Journal of Rehabilitation Research and Development*, vol. 47, no. 4, pp. 317–332, 2010.
- [155] M. V. Weghe, M. Rogers, M. Weissert, and Y. Matsuoka, “The ACT Hand: Design of the Skeletal Structure,” in *International Conference on Robotics and Automation*, Orleans, LA, 2004, pp. 3375–3379.
- [156] R. M. Murray, Z. Li, and S. S. Sastry, *A Mathematical Introduction to Robotic Manipulation*. USA: CRC Press, 1994.

BIBLIOGRAPHY

- [157] V. Potkonjak, B. Svetozarevic, K. Jovanovic, and O. Holland, "The Puller-Follower Control of Compliant and Non-compliant Antagonistic Tendon Drives in Robotic Systems," *Journal of Advanced Robotics Systems*, vol. 8, no. 5, pp. 143–155, 2012.
- [158] D. Kamper, E. Cruz, and E. Siggel, "Stereotypical Fingertip Trajectories during Grasp," *Journal of Neurophysiology*, vol. 90, pp. 3702–3710, 2003.
- [159] S. W. Lee and X. Zhang, "Biodynamic Modeling, System Identification and Variability of Multi-Finger Movements," *Journal of Biomechanics*, vol. 40, no. 4, pp. 3215–22, 2007.
- [160] A. Ghosal, *Robotics: Fundamental Concepts and Analysis*. New Delhi, India: Oxford Press, 2006.
- [161] M. Ciocarlic, A. Miller, and P. Allen, "Grasp Analysis Using Deformable Fingers," in *IEEE/ International Conference on Intelligent Robots and Systems*, Canada, 2005, pp. 4122–4128.
- [162] C. Melchiorri, "Kinematic Model of Robot Manipulators, Online Lecture Notes," university of Bologna, accessed in March 2013.
- [163] S. K. Saha, *Introduction to Robotics*. Mc-Graw Hill, 2010.
- [164] S. Li and Y. Zhang, "Instructions on How To Use Engauge to Digitize Well Logs," <http://digitizer.sourceforge.net/>, Tech. Rep., 2012.
- [165] J. Kaushal, "Comparative Performance Study of ACO and ABC Optimization based PID Controller Tuning for Speed Control of DC Motor Drives," Master's thesis, Thapar University, Patiala, June 2013.
- [166] Escapc, "Portescap, La Chaux de Fonds, Switzerland," www.portescap.com.
- [167] J. Zhong, "PID Controller Tuning: A Short Tutorial," Purdue University, Tech. Rep., Spring 2006.
- [168] I. Carpinella, J. Jonsdottir, and M. Ferrarin, "Multi-Finger Coordination in Healthy Subjects and Stroke Patients: A Mathematical Modelling Approach," *IEEE transaction on Automation and Control*, vol. 8, no. 19, pp. 1–19, 2011.

BIBLIOGRAPHY

- [169] E. A. Biddiss and T. T. Chau, "Upper Limb Prosthesis Use and Abandonment: A survey of the last 25 years," *Prosthet. Orthot. Int.*, vol. 31, no. 3, pp. 236–257, 2007.
- [170] C. Pylatiuk, S. Schulz, and L. Doderlein, "Results of an Internet Survey of Myoelectric Prosthetic Hand Users," *Journal of Prosthetics and Orthotics*, vol. 31, no. 4, pp. 362–370, 2007.
- [171] J. T. Belter and A. M. Dollar, "Performance Characteristics of Anthropomorphic Prosthetic Hands," in *IEEE International Conference on Rehabilitation Robotics*, Zurich, 2011, pp. 921–927.
- [172] H. W. Kay and M. Rakic, "Specifications for Electromechanical Hands," in *4th International Symposium on the External Control of Human Extremities*, Garmen, 1972, pp. 137–155.
- [173] C. M. Light and P. Chappell, "Development of A Lightweight and Adaptable Multiple-Axis Hand Prosthesis," *Journal on Medical Engineering and Physics*, vol. 22, pp. 679–684, 2000.
- [174] M. Malhotra and Y. Matsuoka, "The Relationship between Actuator Reduction and Controllability for a Robotic Hand," in *IEEE RAS/ EMBS International Conference on Biomedical Robotics and Biomechatronics*, Japan, 2010, pp. 331–336.
- [175] N. Fukaya, S. Toyama, T. Asfour, and R. Dillmann, "Design of the TUAT/Karlsruhe Humanoid Hand," in *IEEE/ International Conference on Intelligent Robots and Systems*, Takamatsu, 2000, pp. 1754–1759.
- [176] T. N. Nguyen and H. E. Stephanou, "A Topological Model of Multifingered Prehension," in *IEEE International Conference on Robotics and Automation*, Scottsdale, 1989, pp. 446–451.
- [177] C. Pylatiuk, S. Mounier, A. Kargov, S. Schulz, and G. Bretthauer, "Progress in the Development of a Multifunctional Hand Prosthesis," in *Proceedings of IEEE Engineering in Medicine and Biology Society*, USA, 2004, pp. 4260–4263.

BIBLIOGRAPHY

- [178] J. L. Pons, R. Ceres, E. Rocon, D. Reynaerts, B. Saro, S. Levin, and W. V. Moorleghem, "Objectives and Technological Approach to the Development of the Multifunctional MANUS Upper Limb Prosthesis," *Autonomous Robot*, vol. 23, no. 3, pp. 301–310, 2005.
- [179] M. A. Smith and J. F. Soechting, "Modulation of Grasping Forces During Object Transport," *Journal Neurophysiology*, vol. 93, no. 1, pp. 137–145, 2005.
- [180] A. C. de P. Filho, *Humanoid Robots; New Developments*. Austria: Advanced Robotic Systems International, 2007.
- [181] D. A. McAdams and K. L. Wood, "A Quantitative Similarity Metric for Design-by-Analogy," *Journal of Mechanical Design*, vol. 124, no. 2, pp. 173–182, 2002.
- [182] J. Bourke and B. R. Duffy, "Emotion Machines: Projective Intelligence and Emotion in Robotics," in *IEEE Systems, Man and Cybernetics Workshop*, UK, 2003, pp. 1–5.
- [183] A. Sarmah, S. M. Hazarika, and S. K. Sinha, "Security pattern lattice: A formal model to organize security patterns," in *IEEE/ 19th International Conference on Database and Expert Systems Application*, USA, 2008, pp. 292–296.
- [184] M. C. Carrozza, G. Cappiello, S. Micera, B. B. Edin, L. Beccai, and C. Cipriani, "Design of a Cybernetic Hand for Perception and Action," *Biological Cybernetics*, vol. 95, no. 6, pp. 629–644, 2006.
- [185] B. Ganter and R. Wille, *Formal Concept Analysis*, 2nd ed. New York: Springer-Verlag, 1996.
- [186] S. A. Yevtushenko, "System of data Analysis Concept Explorer, KII-2000," in *7th National conference on Artificial Intelligence*, Russia, 2000, pp. 127–134.
- [187] T. Feix, J. Romero, C. H. Ek, H.-B. Schmiedmayer, and D. Kragic, "A Metric for Comparing the Anthropomorphic Motion Capability of Artificial Hands," *IEEE transactions on Robotics*, vol. 29, no. 1, pp. 82–93, 2013.

Appendix-I: IEMG and nIEMG Signals

EMG is easily affected by undesired signal that come from different sources such as electromagnetic interference between the signal carrying conductors with other signal carrying conductors, ground lines, power lines, electromagnetic radiation etc. In addition, for surface electrode instrumentation, subjective issues may arise due to its coupling with skin. After acquisition, EMG signal was filtered using a band-pass filter to reduce noise. The signal was next amplified with a high CMRR amplifier. Also a notch filter at 50 Hz to eliminate power line noise was exerted. Finally the signal was sampled at 10 KHz sampling rate and transferred to an HP based personal computer for further analysis. This appendix shows the IEMG signals for the six grasp types in Figure I.1 through to Figure I.6 for a single subject.

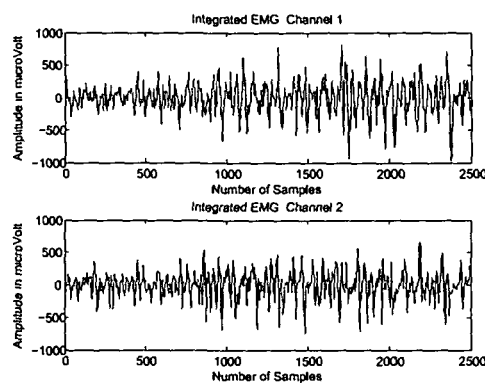


Figure I.1: IEMG signal for Power Grasp

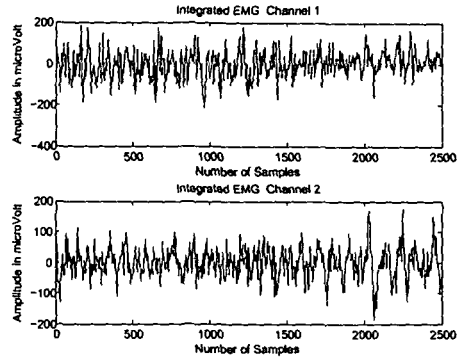


Figure I.2: IEMG signal for Palm-up Grasp

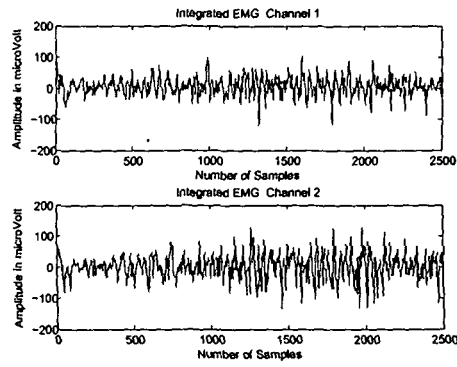


Figure I.3: IEMG signal for Hook Grasp

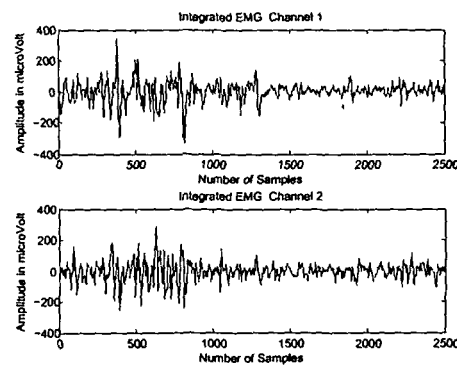


Figure I.4: IEMG signal for Oblique Grasp

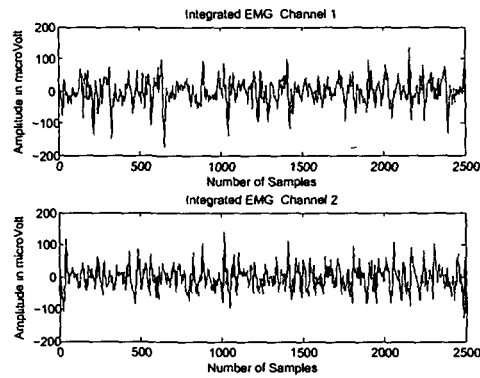


Figure I.5: IEMG signal for Precision Grasp

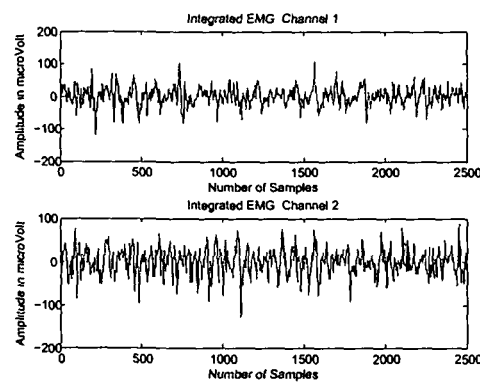


Figure I.6: IEMG signal for Pinch Grasp

In order to overcome the subjectivity of the signals, MVC normalization was used. The specifications of the preprocessing unit is as stated in section 3.2.2 in Chapter 3. The nIEMG signals for the six grasp types are shown in Figure I.7 through Figure I.12 in this appendix. The preprocessed two channel nIEMG signals shown in this appendix are for six grasp types of one subject.

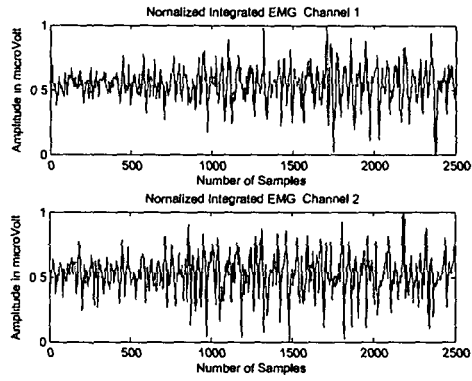


Figure I.7: Normalized IEMG signal for Power Grasp

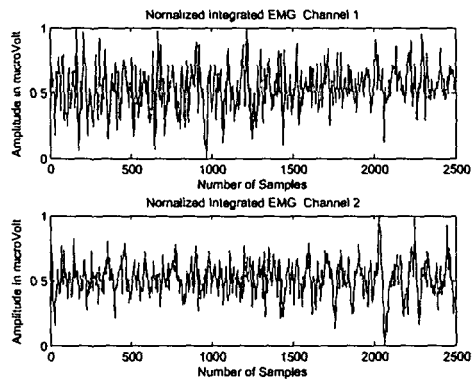


Figure I.8: Normalized IEMG signal for Palm-up Grasp

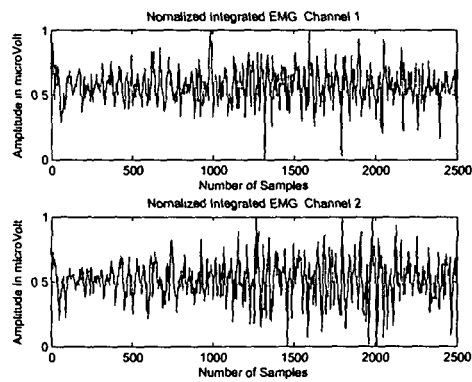


Figure I.9: Normalized IEMG signal for Hook Grasp

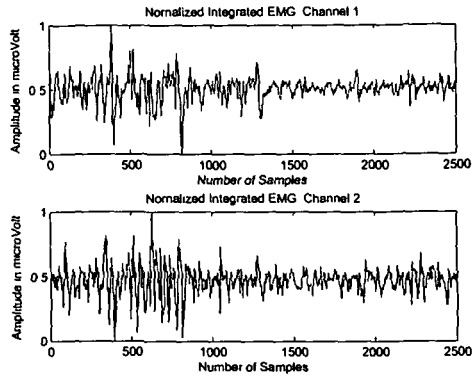


Figure I.10: Normalized IEMG signal for Oblique Grasp

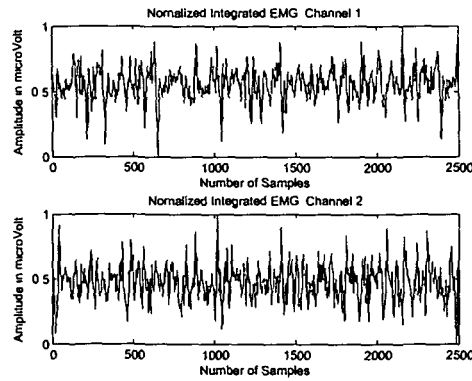


Figure I.11: Normalized IEMG signal for Precision Grasp

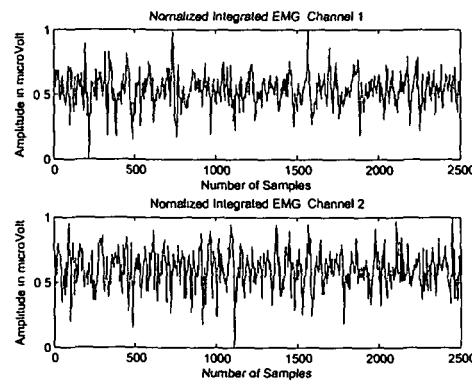


Figure I 12: Normalized IEMG signal for Pinch Grasp

Appendix-II: EMG Signals in Time/ Frequency Domain

WT is one of the most powerful signal processing tools for EMG recognition. I have investigated the EMG features from third level wavelet decomposition of the EMG signal as reported in Chapter 4. The results in this appendix shows the approximate WT coefficients at first, second and third level of decomposition using five mother wavelet functions: Biorthogonal, Symlet 4, Coiflet 2, Daubichies 2 and Haar for two channel EMG signals for one subject performing six grasp types. The approximate coefficients obtained at first, second and third level of decomposition through Biorthogonal WT for the six grasp types under study are shown in Figure II.1 through Figure II.12.

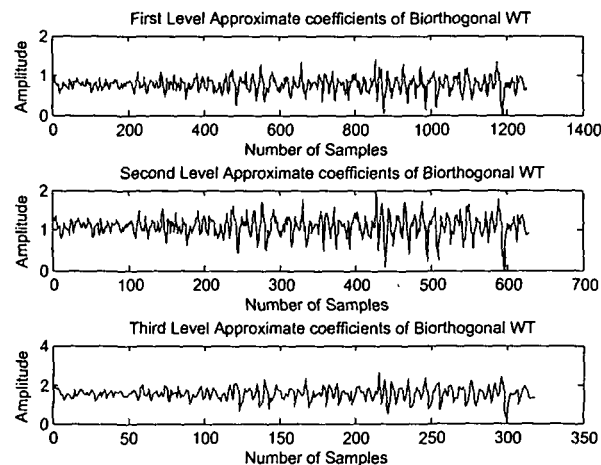


Figure II.1: Biorthogonal WT coefficients of EMG channel 1 for power grasp

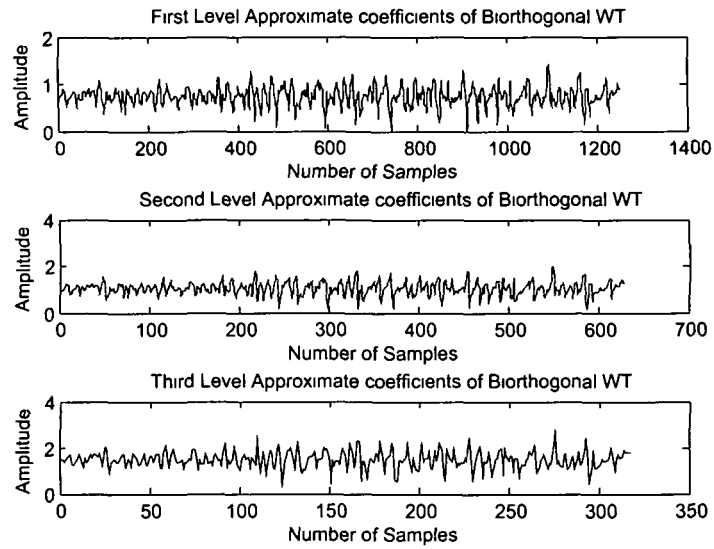


Figure II 2 Biorthogonal WT coefficients of EMG channel 2 for power grasp

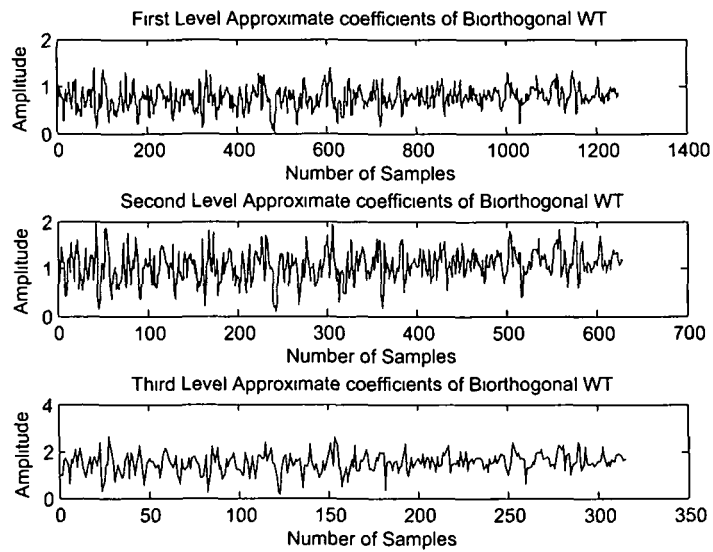


Figure II 3 Symlet 4 WT coefficients of EMG channel 1 for palm-up grasp

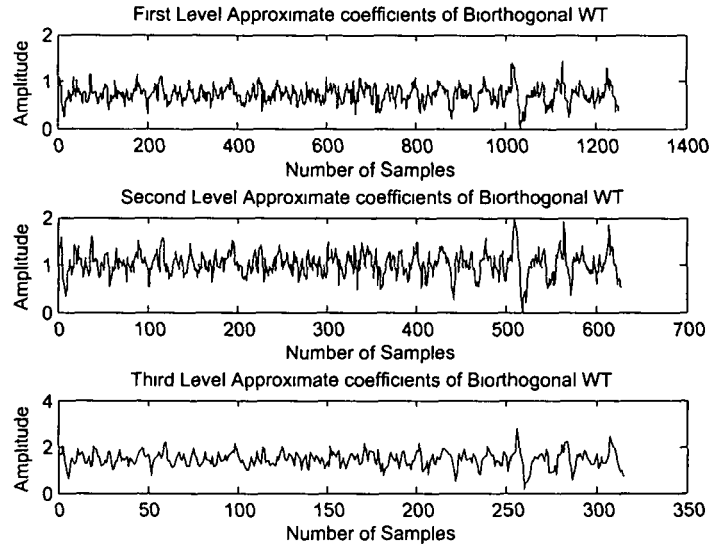


Figure II 4 Biorthogonal WT coefficients of EMG channel 2 for palm-up grasp

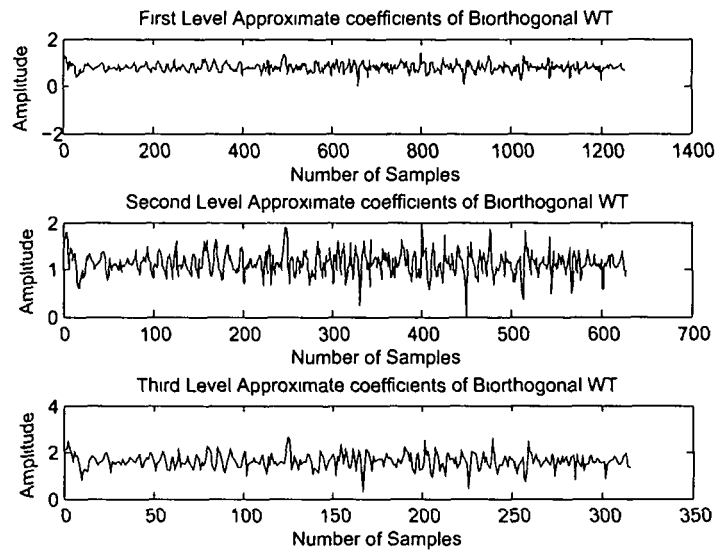


Figure II 5 Biorthogonal WT coefficients of EMG channel 1 for hook grasp

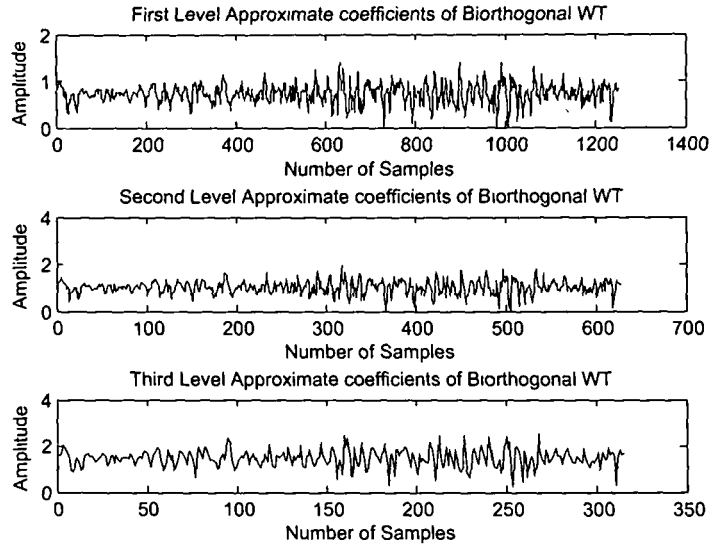


Figure II.6: Biorthogonal WT coefficients of EMG channel 2 for hook grasp

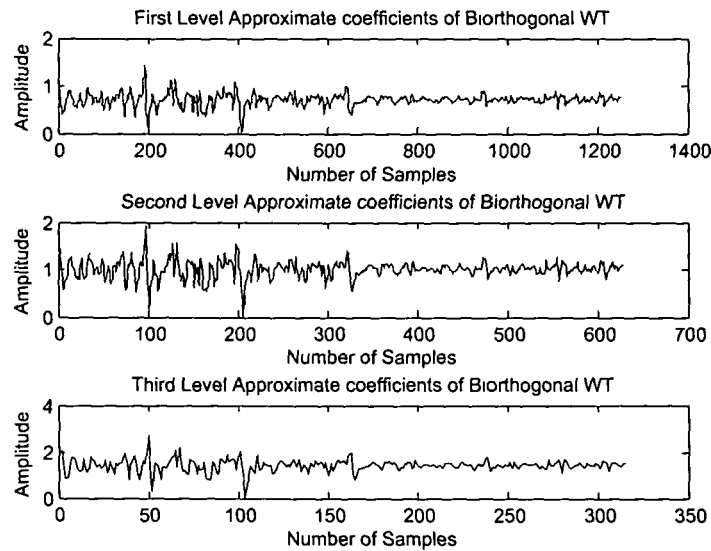


Figure II.7: Biorthogonal WT coefficients of EMG channel 1 for oblique grasp

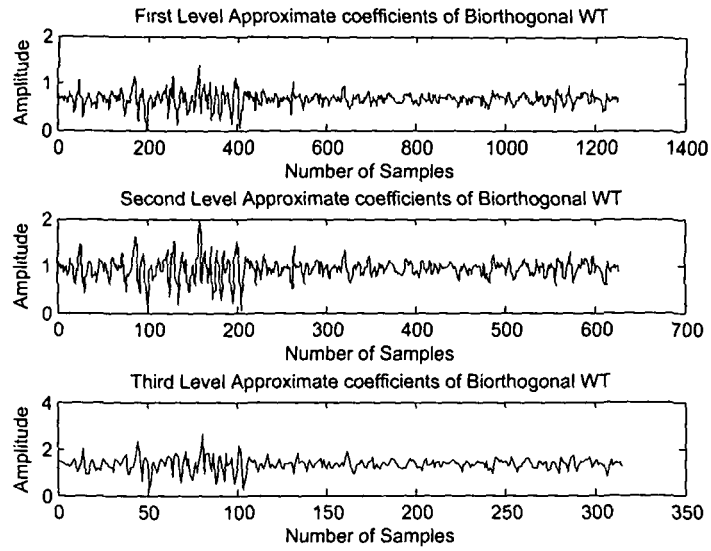


Figure II.8: Biorthogonal WT coefficients of EMG channel 2 for oblique grasp

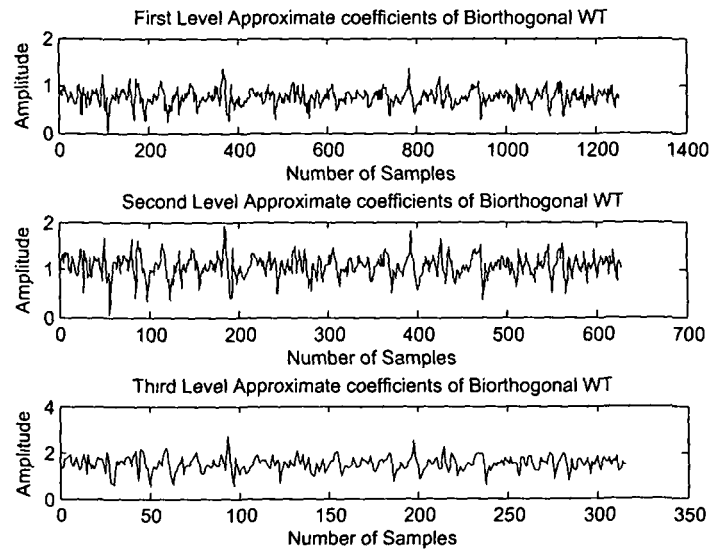


Figure II.9: Biorthogonal WT coefficients of EMG channel 1 for pinch grasp

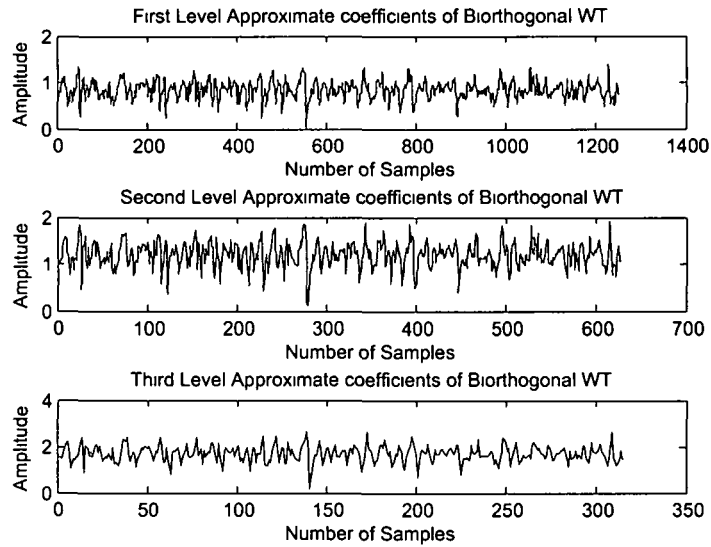


Figure II.10. Biorthogonal WT coefficients of EMG channel 2 for pinch grasp

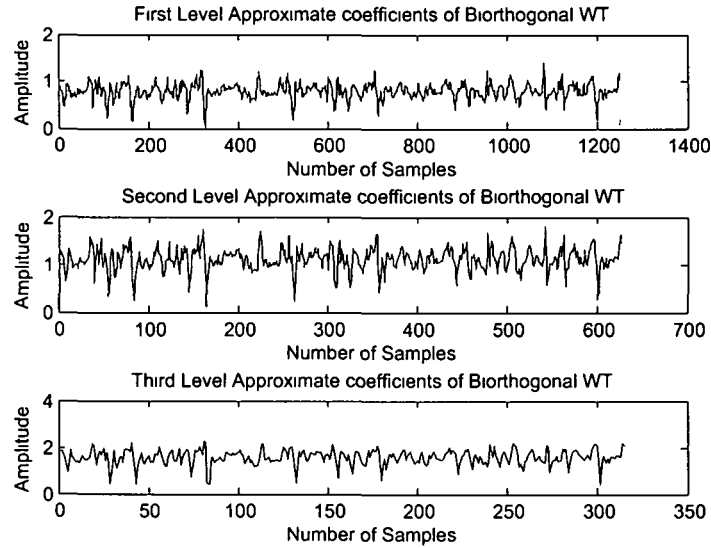


Figure II.11: Biorthogonal WT coefficients of EMG channel 1 for precision grasp

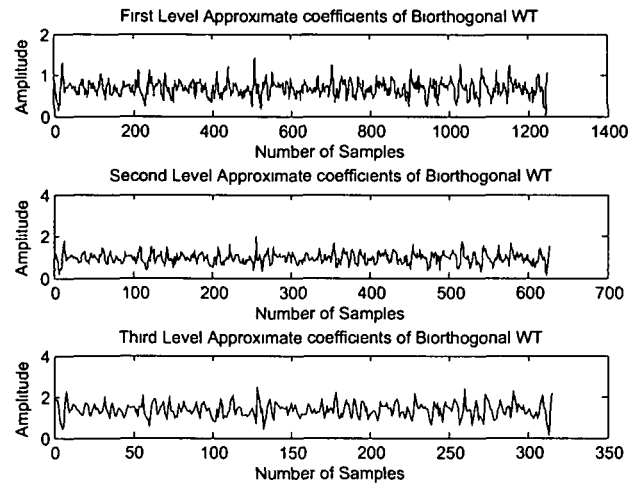


Figure II 12 Biorthogonal WT coefficients of EMG channel 2 for precision grasp

The approximate coefficients obtained at first, second and third level of decomposition through Coiflet 2 WT for two channel EMG of six grasp types under study are shown in Figure II.13 through Figure II.24.

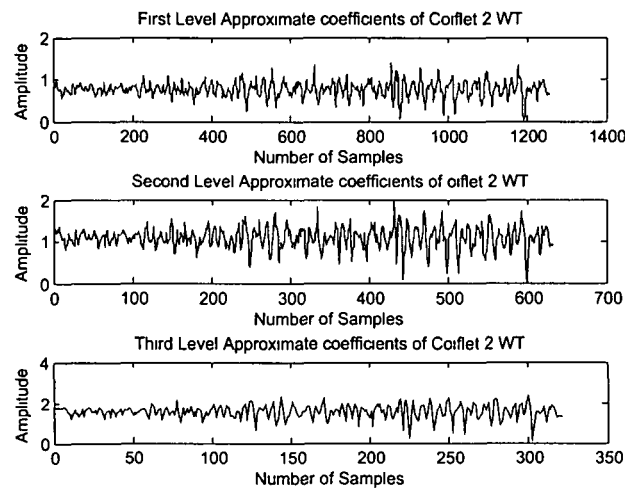


Figure II.13 Coiflet 2 WT coefficients of EMG channel 1 for power grasp

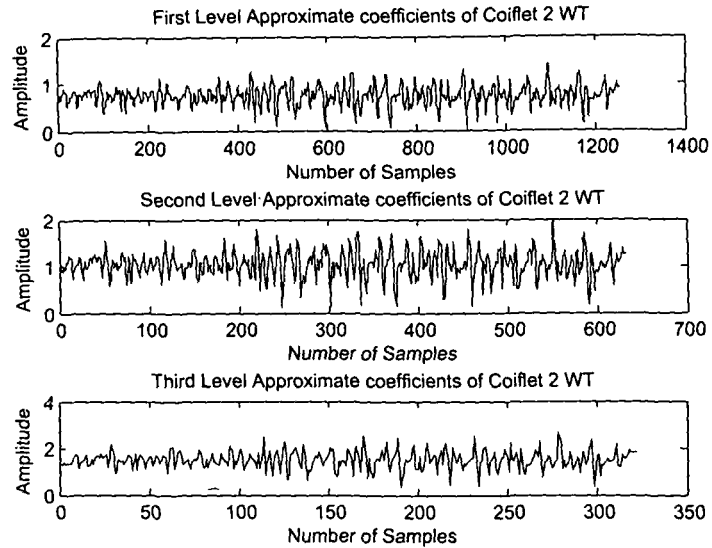


Figure II.14: Coiflet 2 WT coefficients of EMG channel 2 for power grasp

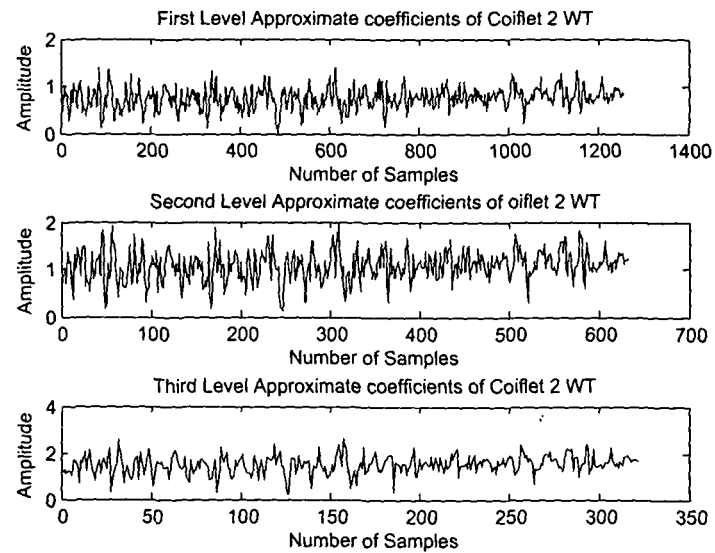


Figure II.15: Coiflet 2 WT coefficients of EMG channel 1 for palm-up grasp

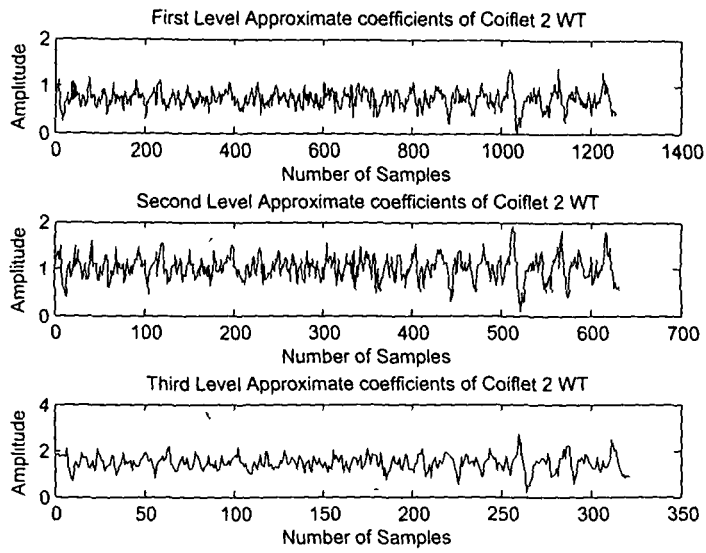


Figure II.16: Coiflet 2 WT coefficients of EMG channel 2 for palm-up grasp

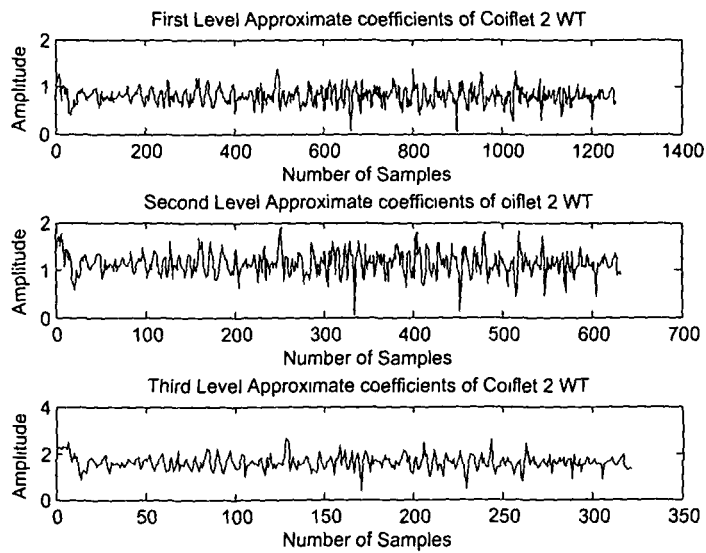


Figure II.17: Coiflet 2 WT coefficients of EMG channel 1 for hook grasp

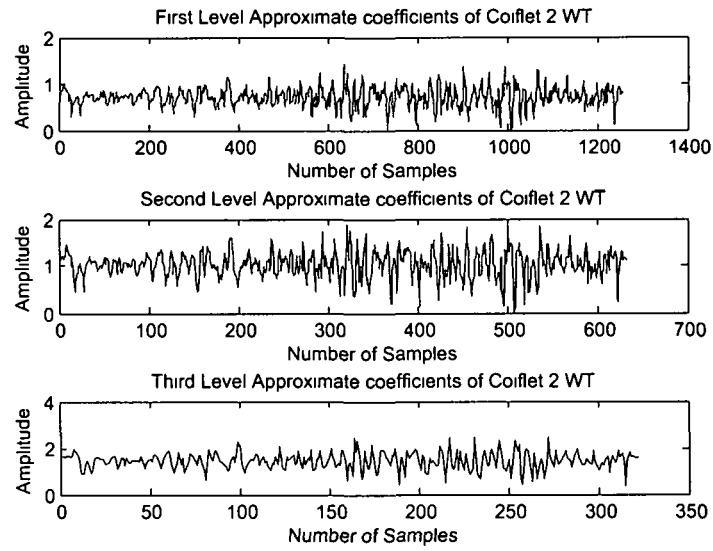


Figure II.18 Coiflet 2 WT coefficients of EMG channel 2 for hook grasp

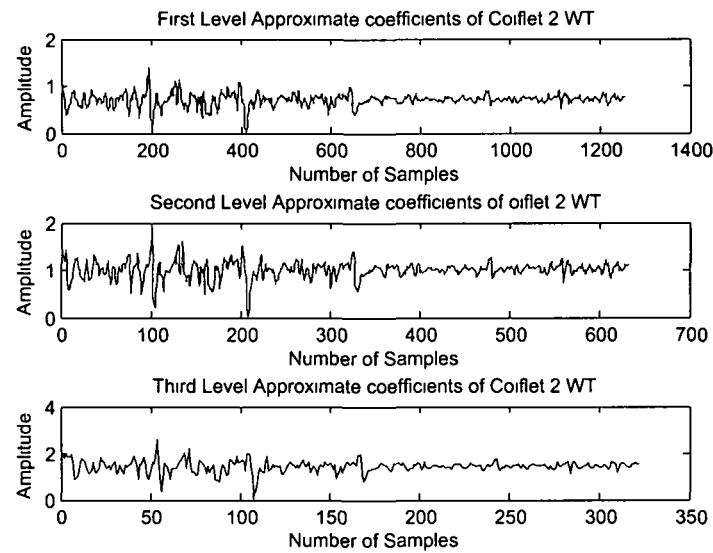


Figure II.19: Coiflet 2 WT coefficients of EMG channel 1 for oblique grasp

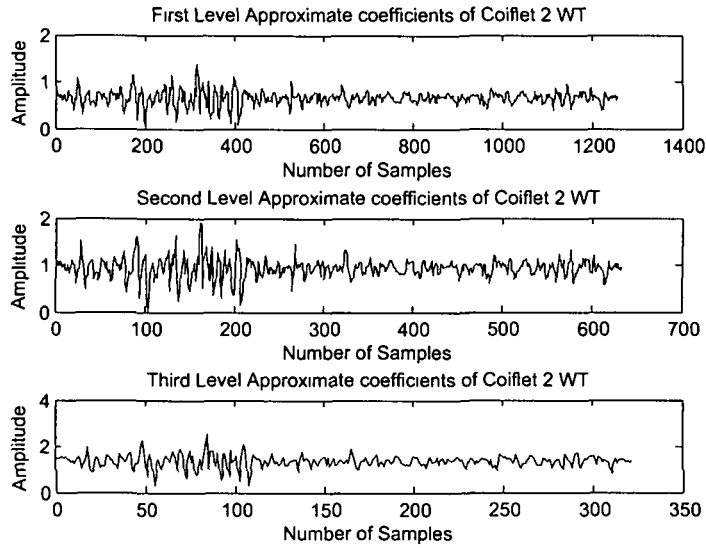


Figure II.20: Coiflet 2 WT coefficients of EMG channel 2 for oblique grasp

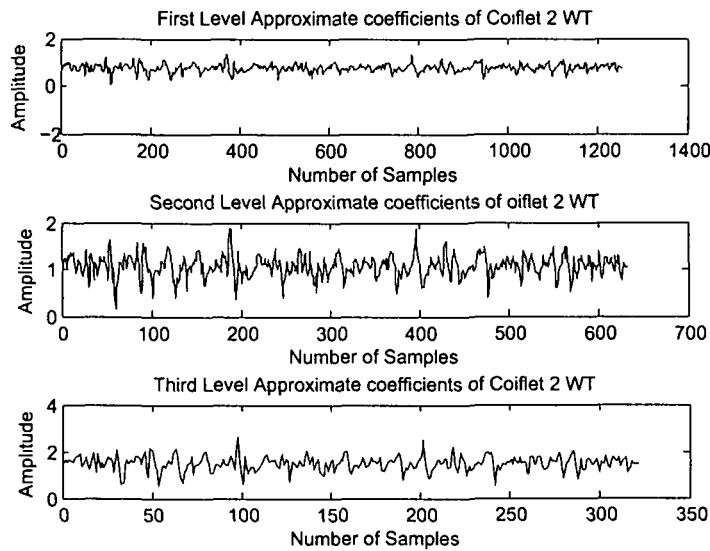


Figure II.21: Coiflet 2 WT coefficients of EMG channel 1 for pinch grasp

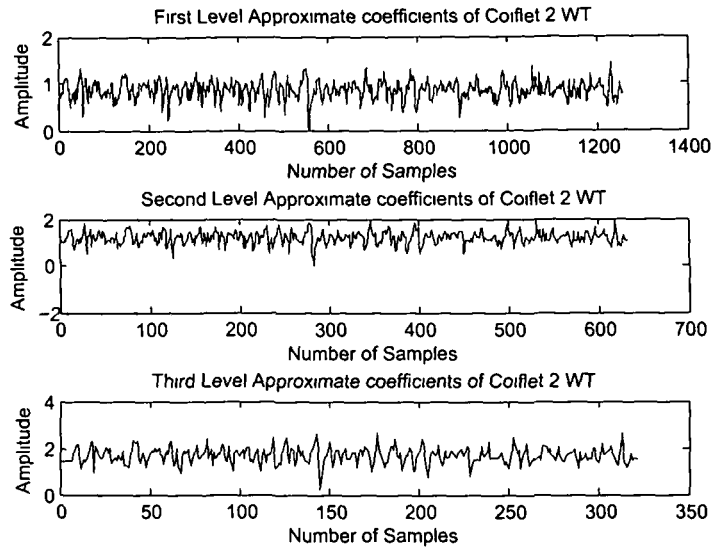


Figure II 22 Coiflet 2 WT coefficients of EMG channel 2 for pinch grasp

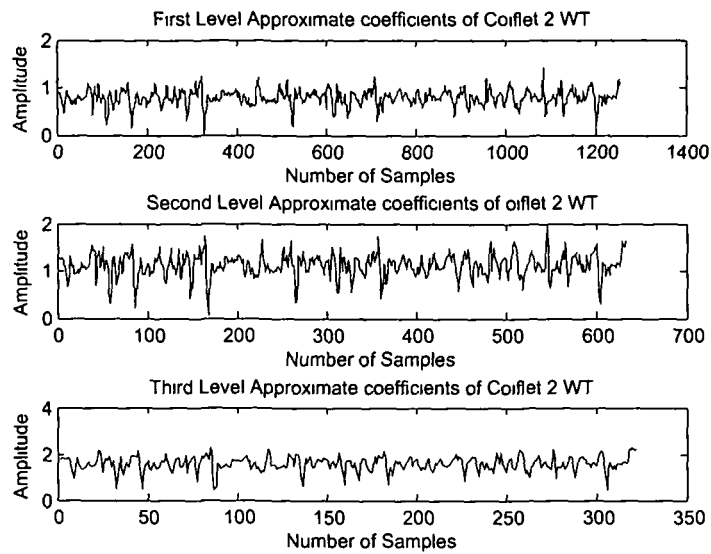


Figure II 23 Coiflet 2 WT coefficients of EMG channel 1 for precision grasp

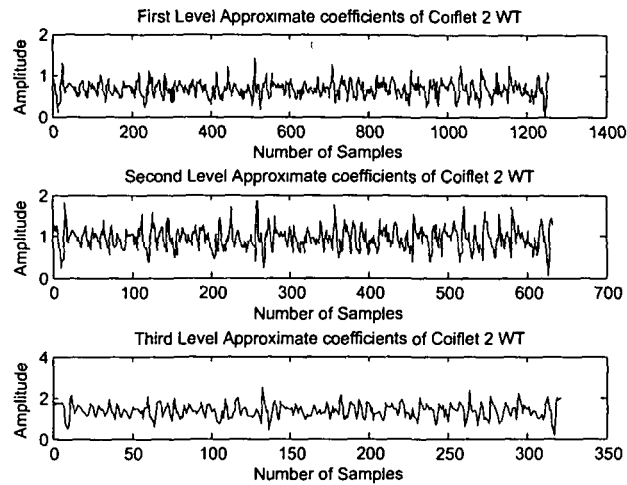


Figure II.24: Coiflet 2 WT coefficients of EMG channel 2 for precision grasp

The approximate coefficients obtained at first, second and third level of decomposition through Daubechies WT for two channel EMG of six grasp types under study are shown in Figure II.25 through Figure II.36.

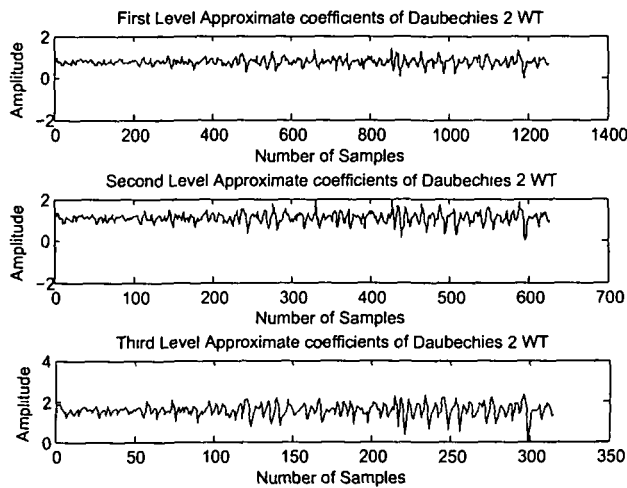


Figure II.25: Daubechies WT coefficients of EMG channel 1 for power grasp

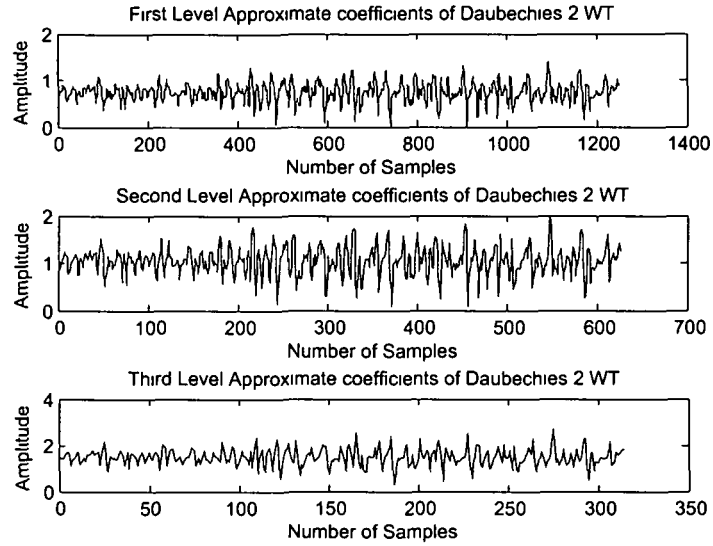


Figure II 26 Daubechies WT coefficients of EMG channel 2 for power grasp

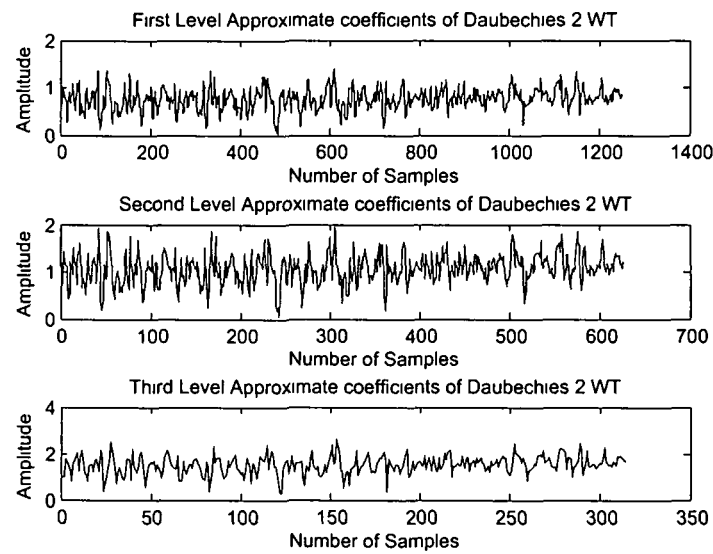


Figure II 27 Daubechies WT coefficients of EMG channel 1 for palm-up grasp

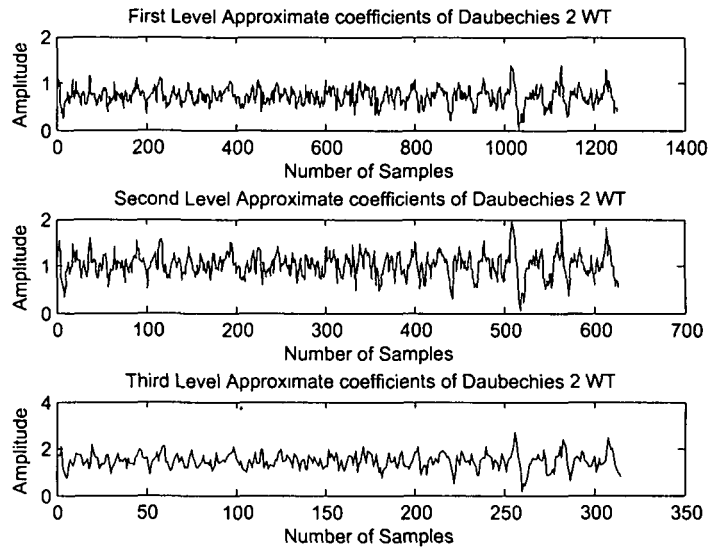


Figure II.28: Daubechies WT coefficients of EMG channel 2 for palm-up grasp

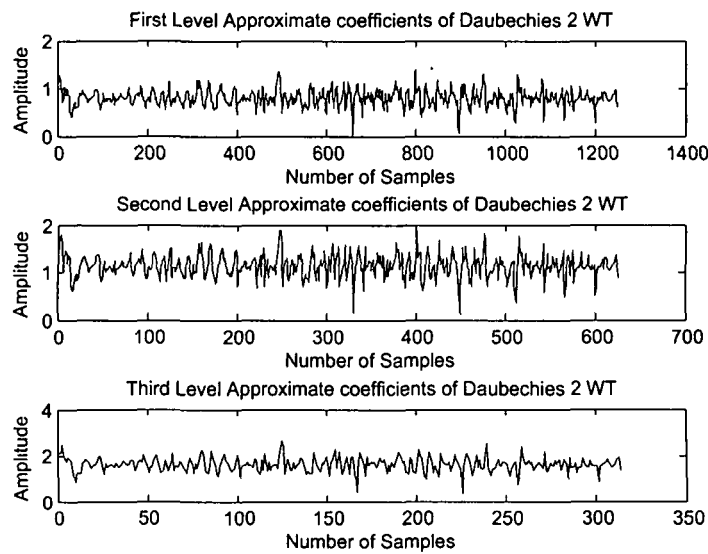


Figure II.29: Daubechies WT coefficients of EMG channel 1 for hook grasp

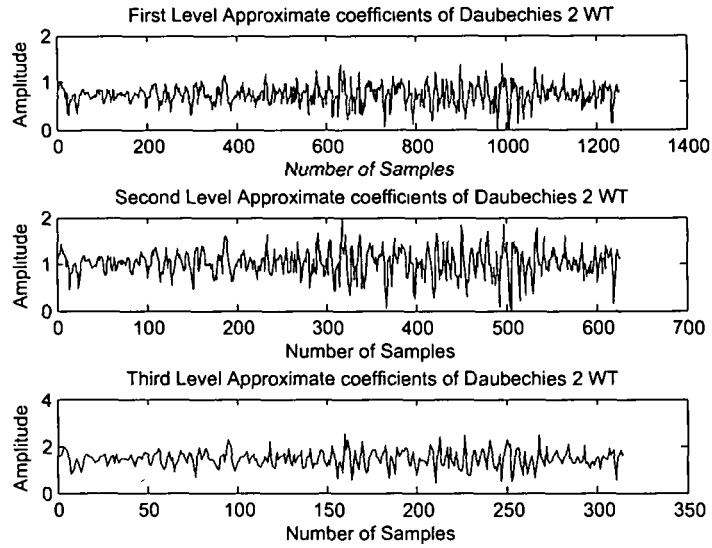


Figure II.30: Daubechies WT coefficients of EMG channel 2 for hook grasp

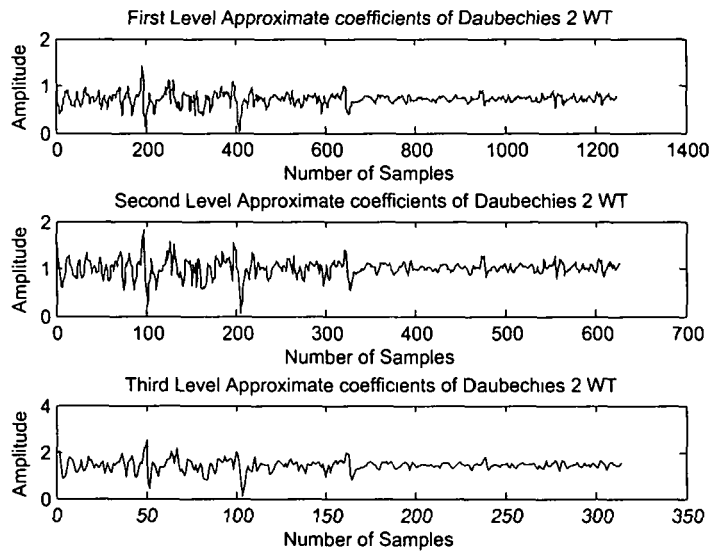


Figure II.31: Daubechies WT coefficients of EMG channel 1 for oblique grasp

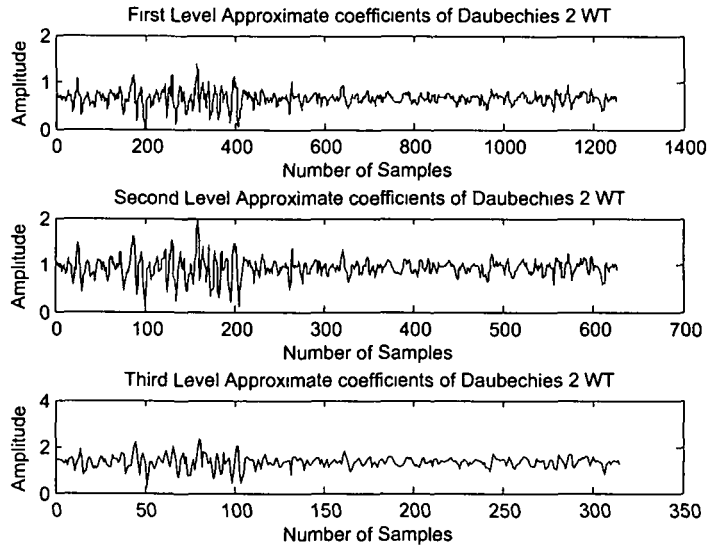


Figure II.32: Daubechies WT coefficients of EMG channel 2 for oblique grasp

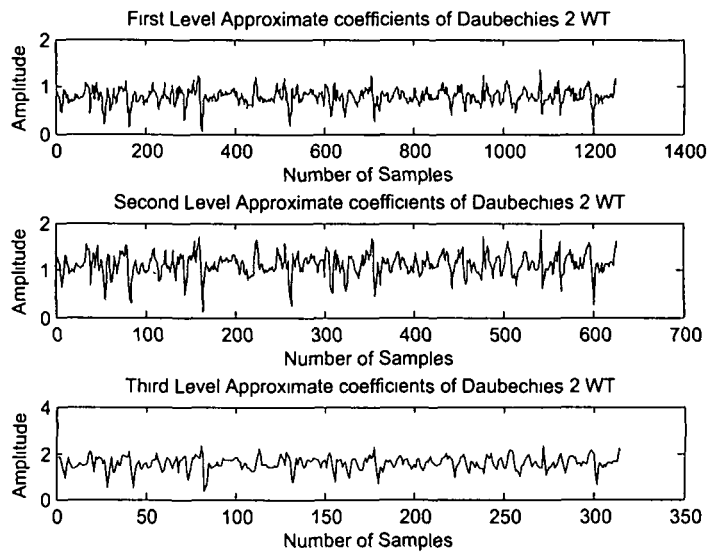


Figure II.33: Daubechies WT coefficients of EMG channel 1 for precision grasp

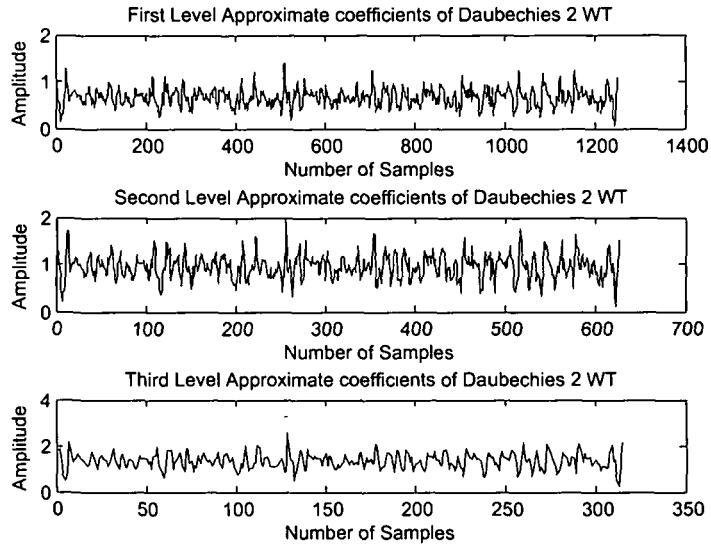


Figure II.34: Daubechies WT coefficients of EMG channel 2 for precision grasp

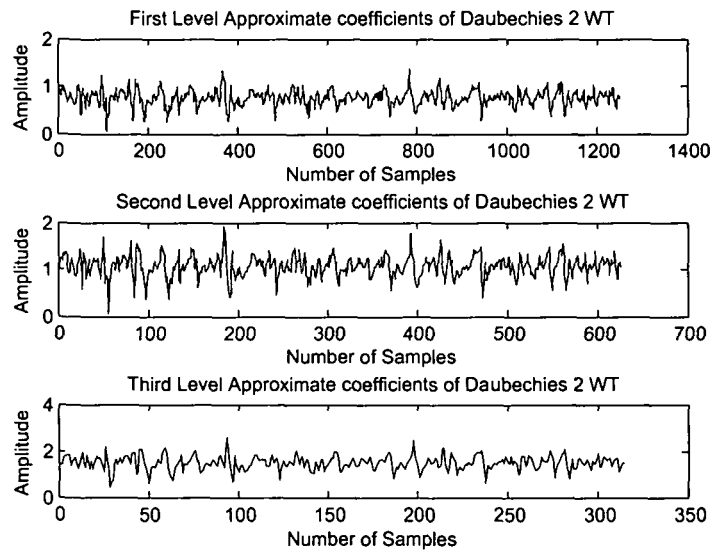


Figure II.35: Daubechies WT coefficients of EMG channel 1 for pinch grasp

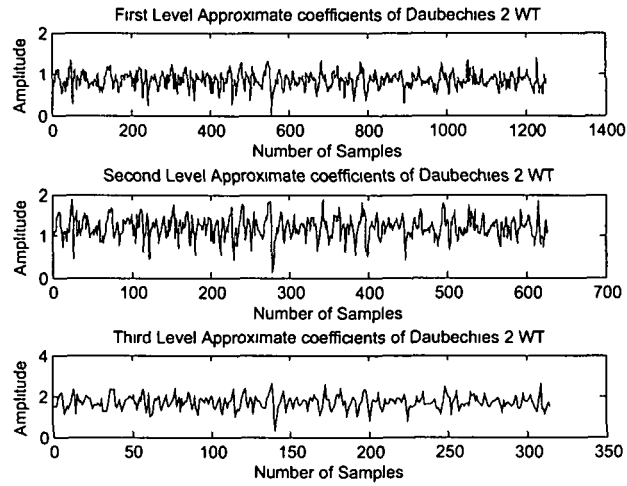


Figure II.36 Daubechies WT coefficients of EMG channel 2 for pinch grasp

The approximate coefficients obtained at first, second and third level of decomposition through Haar WT for two channel EMG of six grasp types under study are shown in Figure II.37 through Figure II.48.

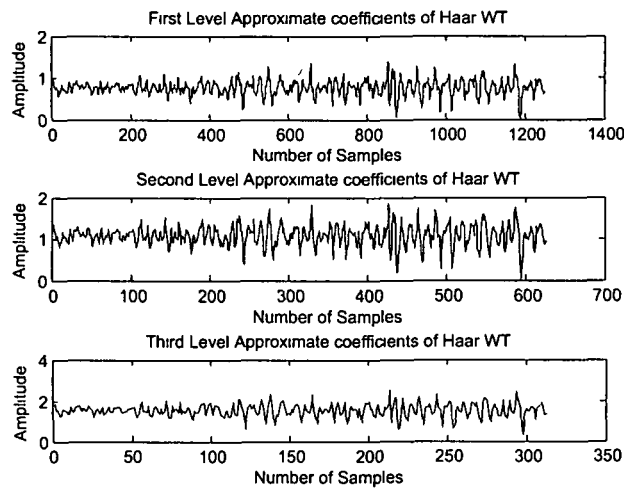


Figure II.37: Haar WT coefficients of EMG channel 1 for power grasp

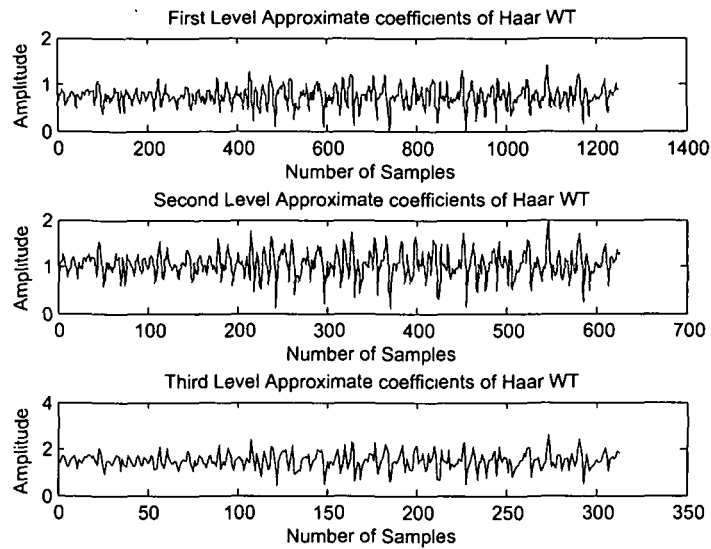


Figure II.38: Haar WT coefficients of EMG channel 2 for power grasp

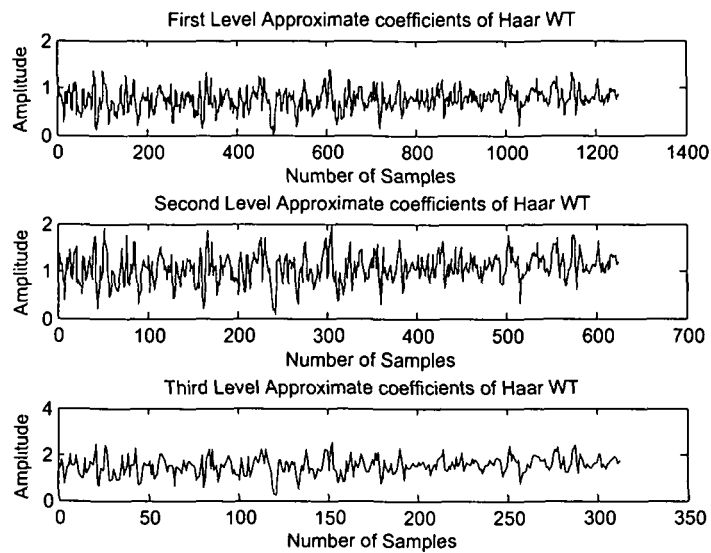


Figure II.39: Haar WT coefficients of EMG channel 1 for palm-up grasp

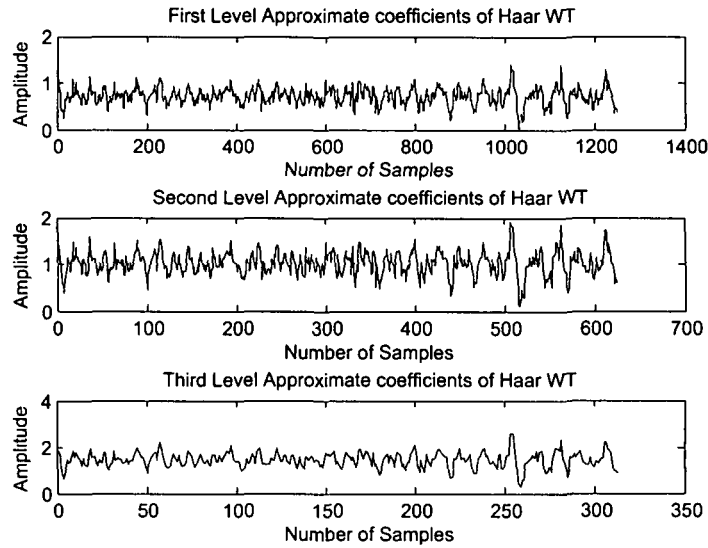


Figure II.40: Haar WT coefficients of EMG channel 2 for palm-up grasp

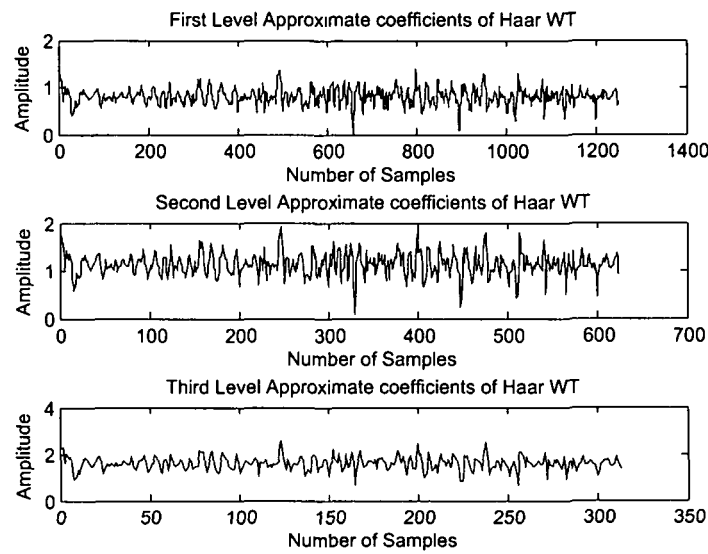


Figure II.41: Haar WT coefficients of EMG channel 1 for hook grasp

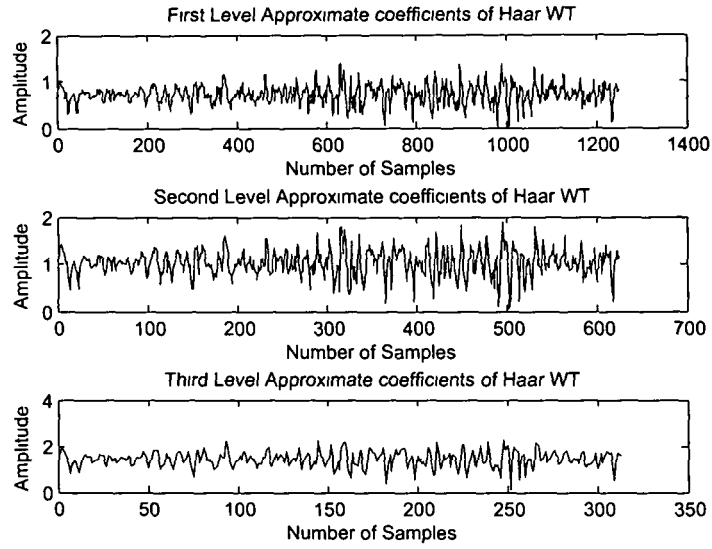


Figure II 42 Haar WT coefficients of EMG channel 2 for hook grasp

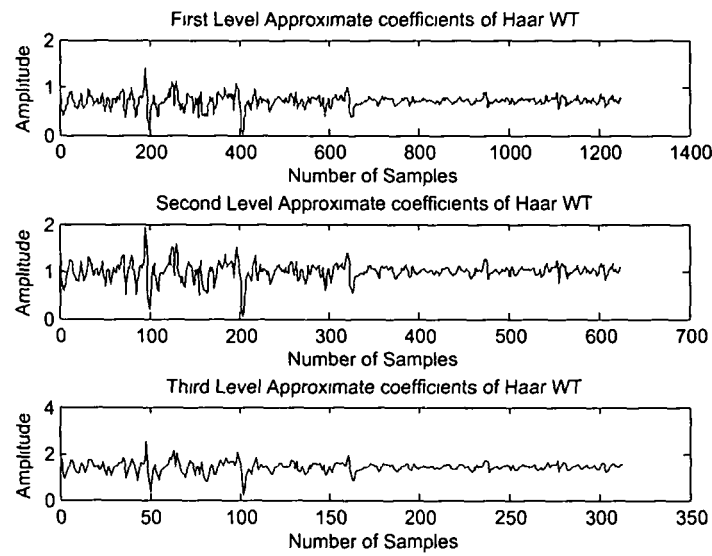


Figure II 43 Haar WT coefficients of EMG channel 1 for oblique grasp

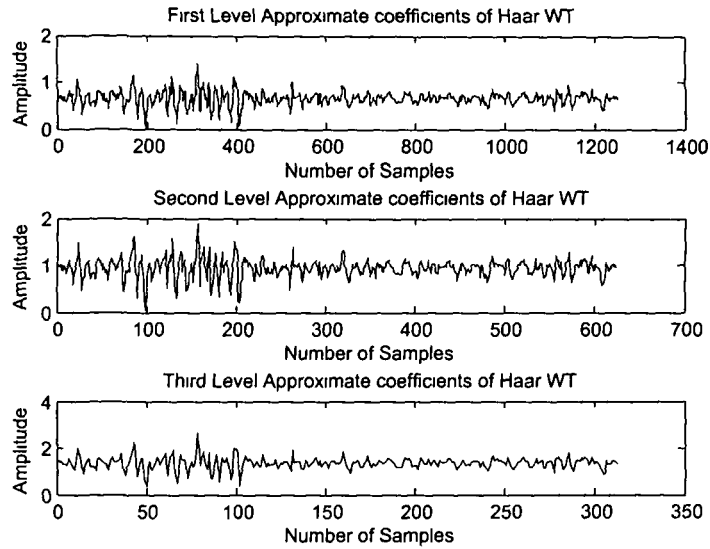


Figure II 44 Haar WT coefficients of EMG channel 2 for oblique grasp

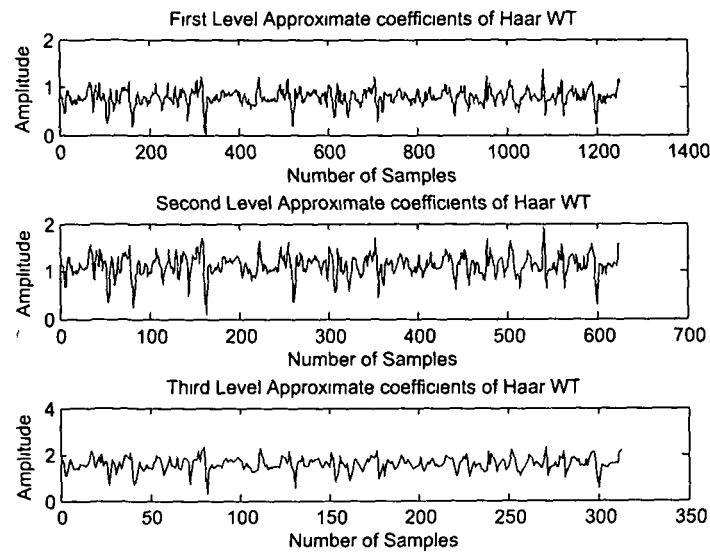


Figure II 45 Haar WT coefficients of EMG channel 1 for precision grasp

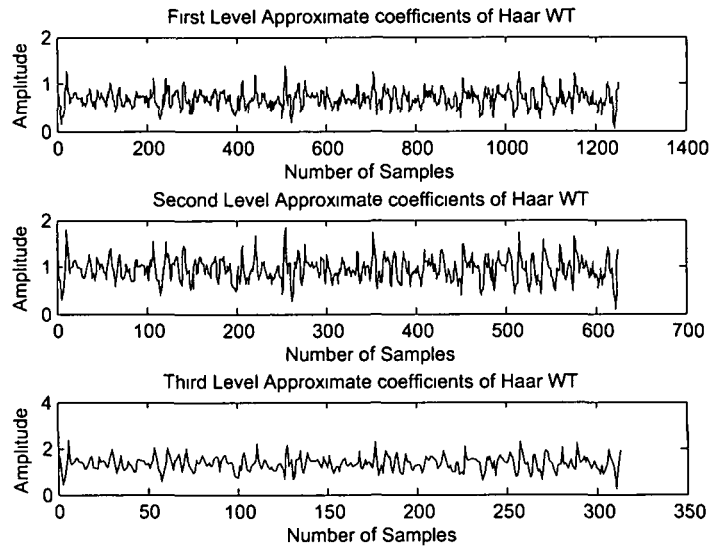


Figure II.46 Haar WT coefficients of EMG channel 2 for precision grasp

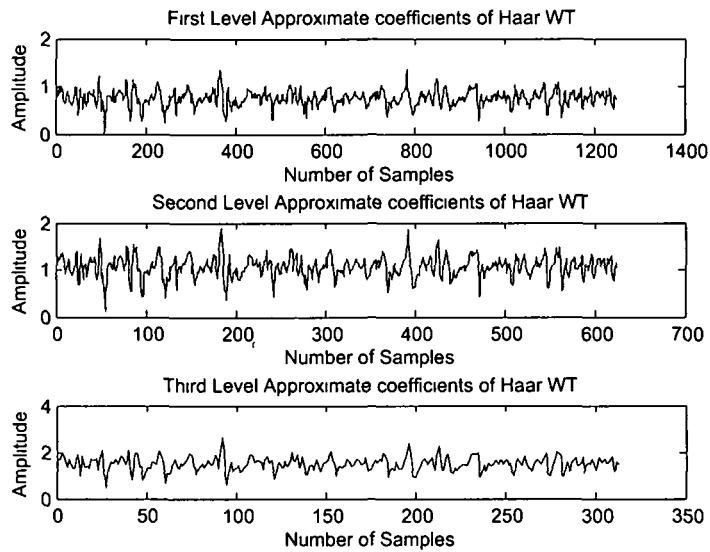


Figure II.47 Haar WT coefficients of EMG channel 1 for pinch grasp

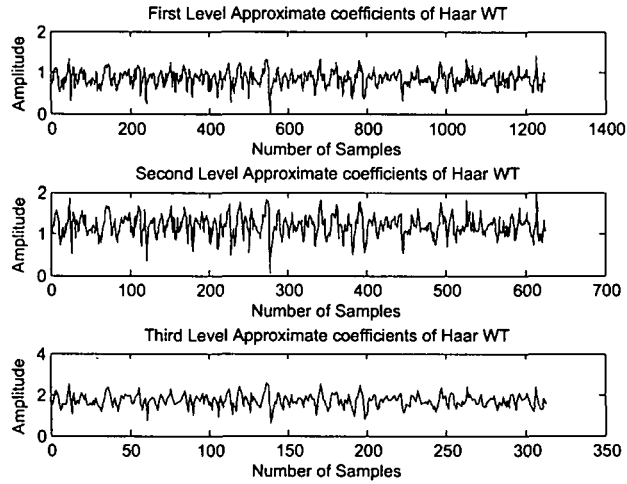


Figure II.48: Haar WT coefficients of EMG channel 2 for pinch grasp

The approximate coefficients obtained at first, second and third level of decomposition through Symlet WT for two channel EMG of six grasp types under study are shown in Figure II.49 through Figure II.60.

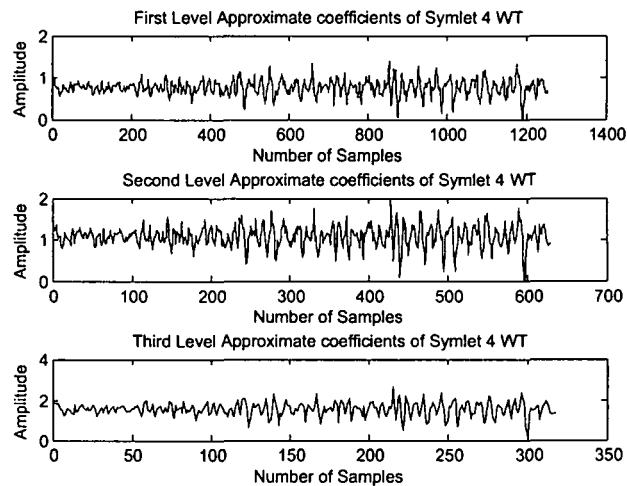


Figure II.49: Symlet 4 WT coefficients of EMG channel 1 for power grasp

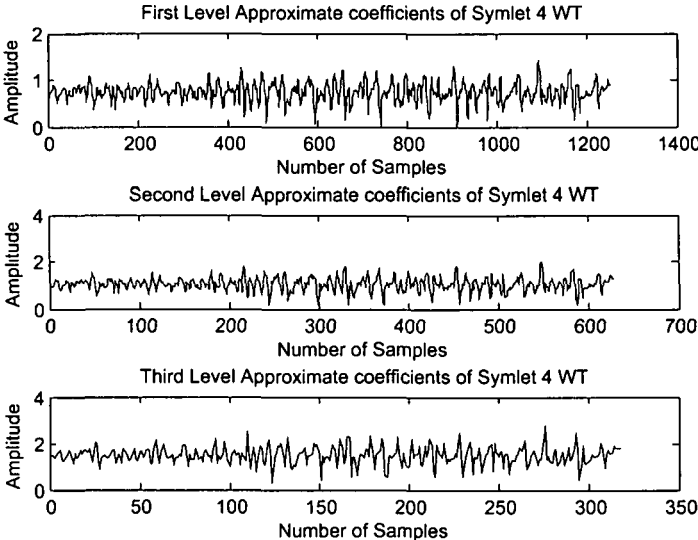


Figure II.50: Symlet 4 WT coefficients of EMG channel 2 for power grasp

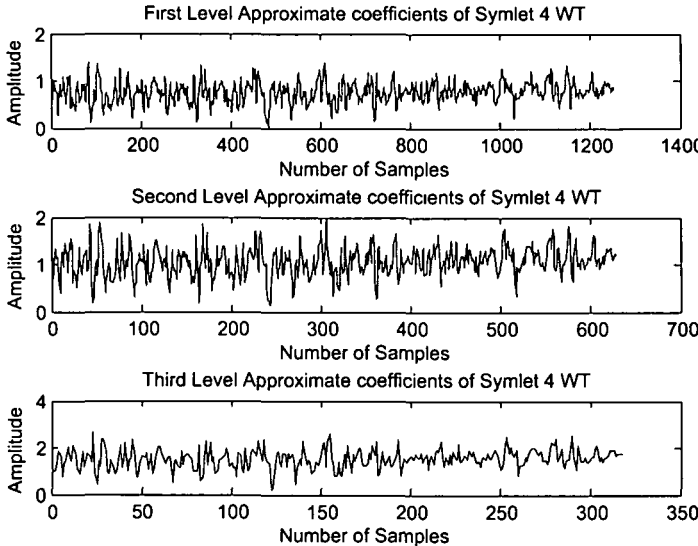


Figure II.51: Symlet 4 WT coefficients of EMG channel 1 for palm-up grasp

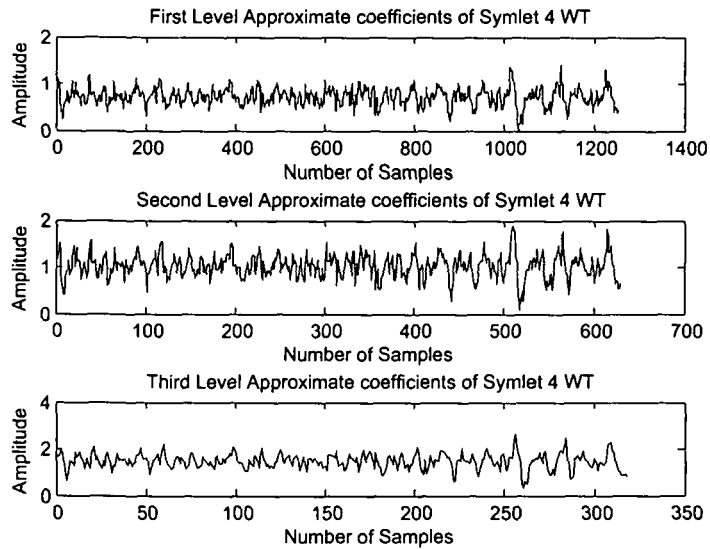


Figure II.52: Symlet 4 WT coefficients of EMG channel 2 for palm-up grasp

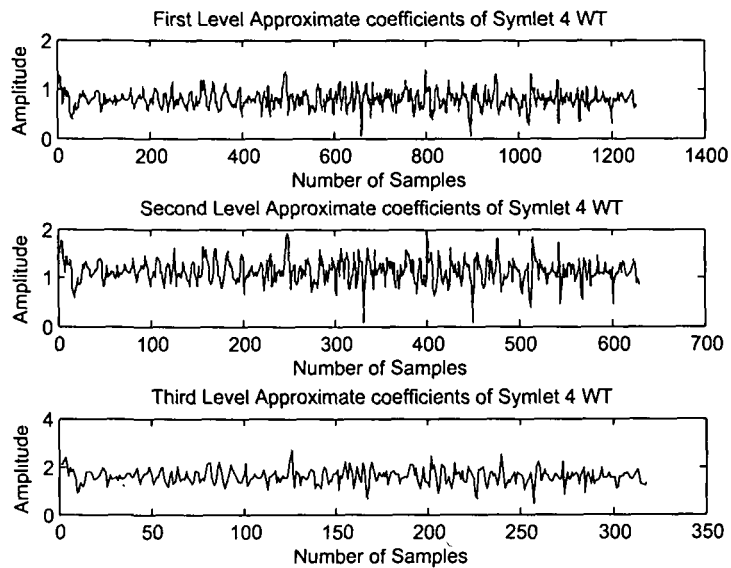


Figure II.53: Symlet 4 WT coefficients of EMG channel 1 for hook grasp

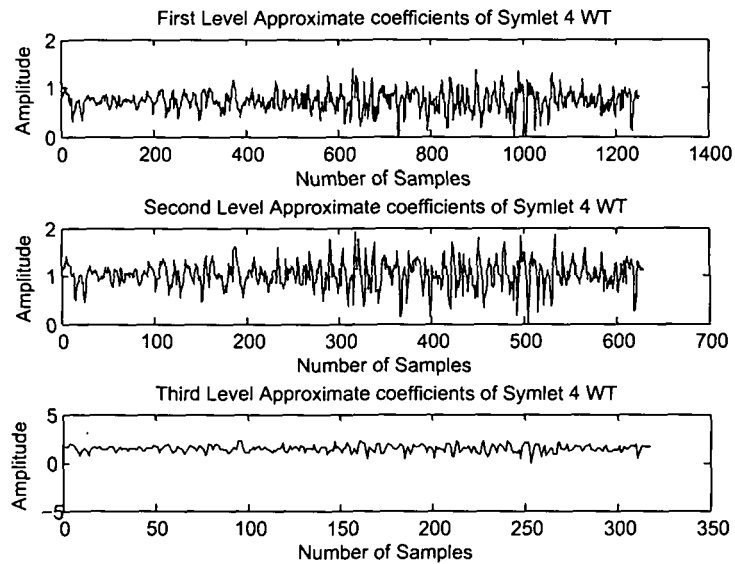


Figure II.54: Symlet 4 WT coefficients of EMG channel 2 for hook grasp

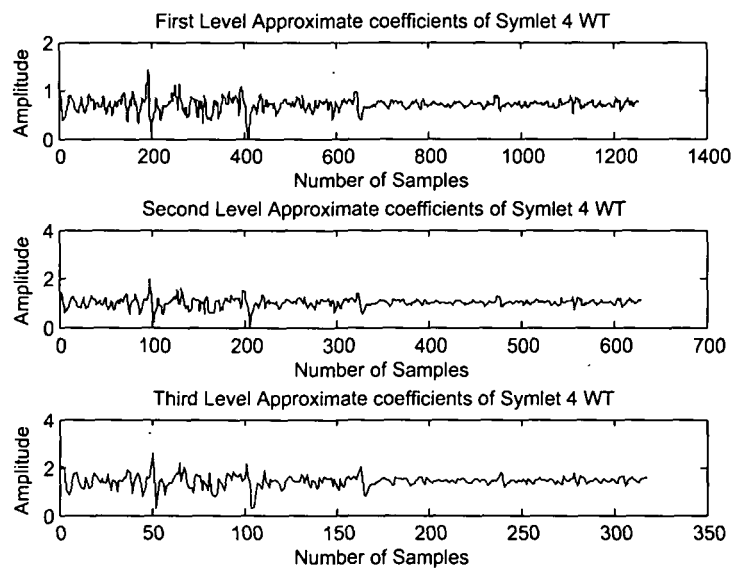


Figure II.55: Symlet 4 WT coefficients of EMG channel 1 for oblique grasp

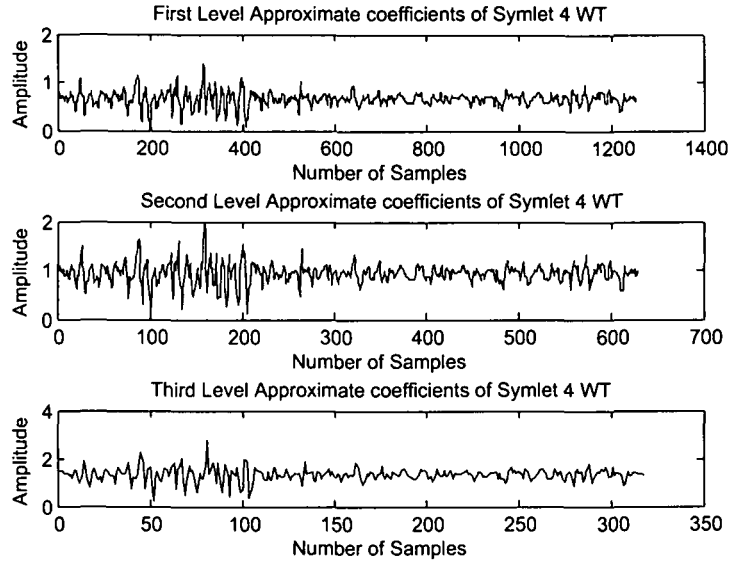


Figure II.56: Symlet 4 WT coefficients of EMG channel 2 for oblique grasp

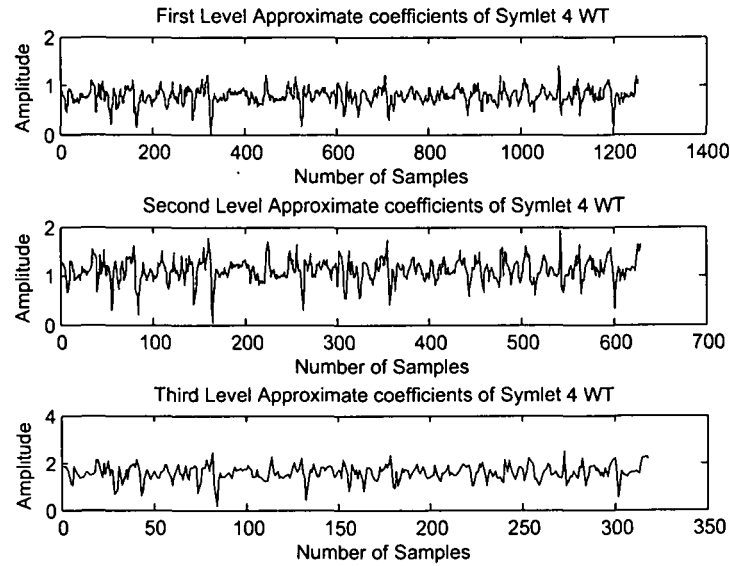


Figure II.57: Symlet 4 WT coefficients of EMG channel 1 for precision grasp

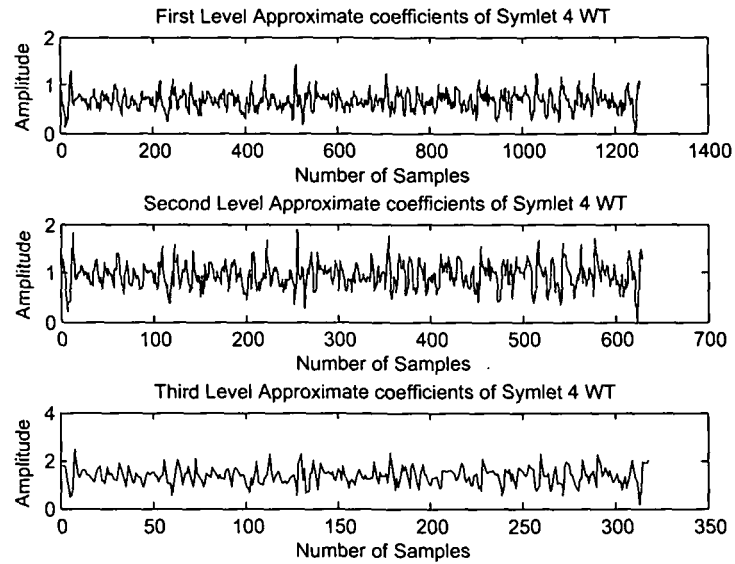


Figure II.58: Symlet 4 WT coefficients of EMG channel 2 for precision grasp

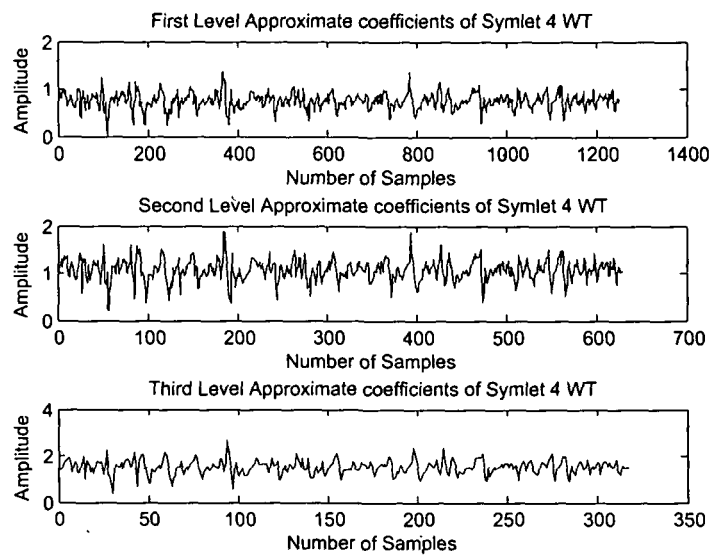


Figure II.59: Symlet 4 WT coefficients of EMG channel 1 for pinch grasp

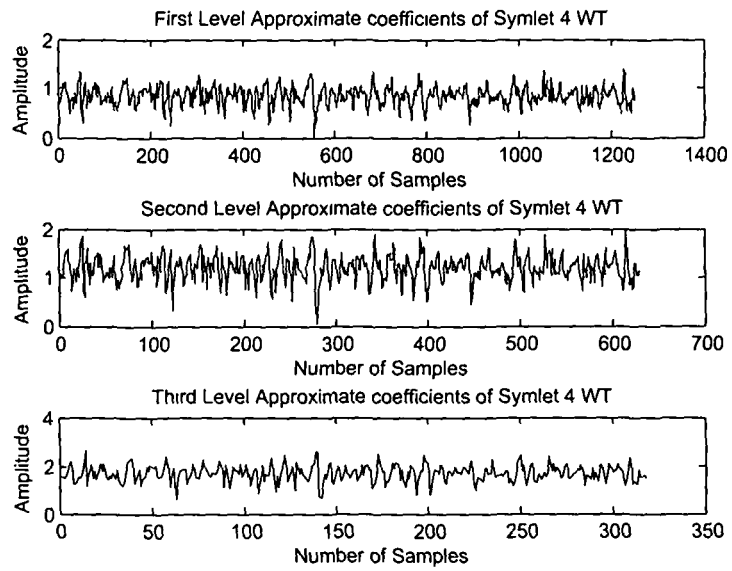


Figure II 60: Symlet 4 WT coefficients of EMG channel 2 for pinch grasp

Appendix-III: Simulation Results of Prototype 1.0

For stable grasping, the finger joint trajectories of Prototype 1.0 should follow the human finger joints trajectories. For finding the torques (as tabulated in Table 5.8) to be applied to the finger joints of Prototype 1.0 to follow natural trajectories, the corresponding finger joint trajectory, velocity and acceleration have been computed. The results of finger joint trajectories, velocities and accelerations are shown in this appendix in Figure III.1 through Figure III.12.

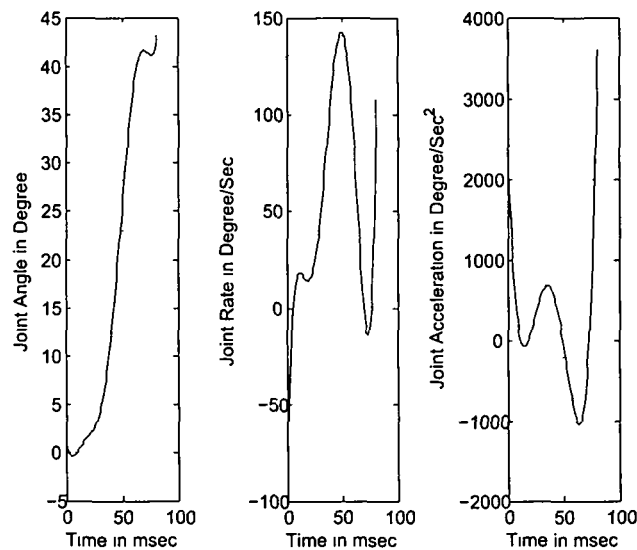


Figure III.1: Joint trajectory, velocity and acceleration of the Index Finger DIP joint

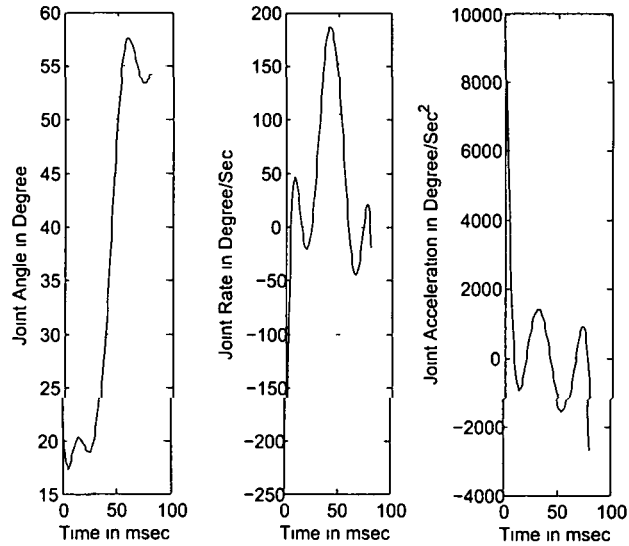


Figure III.2: Joint trajectory, velocity and acceleration of the Index Finger PIP joint

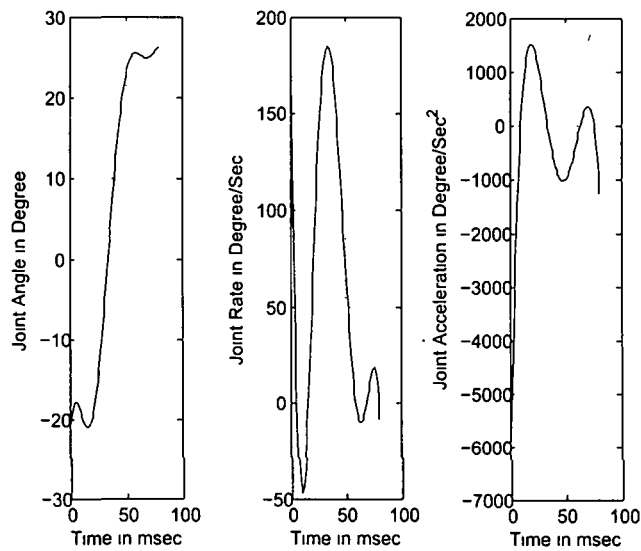


Figure III.3: Joint trajectory, velocity and acceleration of the Index Finger MCP joint

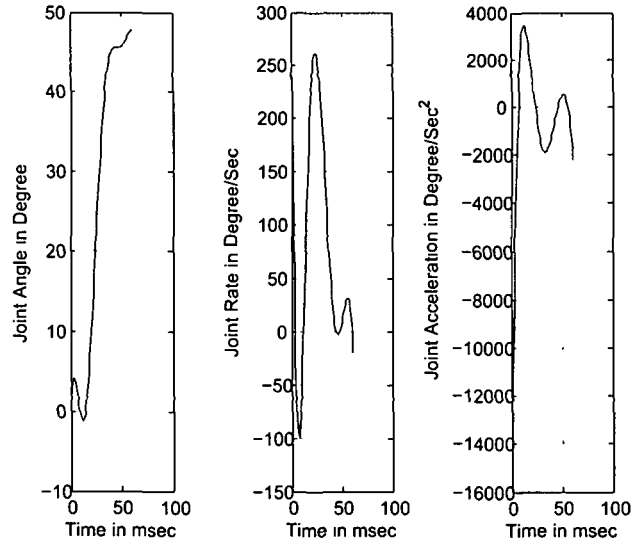


Figure III.4: Joint trajectory, velocity and acceleration of the Middle Finger DIP joint

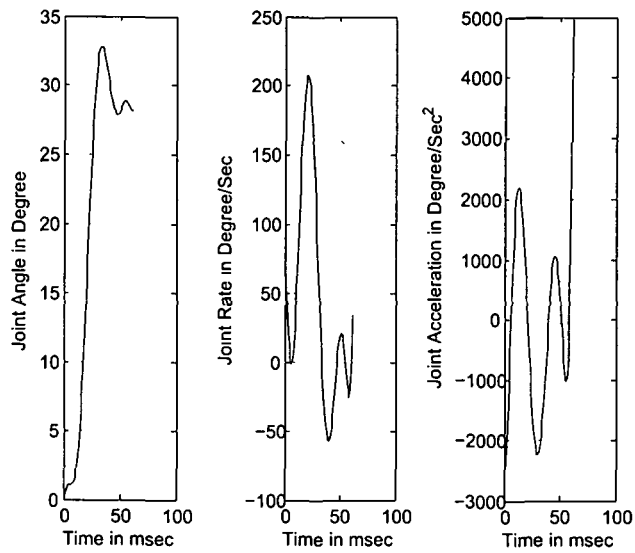


Figure III.5: Joint trajectory, velocity and acceleration of the Middle Finger PIP joint

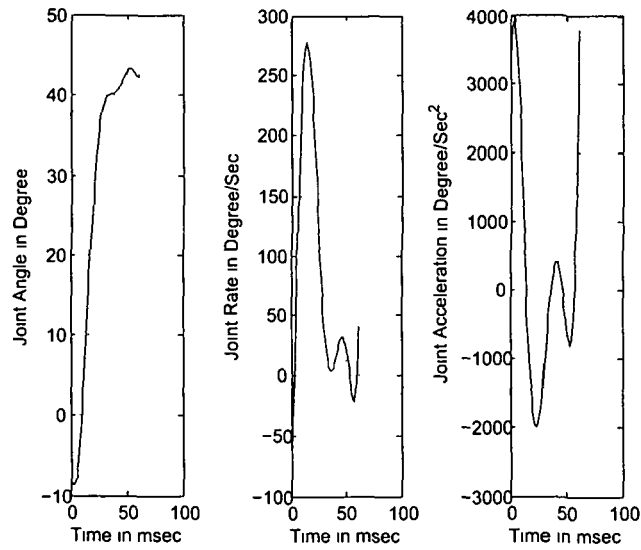


Figure III 6: Joint trajectory, velocity and acceleration of the Middle Finger MCP joint

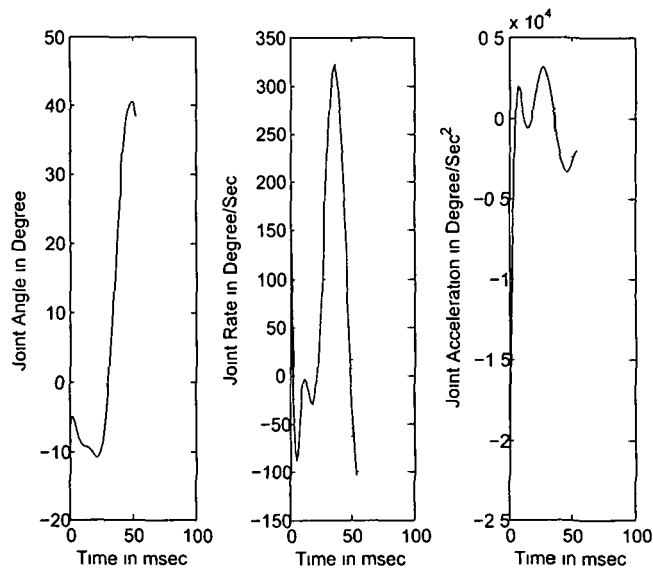


Figure III.7: Joint trajectory, velocity and acceleration of the Ring Finger DIP joint

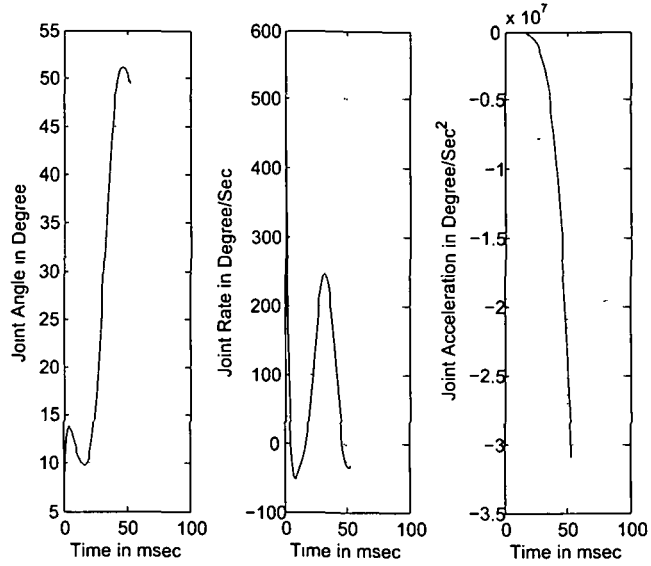


Figure III.8: Joint trajectory, velocity and acceleration of the Ring Finger PIP joint

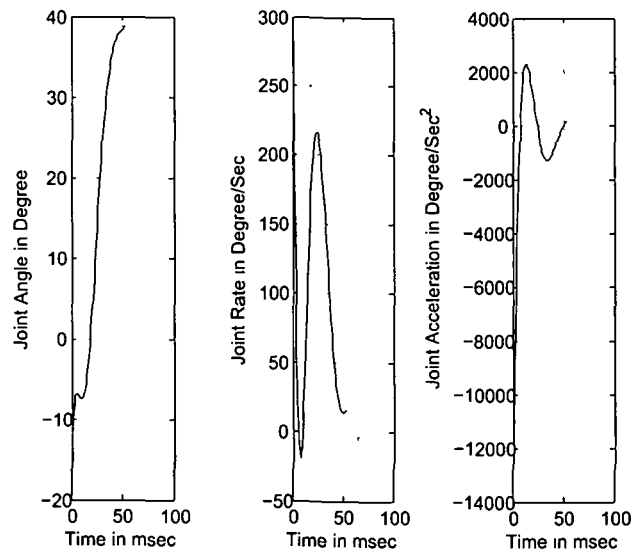


Figure III.9: Joint trajectory, velocity and acceleration of the Ring Finger MCP joint

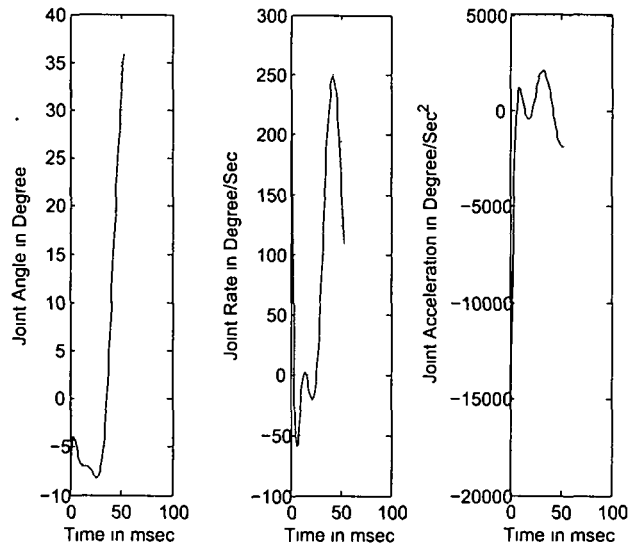


Figure III 10: Joint trajectory, velocity and acceleration of the Little Finger DIP joint

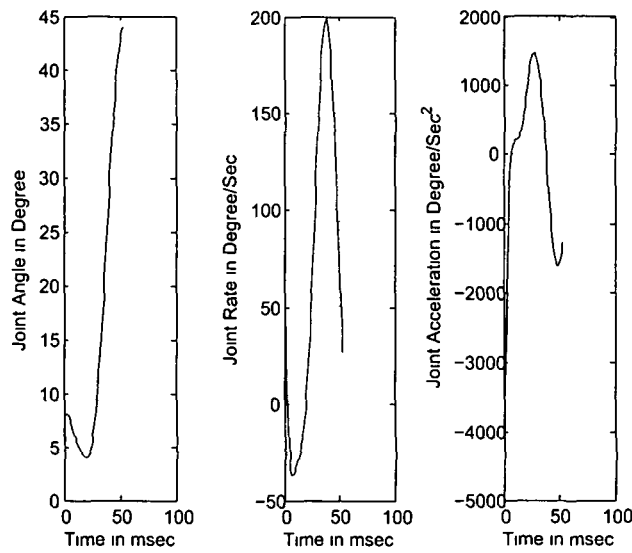


Figure III 11: Joint trajectory, velocity and acceleration of the Little Finger PIP joint

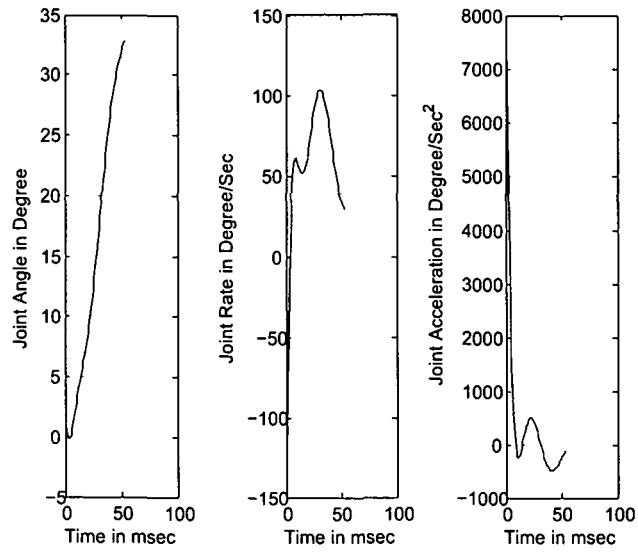


Figure III.12: Joint trajectory, velocity and acceleration of the Little Finger MCP joint

List of Publications

List of Publications

International Peer-Reviewed Journal Publications

1. Nayan M. Kakoty and Shyamanta M. Hazarika. A Two Layered Control Architecture for Prosthetic Grasping, Paladyn. Journal of Behavioral Robotics, Springer, vol. 4, No. 1, pp. 1-9, 2013.(Citation Index: 02)
2. Nayan M Kakoty, Adity Saikia and Shyamanta M Hazarika. Exploring a Family of Wavelet Transforms for EMG based Grasp Recognition. Journal of Signal Image and Video Processing, Springer. (Published Online First on 21st April, 2013) (Citation Index: 01)
3. Nayan M. Kakoty, Mantoo Kaiborta and Shyamanta M. Hazarika. Electromyographic Grasp Recognition for a Five Fingercd Robotic Hand. International Journal of Robotics and Automation - IAES. Vol. 2, No. 1, pp. 1-10, 2013.(Citation Index: 01)
4. Nayan M. Kakoty and Shyamanta M. Hazarika. Development of an Electromyographic Controlled Biomimetic Prosthetic Hand. International Journal of Computational Vision and Robotics, Inderscience. Vol. 4, No. 1, pp. 115-133, 2014.
5. Nayan M. Kakoty and Shyamanta M. Hazarika. Towards Electromyogram based Grasps Classification. International Journal of Biomechatronics and Biomedical Robotics, Inderscience. (Accepted on 29th July, 2013), In Press.

National Journal Publications

6. Nayan M. Kakoty and Shyamanta M. Hazarika, Towards A Bio-signal Controlled Prosthetic Hand, Journal of Assam Science Society, vol. 50, No. 1, 2009.

International Peer-Reviewed Conference Publications

7. Nayan M. Kakoty and Shyamanta M. Hazarika. A Biomimetic Similarity Index for Prosthetic Hands. IEEE Symposium Series on Computational Intelligence in Rehabilitation and Assistive Robotics, Singapore, 2013, pp. 32 - 39.
8. Nayan M. Kakoty and Shyamanta M. Hazarika. Local Hand Control for Tezpur University Bionic Hand Grasping. International Conference on Advances in Robotics, ACM Publication, Pune, 2013, pp. 1 - 7. (**Awarded as the Best Poster Paper in the International Conference on Advances in Robotics 2013, Robotics Society of India.**)
9. Nayan M. Kakoty and Shyamanta M. Hazarika, Recognition of Grasp Types through Principal Components of DWT based EMG Features. IEEE/ International Conference on Rehabilitation Robotics, Zurich, 2011, pp. 477 - 482. (**Citation Index: 11.**)
10. Adity Saikia, Nayan M. Kakoty and Shyamanta M. Hazarika, Wavclet Selection for EMG based Grasp Recognition through CWT. International Conference on Advances in Computing and Communications, Springer, Kerala, 2011, pp. 1116 - 1125.
11. Nayan M. Kakoty and Shyamanta M Hazarika, Classification of Grasp Types through Wavclet Decomposition of EMG Signals. IEEE/ 2nd International Conference on Biomedical Engineering and Informatics, China, 2009, pp. 551 - 555. (**Citation Index: 03**)
12. Nayan M. Kakoty and Shyamanta M. Hazarika, EMG actuated Intelligent Control Architecture for Extreme Upper Limb Prosthesis customized with Sensory Feedback. Poster presented at the International School in Robotics and Intelligent Systems, Iasi, Romania, July, 2009.

13. Nayan M. Kakoty and Shyamanta M. Hazarika, Recognition of Grasp Types Based on Electromyogram Signals, IEEE/ International Conference on Computing, Communication and Networking, December 2008.
14. Nayan M. Kakoty and Shyamanta M. Hazarika, EMG Based Human Robot Interface: Exploiting BZC for Categorizing Hand Movements, 17th International Conference on Computing Mexico City, Mexico, December 2008.

National Peer-Reviewed Conference Publications

15. Nayan M. Kakoty and Shyamanta M. Hazarika. Biomimetic Design and Development of a Prosthetic Hand: Prototype 1.0. 15th National Conference on Machines and Mechanism, IIT Madras, 2011, PP. 499 - 506. (**Citation Index: 06.**)
16. Nayan M. Kakoty and Shyamanta M. Hazarika, Bio-Signal Controlled Prosthetic Hand, National Conference on Design and Manufacturing Issues in Automotive and Allied Industries, IIT Madras, 2009, pp. 267 - 274.
17. Shyamanta M. Hazarika and Nayan M. Kakoty. Development of a Bionic Hand: Prototype 1.0. National Conference Computational Intelligence and Signal Processing, Guwahati, 2011. (Invited Paper).